Settlement during vibratory sheet piling

Piet Meijers

Settlement during vibratory sheet piling

Proefschrift

ter verkrijging van de graad van doctor
aan de Technische Universiteit Delft,
op gezag van de Rector Magnificus prof. dr. ir. J.T. Fokkema,
voorzitter van het College voor Promoties,
in het openbaar te verdedigen op 17 december 2007 om 10:00 uur

door Pieter MEIJERS
civiel ingenieur
geboren te Utrecht

Dit proefschrift is goedgekeurd door de promotor:
Prof. ir. A.F. van Tol

Samenstelling promotiecommissie:

Rector Magnificus,	voorzitter
Prof. ir. A.F. van Tol,	Technische Universiteit Delft, promotor
Prof. A. Sawicki,	Institute of Hydroengineering of the Polish Academy of Sciences
Prof. dr. ir. A. Holeyman,	Université Catholique de Louvain
Prof. dr. ir. F. Molenkamp,	Technische Universiteit Delft
Prof. ir. J.W. Bosch,	Technische Universiteit Delft
Dr. A. Schmitt,	ArcelorMittal
Dr. ir. P. Hölscher,	GeoDelft

ISBN 978-90-9022570-8.

Printed in The Netherlands.

Acknowledgement

The study reported in this thesis is performed as part of two Delft Cluster projects. The main part is part of Delft Cluster project: Risk management of underground construction, 'Delft controls the underground'. The Raamsdonksveer sheet pile test is executed as part of Delft Cluster project 'new perspective for foundations and deep excavations', work package 3.1 'controlled use of the subspace'.

Being active in the field of geotechnical engineering for many years one gets a special affinity with a number of specialised subjects. For me this is the behaviour of soil during dynamic and cyclic loading. In the hustle of day-to-day work the possibilities to delve deeper into the matter for understanding the underlying mechanisms are limited. This study was therefore a welcome opportunity to increase my knowledge in this field.

To perform and finalise this study would not be possible without the help of many persons who contributed in different ways. First of all I want to thank the management of GeoDelft for giving me the time to start with and complete this study. Willem van Pernis and Aad Slingerland did a lot on the laboratory testing. The professional, enthusiastic and constructive attitude with which the monitoring crew of GeoDelft and the piling crew of WoudWormer executed the field test at Raamsdonksveer contributed greatly to its success. It was a pleasure working together with these people.
Financial and practical support for this study was obtained from the following parties: Delft Cluster, GeoDelft, Dutch Directorate-General for Public Works and Water Management, Municipality of Rotterdam, Ballast Nedam, Volker Wessel Stevin, ArcelorMittal, Spanbeton, PSD, NVAF, WoutWormer and Dieseko. This support is gratefully acknowledged.
Many more people contributed in one way or another. Those who are not mentioned, please excuse me. It is not that I do not appreciate their contribution, but the list simply becomes too long.

Abstract

The purpose of the research described in this thesis is to develop a model that is capable of predicting the settlement due to vibratory sheet piling with reasonable accuracy. The research is limited to sheet piling in sand.

As a start, first a description is given of the processes during vibratory sheet piling. This description forms the outline of the model to be developed. From this description the most likely mechanisms that are responsible for the settlement during vibratory sheet piling are identified. These are the densification of the soil and the displacement of a soil volume due to the volume of the sheet pile.
To get an idea on the amount of settlement occurring in practise, reported data on surface settlement from a database collected by GeoDelft are analysed. From this analysis it follows that close to the sheet pile the average settlement is about 0.1 m. Significantly larger settlements, in the order of 0.5 m to 1 m, are also reported.

From the literature an inventory of already available models to predict the surface settlement is made. Presently available numerical models, that are intended for or may be used for assessing the surface settlement, are described. All models are relatively simple and are to be combined with other models to get the surface settlement. Some of the available models do not correctly describe the relevant mechanisms during vibratory sheet piling. Other models show unrealistic trends when varying some of the parameters (e.g. the frequency or the density of the sand) or are intended for a first estimate only. From this observation it is concluded that a need for a model that describes the actual processes more accurately still exists.

As the densification of the soil is a major aspect of the behaviour this is investigated in more detail. The first step is a literature search on the most important aspects of behaviour of sand during cyclic loading during vibratory sheet piling. These are the combined effect of generation and dissipation of excess pore pressure and the possible existence of a threshold value for the shear strain amplitude below which no densification occurs.
Next an investigation is made of available models for calculating the amount of densification or the generation of excess pore pressure. During the investigation the attention is focussed on models that can be used to predict the behaviour for large numbers of loading cycles. If possible, also correlations between the empirical coefficients in these models and the relative density of the sand are established.
From this investigation three models are selected for further comparison in the actual model. One of the selected models is a densification model. The other two are pore pressure generation models. The selected densification model is the C/L model developed by Sawicki. The two pore pressure generation models are the energy dissipation model, for which different researcher present different expressions and the model developed by Seed and Rahman.

To supplement the findings from the literature a series of cyclic triaxial tests is performed. Three types of tests are performed, drained tests, undrained tests and

undrained tests where at some stage a drainage step is included. The objective of these tests is twofold:

- obtain empirical parameters for the selected densification models
- gain an insight into some aspects of the behaviour of sand during cyclic loading.

In particular the tests with interim drainage show interesting results. Drainage of the sand after some excess pore pressures are generated, but before full liquefaction occurs, is found to increase the resistance against liquefaction. This effect is known as ‘preshearing’ or ‘history’ effect. Another finding is that large deformation (a large plastic shear strain) decreases of the resistance against liquefaction.

Using the previously given description of the processes during vibratory sheet piling a numerical model (called TRILDENS3) is developed that takes into account the different sub processes (interface behaviour sheet pile – soil, propagation of vibrations, densification, dissipation excess pore pressure and summation of the local volume strains). For the propagation and the densification different options are considered and implemented. The previously selected constitutive models are extended to handle both undrained and drained soil behaviour.

To test the developed model a well instrumented field test is designed and executed. This test is performed at Raamsdonksveer, The Netherlands. In the test 10 double sheet piles are installed and removed. Data measured are the vibrations near the sheet pile, the pore pressure, the local densification, the settlement at surface and at two depths and the change in cone resistance. The measured data are processed and interpreted.

The data from the field test are used to validate the different sub models in the overall model. In addition, measured surface settlements from a number of other projects are also used to compare the predictions with the developed model against the actual behaviour. Considering the contribution of the densification on the surface settlement only the predicted settlements are within the range of 0.5 to 2 of the measured data. Considering the contribution of densification and volume of the sheet pile together this range becomes 0.3 to 3.

The result of the described research is an improved understanding of the different processes during vibratory sheet piling and a numerical model to predict the surface settlement.

Samenvatting

Dit proefschrift beschrijft het onderzoek dat heeft geleid tot de ontwikkeling van een numeriek model om de zettingen tijdens in- of uittrillen van damwanden met redelijke nauwkeurigheid te voorspellen. Het onderzoek beperkt zich tot situaties waar de ondergrond uit zand bestaat.

Gestart wordt met een beschrijving van de diverse processen tijdens het in- of uittrillen. Deze beschrijving vormt de basis van het op te stellen model. Uit de beschrijving volgt dat de meest waarschijnlijke mechanismen die de zetting veroorzaken zijn de verdichting van de ondergrond door de trillingen en het inbrengen of verwijderen van het volume van de damwand.
Om enig inzicht te krijgen van de hoeveelheid zetting die in de praktijk optreedt zijn gegevens uit de GeoBrain databank, die door GeoDelft wordt beheerd, op dit punt geanalyseerd. Uit die analyse volgt dat nabij de damwand de zetting gemiddeld 0,1 m bedraagt. Grotere zettingen, van 0,5 m tot 1 m, worden echter ook gemeld.

In de internationale literatuur is vervolgens gezocht naar bestaande modellen om de zetting te voorspellen. Verschillende modellen zijn gevonden die hiervoor bedoeld zijn of hiervoor kunnen worden gebruikt. Alle bestaande modellen zijn relatief eenvoudig en moeten met andere modellen worden gecombineerd om een voorspelling van de maaiveldzetting te krijgen. Een aantal van de beschikbare modellen beschrijven het feitelijke fysische proces niet correct. Andere modellen geven onrealistische resultaten wanneer een bepaalde parameter wordt gevarieerd of zijn alleen bedoeld voor een eerste schatting. Uit deze inventarisatie volgt dat er behoefte is aan een model wat de werkelijke processen beter beschrijft en daarmee tot een betere voorspelling komt.

Een belangrijke bijdrage aan de zakking wordt geleverd door de verdichting van het zand. Daarom is met een literatuurstudie een aantal aspecten van het gedrag van zand onder wisselende belasting, die bij het in- en uittrillen van belang zijn, in meer detail bestudeerd. Deze aspecten zijn het gecombineerde effect van generatie en dissipatie van wateroverspanning en de mogelijke drempelwaarde voor de schuifrekamplitude, waaronder geen verdichting meer plaats vindt. Daarnaast is geïnventariseerd welke modellen in de literatuur worden beschreven waarmee de verdichting en/of de generatie van wateroverspanning van zand bij cyclische belasting te voorspellen. De aandacht is daarbij gericht op modellen die gebruikt kunnen worden om het gedrag bij een groot aantal belastingwisselingen te voorspellen. Waar mogelijk zijn tevens correlaties tussen de empirische parameters in de modellen en de relatieve dichtheid van het zand afgeleid. Uiteindelijk zijn drie modellen geselecteerd voor verdere analyse. Dit zijn twee modellen om de generatie van wateroverspanning te voorspellen en een model om de verdichting van droog zand te voorspellen.

In aanvulling op de gegevens uit de literatuur is een serie cyclische triaxiaalproeven uitgevoerd. Daarbij zijn drie verschillende drainage condities gebruikt, namelijk gedraineerde proeven, ongedraineerde proeven en

ongedraineerde proeven waarbij halverwege de proef een drainagestap is toegepast. Het doel van deze proeven is tweeledig:

- bepalen grootte van empirische parameters in de verschillende verdichtingsmodellen te bepalen
- verkrijgen van inzicht in een aantal aspecten van het gedrag van zand onder cyclische belasting.

Vooral de testen met tussentijdse drainage tonen een interessant gedrag. Drainage van het zand voordat volledige verweking is opgetreden geeft een sterke toename van de weerstand tegen verweking. Anderzijds geeft een grote statische (plastische) vervorming een sterke afname van de weerstand tegen verweking.

Op basis van de eerder opgestelde beschrijving van de diverse processen tijdens het in- of uittrillen van damwandplanken is een numeriek model opgesteld. Voor diverse subprocessen zijn verschillende formuleringen onderzocht. Waar nodig zijn de eerder beschreven verdichtingsmodellen uitgebreid zodat ze zowel voor ongedraineerde, gedraineerde en drainerende situaties kunnen worden gebruikt. De gevoeligheid van het model voor verschillende invoerparameters is onderzocht.

Om de juistheid van het opgestelde model te testen is in Raamsdonksveer een test uitgevoerd waarbij 10 dubbele damwand planken zijn in- en uitgetrild. Daarbij zijn diverse grootheden gemeten zoals de zakking op maaiveld en op diepte, de trillingen in de omgeving, de opbouw en dissipatie van wateroverspanningen, de locale verdichting en de verandering van de conusweerstand. De gemeten waarden zijn geanalyseerd en geïnterpreteerd.

Met de meetgegevens uit deze proef zijn de diverse subprocessen gevalideerd. In aanvulling op deze meting zijn gegevens van een aantal andere projecten, waarbij de maaiveldzakking is gemeten, gebruikt om berekende en gemeten zakking te vergelijken.
Uit de vergelijking volgt dat de bijdrage van de verdichting aan de maaiveldzakking voorspeld wordt gevonden dat de voorspelde zakking meestal ligt binnen een bandbreedte van 0,5 tot 2 keer de gemeten zakking. Als de bijdrage van verdichting en ingebracht volume van de damwand wordt gecombineerd wordt deze bandbreedte 0,3 tot 3.

Het eindresultaat van het hier beschreven onderzoek is een verbeterd begrip van de diverse processen die bij het in- en uittrillen een rol spelen en een numeriek model om de maaiveldzakking ten gevolge van deze processen te voorspellen.

Table of contents

Acknowledgement		i
Abstract		iii
Samenvatting		v
Table of contents		vii
List of symbols		xi
1.	Introduction	1
1.1	Background	1
1.2	Objective and scope	1
1.3	Outline of the dissertation	2
2.	Problem description	3
2.1	Settlement during vibratory sheet piling	3
2.2	General description of the process during vibratory sheet piling	4
2.3	Situation during removal of sheet piles	10
2.4	Observations from model tests	11
2.5	Empirical data	14
2.6	Discussion and conclusion	17
3	Available methods for assessing densification during vibratory sheet piling	19
3.1	General	19
3.2	Method of Massarsch 1992	19
3.3	Method of Massarsch 2000	20
3.4	Method of Massarsch 2004	21
3.5	Method of Drabkin, Kim et al.	23
3.6	Method of Bement	24
3.7	Method of Hergarden	24
3.8	Method of Lukas and Gill	27
3.9	FEM calculations	28
3.10	Comparison and discussion of the different models	28
3.11	Conclusion	32
4.	Behaviour of sand under cyclic loading	33
4.1	General	33
4.2	Qualitative description behaviour of sand under cyclic loading	33
4.3	Methods of cyclic testing on sand	38
4.3.1	General	38
4.3.2	Cyclic triaxial tests	39
4.3.3	Cyclic simple shear tests	40
4.3.4	Cyclic torsional shear tests	41
4.3.5	Vertical shaking	42

4.3.6	Comparison cyclic simple shear and cyclic triaxial tests	44
4.4	Effect preshearing	48
4.5	Threshold load amplitude	53
4.6	Discussion on sand behaviour during cyclic loading	56
4.7	Overview available densification models	57
4.7.1	General	57
4.7.2	Model of Barkan	57
4.7.3	C/L model, description	60
4.7.4	C/L model, empirical data	61
4.7.5	Cyclic fatigue model	63
4.7.6	Finn's model	65
4.7.7	Energy dissipation model, description	67
4.7.8	Energy dissipation model, empirical data	68
4.7.9	Seed and Rahman model	74
4.7.10	Accumulation model	75
4.8	Discussion on the densification models	77
5.	Cyclic triaxial tests on sand from Raamsdonksveer	81
5.1	Testing procedure	81
5.1.1	Purpose of the testing	81
5.1.2	Selection testing conditions	81
5.1.3	General procedure	83
5.1.4	Description of the used sand	84
5.1.5	Test program	85
5.2	Test results and interpretation	85
5.2.1	Post processing test data	85
5.2.2	Results cyclic testing	87
5.2.3	Method deriving parameters energy dissipation model	88
5.2.4	Empirical parameters energy dissipation model from results undrained tests	90
5.2.5	Method used for deriving parameters Seed&Rahman model	91
5.2.6	Empirical parameters Seed and Rahman model from results undrained tests	94
5.2.7	Method deriving parameters C/L model	96
5.2.8	Empirical parameters C/L model from results drained tests	97
5.3	Effect interim drainage	100
5.4	Comparison drained and undrained tests	103
5.5	Threshold value shear strain amplitude	107
5.6	Check of sand properties after the testing	108
5.7	Discussion of the test results	110
5.8	Application of the results to the situation during sheet piling	111
6.	Development new model	113
6.1	Introduction	113
6.2	Outline of the model	113
6.3	Assumptions and simplifications	116
6.4	Source model	117
6.4.1	General	117
6.4.2	Speed of installation	117

6.4.3	Modelling shape of the sheet pile	118
6.4.4	Interface sheet pile – soil	120
6.4.5	Tip resistance	124
6.4.6	Out-of-plane bending sheet pile	125
6.4.7	Summary modelling source model	127
6.5	Propagation model	128
6.5.1	General	128
6.5.2	Shear stress attenuation	129
6.5.3	Attenuation of velocity amplitude	129
6.5.4	Stokes	130
6.5.5	Conclusions on the propagation model	133
6.6	Generation model	133
6.6.1	General	133
6.6.2	Densification model Barkan standard	135
6.6.3	Advanced densification model Barkan/Hergarden	135
6.6.4	C/L model	137
6.6.5	Energy dissipation model	137
6.6.6	Seed&Rahman model	140
6.6.7	Threshold value vibration amplitude	140
6.7	Dissipation model	140
6.8	Contribution volume of sheet pile	142
6.9	Summation model	142
6.10	Adjustment shear modulus during the calculation	145
6.11	Effect additional sheet piles on amount of densification	147
6.12	Sensitivity of the model	149
6.12.1	General	149
6.12.2	Influence densification and propagation models	150
6.12.3	Influence installation and removal	151
6.12.4	Influence frequency vibrator	151
6.12.5	Influence tip resistance	152
6.12.6	Influence relative density	152
6.12.7	Influence time of vibrating	153
6.12.8	Conclusions from the sensitivity analysis	153
7.	Execution and results Raamsdonksveer sheet pile test	155
7.1	Purpose of the test	155
7.2	Location	155
7.3	Subsoil conditions	156
7.4	Test program	159
7.5	Used instrumentation	160
7.6	Test results	162
7.6.1	Driving depth sheet piles	162
7.6.2	Speed of installation and removal	163
7.6.3	Vibration level sheet piles	165
7.6.4	Vibration levels surrounding	166
7.6.5	Excess pore pressure	169
7.6.6	Local densification	171
7.6.7	Settlement at surface and at depth	177
7.6.8	Net volume change	180

7.6.9	Creep	182
7.6.10	Horizontal displacements	184
7.6.11	Change in cone resistance	185
7.7	Summary main results	187
8.	Validation of the model	189
8.1	Introduction	189
8.2	Raamsdonksveer sheet pile test	189
8.2.1	General	189
8.2.2	Selection of the relevant soil parameters	189
8.2.3	Comparison measured and calculated velocity amplitude	190
8.2.4	Comparison measured and calculated attenuation shear strain amplitude	194
8.2.5	Comparison measured and calculated local densification	197
8.2.6	Comparison measured and calculated excess pore pressures	198
8.2.7	Comparison measured and calculated surface settlement due to installation	199
8.2.8	Comparison measured and calculated surface settlement due to removal	200
8.2.9	Discussion results comparison measured and calculated values	201
8.3	Nijverdal sheet pile test	202
8.4	The Hague sheet pile test	205
8.5	Settlement at A15	208
8.6	Sewage line Haarlem	209
8.7	Pettemer Zeedijk	211
8.8	Building pit Wassenaar	212
8.9	Summary of validation calculations, installation	213
8.10	Summary of validation calculations, removal	218
8.11	Conclusions	219
9.	Conclusions and recommendations	221
9.1	Conclusions	221
9.2	Recommendations for further research	224
References		227
Curriculum Vitae		235
Annexes		

List of symbols

A : cross section sheet pile
A_1, A_2 : empirical constants
A_L : dissipated energy per cycle (area enclosed by hysteresis curve)
A_T : elastic energy
A,B : calibration parameters in relation between electrical resistivity and porosity
a : acceleration
a : radius of contact area (Hertz equation)
a,b : empirical parameters in expression for the number of cycles to liquefaction
a,b : constants
B : B-factor, Skempton coefficient
B_{sheet} : width of sheet pile
B_{ij} : influence width settlement at surface
b_i : width element i
b_{spread} : width of volume spreading
b_{sheet} : thickness of the sheet pile
C : damping
C_p : wave velocity P-wave
C_S : wave velocity S-wave
CSR : cyclic stress ratio
C_R : wave velocity R-wave
C_R : correction factor between cyclic triaxial and cyclic simple shear loading
C_u : coefficient of uniformity, $C_u = d_{60}/d_{10}$
C_1 : constant
C_1, C_2 : empirical constants C/L densification model
C_1, C_2, C_3, C_4,: empirical parameters Finn's model
c : cohesion
c_v : coefficient of vertical consolidation
c_h : coefficient of horizontal consolidation
C_u : coefficient of uniformity $C_u = d_{60}/d_{10}$
D : diameter pile
D : damping ratio
D_c : parameter describing grain size distribution (Bement)
D_{sheet} : average thickness sheet pile (cross section divided by working width of the sheet pile)
D_1, D_2 : empirical constants C/L densification model
d_{10} : grain size at which 10% passes by weight
d_{30} : particle size with 30% passing by weight
d_{50} : grain size at which 50% passes by weight
d_{60} : grain size at which 60% passes by weight
d_{90} : particle size with 90% passing by weight
E : Young's modulus
E_{dis} : dissipated energy
$E_{dis,cycle}$: dissipated energy per loading cycle
E_{ur} : elastic unloading/reloading modulus

e : void ratio
e_{min} : minimum void ratio
e_{max} : maximum void ratio
e_0 : initial void ratio
F : force
F_{clutch} : clutch friction
F_{dyn} : exerted force vibrator
F_{fric} : friction force at interface sheet pile - soil
F_{pull} : pulling force piling rig
F_{tip} : tip resistance
f : friction ratio, $f = f_s/q_c$
f : friction coefficient
f : frequency
f_s : local friction
f_1 : empirical parameter (method Massarsch 2000)
G : weight
G : shear modulus
G_{max} : initial (small strain) shear modulus
G_{ref} : shear modulus at reference stress p_{ref}
$G_{vibrator}$: weight of the vibrator
G_{sheet} : weight of the sheet pile
GL : ground level
g : acceleration of gravity
g_{Rz} , $g_{\varphi z}$: Green's function
ΔH : thickness soil layer
h_j : thickness of sublayer j
i : width parameter (distance centre to point of maximum inclination)
i : imaginary unit
I_D : relative density
$I_{D,0}$: initial relative density
$I_{D,f}$: final relative density
J_0, J_1, Y_0, Y_1,: Bessel functions
J_2 : second invariant strain amplitudes deviator
K : compression modulus
K : coefficient of earth pressure, ratio between horizontal and vertical stress
K : factor in expression for surface settlement
K_W : bulk modulus water
K_0 : compression modulus at small strain
K_0 : coefficient of earth pressure at rest
L : wave length
L : empirical liquefaction parameter HYPERVIB model
L : driving depth sheet pile
L_{start} : driving depth sheet pile at start
L_{end} : driving depth sheet pile at end
M : constrained modulus
M : moment
M : mobilization index (cyclic fatigue model)
m : mass
m_z : parameter relating vibration amplitude at depth to vibration amplitude at

surface
N : number of cycles
N : normal force
NAP : Amsterdam Ordnance Datum, reference level for height measurements in The Netherlands
N_{liq} : number of cycles to liquefaction
$N_{liq,0}$: number of cycles to liquefaction if no preshearing is present, for the relative density at start of cyclic loading
n : attenuation parameter
n : parameter for stress dependency stiffness
n : porosity
n_{min} : minimum porosity
n_{max} : maximum porosity
n_0 : initial porosity
Δn : change in porosity
O : circumference of the sheet pile: $O=2*B_{sheet}$
PEC : Pseudo Energy Capacity, dissipated energy at liquefaction in undrained situation
p : isotropic stress
p_{ref} : reference stress
q : deviatoric stress
q_c : cone resistance
$q_{c,tip}$: cone resistance at tip level sheet pile
R : radius of sphere
R : distance
R_C : ratio between C_R and C_S
r : radial coordinate
r_1 r_2 : radial distance point 1 and point 2
r_{equi} : equivalent radius
r_u : the relative excess pore pressure (ratio between excess pore pressure and initial effective vertical stress, $r_u = u/\sigma'_{v0}$)
r_0 : width first element mesh
r_0 : radius of cavity
r_0 : reference distance
S : structure parameter, parameter that describes the increase in liquefaction resistance due to preloading
S_{max} : settlement at tunnel centre line
s, S : settlement
s_{avg} : average settlement
s_{max} : maximum settlement
T : shear force (Hertz equation)
t : time
t_{max} : maximum time
t_{start} : start time
Δu : change in pore pressure
$du_{generat}$: change in pore pressure due to densification
$du_{dissipat}$: change in pore pressure due to dissipation
u : (excess) pore pressure

u : radial displacement
u_0 : radial displacement amplitude at $r = r_0$
V : volume
v : velocity
v_0 : reference amplitude velocity (velocity amplitude at reference distance r_0)
W : section modulus
ΔW : dissipated energy
w : water content
X : history parameter
x : horizontal coordinate
x : distance considered point to tunnel centre line
x_1, x_2, x_3, x_4, x_5, x_6 : coding parameters in method Drabkin, Lacey, Kim
Y : settlement in method Drabkin, Lacey, Kim
z : vertical coordinate
z : surface settlement
z_0 : reference settlement
z : parameter in C/L model, $z=JN=¼\gamma_0^2N$
Δz_i : settlement for column i
Δz_{ij} : settlement due to volume change element ij

α : acceleration amplitude sheet pile, expressed as fraction of the gravitational acceleration
α : a parameter describing soil damping
α : compression factor, an empirical constant in method Massarsch 2004
α : compressibility of the soil
α_B : coefficient of vibratory compaction, parameter in expression for densification (Barkan)
β : time factor
β : relative pore pressure generation per loading cycle
β : compressibility pore water
γ : shear strain
γ : unit weight
γ_{dry} : dry unit weight
γ_{max} : shear strain amplitude
γ_r : reference shear strain (Hardin-Drnevich)
γ_w : unit weight water
γ_{yield} : shear strain at yield (Hertz equation)
δ : lateral displacement (Hertz equation)
δ : angle of interface friction
δ_{yield} : lateral displacement at yield (Hertz equation)
$\Delta\gamma$: shear strain amplitude
$\Delta\tau$: shear stress amplitude
$\varepsilon_{vol,ij}$: volume strain of element i,j
ε^p : plastic strain
ε_{vol} : volume strain
ε^{pl}_{vol} : plastic volume strain

ε^{el}_{vol} : elastic volume strain
ε_{rad} : radial strain
ε_z : vertical strain
η : dynamic viscosity
η : acceleration amplitude, expressed as fraction of acceleration of gravity
η_0 : threshold value acceleration amplitude, expressed as fraction of acceleration of gravity
θ : empirical parameter
θ : angle of volume change spreading
θ : angle between vertical and line through source and receiver
θ : empirical parameter in expression for development of excess pore pressure under cyclic loading
ν : Poisson ratio
ρ : unit mass
ρ_s : unit mass of solids
ρ_{soil} : specific electrical resistance soil
ρ_{water} : unit mass of water
ρ_{water} : specific electrical resistance of water
σ : stress
σ_c : normal stress between spheres
σ_c : cell pressure
σ_d : deviatoric stress
σ_h : horizontal stress
σ_{mc} : mean effective stress
σ_n : normal stress
σ_v : vertical stress
σ'_{v0} : initial vertical effective stress
σ_z : vertical stress
σ_1, σ_3 : major and minor principle stress
τ : shear stress
τ_d : driving shaft unit resistance
τ_l : liquefied soil shaft resistance
τ_{max} : shear stress amplitude
τ_s : local friction
τ_{yield} : shear stress at yield
Φ : compaction
ϕ : angle of internal friction
Ω_P, Ω_S : dimensionless frequency for respectively P and S waves
ω : angular velocity

1. Introduction

1.1 Background

Building pits are often constructed using sheet piles. Methods used to install or remove the sheet piles are vibratory driving, impact driving and jacking. The most economical method, and therefore the most used method, is vibratory driving. In The Netherlands 70 to 80 % of all sheet piling is installed using vibratrory driving (NVAF and PSD, 2002).
Vibratory driving however may have some negative effects on the surrounding. These negative effects are are vibrations, settlements and noise. In order to overcome or reduce these environmental effects other methods for constructing the building pit, like pressing the sheet piles or the use of a diaphragm walls or secant bored pile wall, are sometimes used. These methods are in general more expensive and may introduce other problems. Therefore, the use of vibratory driven sheet piles is still the favourite method.

A general trend in society is that environmental concern is growing and acceptance of discomfort is declining. Therefore there is a growing need to pay attention to environmental aspects and potential risks during building activities, especially in built-up areas. Part of this is to predict with a reasonable accuracy the level of the environmental effects.
Prediction of the effect on vibratory installation of sheet piles on the surrounding is still a difficult job. Over the years much effort has been paid to predicting the vibrations due to vibratory installation of sheet piles. In a recent research program (Hölscher and Waarts, 2003), (Waarts and Wit, 2004) it is shown that the accuracy of vibration predictions is limited. The average of the predicted vibration amplitudes, made by different companies and using different methods agrees well with the measured values. For an individual prediction however the predicted and observed vibration amplitude may differ by a factor up to 10.

Not much research has been performed on the subject of settlement during vibratory sheet piling. In the course of time some simple methods have been developed for predicting the settlement due to vibratory sheet piling. As far as known no extensive comparison between predicted and measured settlements has been made. The reliability of the available methods is therefore not known.
A need is felt to gain more insight in the process of vibratory induced settlement in order to develop a reliable model for predicting these settlements. This knowledge and model will be of use when considering the risks of installing sheet piles using a vibrator, so a well balanced decision on selecting the type of walls for a building pit and the preferred method of installation of the sheet piles can be made. The development of such a model is the topic of this dissertation.

1.2 Objective and scope

The objective of the research presented in this thesis is to develop a model that is capable to predict the settlements during vibratory sheet piling with reasonable

accuracy. A ‘reasonable accuracy’ is considered to be reached when in 90% of the cases the measured settlements are within a range of 0.5 to 2 times the predicted settlements.
The research focuses on sheet piles in sand, as it is the general opinion that settlements are due to densification of sand during cyclic loading. No attention is paid to the possible densification in clay and peat.

1.3 Outline of the dissertation

First a description of the process during vibratory sheet piling is given (chapter 2). This chapter serves as basis for the model to be developed. To illustrate the relevance of the model also an overview of possible problems due to settlements is given. An assessment of the amount of settlement during vibratory sheet piling is made using data from a database.
Chapter 3 summarises published methods for assessing the settlement vibratory sheet piling.
It is expected that main cause for the settlements is the cyclic loading of the soil. Quantifying this effect is a major part of the new model. Therefore, a review of available knowledge on this aspect is presented in chapter 4. Special attention is paid to aspects relevant for the situation during vibratory sheet piling.
In chapter 5 a series of cyclic triaxial tests is described. The objective of these tests is twofold. One purpose is to elucidate some aspects of cyclic loading that are hardly, if at all, considered in the available literature but of importance for the situation during vibratory sheet piling. The other purpose is to asses the parameters of the sand at the location of the field test (as described in chapter 7). All the available information is used for developing a new model. This model is described in chapter 6.
In order to validate the model a large scale test is performed at Raamsdonksveer, The Netherlands. This test and the results are described in chapter 7.
Chapter 8 describes the validation of the new model. For this validation first the results of the Raamsdonksveer sheet pile test are used.
In addition to this test data from other projects, where the surface settlement during vibratory sheet piling is measured, are used.
Conclusions from the analysis and the validation are summarised in chapter 9. In this chapter also recommendations for further research are given.

2. Problem description

2.1 Settlement during vibratory sheet piling

The use of vibratory installed steel sheet piling is by far the most economical method to construct the vertical boundary of a building pit. In many cases the method can be used without problems or fear for problems in the surrounding. However, in some cases problems will occur or fear for problems arise. One of the problems is settlement in the surrounding on installing or removal of the sheet piling.

The settlement may become quite excessive. Settlements in the order of 0.5 m and more have been observed close to sheet piles installed in loose sand. Figure 2.1 shows one example. Examples of measured settlements due to vibratory or impact driving of sheet piles are shown in e.g. (Heckman and Hagerty, 1978), (Clough and Chameau 1980), (Lacy and Gould 1985), (Picornell and Del Monte 1985), (Dalmatov et al. 1986), (Lineham et al 1992), (Fujita 1994) and (Glatt et al. 2004).

Figure 2.1 Example of excessive settlement during vibratory installation of sheet piles

Typically close to the sheet pile the largest settlements occur, diminishing with increasing distance from the sheet pile. In general the settlements become negligible at a distance of about half the driving depth. In case of loose sand or hard driving the area of influence may be larger.

In a greenfield area settlements will not be a problem. When structures are present near the sheet pile wall problems may arise. Buildings may suffer from uneven settlement or horizontal deformations, resulting in cracks in the walls and possible loss of structural integrity. Existing roads and railways may show local settlements, resulting in discomfort to the traffic and, in case of railways, risk of derailment.

Lifelines as sewage lines and water mains may suffer differential settlement, bending and cracking. A special case is the situation where a pipeline is partly constructed by micro tunnelling. When removing the sheet piles of the start or end shaft the newly constructed pipeline may undergo locally large settlements. Another problem may be the development of excess pore pressures. In saturated sand excess pore pressures precede the settlement. These temporary excess pore pressures may endanger the stability of buildings, dikes etc.

Only a limited number of models has been developed in the past to predict the amount of surface settlement. An overview of these models is given in chapter 3.

2.2 General description of the process during vibratory sheet piling

First a global description of the process is given in order to understand what is happening during vibratory sheet piling. The whole process starts with a sheet pile and a vibrator. Installation or removal of the sheet pile starts by placing the vibrator on the top of the sheet pile. The vibrator can be either a free-hanging vibrator, a leader guided vibrator or an excavator mounted vibrator. The operator selects the place where the vibrator is placed at the sheet pile. This is not necessarily at the centre line (neutral axis) of the sheet pile profile. In case of a single U-profile and a single clamp it is not even possible to place the vibrator at the neutral axis of the sheet pile. After the vibrator is clamped to the sheet pile the vibrator is switched on.

At the interface sheet pile – soil the vibrations are transferred to the soil. Vibration waves start to travel into the soil. In this process the amplitude of the waves decreases with distance. The soil is loaded cyclically due to these vibrations. It is this loading that is responsible for the densification and the excess pore pressures. In case of saturated soil at first some excess pore pressure is developed. Dissipation of the excess pore pressure results in densification. In figure 2.3 the process is illustrated.

Figure 2.2 Sheet pile and vibrator

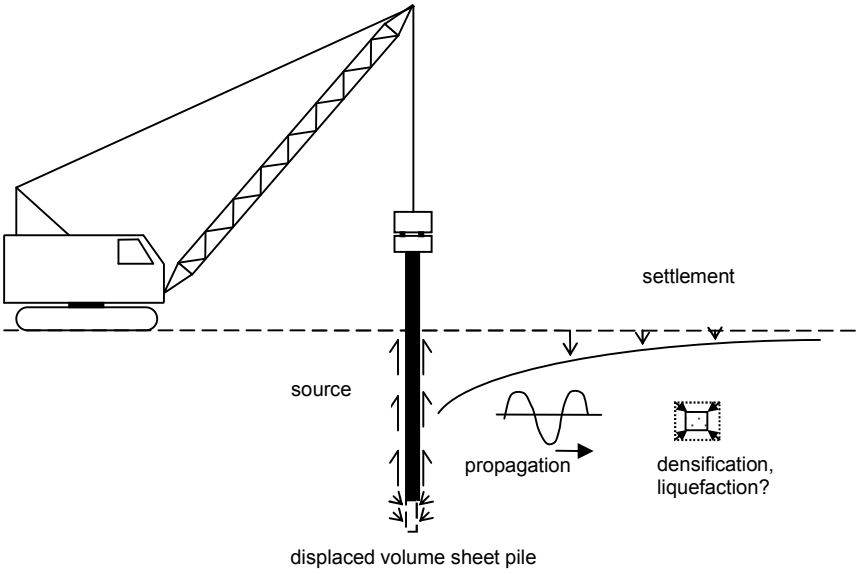

Figure 2.3 Sketch showing the process during vibratory sheet piling.

Different types of vibrators are available. The commonly used types are a low frequency vibrator, a high frequency vibrator and a variable moment vibrator. A low frequency vibrator operates at a frequency of about 25 Hz to 30 Hz (1300 to 1700 rpm). A high frequency vibrator operates at a frequency of 35 Hz to 40 Hz (2000 rpm to 2500 rpm). Variable moment vibrators mostly run at a frequency of 30 to 40 Hz.
Excitations are generated by an even number of eccentric weights rotating in opposite direction. During start-up or switch off of the vibrator the sheet pile is loaded with all frequencies between zero and the working frequency of the vibrator. Quite often it is noticed that during this phase the largest vibrations in the surrounding occur. The variable moment vibrator has been developed to overcome these problems. This vibrator uses four or eight eccentric weights. During start-up and shut-down of the vibrator the eccentric weights are out of phase, resulting in a net zero eccentric load. After reaching the required frequency the eccentric weights are shifted to act out-of-phase. In this way the moment and thus the vibration during start-up and shut-down of the vibrator is zero.

Two types of vibrators that are hardly, if at all, used are the sonic driver and the impact vibrator hammer (USACE 1998). The sonic or resonance driver (e.g. a Bodine-Guild resonance driver) operates at a frequency of 90 to 120 Hz. The working principle of this type of vibrator is to induce a resonant response of the pile.

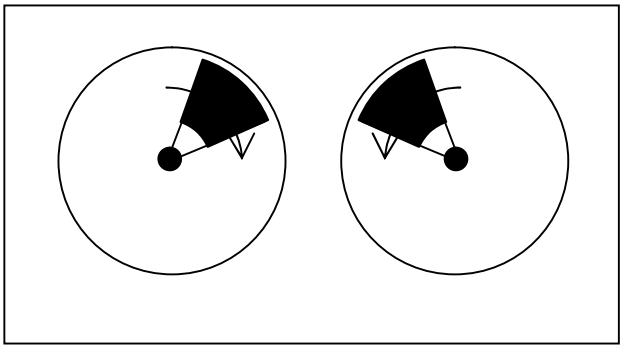

Figure 2.4 Illustration counter rotating eccentric weights

The impact vibrator hammer combines a vibration with an impact force.
A recent development is the 'directional vibrator' by ABI (ABI 2004, Viking 2006). The dynamic vertical load exerted by common vibrators is a sine function. The 'directional vibrator' has a downward load amplitude that is larger than the upward load amplitude. This is achieved with a more complex driving of the eccentric weights.

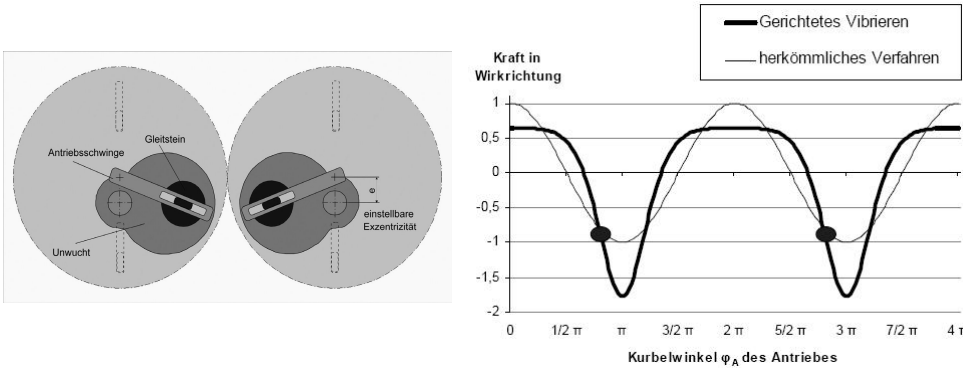

Figure 2.5 Principle of a 'directional vibrator'

Different researchers have investigated the process during vibratory sheet piling (e.g. Holeyman et al 1996). An overview of the different methods is given in e.g. (Berghe 2001), (Viking 2002) and (Azzouzi 2003). One convenient way to describe the process is to consider the forces at a sheet pile. The following forces are distinguished.

1. weight of the sheet pile (G_{sheet} = m*g)
2. weight of the vibrator (bias mass, clamp, exciter block) ($G_{vibrator}$)
3. line pull (F_{pull})
4. centrifugal force from the vibrator (F_{dyn})
5. tip resistance (F_{tip})

6. friction at the interface wall-soil (F_{fric})
7. clutch friction(F_{clutch})
8. inertia of the sheet pile (m*a).

The first four forces give the driving force during installation, the last four the resisting force. Figure 2.6 shows the forces during downward and upward movement respectively.

Usually it is assumed that the tip resistance is zero on upward movement of the sheet pile, see e.g. (Holeyman et al 1999). For non-saturated soil this may be a reasonable assumption, for saturated soils suction at the pile tip may develop during the upward movement and excess pore pressure during the downward movement.

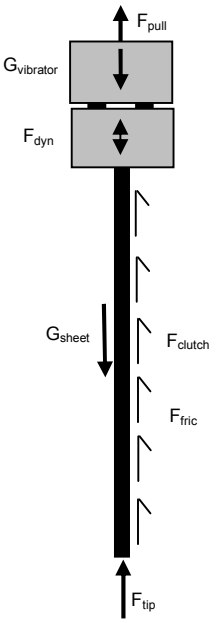

Figure 2.6 Forces at a sheet pile

De net force (as function of time t) during downward movement of the sheet pile is:

$$F(t) = m * a = -F_{pull} + G_{vibrator} + G_{sheet} - (F_{fric} + F_{clutch}) - F_{tip} + F_{dyn} \quad (2.1)$$

and during upward movement:

$$F(t) = m * a = -F_{pull} + G_{vibrator} + G_{sheet} + (F_{fric} + F_{clutch}) - F_{dyn} \quad (2.2)$$

In general it is assumed that the vibration of the sheet pile is in the vertical direction. When the vibrator is mounted eccentric at the sheet pile the head of the sheet pile is loaded with both a cyclic vertical and a cyclic bending moment (see figure 2.7). The last load will result in horizontal vibrations of the sheet pile as well. Viking (2002) measured the horizontal and vertical acceleration of a single sheet

pile (U-profile) on installation. One of his measurements is shown in figure 2.8. His measurements show that, for this case, the horizontal acceleration is about 75% of the vertical acceleration when the transducer is above ground level. For the part of the sheet pile in the soil the horizontal acceleration is limited, but not zero. It is most likely that the sheet pile generates now horizontal waves.
Even with a vibrator mounted at the neutral axis of the sheet pile horizontal movements are possible. The mode is bending of the sheet pile on the applied normal force.

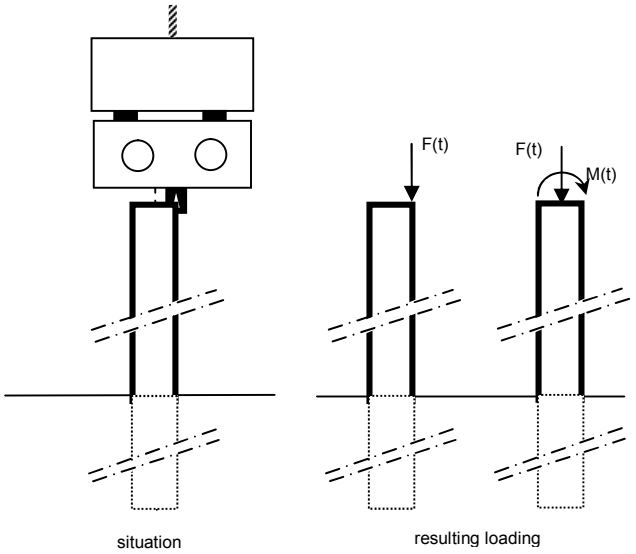

Figure 2.7 Illustration effect of location vibrator at top of sheet pile on applied forces

The common explanation for the working principle of vibrating is the generation of excess pore pressure around the sheet pile. This excess pore pressure reduces the friction and tip resistance. Sinking of the sheet pile results from the weight of the sheet pile and vibrator. For lifting the winch of the piling rig is needed.

Viking and Bodare (1999) investigated the effect of vibrations on the shaft friction using model tests. In their tests a model is placed in a cylinder filled with sand. The load displacement curve of the model pile is measured after installation and after the pile is vibrated. Frequency and time of vibrating are not mentioned. A comparison of the load displacement curves before and after vibro driving shows that the shaft resistance is greatly reduced. From the measured data the reason for this reduction cannot be assessed.

From the preceding it follows that generation of excess pore pressure may not be the only mechanisms responsible for a (temporary) reduction of the soil resistance. Other mechanism may be decrease of horizontal stress, crushing of grains at the interface and a decrease of the friction angle between steel and soil.

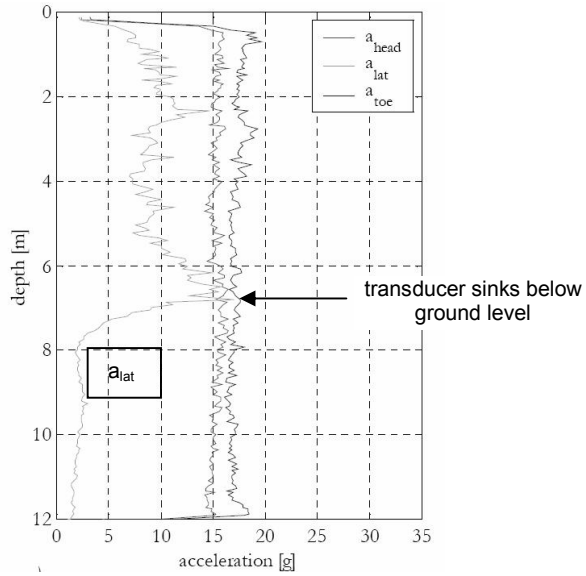

Figure 2.8 Measured horizontal and vertical accelerations in a sheet pile during vibratory driving (Viking 2002), length of sheet pile 14 m, acceleration transducer located at mid depth (7 m from top)

Apart from vibrations emitted from the sheet pile installed or removed other sources of vibrations at the building site may be identified:

- piling rig
- power pack
- traffic at the building site
- densification activities at the building site
- heavy machinery (e.g. demolition, sand sieves) at the site or at neighbouring locations
- traffic at neighbouring roads and railways
- heavy industrial equipment at neighbouring locations.

The first 5 sources are related to building activities. For this study it is assumed that these vibrations do not influence (at least not significantly) the densification near the sheet pile wall. The last two sources are present independent of building activities. Possible densification due to these external sources most likely already occurred before the vibratory sheet piling started. Therefore these can be ignored. Theoretically it may be possible that the combination of vibrations from external sources with vibratory sheet piling increases the shear stress/strain amplitude and thus increases the densification. This aspect will be ignored as well.

One of the tasks of the contractor is to select the proper type of vibrator. Often a requirement is set for the speed of installation, e.g. at least 2 m/minute. In general a larger the speed is present. The time of vibrating for installing one sheet pile is typically in the order of 2 to 5 minutes. This gives that the number of load cycles for installing one sheet pile is in the order of 3,000 to 20,000.

2.3 Situation during removal of sheet piles

During removal the process is mainly the same. Mostly the upward velocity of the sheet pile at start is small or even zero. At this stage all kind of things may happen in the soil like generation of excess pore pressure around the sheet pile, stretching of the sheet pile, degradation of the clutch friction and decrease of the interface friction between sheet pile and soil. Possibly a degraded zone develops, starting at the top and growing towards the tip. When the degradation (including liquefaction) reduced the friction between sheet pile and soil enough the sheet pile starts to move. It is possible that the horizontal stresses in the soil next to the sheet pile are changing as well in this stage.
After this stage the sheet pile is pulled out of the soil, mostly at an increasing speed. The sheet pile represents a volume and removing of the sheet pile will thus leave some space in the subsoil. The removed volume will be in excess of the net steel volume when soil sticks to the sheet pile. In sand this effect is small (in the order of 1 mm or less) but in clay large lumps may stick to the sheet pile. This void will not remain intact. Sand will flow to this void to fill it. This will result in additional settlements.
When the sheet pile is removed the stresses at both sides of the location of the former sheet pile will be in equilibrium. Before the extraction difference in the horizontal stress at both sides of the sheet pile can, and will be, present. This levelling of the stresses may result in some soil deformations as well.
Also stretching of the sheet pile may result in some soil deformations. Mostly the sheet pile is deformed towards the former building pit. Stretching implies that a section of the sheet pile moves a little horizontally, away from the former building pit and into the surrounding. This may result in a void at the side of the former building pit and some compression of the soil at the other side.

For the situation during removal the soil cannot be considered as virgin soil. Installation of the sheet piles and subsequent construction of the building pit may have altered the soil fabric (the way grains are in contact with each other and the actual stress paths in the sand skeleton). During installation already some densification of the soil will occur. Usually the soil at one side of the sheet pile is excavated after installation and anchors or struts are installed. This results in bending of the sheet pile. The horizontal stress behind the sheet pile over some height will decrease towards the active earth pressure. Possible also some dilation (loosening) of the soil will occur. This effect reduces the densification during installation.
After the building job is completed the building pit is backfilled and the anchors and struts are removed. The wall itself may be bended during this job or from previous jobs. Therefore the sheet pile is not necessary free of internal stresses. Also differences in horizontal and vertical stress will be present over the sheet pile.
At the side of the backfilled building pit virgin soil will be present. At the other side the situation is less clear. On one hand the installation phase may have increased the resistance against densification. On the other hand the deformations during the building stage may have altered the fabric of the soil and probably the resistance against densification.

2.4 Observations from model tests

For some insight in the behaviour, the results of a series of model tests, performed at GeoDelft, are described. The objective of these tests is to observe the behaviour during vibratory sheet piling in order to get an insight in the actual behaviour of the soil during sheet pile extraction. The tests are performed in a tank with dimensions 2*1*1 m. Figure 2.9 shows the test set-up. The tank is partly filled with sand (to a depth of approx. 0.6 m) with a uniform relative density of 50%. A plywood sheet is installed in the sand. Tests are conducted with static pulling, vibrating without pulling and a combination of pulling and vibration. The vibrator is connected to a steel frame, resting on the floor of the hall. The tank itself is placed on this frame as well, separated from it with rubber bearings.

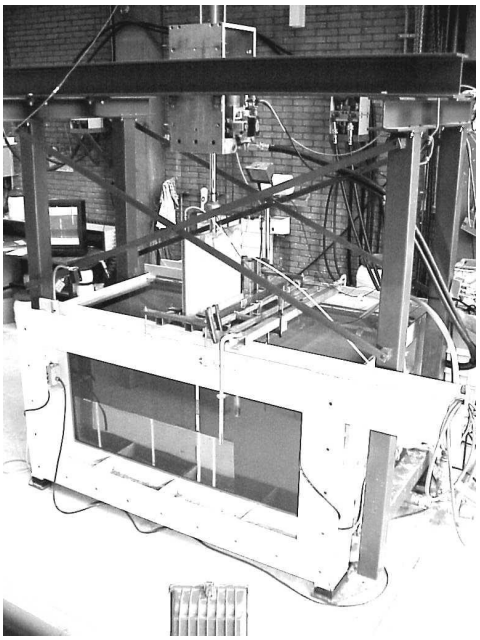

Figure 2.9 Test set-up

During the tests the following parameters are measured:
- excess pore pressures at the tip of the sheet pile and 5 locations in the soil
- the horizontal and vertical soil stress at two locations
- the acceleration of the sheet pile and of the tank
- the surface of the sand before and after the test
- displacement of coloured markers in the sand
- movement of the soil using a high speed video camera.

Of course there are some drawbacks in translating the results of these tests to the prototype situation. Most obvious are the limited size of the tank and thus the possible influence of the walls of the tank on dissipation of excess pore pressure

and reflection of vibrations. Therefore, the results are to be considered qualitatively.

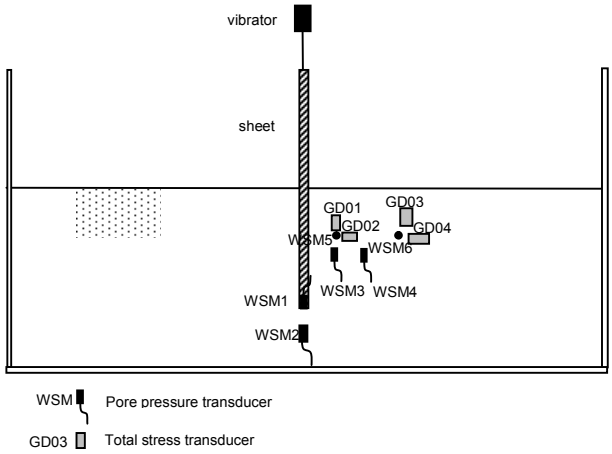

Figure 2.10 Location of transducers

The average densification of the sand is assessed from the change in top level of the sand. Figure 2.11 shows the results of the assessment.

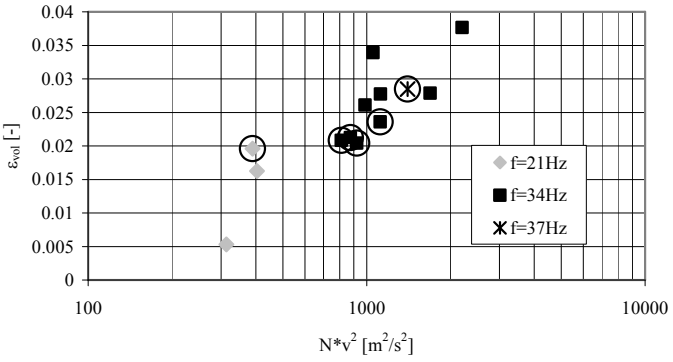

Figure 2.11 Average densification in performed tests

On the horizontal axis a parameter $N*v^2$ is used. In this figure N is the number of vibrations and v the amplitude of the velocity of the sheet pile. The reason for selecting this parameter is that, according to the C/L model the volume strain is a function of the product of the applied number of cycles and the square of the shear strain amplitude. The C/L model (Compaction/Liquefaction model) is further described in section 4.7.3. In figure 2.11 both the results of the tests with and without pulling are plotted. To distinguish them the tests without pulling are encircled.
The average trend is that the densification increases with the number of cycles and with the velocity amplitude of the sheet pile. There is some scatter around the average trend. The tests with and without pulling show almost the same amount of

densification. With an average volumetric strain of 2 to 3 % in these tests with medium dense sand it is obvious that densification during sheet pile removal with vibratory pull cannot be denied.
Figure 2.12 shows the change in surface level for one test (test DWD26C3). In this test the thickness of the sheet is 26 mm, the frequency of vibration is 34 Hz and the pulling speed 0.7 cm/s.

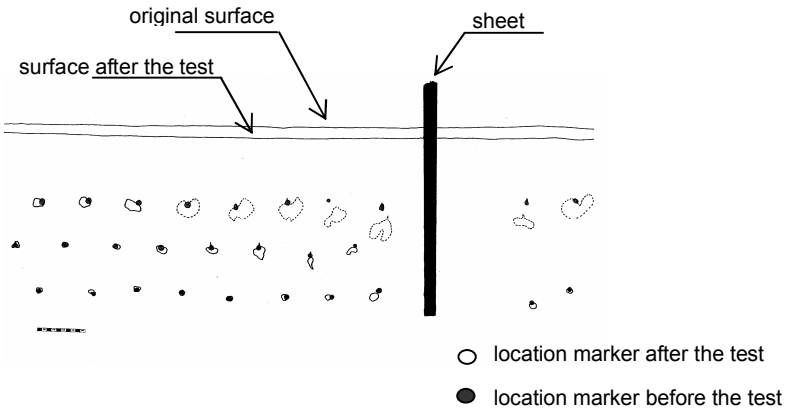

Figure 2.12 Settlements at test DW26C3

The displacements of the markers indicate that the settlement is largest close to the sheet pile and decreases with depth and with distance. The sand surface is quite flat and does not correspond with the displacement profile of the markers. This effect is attributed to flow of liquefied sand near the surface towards the sheet, thus filling the trough created by the densification.

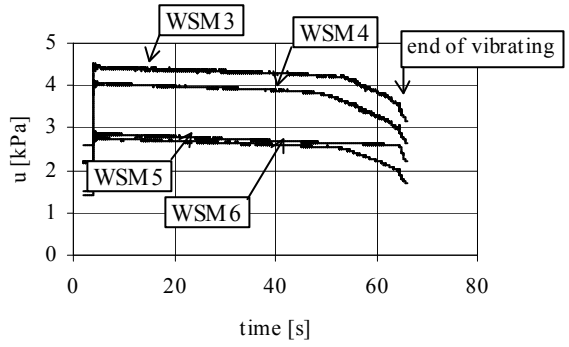

Figure 2.13 Average pore pressures during test DW26C3

The development of the pore pressure during the test is shown in figure 2.13. The moving average of the excess pore pressures is presented. Interesting is to examine the development of the excess pore pressure during the test. At start of vibrating a fast increase in the excess pore pressure is observed. The average pore pressure reaches a value that is identical to the total vertical stress. This

indicates that the sand liquefied during the test. After this the excess pore pressure decreases. At first, this is a slow decrease, corresponding to the settlement of the surface. Towards the end of the test the decrease is faster. It is known that as the soil becomes denser the tendency to densify decreases. Apparently, toward the end of the test this tendency has decreased so far that dissipation of excess pore pressure is in excess of generation of excess pore pressure. This results in a net decrease in the excess pore pressure.

For the tests with static pulling, a settlement trough is observed. The width of this trough is about 30 to 60 cm. This corresponds more or less to an active failure plane, starting at the tip of the sheet.
From an interpretation of the observed settlement in the tests with vibrating and puling, with vibrating only and with pulling only Hergarden (2000) concluded that the total settlement can be considered as a summation of the settlement due to densification and the settlement due to the removed volume of the sheet pile.

2.5 Empirical data

In order to get some quantitative insight in the occurrence of settlement during vibratory sheet piling an analysis of experience data is analysed. For this a data base that is expected to be unbiased is searched for. Using data from the files of a research institute or university bears the risk that projects with relative large settlements are overrepresented. This is because cases where large settlements are expected or cases where large settlements did occur are typically the cases where an expert opinion is searched for.

An unbiased data base will be a data base where data from a large number of projects is collected, independent of the size of the project, the degree of complexity of the project and the occurrence of damage during the construction. Such a data base is the GeoBrain experience data base (Hemmen 2005).

GeoBrain is an experience database, maintained at GeoDelft. In this data base experience data for different geotechnical activities are collected in a systematic way. The purpose of GeoBrain is to bridge the gap between designers and practitioners. One of the activities for which data are collected is vibratory sheet piling. Among the many data collected are the surface settlements close to the sheet pile, at 1 m from the sheet pile and at 3 m from the sheet pile. The number of projects in the database is still increasing.

An analysis of the available projects as per August 2005 is made. At that time 208 case histories from 64 projects are available. At a single project more than one case history may be obtained, e.g. when using different sheet pile profiles or different vibrators. Not always the surface settlements are reported. Only for 28 projects settlements near the sheet pile wall are reported. In a few cases the reported settlements are measured values (5 projects) but in the majority of cases the reported settlements are based on visual observations.

For the analysis one case history of each project is used. The reason for this is that otherwise projects with a large variation in used sheet piles and/or vibrators may dominate the result. For projects with more than one case history the situation with the largest settlement is selected. The reason for this is that the largest settlement is decisive for judging the project performance. In a few cases the surface settlement at only one point is reported. In most cases three values per project are available. After this selection 77 data points are available for further processing. Figure 2.14 shows the distribution of the measured settlement at 1 m distance from the sheet pile over the number of projects.

All cases where the settlement has been measured report a non-zero settlement. In many cases where the settlement is estimated from visual observation a zero settlement is reported. Most likely some settlement did occur in these cases but has not been observed by the naked eye. Therefore this is not to be interpreted as 'no settlement' but as 'no noticeable settlement'.

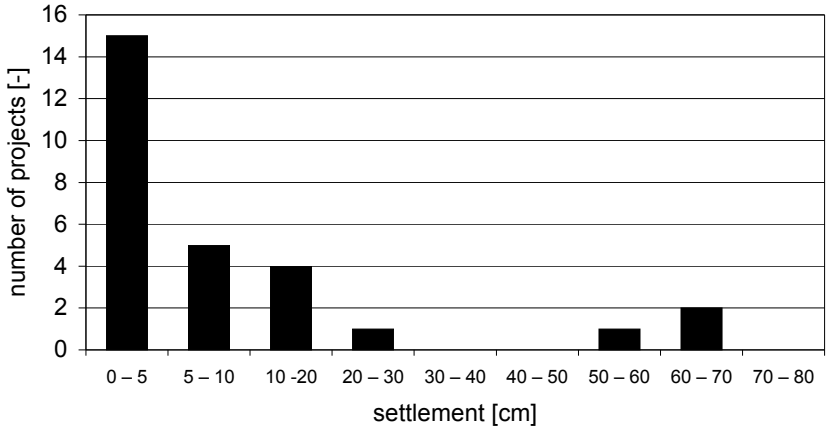

Figure 2.14 Histogram with reported settlement close to the sheet pile

It may be expected that the width of the settlement trough and the total amount of densification are a function of the driving depth of the sheet pile. The width of the settlement trough is assumed proportional to the driving depth of the sheet pile. Therefore the reported distance to the sheet pile is normalised with the driving depth of the sheet pile. The volume of the settlement trough is assumed to be proportional to the driving depth of the sheet pile as well. As the width is already taken proportional to this parameter the absolute settlement becomes independent of the driving depth. This is a simplification as a longer sheet pile will result in a longer duration of vibrating and thus some more densification. For the analysis of the GeoBrain data this aspect is neglected.

Observations of intensively measured projects show that the surface settlement plots almost as a linear line on a graph with a linear scale for the distance to the sheet pile and a logarithmic scale for the surface settlement. This method of presentation is thus selected for presenting the data of GeoBrain. Figure 2.15

shows these data points. For the reported zero settlements a low value (0.1 cm) is used. This holds for 33 out of the 77 data points.

A complication with the further processing of the data is the large number of reported zero settlements. As pointed out before most likely this is not really a zero settlement. It is expected that settlements in excess of 5 to 10 cm will be visually detected. Options for further processing are:

- neglect the data points with zero settlement
- assume a low value of the settlement for the reported points with zero settlement.

The first option results in neglecting a large amount of cases with small settlements. After removing these data the remaining data most likely represent cases with settlement in excess of the average. On the other hand assuming an almost zero settlement for the points with reported zero settlement results in a low value for the average settlement. Therefore an arbitrary value of 3.5 cm is used for cases with reported zero settlement.

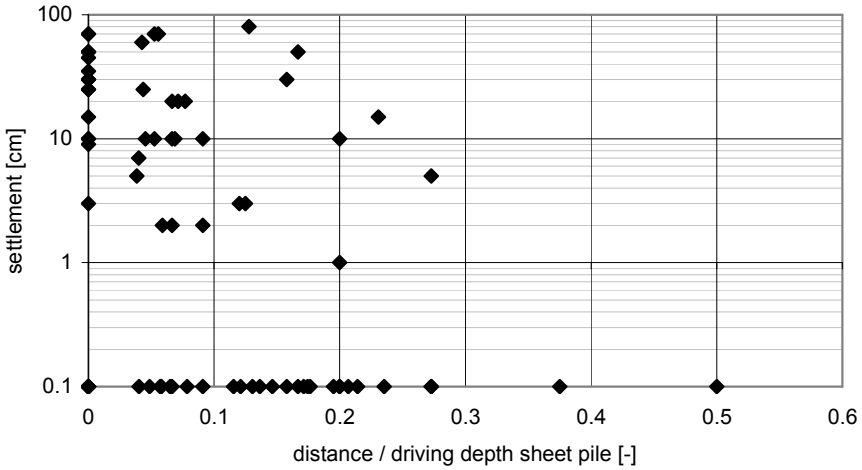

Figure 2.15 Reported settlement as function of distance

The surface settlement will be described with the following formula:

$$\ln(z / z_0) = a + b * (r / L) \qquad (2.3)$$

with:

- z : surface settlement
- z_0 : reference settlement (z_0 = 1m)
- L : driving depth sheet pile
- R : distance to the sheet pile
- a, b : constants.

This gives two unknown parameters: a and b. The first describes the zero intercept and the second the slope of the line. In order to limit the number of unknowns a

fixed value for b will be selected. For this b=-4 is selected. Using a statistical approach the relevant value of a can be selected. For the stochastic parameter a is used. It is assumed without proof that for this parameter a normal probability curve applies. The results are shown in figure 2.16.

It should be realised that all available cases are used. No distinction between different soil types is made. The cases with the largest settlements (settlement in excess of 0.5 m) in the data base are for situations with loose sand.

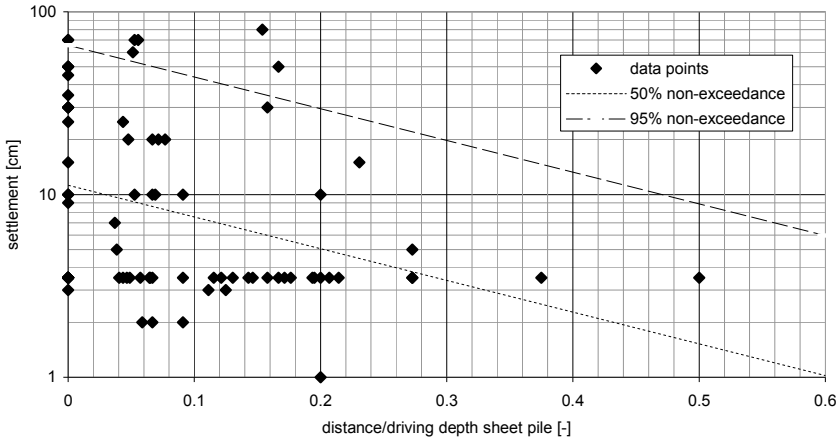

Figure 2.16 Lines of probability of non-exceedance

Unfortunately the number of reported settlements at removal of sheet piles is rather limited (just one project). Therefore it is not possible to perform the same analyses for removal of sheet piles.

2.6 Discussion and conclusion

The available empirical data indicate that settlement during vibratory sheet piling can become quite large.
A description of the processes during vibratory sheet piling gives that the process can be divided in several sub processes. The identified sub processes are:

- vibrating sheet pile
- behaviour (slippage) at the interface sheet pile – soil
- propagation of waves into the subsoil
- densification and possible generation of excess pore pressures
- dissipation of excess pore pressures
- settlement of the surface due to the densification
- displaced soil volume due to the inserted or removed volume of the sheet pile.

From the phase of installation two causes for settlements are identified. These are

- densification of the soil on cyclic loading

- displacements due to insertion in or removal from the soil of the volume of the used sheet piles.

For the phase of removal more processes may be present. Following the conclusions of Hergarden (2000) the two causes mentioned for the phase of installation are considered to be the dominating mechanisms.

3. Available methods for assessing densification during vibratory sheet piling

3.1 General

In the last decade different researchers already tried to develop a method for assessing the surface settlement due to vibratory sheet piling. To date the following researchers presented a method:

- Massarsch (1992, 2000 and 2004)
- Drabkin, Kim et al.
- Bement
- Hergarden
- Lukas and Gill
- Grabe and Mahutka

In this chapter first the different methods are briefly described. A comparison and discussion of the different methods is given in the last section of this chapter.

3.2 Method of Massarsch 1992

In course of time Massarsch has presented three methods for assessing the surface settlement on vibratory sheet piling. The methods are quite different in approach and will be described in separate sections.

The first method is described in (Massarsch 1992). It is straightforward. First the amplitude of the acceleration is to be assessed. When this amplitude is known the corresponding volume strain can be derived from the presented graph (figure 3.1). This graph relates the settlement (as percentage of the layer thickness) with ground acceleration and cone resistance. It is an empirical graph, said to be based on observations during vibratory compaction.

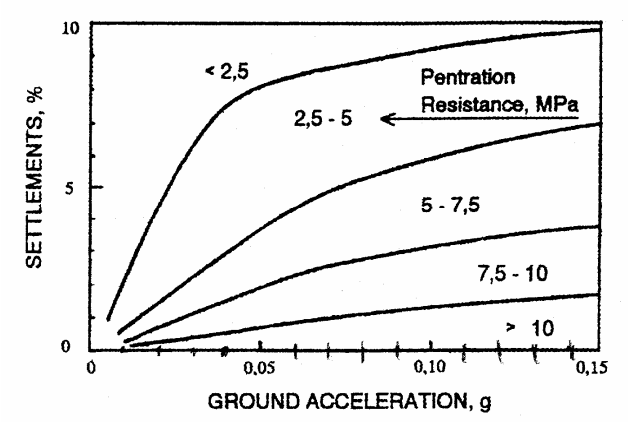

Figure 3.1 Graph for estimating the densification as function of cone resistance and acceleration amplitude (from (Massarsch 1992))

3.3 Method of Massarsch 2000

In (Massarsch 2000) a second method to assess the volume strain due to vibrating is given. Basically the method consists of two steps. The first step is to estimate the shear strain amplitude. The second step is to estimate the volume strain from this shear strain amplitude.

The shear strain amplitude is derived from the vibration velocity amplitude

$$\Delta\gamma = \Delta v / C_s \tag{3.1}$$

with:

- $\Delta\gamma$: shear strain amplitude
- Δv : amplitude vibration velocity
- C_s : shear wave velocity.

For the variation of the vibration amplitude with depth the situation of Rayleigh waves is assumed. It is mentioned that this type of waves will carry most of the energy at some distance from the vibration source. No remarks are made regarding the situation close to the vibration source. Assuming Rayleigh waves the shear strain amplitude will have its maximum value ground level and will diminish with depth. At a depth of approximately one wave length the strain amplitude becomes negligible. It also implies that the shear strain amplitude and the depth over which vibrations are present are independent of the length of the sheet pile. Finally the following expression for determining the settlement is derived:

$$\Delta z = f_1 . m_z . v . \Delta H / (R_C . C_s) \tag{3.2}$$

with:

- Δz : settlement in the considered layer
- f_1 : empirical parameter relating the plastic vertical strain to the shear strain amplitude
- m_z : parameter relating the vibration amplitude at depth z to the vibration amplitude at ground level
- v : : vibration amplitude (velocity amplitude) at ground level
- ΔH : thickness considered layer
- C_S : shear wave velocity
- R_C : ratio between Rayleigh wave velocity and shear wave velocity (taken as 0.93)

The parameter f_1 is the ratio between the vertical strain ε_z and the shear strain amplitude $\Delta\gamma$. It is a function of the shear strain amplitude and the number of equivalent cycles. The value of f_1 is derived from the test results published by (Seed and Silver 1972) and (Youd 1972) and is presented in a graph. This graph is reproduced here as figure 3.2. The parameter m_z*v is in fact the velocity amplitude at depth z. The value of m_z can be obtained from theoretical values derived for a Rayleigh wave. The relation has been simplified as

$$m_z = 0.9 - 0.6 * z / L \tag{3.3}$$

with:

- z : depth below ground level
- L : wave length.

The wave length L follows from $L = C_R/f$ with C_R the Rayleigh wave velocity and f the frequency.

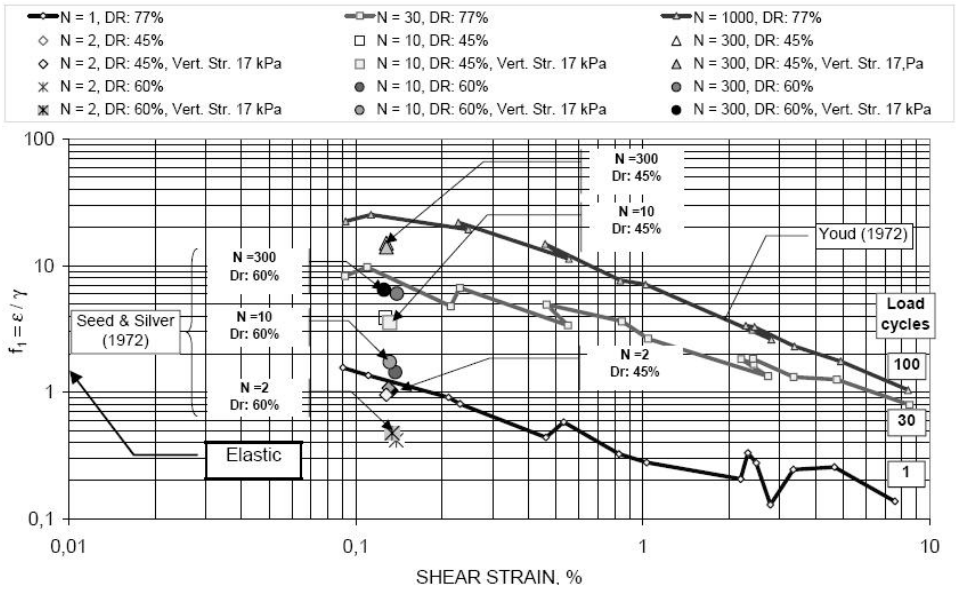

Figure 3.2 Shear strain factor f_1 as function of shear strain amplitude, number of load cycles and relative density of the sand (from (Massarsch 2000))

The calculation procedure is not very clear. In particular it is not mentioned how to determine the value of f_1 for situations different from those used in figure 3.2.

Massarsch notes that the method is intended for the area where the Rayleigh wave is dominant, so at a distance from the sheet pile of more than 1.5 or 2 times the wave length. The method is illustrated with an example, but no validation of the model is presented.

3.4 Method of Massarsch 2004

In (Massarsch 2004) a third method to assess the settlement in homogeneous sand due to pile driving is given. From the publication it is not clear if the presented method is intended for impact driving or for vibratory driving. Given the context of the paper most likely it is intended for impact pile driving. The given procedure is a simple engineering approach, aimed at obtaining a first estimate for the settlements at an early stage of a project. It can be used to estimate settlements in a homogeneous sand deposit adjacent to a single pile. The approach is said to be based on extensive experience from soil compaction projects.

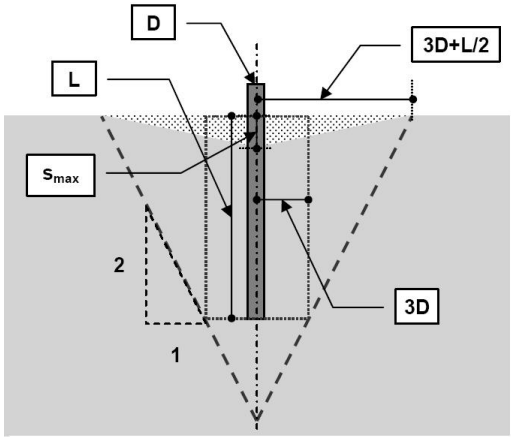

Figure 3.3 Dimensions settlement trough, according to (Massarsch 2004)

In the method it is assumed that intense densification occurs within a zone corresponding to three times the pile diameter. At the surface the densification is manifest as a settlement trough. Half width of the trough is:

$$B = 3D + L/2 \tag{3.4}$$

with:

- D : pile diameter
- L : driving depth of the pile.

The maximum settlement s_{max} and the average settlement s_{avg} follow from the following equations:

$$s_{\max} = \alpha(L + 6D) \tag{3.5}$$

$$s_{avg} = \frac{\alpha(L + 6D)}{3} = s_{\max}/3 \tag{3.6}$$

with:

- α : compression factor, an empirical constant.

In table 3.1 values for the empirical constant α are given.

sand density	driving energy		
	low	average	high
very loose	0.02	0.03	0.04
loose	0.01	0.02	0.03
medium	0.005	0.01	0.02
dense	0.00	0.005	0.01
very dense	0.00	0.00	0.005

Table 3.1 Compression factor α as function of ground condition and driving energy

3.5 Method of Drabkin, Kim et al.

Drabkin and Kim developed an empirical formula for the settlement as function of different parameters (Kim et al 1994) (Kim and Drabkin 1995), (Drabkin et al 1996). The formula is based on the results of a series of 27 cyclic tests on dry and moist sand. In the tests a triaxial cell is attached to a vibratory frame and vertically vibrated. The tests are performed at a frequency of 60 Hz. Variables in the test are the static confining stress, the static deviatoric stress, the sand mixture, the relative density, the vibration amplitude and the duration of vibration. Measured is the vertical deformation of the sample. It is not mentioned if the volume strain of the sample is measured as well.

Table 3.2 shows the parameters that are varied and the used range. This table also shows the 'coding' for the different parameters. This 'coding' is used to describe the effect of each factor in the final equation for the settlement.

factor	tested range	coding of factor	unit
velocity amplitude	2.5 – 18 mm/s	x_1 = -1+(v-0.1)/0.3	[inch/s]
deviatoric stress	14 –104 kPa	x_2 = -1+(q-2)/6.5	[psi]
confining pressure	69 – 207 kPa	x_3 = -1+(p-10)/10	[psi]
sand mixture	coarse (d_{50} = 1.7 mm), medium(d_{50} = 0.7 mm), fine(d_{50} = 0.5 mm)	x_4 is resp. –1, 0, 1	
number of vibrations	N = 60 – 500,000	x_5 = -1+(N-60)/269970	[-]
moisture content	dry, saturated	x_6 is resp. –1 and 2	
initial relative density	loose, medium dense	x_7 is resp. –1 and 2	

Table 3.2 Parameters in method Drabkin, Kim, et al.

From the results of the cyclic tests an empirical formula is derived. This is based on a fit through the results of the performed cyclic tests assuming a second order regression polynomial. No physical models are used in deriving the formula.

The settlement follows from:

$$\ln Y = 2.27 + 1.19x_1 - 0.71x_1^2 + 0.49x_2 - 0.68x_2^2 - 0.80x_3 + 1.09x_3^2 - 0.46x_4 + 0.06x_4^2 + 0.45x_5 - 0.38x_5^2 - 0.19x_6 - 0.1x_7 \quad (3.7)$$

In this Y is the settlement (used unit is 0.001 inch) of a sample with height 150 mm. It should be realised that the used values for the different parameters are not to be given in SI-units but in the units shown in the last column of table 3.2.

The method has been validated by the authors with field data. The considered cases contain situations with impact and vibratory driving of foundation piles and sheet piles. They concluded that a reasonable agreement between observed and calculated settlements exists.

3.6 Method of Bement

Bement (Bement and Shelby 1997) developed an expression to determine the densification of sand during cyclic loading. The expression is based on results of a large series of tests in which a soil sample in a Rowe cell is vertically vibrated. Some tests are run with horizontal vibrations. Different parameters are varied: type of sand, relative density, vertical (static) stress, frequency of loading (25 Hz, 40 Hz and 120 Hz) and degree of saturation. The vertical acceleration in the tests is increased stepwise. In general each 10 to 20 minutes the acceleration level is increased.

From the test results the following expression for the volume reduction is obtained:

$$S = \frac{2.8\ln(D_c)\eta^2}{I_D\sigma'_{v0}} \tag{3.8}$$

$$D_c = \frac{D_{90}}{D_{60}D_{30}} \tag{3.9}$$

with:

- S : settlement (unit: %)
- η : acceleration amplitude (unit: g)
- D_c : parameter describing the grain size distribution (unit mm^{-1})
- I_D : relative density (unit: unity)
- D_{90} : particle size with 90% passing
- σ'_{v0} : vertical stress (unit kPa).

For acceleration levels exceeding 2g it is stated by the authors that fluidisation will occur and a different equation is given. This equation reads:

$$S = \frac{4(\ln(D_c)+0.7)*\ln(\eta)}{0.01*\sigma'_{v0}+0.75*(1-I_D)} \tag{3.10}$$

The author states that the vertical settlement follows from summation of the vertical strain in a vertical at the considered point.

3.7 Method of Hergarden

R. Hergarden (Hergarden 2000), (Hergarden and Tol 2001) developed a method for assessing the settlement due to vibratory sheet piling. The densification is a function of the acceleration amplitude. A summary of this method is given in (Meijers, Tol 2004) as well.
For the source model empirical data from the Dutch manual on sheet piling C 166 (CUR 1993) are used. The horizontal and vertical velocity at 5 m from the sheet pile are given for 6 different soil profiles, that are typical for Dutch subsoil conditions. The given values are valid for a vibrator with a centrifugal force of 350 kN. For vibrators with a higher centrifugal force the velocity amplitude is to be corrected according to:

$$v_{0,cor} = v_{ref} + 0.002*(F_{dyn} - 350) \tag{3.11}$$

with:

- F_{dyn} : centrifugal force (in kN)
- v_{ref} : velocity amplitude (in mm/s) at reference distance r_0, for a centrifugal force of 350 kN
- $v_{ref,cor}$: corrected velocity amplitude at reference distance r_0 (in mm/s), corrected for capacity of the vibrator.

The attenuation of the waves is described using a Barkan type relation:

$$a(r) = a_0 \sqrt{\frac{r_0}{r}} * \exp(-\alpha(r - r_0)) \tag{3.12}$$

with:
- a(r) : amplitude of the acceleration at distance r
- a_0 : amplitude of the acceleration at distance r_0
- α : parameter describing soil damping.

In fact this is a relation for the attenuation of vibrations in the far field.

The densification model is based on a publication by Barkan (1962). Following Barkan he assumes that there is a threshold acceleration below which no densification occurs. This threshold acceleration is a function of the relative density and stress level. The threshold acceleration follows from:

$$\eta_0 = \frac{\ln(1 - I_{D,0})}{-\alpha_B} \tag{3.13}$$

with:
- η_0 : threshold acceleration, η_0 = a/g
- $I_{D,0}$: initial relative density
- α_B : empirical parameter, depending on soil strength and stress level.

The value varies from α_B = 3 (for high stress level and high strength) to α_B = 5 (for low stress level and low strength). Available data are not sufficient to assess this parameter with reasonable accuracy.

The change in relative density as function of acceleration and time is described with the following equation:

$$\Delta I_D(\eta, t) = \left[\exp(-\alpha_B \eta_0) - \exp(-\alpha_B \eta)\right] * \left[1 - \exp(-\beta t)\right] \tag{3.14}$$

According to Hergarden the time factor β is about 1 -/minute. This value is derived from published test results. In the prescribed approach the frequency and/or the number of cycles are no model parameters.
Hergarden states that during vibratory sheet piling the number of cycles is sufficiently large for assuming that, from a practical point of view, the final density is achieved. The last term in the equation for the change in relative density becomes 1.
Knowing the change in relative density the volume strain can be determined.

$$\varepsilon_{vol} = \Delta I_D \frac{e_{max} - e_{min}}{1 + e_0} \tag{3.15}$$

with:
- e_{max} : maximum void ratio

- e_{min} : minimum void ratio
- e_0 : initial void ratio.

The amount of densification can be calculated using the mentioned formulas. It is also possible to use the nomogram of figure 3.4. Starting point is the cone resistance and the vertical effective stress. From this follows in the left hand graph the relative density I_D. For this the correlation of Lunne and Christoffersen (1983) is used. Going to the right hand graph the threshold acceleration can be found when the value of α_B is selected. If the acceleration at the considered point is above the threshold value the relative density after vibrating can be found going from the right hand graph to the left hand graph.

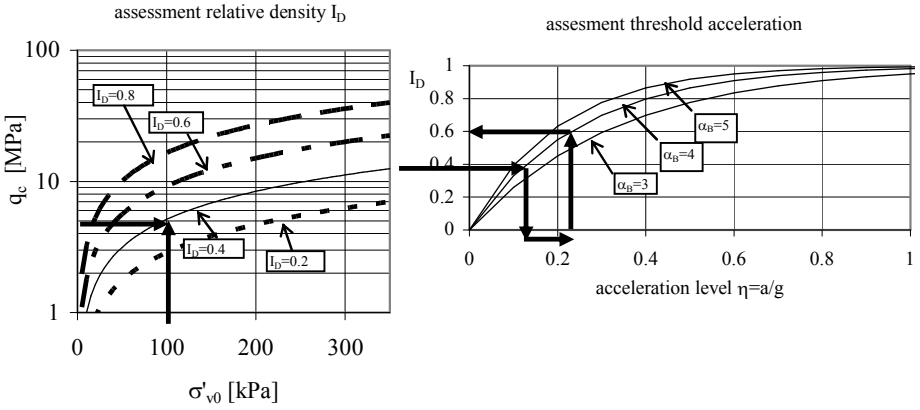

Figure 3.4 Nomogram for assessing the volume strain

The procedure will be illustrated with an example. In the example the cone resistance is 5 MPa, the effective vertical stress is 100 kPa and the acceleration amplitude is 2.3 m/s^2 (η = 0.23). From the left hand graph the relative density is assessed to be I_D = 0.4. This value is used as input in the right hand graph. It is assumed that for this situation α_B =4. Going horizontally from I_d = 0.4 to the line of α_B =4 and than going vertical downward the threshold acceleration is found to be η_0 = 0.13. The actual acceleration amplitude is η = 0.23, so above this value. Densification due to vibrating is expected. The final relative density due to vibrating can be read from the right hand graph. Going from η = 0.23 to the line of α_B =4 and than going to the left the final relative density is found to be I_D = 0.6. This gives a change in relative density of ΔI_D = 0.2. From this the volume strain can be calculated.
This procedure can be performed for each point in the densification zone. The result is the local volume strain in the subsoil due to vibrating. The settlement at surface follows from integration of the effect of all local volume strains.
It is assumed that the effect of local volume change spreads to the surface at an angle θ. For θ a value of 30° is proposed. With this the width of the settlement trough due to densification of element ij becomes:

$$B_{ij} = 2z \tan\theta \qquad (3.16)$$

with:

- B_{ij} : influence width at surface
- z : depth of considered point below ground surface
- θ : angle of volume change spreading.

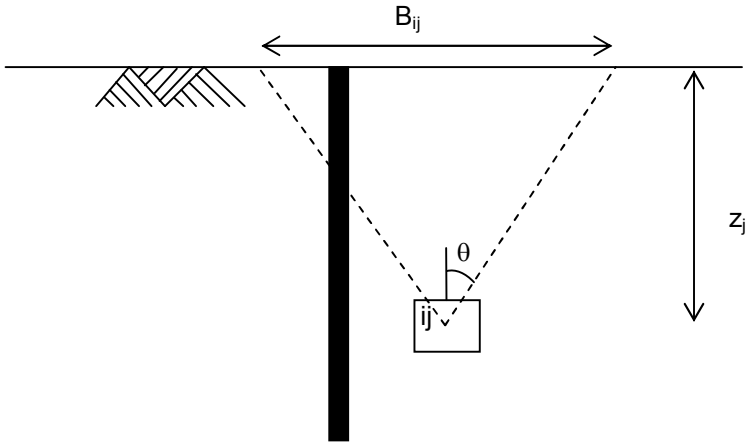

Figure 3.5 Translation of local densification to surface settlement

The contribution to the settlement follows from the volume change of element I divided by the width B_{ij}:

$$\Delta z_{ij} = \frac{\varepsilon_{vol} A_{ij}}{B_{ij}} \tag{3.17}$$

with:

- Δz_{ij} : contribution to surface settlement due to densification of point i
- ε_{vol} : volume strain at point ij
- A_{ij} : representative area (volume per meter) of point ij.

Besides the volume strain due to densification the effect of the installed or removed volume of the sheet pile is to be accounted for. This influence is handled separately. The volume change is lumped at the centre line of the wall. Spreading towards the surface is determined using the same approach as for the local densification. The total settlement is derived by summation of these two effects (densification and volume of sheet pile). The assumptions that the two contributions may be summed is validated by the tests described in section 2.4 of this thesis.

3.8 Method of Lukas and Gill

Lukas and Gill (1992) describe a method to estimate the settlement from pile driving. They make use of methods used for assessing the settlement during earthquake loading. The method involves the following 8 steps:

1. divide the subsoil in different thin layers with equal relative density
2. compute overburden stress for each layer
3. determine the shear modulus for each layer

4. find shear stress amplitude from $\tau = \gamma^*z^*a_{max}^*r_d$
   with:
   - γ^*z : overburden pressure
   - a_{max} : peak acceleration as fraction of the acceleration of gravity
   - r_d : depth factor, varying from 1.0 at ground level to 0.9 at a depth of 9.6 m

   The authors do not give a method for estimating the peak acceleration
5. determine the average shear stress amplitude as $\Delta\tau_{avg} = 0.65^*\Delta\tau_{max}$
6. calculate the shear strain amplitude as $\Delta\gamma = \Delta\tau_{avg}/G$
7. use published data where a relation is given between the shear strain amplitude, the number of loading cycles and the volumetric strain (e.g. from (Silver, Seed, 1971b)) to assess the volumetric strain; if necessary extrapolate the available data for the actual number of loading cycles
8. the settlement follows from an integration of the volumetric strain with depth.

The authors used their method for assessing the settlement at a site with (impact) pile driving and compared the result with observed settlement. A close agreement between the two values is observed.

3.9 FEM calculations

Grabe and Mahutka (Grabe, Mahutka 2005), (Mahutka, Grabe 2006) describe finite element calculations for the vibratory installation of piles. The used soil model is the hypoplasticity model. Presented are among other things speed of installation, development of the radial stress at the pile, the vertical stress and the surface settlement. Results give a clear view of possible mechanisms. In (Mahutka, Grabe 2006) measured and calculated surface settlements when installing a tubular pile (diameter 0.4m) in dense sand are compared. No clear conclusions can be drawn from this comparison.
To date these are the only examples known to the author of efforts using a finite element method for predicting the surface settlements due to vibratory piling.

3.10 Discussion and comparison of the different models

The method of (Massarsch 1992) uses the acceleration amplitude as loading parameter. The soil is described by the cone resistance. Probably this parameter is considered to be representative for the in-situ density of the sand. However the in-situ stress or the depth is not an input parameter. As the cone resistance is a function not only of the relative density but also of the stress level the latter value is needed for a proper interpretation of the cone resistance. Sand at shallow depth with a certain cone resistance may be dense sand while sand at larger depths with the same cone resistance may be loose sand.
The duration of the vibrating (or the number of cycles) is not taken into account in this method. Presumably the method is for a situation with a large number of loading cycles. For situations with vibratory sheet piling this may be an acceptable simplification

The method described in (Massarsch 2000) uses the shear strain amplitude as loading parameter. Test data are used to link the shear strain amplitude to a volume strain. The presented range of loading cycles is limited to 300, which is small compared to the expected number of loading cycles during vibratory sheet piling. The described method assumes the presence of Rayleigh waves. As Rayleigh waves develop only at some distance from the sheet pile the used assumption is valid for the far-field situation but not for the situation close to the sheet pile. Here Raleigh waves are not present and the waves will be mainly body waves (shear waves). It is close to the sheet pile that most of the densification will occur. Therefore, for the vibrations the near-field situation and not the far-field situation is to be considered. An improvement of the method would be to change the type of waves from Rayleigh waves to shear waves.

The method described in (Massarsch 2004) is a simplified method. It's aim is to give a first, engineering, indication of the settlements at an early stage of a project. For this purpose it may be an acceptable method.

The methods by Drabkin, Kim et al. and by Bement are based on result of vertically vibrated soil specimen. This implies that essentially the loading is compression loading. Next to a sheet pile the loading is expected to be mainly shear loading. The type of loading in the tests therefore does not correspond with the expected loading during driving of sheet piles.
The expression by Drabkin, Kim et al. gives qualitatively a reasonable result for situations within the range used in their tests. For situations outside this range their equation may give erroneous results.

Hergarden uses the acceleration amplitude as loading parameter. He is the only author mentioning a method for estimating the vibration amplitude. For the attenuation of the vibration amplitude the well known Barkan relation is used. In fact this relation describes the attenuation of waves at distances in excess of 5 m, so for the far field. Extrapolating this relation to locations close to the sheet pile will underestimate the actual vibration amplitude.
The vibration amplitude following from the presented approach is the velocity amplitude. This value is independent of the frequency of the used vibrator. The acceleration amplitude is calculated from the velocity amplitude.

$$a = v * 2\pi f \tag{3.18}$$

A consequence of this approach is that using high frequency vibrators will yield large acceleration amplitudes and thus more densification as normal frequency vibrators. The method is thus sensitive to the type of vibrator used.

The expressions used by Lukas and Gill (1992) are typically for earthquake loading. The situation during vibratory sheet piling is quite different. Therefore this method is not considered to give a good representation of the actual mechanisms.

In table 3.3 the main characteristics of the different models are summarised. Most of the methods assess the local volume strain or vertical strain. For assessing the surface settlements mostly a vertical integration of the assessed strains is used. This implies that spreading is neglected. Also the effect of the sheet pile volume on

the settlement is neglected. In fact Hergarden is the only author that takes this aspect into account.

model	driving force for densification	number of cycles incorporated	excess pore pressure generation	density of sand considered	type of piling	remarks
Massarsch 1992	acceleration	no	no	yes	vibratory pile driving	
Massarsch 2000	shear strain amplitude	yes	no	partly (only I_D = 45% and 60%)	not mentioned	
Massarsch 2004	none	no	no	yes	not mentioned	
Drabkin, Kim et al.	velocity amplitude	yes	no	yes	not mentioned	
Hergarden	acceleration	no (considered negligible)	no	yes	vibratory sheet piling	
Lukas and Gill	shear amplitude	yes	no	yes	not mentioned	
Bement	acceleration	no	no	yes	vibratory sheet piling	grain size distribution is accounted for
Grabe, Mahutka		yes	no	no	vibratory piling	EEM model

Table 3.3 Comparison models for assessing settlement due to sheet piling

Most models use the acceleration as the loading parameter for densification. Some use the velocity amplitude or the shear strain amplitude. There will be a relation between these parameters. If it is assumed that vibrations are mainly shear waves, the following relation between the different amplitudes exists

$$\Delta\tau = G\Delta\gamma = G\frac{\Delta v}{C_s} = G\frac{\Delta a}{2\pi f C_s} \tag{3.19}$$

with:

- $\Delta\tau$: shear stress amplitude
- $\Delta\gamma$: shear strain amplitude
- Δv : velocity amplitude
- Δa : acceleration amplitude
- G : shear modulus
- C_s : shear wave velocity $C_s = \sqrt{(\rho/G)}$
- f : frequency.

The shear stress amplitude, the shear strain amplitude and the velocity amplitude are proportional to each other. The acceleration amplitude is different as the frequency of loading comes into play. This implies that quite different results are obtained with the different methods when the effect of the vibration frequency is considered. When it is assumed that the velocity amplitude is independent of the vibration frequency, models that use the acceleration amplitude will predict that the settlement increases with increasing frequency. When it is assumed that the acceleration amplitude is independent of the vibration amplitude the velocity amplitude decreases with increasing vibration frequency. Models using the velocity

amplitude or shear strain amplitude as driving force for densification will predict a decrease in settlement with increasing frequency.
Whether the acceleration amplitude is the correct parameter to describe the cyclic loading of sand is still a matter of discussion.

None of the models predict the amount of excess pore pressure during vibratory sheet piling. In cases where excess pore pressure may be of importance (e.g. when driving sheet piles close to or in slopes) these models cannot be used. This limits the use of these models to their primary purpose, to estimate the amount of surface settlement.

In order to compare the models quantitatively a hypothetical case is defined. The following situation is considered:
- homogeneous half space consisting of sand with uniform density
- relative density of the sand is 40%
- duration of vibrating is 6 minutes, irrespective of type of vibrator
- volumetric strain at 7 m depth is determined
- a normal frequency (NF, f = 23 Hz) vibrator and a high frequency (HF, f = 38 Hz) are used.

The required eccentric force of the vibrator is assessed using a program for modelling the sheet pile installation. This resulted for the loose sand (I_D = 0.4) in a required eccentric forces of F = 600 kN.

The vibration amplitude is assessed using the model described in section 3.7 (model Hergarden).
The method by Bement requires information on the grain size distribution. For this comparison the following parameters are used:
- D_{30} = 0.18 mm
- D_{60} = 0.25 mm
- D_{90} = 0.45 mm.

From this follows D_c = 10 -/mm.

In table 3.4 the volume strain predicted by the different methods is presented. The results are also shown in figure 3.6.

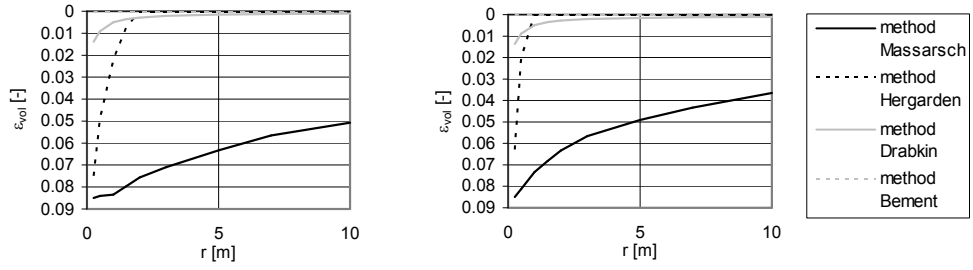

Figure 3.6 Comparison predicted volume strain using different methods

distance to sheet pile		volumetric strain					
		0.5 m	1 m	2 m	3 m	5 m	10 m
method	vibrator						
Massarsch 1992	HF	0.085	0.084	0.077	0.071	0.064	0.050
	NF	0.084	0.073	0.065	0.058	0.049	0.037
Hergarden	HF	0.049	0.022	0	0	0	0
	NF	0.02	0	0	0	0	0
Drabkin	HF	0.0091	0.0051	0.0029	0.0021	0.0015	0.0011
	NF	0.0089	0.0049	0.0028	0.0021	0.0015	0.0010
Bement	HF	$147\ 10^{-6}$	$72\ 10^{-6}$	$35\ 10^{-6}$	$22\ 10^{-6}$	$12\ 10^{-6}$	$5\ 10^{-6}$
	NF	$54\ 10^{-6}$	$26\ 10^{-6}$	$13\ 10^{-6}$	$8\ 10^{-6}$	$4\ 10^{-6}$	$2\ 10^{-6}$

Table 3.4 Predicted volume strain at z=7m, using different methods and vibrators

All methods show that using a high frequency vibrator increases the settlement. This can be understood from the fact that a high frequency vibrator increases the number of cycles during the same time period. For most methods the effect is small. The method by Hergarden indicates that using a high frequency vibrator instead of a normal frequency vibrator will result in a large increase in predicted settlement. The reason for this is that his method uses the acceleration as input variable. The acceleration follows from the velocity as follows:

$$a(t) = \frac{dv}{dt} = \hat{v}\omega\cos(\omega t) \tag{3.20}$$

Increasing the frequency of the vibrator results in an increase of the acceleration amplitude (for the same velocity amplitude). This explains the large influence of the frequency in his method.

3.11 Conclusion

Different methods are available to aid a design engineer in assessing the surface settlement due to vibratory piling.
Some of the models are considered to describe the relevant mechanisms during vibratory sheet piling not correctly. The other models show unrealistic trends when varying some of the parameters (e.g. the frequency or the density of the sand)
The final conclusion is that the available models yield quite different results for the same loading situation. Different models also yield unrealistic results when varying certain parameters (e.g. the frequency of the used vibrator). Important parameters as the amount of excess pore pressure are not predicted with these models.

4. Behaviour of sand under cyclic loading

4.1 General

As densification of sand under cyclic loading is expected to be the main cause of settlement during vibratory sheet piling it is necessary to pay attention to this aspect

Typical aspects of the situation during vibratory sheet piling are the time of vibrating, the number of load cycles and the variation of the load amplitude.
The time for installation or removal of a sheet pile is typical in the order of 2 to 6 minutes. In favourable situations it may be one minute, in case of hard driving (obstacles in the subsoil, inadequate vibrator) it may exceed half an hour. For processes with this duration of time the situation in sand is neither undrained nor fully drained. During the process drainage of excess pore pressure will occur. Therefore it is relevant to understand the effect of drainage on the cyclic behaviour.
The frequency of the vibrator is usually 25 Hz to 50 Hz. With a common time of vibrating the number of load cycles per sheet pile becomes 3000 to 20,000. It is therefore relevant to understand the effect of large number of loading cycles on the cyclic behaviour.
In view of the importance of these aspects a literature survey is conducted to gain an understanding of these aspects.

First a qualitative description of the cyclic behaviour at grain size level (micro scale) is given. The purpose of this description is to get some understanding of the particular aspects of the behaviour of sand during cyclic loading. Going from a micro scale to a macro scale the behaviour of a sand volume is illustrated with published test results. After this attention is paid to some specific aspects which are of particular relevance for the situation during vibratory sheet piling. These are the effect of drainage during cyclic loading and the number of load cycles.

Last but not least some available models to quantify the amount of densification or generation of excess pore pressure are described. Attention is focussed on models capable of handling the average behaviour for large number of cycles.

4.2 Qualitative description behaviour of sand under cyclic loading

In geotechnical engineering the soil is usually treated as a continuum. Each soil layer is considered homogeneous and is described with bulk parameters like stiffness, angle of internal friction, cohesion and density. In reality however sandy soil consists of sand grains with different sizes and shapes that are in contact with each other. Together they form a matrix capable of taking the applied loads. The behaviour of the continuum is in fact a result of the behaviour at the numerous contact areas of the grains. In order to get a more basic understanding of the behaviour of sand during cyclic loading first a qualitative description of the behaviour of grains at micro scale during cyclic loading is given. The description is based on dry (or at least drained) conditions.

The soil matrix is influenced by the (geological or stress) history of the soil. Calculations with discrete element models show that the stress in the soil is not evenly distributed. At grain size scale, there are preferred paths where high contact stresses between the soil particles exists while other particles are not or hardly loaded.
On loading the sand skeleton deforms in order to accommodate the new stress situation. During cyclic loading this is a continuous process as the load changes continually. This deformation will result in some continuous changes in the soil matrix. Youd (1977) shows a picture indicating the displacements within a grain skeleton during cyclic shear loading (reproduced as figure 4.1).
Grains that are first tightly constrained by their neighbours may loose their confining stress and tumble in voids within the soil matrix. Other grains rotate a little while others may start to slide over each other. The result is that the soil matrix changes a little, attains a new fabric and possibly also a new density. Some crushing of grains may occur like breaking off small asperities.
Part of the deformations is plastic deformation. On reversal of the stress not all deformations are recovered. This process will continue. However more and more grains will obtain a stable situation and thus the tendency for deformation will reduce.

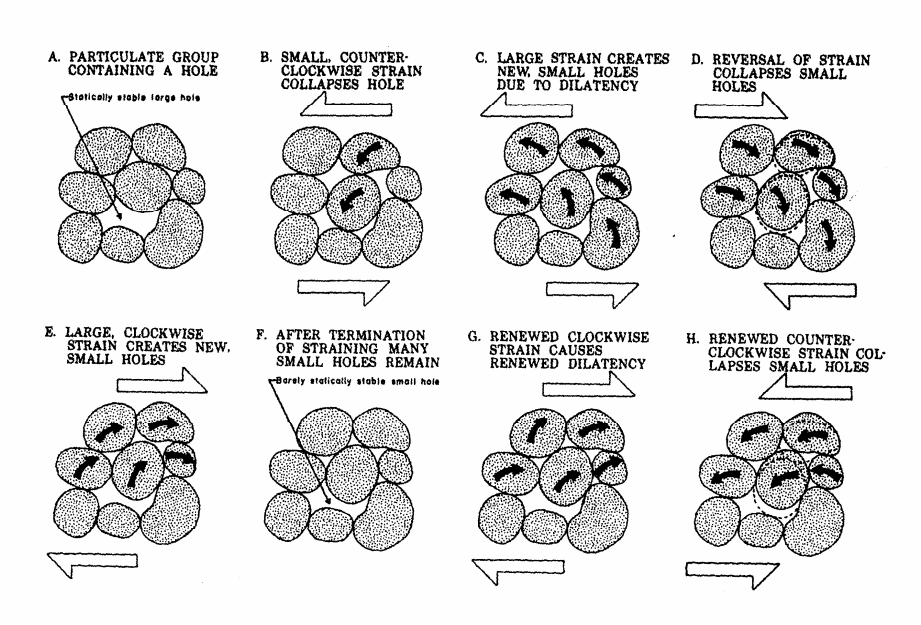

Figure 4.1 Sketch of a group of soil particles illustrating the change in packing during cyclic loading (from Youd 1977)

Describing the behaviour of the total soil volume at grain size level requires the use of discrete element models. For two elastic spheres in contact with each other the well known Hertz theory (see e.g. Deresiewicz 1953) describes the behaviour at the contact point.
First consider two perfect spheres with equal radius R that are pressed against each other with a force N.

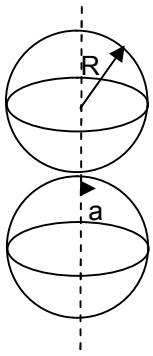

Figure 4.2 Two spheres in contact

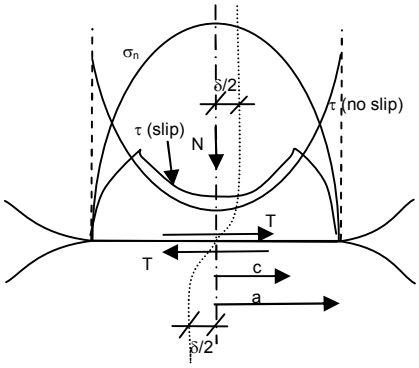

Figure 4.3 Contact stresses at sphere-sphere contact

The radius a of the contact area is given as:

$$a = \left[\frac{3(1-\nu^2)RN}{4E} \right]^{1/3} \tag{4.1}$$

The contact stress σ_c is a function of the distance ρ from the centre of the contact area and is given as:

$$\sigma_c = \frac{3N}{2\pi a^3} \left(a^2 - r^2 \right)^{0.5} \tag{4.2}$$

with:

- R : radius of the spheres
- N : normal force
- a : radius of contact area
- ν : Poisson's ratio
- σ_n : normal stress between spheres
- r : distance from centre of contact area
- E : Young's modulus.

When a shear force T is exerted, shear stresses develop in the contact area. At the fringe of the contact area failure occurs while at the centre the deformation is still elastic. Thus at the contact area an outer fringe with plastic shear develops and increases in width with increasing shear stress. The radius r_{el} of the zone without slippage follows from:

$$r_{el} = a\left(1 - \frac{T}{fN}\right)^{1/3} \tag{4.3}$$

with:

- r_{el} : radius zone without slippage
- f : friction coefficient
- T : shear force
- N : normal force.

Deresiewicz (1953) shows results of tests with two spheres in contact. Scratches at the contact area show that there is indeed a central area without slippage and a fringe with slippage.

Figure 4.4 Scratches showing area with plastic deformation at sphere-sphere contact (from (Deresiewicz 1953))

With increasing shear stress the lateral displacement of one sphere with respect to the other grows. This lateral displacement δ is given by:

$$\delta = \frac{3(2-\nu)(1+\nu)fN}{4Ea}\left[1 - \left(1 - \frac{T}{fN}\right)^{2/3}\right] \tag{4.4}$$

It is postulated here that the displacement is reversible when the centre of the contact area is still not slipping. Irreversible displacements, and thus irreversible plastic deformation, occurs when the radius of the zone of slippage is equal to the radius of the contact area, so when c = a. This is the case when T = fN.
The corresponding lateral displacement at yield becomes:

$$\delta_{yield} = \frac{3(2-\nu)(1+\nu)fN}{4Ea} \tag{4.5}$$

To assess the contact area the normal force is expressed as a function of the normal stress σ_v. It is assumed that the representative area of one sphere is equal to $A = D^2 = 4R^2$.
This gives $N = 4R^2 * \sigma_v$ and from that for the radius of the contact area:

$$a = R\left[\frac{3(1-\nu^2)\sigma_v}{E}\right]^{1/3} \tag{4.6}$$

With this the expression for the lateral displacement at yield becomes:

$$\delta_{yield} = \frac{3(2-\nu)(1+\nu)fR}{\left[3(1-\nu^2)\right]^{1/3}}\cdot\left(\frac{\sigma_v}{E}\right)^{2/3} \tag{4.7}$$

The shear strain is the ratio between the lateral displacement and the centre-to-centre distance of the spheres. This gives for the yield shear strain:

$$\gamma_{yield} = \frac{\delta_{yield}}{2R} = \frac{3(2-\nu)(1+\nu)f}{2\left[3(1-\nu^2)\right]^{1/3}}\cdot\left(\frac{\sigma_v}{E}\right)^{2/3} \tag{4.8}$$

This model indicates that the threshold shear strain amplitude is a function of the stress level. With increasing vertical stress (increasing depth) the threshold amplitude increases. With increasing initial shear stress the threshold strain decreases. Using realistic values of the stiffness parameters of quartz (E = 86 GPa, ν=0.3, f=0.6) the yield shear strain varies between 0.4 10^{-4} (at σ'_v = 25 kPa) to 1.5 10^{-4} (at σ'_v = 200kPa). The relative shear stress amplitude (T/N at which irreversible shearing occurs) is 0.6. The yield shear strain is compares well with data from literature (see section 4.5 on threshold strain amplitude). The shear stress amplitude is far above experience from laboratory tests.

The considered situation is an idealised situation. The actual soil matrix is not a simple stacking of spheres but a complex arrangement of irregular shaped grains. Therefore in reality deviations from the idealised situation are present. One of the differences is the presence of an initial shear stress at the contact area. This may be the case even when the average shear stress is zero. With an initial local shear stress, and thus an initial local shear strain, the required increase in shear stress before slippage occurs will be less.
The theoretical analysis helps to understand the particulate behaviour of sand but is not a quantitative description of the actual soil behaviour. For this more sophisticated models (Discrete Element Models) are needed.

So far no attention is paid to the effect of acceleration. As found in chapter 3 many of the presently available models to assess the densification during vibratory sheet piling assume this to be the main loading parameter for densification. Therefore attention is paid to this parameter.
With acceleration inertia effects come into play. For a plane perpendicular to the travel direction of a compression wave this results in a varying increase and decrease the normal stress at the considered plane and thus increase and decrease the resistance against sliding. Shear waves will induce a variable shear stress. In fact this is the cyclic loading of the soil.

The order of magnitude of the change in normal stress can be derived from a simple expression for a P-wave in a bar.

$$\Delta\sigma_n = E\Delta v / C_p \qquad (4.9)$$

with:

- $\Delta\sigma_n$: stress amplitude
- Δv : velocity amplitude
- E : Young's modulus
- C_P : P-wave velocity.

For the situation during vibratory sheet piling the velocity amplitude close to the sheet pile is typically in the order of Δv = 0.1 m/s. Assuming further E= 100 MPa and ρ = 1700 kg/m3 this gives (C_p = 242 m/s) σ_n = 4 kPa. For situations at a few meters below surface the change is negligible compared to the normal stress at rest. Therefore it is expected that the influence of a varying normal stress due to accelerations is limited there. For shallow depths the change in normal stress is in the order of the normal stress at rest. For this situation the acceleration may have some effect.

The preceding discussion is about dry sand. In many cases the sand is saturated. The fluid filling the voids will influence the behaviour of the sand. When the situation can be considered as drained (this is the case when the speed of deformation is low and the excess water in the voids has sufficient time to drain away) the effect will be negligible.
In case of fast deformations (the speed of deformation is high and the excess water in the voids does not have sufficient time to drain away) no or hardly any volume strains can occur. The total volume does not change. This does not imply that the position of the grains cannot change. A re-arrangement of the grains is still possible and will occur. As a result the interparticle stress will reduce. When the total (external) stress does not change the water pressure will increase and the stresses at the particle contact points will decrease. In the extreme case the contact stress will almost vanish and the soil behaves as a viscous fluid.

4.3 Methods of cyclic testing on sand

4.3.1 General

Our understanding of the behaviour of sand during cyclic loading is mainly acquired by performing cyclic loading tests on sand. In order to gain some understanding in the possibilities and limitations of the different used methods a brief description of them is given. This will help in understanding and appreciation of the methods.
Tests on behaviour of sand during cyclic loading can be divided in three categories:

- tests to determine the elastic (small strain) shear modulus and damping of the soil
- tests to determine the pore pressure generation of the soil during cyclic loading
- tests to determine the plastic deformation (volume strain) of the soil.

For measuring the elastic (small strain) properties of the soil mostly resonance column or free vibration torsion tests are used.
For measuring the development of excess pore pressure or volume strain on cyclic loading mostly cyclic triaxial and cyclic simple shear tests are performed.
For more fundamental research, including aspects like stress rotation, torsional shear tests (also referred to as hollow cylinder tests) are used.
Shakers or shaking tables are used to tests larger sized samples. Model tests, either at 1g or in a geocentrifuge, are performed to check the behaviour of the soil below a particular type of structure during cyclic loading.

Given the purpose of this study we are mainly interested in the development of plastic volume strain or excess pore pressure during cyclic loading. Therefore the following tests are described in more detail:
- cyclic triaxial tests
- cyclic simple shear tests
- cyclic torsional shear tests
- vertical shaking.

4.3.2 Cyclic triaxial tests

A cyclic triaxial test is performed in a triaxial test apparatus. The main difference with a standard (static) triaxial test is the alternating loading of the sample. During the test different loading conditions can be used, like:
- drained or undrained sample
- stress controlled or strain controlled loading
- alternating axial stress/strain
- alternating radial stress
- combination of axial and radial stress cycling, e.g. to obtain a pure deviatoric stress variation.

Measured parameters can be:
- axial stress and strain
- radial strain, using gap sensors
- pore pressure in the sample
- volume strain (mostly indirect from the outflow of water in a drained test on a saturated sample).

Mostly triaxial tests are performed using samples with a height to diameter ratio of 2. The reason for this is that at the sample ends radial displacement of the sample is prevented by the end platens. There some stress concentration will develop. Using the quoted aspect ratio is believed to reduce the effect of this inhomogeneity on the test results.
Ibsen (1994), following Jacobsen, recommends to use samples with height to diameter ratio of 1 and lubricated ends. The purpose is to achieve a homogeneous stress and strain condition in the sample and thus overcome the above mentioned limitation.

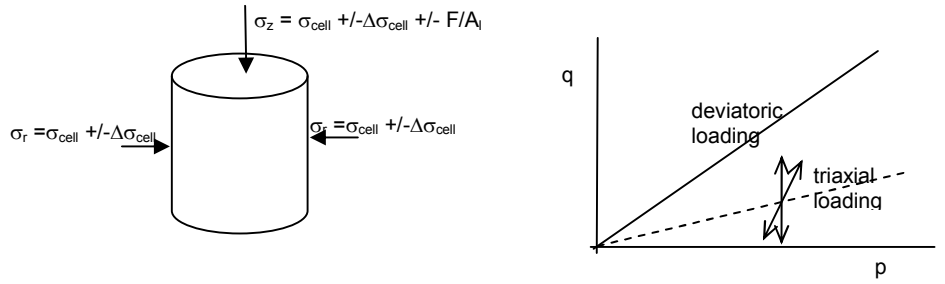

Figure 4.5 Loading in a cyclic triaxial test

The options for the applied stress path in a cyclic triaxial test are limited. Rotation of the principle stresses is not possible. The major principle stress is either the vertical stress or the radial stress. Stress paths are mainly triaxial compression, triaxial extension or deviatoric loading. For the first two stress paths the radial stress (cell pressure) is kept constant. For a deviatoric stress path the cell pressure is to vary with the axial stress.

The maximum shear stress occurs at an angle of 45° with the vertical. At this plane the stress components (shear stress and normal stress) are:

$$\tau = \tfrac{1}{2}(\sigma_1 - \sigma_3) \quad (4.10)$$

$$\sigma_n = \tfrac{1}{2}(\sigma_1 + \sigma_3) \quad (4.11)$$

4.3.3 Cyclic simple shear tests

An alternative for the cyclic triaxial test is the cyclic simple shear test. In this test the soil sample is contained in a wire reinforced rubber membrane. The wire reinforcement is supposed to prevent radial expansion the sample. The sample is loaded vertically and horizontally. Mostly the vertical stress is a static load. The horizontal load may be either stress controlled or strain controlled cyclic load.

The type of loading in cyclic simple shear testing is mostly one-way shearing. Sometimes the tests are run as ‘constant volume’ tests, simulating the undrained behaviour of the soil. In this test the vertical strain is kept constant, thus simulating the constant volume during undrained loading of saturated soil. The change in vertical stress needed to obtain no vertical strain is believed to be equal to the generated excess pore pressure in a real undrained test.
In the simple shear test inhomogeneities develop at the edge of the sample. At the vertical side of the sample the shear stress will be zero or near zero, as illustrated in figure 4.7.

It is questionable if the shear stress at the vertical boundary of the sample in a simple shear test is actually zero, as indicated above. The required elongation of the membrane in axial direction during shearing may induce some shear stress variation at this boundary as well.

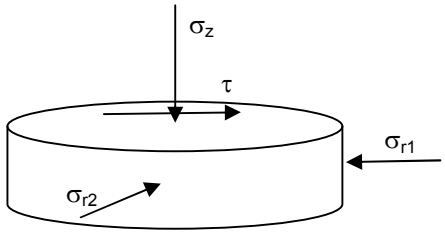

Figure 4.6 Stresses during simple shear test

Figure 4.7 Difference in true shear and simple shear

The test results are mostly interpreted as if the stress situation is a well known pure shear loading. This assumption is however questionable. The horizontal (radial) stress at the sample is hardly ever measured and thus not known. Some researchers investigated this aspect.

Budhu (1985) and O-Hara and Yamamoto (1990) measured the development of the radial stress during cyclic loading. These test results show that the radial stress increases during this process. O-Hara and Yamamoto (1990) also measured the radial stress perpendicular to the direction of shearing. This stress increases as well, however less as the radial stress in the direction of shearing.

Whang (2001) reviewed available data on the influence of the boundary conditions. His conclusion (based on test results by De Alba, Franke and Vucetic and Lacasse) is that the error due to the stress concentration in static small scale simple shear tests may not be large. On the other hand De Alba et al (1976) concluded from a comparison of large scale shaking table tests that the tests results are influenced by the height-to-diameter ratio. Increasing this ratio results is an increase of the number of cycles to liquefaction.

4.3.4 Cyclic torsional shear tests

For fundamental research sometimes torsional shear tests are used. These tests are also referred to as hollow cylinder tests. In the test a hollow cylinder of sand is prepared. Loading consist of a radial stress at the inner radius of the sample, a radial stress at the outer radius of the sample, a vertical stress and a moment loading. The latter component introduces a shear stress at the top of the sample. A major advantage of this test is that a large variation of stress paths can be applied, including stress rotation. A disadvantage is the complexity of the test device.

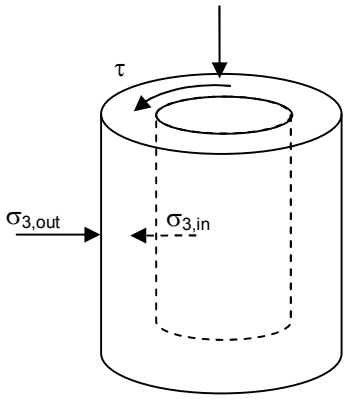

Figure 4.8 Loading in a torsional shear test

4.3.5 Vertical shaking

In the past different researchers investigated the behaviour of sand during cyclic loading using vertical (e.g. (Leussink and Kutzner 1962), (Bement and Shelby 1997)) or horizontal (e.g. (Youd 1970) shakers. The method has become less popular during the last decades but is still sometimes used.
Figure 4.9 shows the test device used by Leussink and Kutzner (1962). In these tests the sample is usually contained in a cylindrical mold. A vertical load is applied at the top. The load may be either a static load, a prestressed spring or a combination of these. The system is vertically vibrated. This implies that the cyclic loading is typically a cyclic variation of the compression stress. Sometimes the vertical acceleration exceeds the acceleration of gravity. In such a case the vertical stress may become zero during part of the testing, resulting in a significant increase in densification. Figure 4.10 shows an example of this behaviour.

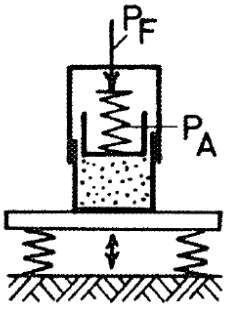

Figure 4.9 Test device of Leussink and Kutzner (1962)

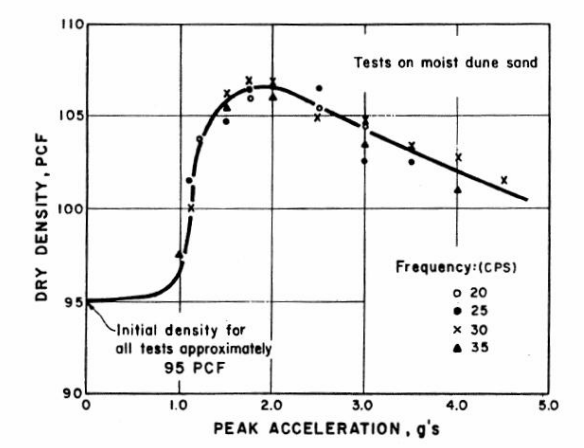

Figure 4.10 Test result cyclic loading by vertical vibrating, zero surcharge load (from (D'Appolonia et al 1969))

Some researchers investigated the effect of shearing in multiple directions, using specially designed simple shear testing devices or shaking tables. An example is (Pyke et al 1975). He compared the settlement in a sample, placed at a large scale shaking table, with loading in one direction and in two directions. One of the results of their tests is shown in figure 4.11. The test results indicate that with multi directional shaking the settlement increases, and almost doubles.

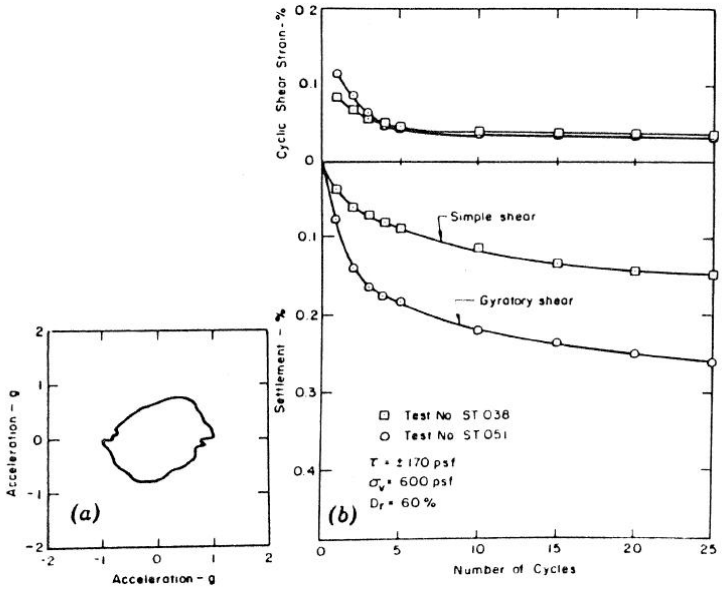

Figure 4.11 Example testing with shearing in two directions (Pyke et al 1975)

4.3.6 Comparison cyclic simple shear and cyclic triaxial tests

Mostly cyclic tests are cyclic triaxial tests or cyclic simple shear tests. In this section a comparison between the two methods is made. Basis for the comparison is the amplitude of the shear stress ratio $\Delta\tau/\sigma_n$ in the tests.

In a cyclic simple shear test this parameter follows directly from the applied forces at the top of the sample.

In a triaxial test the maximum shear stress occurs in a plane with a normal of 45° with the major and minor principal stress direction. Some mathematical exercises with formula are needed to derive the expression for the amplitude of the shear stress ratio.
The normal and shear stress at a plane of 45° are:

$$\sigma_n = \tfrac{1}{2}(\sigma_1 + \sigma_3) \tag{4.12}$$

$$\tau = \tfrac{1}{2}(\sigma_1 - \sigma_3) \tag{4.13}$$

The shear stress ratio at this plane is thus:

$$\frac{\tau}{\sigma_n} = \frac{\sigma_1 - \sigma_3}{\sigma_1 + \sigma_3} = \frac{\sigma_d}{\sigma_d + 2\sigma_3} \tag{4.14}$$

The relative shear stress amplitude becomes

$$\Delta\left(\frac{\tau}{\sigma_n}\right) = 0.5 * \left(\frac{\tau_1}{\sigma_{n1}} - \frac{\tau_2}{\sigma_{n2}}\right) = 0.5 * \left(\frac{\sigma_1 + \Delta\sigma_1 - \sigma_3 - \Delta\sigma_3}{\sigma_1 + \Delta\sigma_1 + \sigma_3 + \Delta\sigma_3} - \frac{\sigma_1 - \Delta\sigma_1 - \sigma_3 + \Delta\sigma_3}{\sigma_1 - \Delta\sigma_1 + \sigma_3 - \Delta\sigma_3}\right) \tag{4.15}$$

After some elaboration this gives:

$$\Delta\left(\frac{\tau}{\sigma_n}\right) = 2\left(\frac{\sigma_3\Delta\sigma_1 - \sigma_1\Delta\sigma_3}{(\sigma_1 + \sigma_3)^2 - (\Delta\sigma_3 + \Delta\sigma_1)^2}\right) \tag{4.16}$$

For vertical cyclic loading only ($\Delta\sigma_3 = 0$) this becomes:

$$\Delta\left(\frac{\tau}{\sigma_n}\right) = 2\left(\frac{\sigma_3\Delta\sigma_1}{(\sigma_1 + \sigma_3)^2 - (\Delta\sigma_1)^2}\right) \tag{4.17}$$

For pure deviatoric loading ($\Delta\sigma_3 = -0.5*\Delta\sigma_1$) 4.16 becomes:

$$\Delta\left(\frac{\tau}{\sigma_n}\right) = 2\left(\frac{(\sigma_3 + 0.5\sigma_1)\Delta\sigma_1}{(\sigma_1 + \sigma_3)^2 - (1.5\Delta\sigma_1)^2}\right) \tag{4.18}$$

Taking the stress amplitude $\Delta\sigma_1$ small compared to the initial stress σ_3 the expression for vertical cyclic loading is:

$$\Delta\left(\frac{\tau}{\sigma_n}\right) = 2\left(\frac{\sigma_3\Delta\sigma_1}{(\sigma_1 + \sigma_3)^2}\right) = \frac{2\Delta\sigma_1}{\left(\frac{\sigma_1}{\sigma_3} + 1\right)^2 \sigma_3} = \frac{4}{\left(\frac{1}{K} + 1\right)^2}\frac{\Delta\sigma_1}{2\sigma_3} \tag{4.19}$$

For deviatoric cyclic loading the expression becomes:

$$\Delta\left(\frac{\tau}{\sigma_n}\right)=2\left(\frac{(\sigma_3+0.5\sigma_1)\Delta\sigma_1}{(\sigma_1+\sigma_3)^2}\right)=\frac{2\left(1+0.5\frac{\sigma_1}{\sigma_3}\right)\Delta\sigma_1}{\left(\frac{\sigma_1}{\sigma_3}+1\right)^2\sigma_3}=\frac{4\left(1+0.5\frac{1}{K}\right)}{1.5\left(\frac{1}{K}+1\right)^2}\cdot\frac{1.5\Delta\sigma_1}{2\sigma_3} \qquad (4.20)$$

The last term in both expressions is the relative amplitude of the deviatoric stress. For K=1 the first part becomes 1.
From this follows that for initial isotropic effective stress (K=1) the shear stress ratio in a cyclic triaxial test is to be taken as $\Delta\sigma_d/2\sigma_3$. For an anisotropic initial stress situation a different value is to be used, depending on the value of K and the type of cyclic loading (vertical or deviatoric).

The preceding is a theoretical comparison. Some researchers compared the results of cyclic simple shear testing and cyclic triaxial testing. They found that in general the number of cycles to liquefaction in undrained cyclic triaxial tests is larger as in cyclic simple shear tests. This can also be interpreted that the relative shear stress ratio required for liquefaction within a given number of load cycles is smaller in a cyclic simple shear test as in a cyclic triaxial tests. To account for this effect correction factors to the shear stress ratio in a cyclic triaxial test have been proposed. The type of expression used is:

$$\left(\frac{\Delta\tau}{\sigma'_{v0}}\right)_{simpleshear}=C_R\left(\frac{\Delta\sigma_d}{2\sigma_c}\right)_{triax} \qquad (4.21)$$

with:
- C_R : correction factor.

For this correction factor C_R different researchers present different values. An overview is given below.

Seed and Peacock (1971) analysed theoretically the differences in cyclic triaxial and cyclic simple shear testing. The followed approach differs from the one presented at the start of this section. For the simple shear test they take into account the difference between vertical and horizontal stress. The maximum shear stress ratio in the simple shear test is defined by them as:

$$\frac{\Delta\tau_{\max}}{\sigma_{mc}}=\frac{3\Delta\tau}{\sigma'_{v0}(1+2K_0)} \qquad (4.22)$$

with:
- $\Delta\tau_{max}$: maximum shear stress amplitude in the sample
- σ_{mc} : mean effective principal stress during consolidation
- $\Delta\tau$: shear stress amplitude at the horizontal plane
- σ'_{v0} : effective vertical stress
- K_0 : ration between horizontal and vertical stress.

From this they derive the following relation between the shear stress amplitude in a simple shear test and in a triaxial test. Please note that the value of K_0 is for the stress condition in a direct simple shear test. The stress condition in the triaxial test is isotropic.

$$\left(\frac{\Delta\tau}{\sigma'_{v0}}\right)_{simpleshear} = \frac{1+2K_0}{3}\left(\frac{\Delta\sigma_d}{2\sigma_c}\right)_{triax} \qquad (4.23)$$

After this they compare the results of cyclic simple shear tests and cyclic triaxial tests. From this comparison they conclude that two corrections are to be made to the shear stress amplitude in a cyclic triaxial test. The first is a correction for the difference between the stress conditions (different K_0 condition) in the field and in the laboratory testing. The second is a correction for the limitations in test equipment and procedures.

relative density I_D [-]	correction for difference in test and field conditions	correction for limitations equipment and procedures	total value C_R
0.4	0.47	1.15	0.55
0.6	0.47	1.30	0.61
0.85	0.47	1.50	0.7

Table 4.1 Correction factors for the shear stress amplitude in cyclic testing to obtain the equivalent shear stress amplitude in field conditions

Seed and Idriss (1971) present a graph with the value of C_R as function of the relative density. The graph is based on three points and equal to the graph presented by Seed and Peacock (1971).

Lee and Focht (1975) use in their analysis correction factors between triaxial test data and field conditions based on the study by Seed and Peacock (1971). They mention the following values:
- I_D = 0.63: C_r = 0.63
- I_D = 0.77: C_r = 0.7
- I_D = 1.00: C_r = 0.8.

These values are in line with the given graph in (Seed and Peacock 1971).

Castro (1975) compares the theoretical relation between the shear stress amplitude in the field and in the triaxial test. For the shear stress amplitude he uses the ratio of the octahedral shear stress and the octahedral normal stress. From this he derives the following factor:

$$C_R = \frac{2(1+2K_0)}{3\sqrt{3}} \qquad (4.24)$$

For K_0 = 1 this gives C_R = 1.14 and for K_0 = 0.5 the factor becomes C_R = 0.77.

De Alba et al (1976) compare the results of shaking table tests and cyclic triaxial tests. From this comparison they derive a value for C_R between 0.6 and 0.65. This value is independent of the relative density.

Seed (1979) gives a relation between the loading in the field, the loading in a simple shear test and the loading in a triaxial test.

$$\left(\frac{\tau}{\sigma'_{v0}}\right)_{field} \approx 0.9\left(\frac{\tau}{\sigma'_{v0}}\right)_{simple\ shear} \approx C_R\left(\frac{\sigma_d}{2\sigma'_0}\right)_{triaxial} \qquad (4.25)$$

The value of C_R is said to be about 0.57 for $K_0 = 0.4$ and 0.9 for $K_0 = 1$.

Peacock and Seed (1968) show a comparison between the cyclic strength in triaxial tests and simple shear tests. According to their data the liquefaction strength in triaxial testing is about three times the strength in simple shear testing. From this follows a correction factor $C_R = 0.33$. This factor is low compared to values mentioned by other researchers.

In (Yoshimi et al 1994) the following relation for the liquefaction resistance is mentioned. It is based on the relation given by Seed (1979).

$$\left(\frac{\tau}{\sigma'_{v0}}\right)_{field} = 0.9\frac{1+2K_0}{3}\left(\frac{\sigma_d}{2\sigma'_c}\right)_{triaxial} \qquad (4.26)$$

This relation differs slightly from the theoretical relation given at the beginning of this section.

Thus far the attention is focussed on stress controlled conditions. For strain controlled conditions a similar relation between direct simple shear and triaxial loading exists. This is illustrated in the test data of Berghe (2001). He performed both cyclic triaxial tests and cyclic simple shear tests on Brussilian sand. The tests are undrained and strain controlled. He did not compare the results of the two types of testing. The reported results allow to make this comparison. Figure 4.12 shows the number of cycles to liquefaction as function of the relative density and shear strain amplitude for the two types of testing.

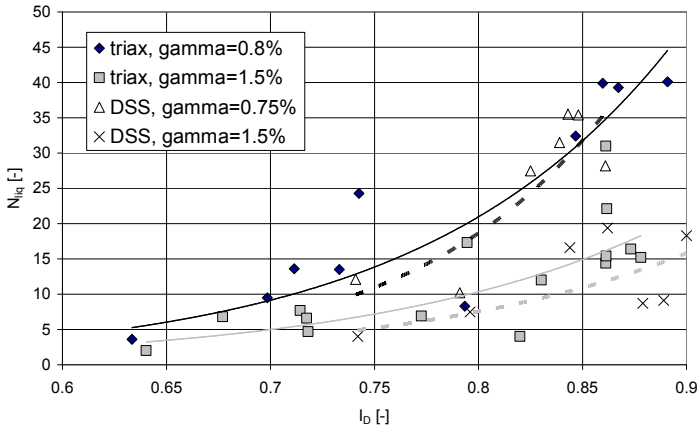

Figure 4.12 Comparison number of cycles to liquefaction for cyclic simple shear and cyclic DSS tests (solid lines are trend lines for the triaxial tests, dotted lines are trend lines for the direct simple shear tests)

To view the difference between cyclic simple shear and cyclic triaxial testing trend lines are added. For tests with a shear strain amplitude of 1.5% both lines can be compared directly. It shows that the trend line for simple shear testing plots below the line for triaxial testing. The ratio between the number of cycles to liquefaction is about 0.7. The other two lines nearly coincide. The situation is however not really the same. The triaxial tests are performed with shear strain amplitude of 0.8% while the simple shear tests are performed with shear strain amplitude of 0.75%. The number of cycles for simple shear testing at 0.75% plots below the line for the triaxial tests at 0.8%. This shows that the simple shear test has a lower liquefaction resistance as the triaxial testing.

4.4 Effect preshearing

Nearly all published cyclic test results are either drained or undrained on virgin samples. In cases like wind loading and vibratory sheet piling, the situation is neither fully drained nor fully undrained. Generation and dissipation of excess pore pressure occur simultaneously. It has been found that the interim drainage results in a significant decrease in pore pressure generation. This type of preloading is usually referred to as 'preshearing'. Other types of preshearing are isotropically loading and unloading the sample (thus creating a kind of overconsolidation), deviatoric loading and unloading of the sample and preloading with a large number of small amplitude cycles.

As during vibratory sheet piling a situation exists where generation and dissipation of excess pore pressure occurs simultaneously it is relevant to know the influence of this on the generation of excess pore pressure. This aspect is discussed in this section.
The effect of simultaneous generation and dissipation has been observed in a number of element tests. The model tests on vibratory sheet piling, already described in section 2.4, are an example. Other examples are the model tests with wave loading on a sandy seabed e.g. (Sassa and Sekiguchi 1999) and (Sumer et al 1999).

Sassa and Sekiguchi (1999) executed model tests on the development of excess pore pressure in the seabed. The tests are performed by placing a small scale wave tank in a geocentrifuge. Results of one of the performed tests are reproduced here as figure 4.13.
During the test the wave loading is constant. In the test generation and dissipation of excess pore pressure occurs simultaneously. The test shows that the excess pore pressure first increases. At this stage the generation of pore pressure is in excess of the dissipation. After some time the excess pore pressure decreases. This indicates that the generation of excess pore pressure is decreasing. Two mechanisms can beheld responsible for this effect. The first is the densification of the sand due to the dissipating water. The other effect is the change in soil fabric during densification.

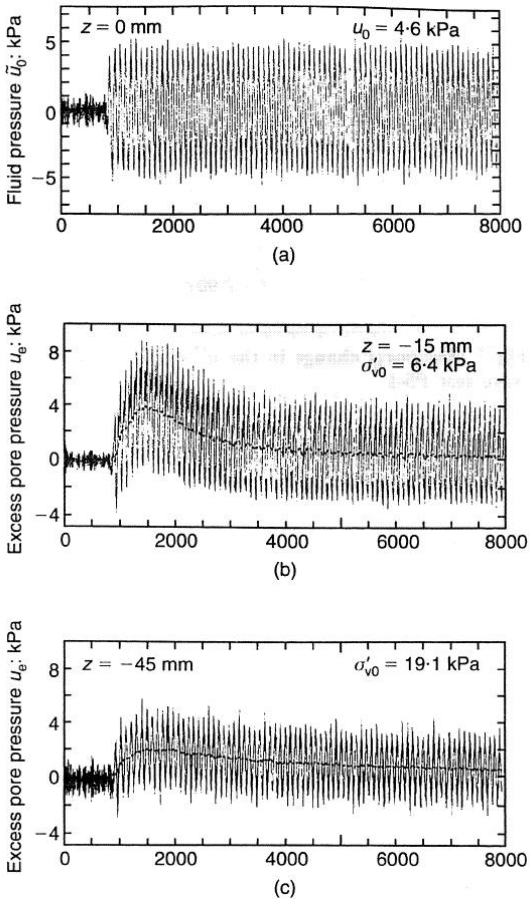

Figure 4.13 Development of excess pore pressure in a seabed during model (geocentrifuge) tests (Sassa and Sekiguechi, 1999)

The same effect is observed in the tests by Sumer et al (1999) in a small tank at ISVA, Danmark. In the tests the development of excess pore pressure in a sandy/silty seabed due to wave loading is measured. Results of one of the tests are shown in figure 4.14. The excess pore pressure at first rises quickly. Even complete liquefaction is observed in the test. After some time the excess pore pressure decreases. Towards the end of the test the excess pore pressure is completely vanished, although the wave loading remained constant

These model tests show that dissipation of excess pore pressure increases the resistance against liquefaction. The number of single element tests with simultaneous generation and dissipation of excess pore pressure is limited. Mitchell and Dubin (1986) used a very interesting test device. In the cyclic triaxial apparatus a column filled with sand is connected to the drainage valve. The column is used to simulate the flow resistance encountered in reality by dissipating excess pore pressure. With this device the amount of dissipation could be controlled. Unfortunately the results of only one test are given, other test results are indicated

in wording only. The result indicates that at first the pore water pressure increases, remains constant for some time (cycles) and then decreases rapidly. The volumetric strain is not accurately recorded.

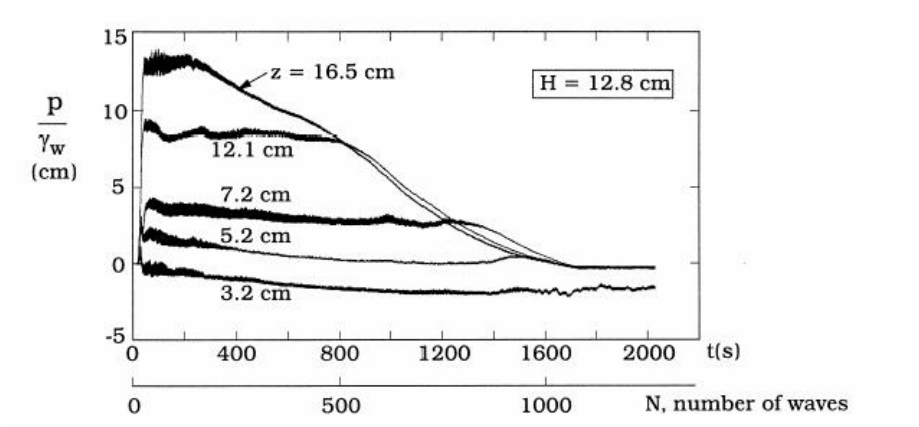

Figure 4.14 Development of excess pore pressure in a seabed during model tests (Sumer et al 1999)

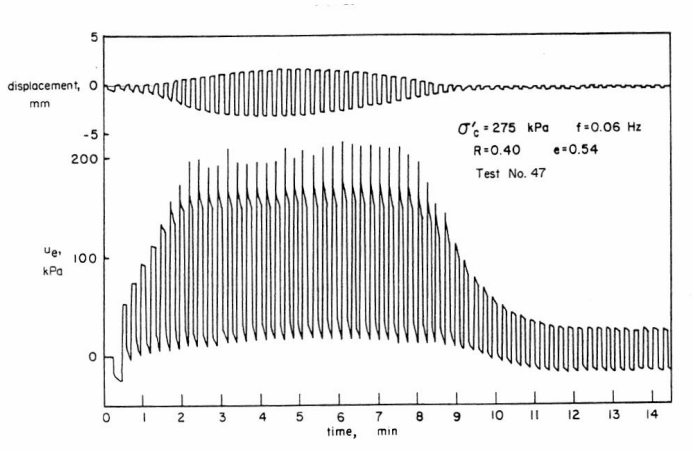

Figure 4.15 Result cyclic triaxial test with continuous drainage (Mitchell and Dubin 1986)

O-Hara et al (1985) also simulated the effect of continuous dissipation in a cyclic triaxial test. Partial drainage is achieved by opening the drain valve after each cycle to dissipate a predetermined amount of excess pore pressure. This amount of dissipation per drainage step is not very accurate, yet the presented data are interesting and worthwhile some attention.

To check the influence of the drainage the authors summed the increase of the excess pore pressure at each cycle. This resulted in a graph representing the total

amount of generated excess pore pressure. The resulting value is far below the excess pore pressure that would develop in undrained conditions.

Lee and Focht (1975) performed 35 cyclic undrained triaxial tests for the design of the Ekofisk tank. In some of these tests the sample is allowed to reconsolidate after a certain amount of excess pore pressures has been generated. This resulted in a large increase in the number of cycles to liquefaction when the loading is resumed. A special procedure is followed in some of the tests to simulate the effect of partial drainage. After 12.5 or 50 undrained loading cycles the test is stopped. The backpressure is increased to 90% of the measured excess pore pressure at that time and the drainage valve is opened. With this method 10% of the excess pore pressure is allowed to dissipate. After this, the drainage valve is closed and another parcel of 12.5 or 50 undrained loading cycles is performed. This process is repeated until the sample liquefied or the increase in pore pressure due to undrained cyclic loading is less as the decrease in pore pressure during the dissipation step. This procedure reduced the liquefaction potential. For some cases the number of cycles to liquefaction doubled while for other situations no liquefaction is reached and the excess pore pressure starts to decrease after some time. The last observation indicates that after some time the dissipation exceeds the generation of excess pore pressure.

Most researchers who tried to investigate the effect of drainage on the liquefaction resistance use a less subtle approach. The tests are performed in three stages. First an undrained test is performed until a certain amount of excess pore pressure is generated. After this the sample is allowed to drain and the undrained cyclic loading is resumed. Some test data are summarised below.

Sato et al (1997) performed cyclic tests (hollow cylinder, stress controlled) on Toyoura sand. In the test the excess pore pressure is drained after approximately 5 cycles. After drainage the cyclic loading is resumed. When no liquefaction is reached in the first series the pore pressure generation in the second series is less, when liquefaction is achieved in the first series the pore pressure generation in the second series is higher.

Finn et al (1970) investigated the effect of strain history on the liquefaction potential. They performed both undrained cyclic simple shear tests and undrained cyclic triaxial tests on Ottawa sand. Cyclic loading is continued until the sample liquefied. After reaching liquefaction the loading is continued for a few cycles. In this stage the sample shows large shear strain amplitudes (strain amplitude is about 10% to 20%). After reconsolidation the undrained loading is resumed. They observed that during the second phase of cyclic loading the sample liquefied in a few cycles, despite the increase in density during the reconsolidation stage. In addition to these tests a series of tests is performed in which the shear deformation during the test is prevented to exceed a preset threshold value. Different threshold values have been used. After reconsolidation the undrained cyclic loading is resumed. The number of cycles to liquefaction before and after the reconsolidation stage is compared. From the test results it is observed that the ratio of number of load cycles until liquefaction before and after the reconsolidation stage decreases with increasing threshold shear strain.

The effect of the shear strain amplitude on the liquefaction resistance is also investigated by Oda et al (2001). In his 'test serie B' the sample is first loaded cyclically to a predefined double amplitude and then allowed to reconsolidate. Then the undrained cyclic loading is resumed. From their tests it follows that preshearing with small amplitude (double amplitude <1%) results in a small increase in liquefaction resistance. Preloading with large prestrain (>2%) reduces the liquefaction resistance, despite the increase in relative density. He attributes this decrease on resistance to the development of shear bands in presheared specimens. This is supported by calculations with a discrete element model. The shearing results in bands with extreme large voids that can easily collapse in subsequent cyclic loading.

The research mentioned so far investigate the qualitatively the effect of preshearing. For practical problems some guidance in the quantitative effect is needed. The research by Smits et al (1978) can be used for this purpose. As part of the design activities for the Eastern Scheldt Storm Surge Barrier they executed a large number of cyclic triaxial tests with intermittent drainage stages. The exact procedure used in the tests is not described. The test results are interpreted by comparing the amount of relative pore pressure generation per cycle ($\beta = \Delta r_u/\Delta N = \Delta(u/\sigma'_v)/\Delta N$) as function of the preshearing (expressed as a change of the porosity n) in the previous drainage steps. Results are shown in figure 4.16.

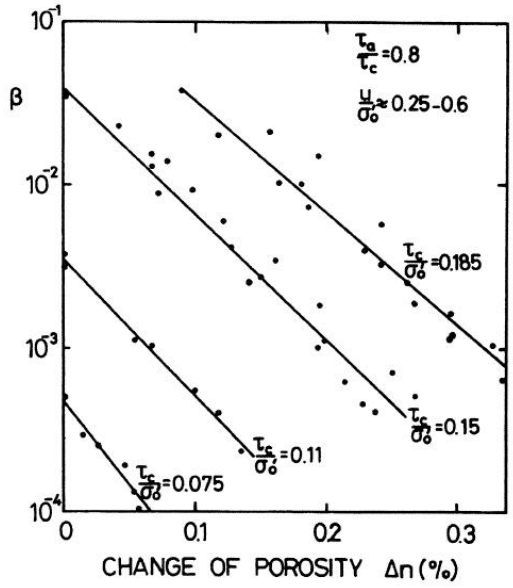

Figure 4.16 Effect of preshearing on the generation of excess pore pressure (Smits et al 1978); please be aware that in this graph a positive value of Δn denotes a decrease in porosity

The authors do not present an expression for the effect of preshearing on the pore pressure generation. From figure 4.16 such an expression can be derived:

$$\log \beta = A + X.\Delta n \tag{4.27}$$

From this follows:

$$\beta = 10^{A}.10^{+X.\Delta n} \tag{4.28}$$

The term 10^{A} is the pore pressure generation for $\Delta n = 0$, so for the situation without drainage or preshearing. The effect of drainage on the pore pressure generation is given by the factor $10^{+X_{\Delta n}}$. The value of X, as derived from figure 4.16, is about +700 (when Δn is in unity).

Tokimatsu and Hosaka (1986) show two different effects of preshearing on the liquefaction resistance. These are illustrated in figure 4.17. The liquefaction resistance of a virgin sample is shown in the left hand plot. This sample is sheared with 10,000 cycles with a single axial amplitude of 0.1%. The result is called 'ideal sample'. The liquefaction resistance is shown in the right hand plot of figure 4.17. A large increase in resistance is found. The samples are compressed to a prescribed axial strain and unloaded before cyclic testing. They found that for small axial strain (0.3%) the effect is marginal. For larger axial strains (>0.5%) the resistance against liquefaction greatly reduces

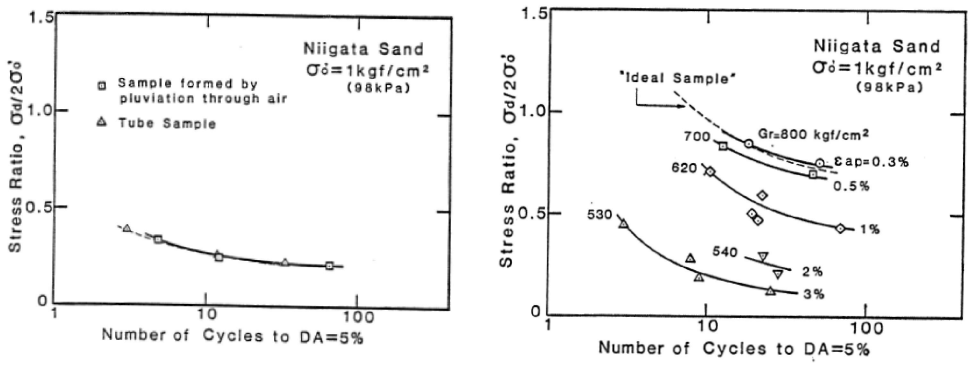

Figure 4.17 Effect preloading on the number of cycles to liquefaction; left tests on virgin ample, right test on sample after preshearing (Tokimatsu and Hosaka 1986)

4.5 Threshold load amplitude

The description of the Hertz model (section 4.2) indicates that there is a kind of threshold for the shear strain amplitude below which no permanent densification occurs. Many researches claim the same, based on their test results. Two kind of threshold values may be distinguished, a strain threshold and a stress threshold.

One of the leading researchers investigating this aspect is Vucetic. In (Vucetic 1994) he tries to derive the threshold shear strain from published test data.
The threshold shear strain amplitude is derived by plotting the volume strain as function of the shear strain amplitude. Extrapolating the results until zero volume

strain gives the threshold value for the shear strain amplitude. For sand the threshold strain amplitude is in the range of 0.5 10^{-4} to 3.10^{-4}. The number of cycles in the tests used by the different researchers is not mentioned. In the quoted examples it is 5 to 10.
Comparable results can be found in (Hsu and Vucetic 2004).

The question may be posed whether the mentioned threshold shear strain amplitude is actually the value below which the permanent volume strain is zero or if still some marginal volume strain is present. Extrapolating always introduces the risk of overlooking some mechanisms. Even if the measured volume strain is zero this only indicates that it is, for the small number of applied loading cycles, within the measuring accuracy. For situations with a large number of cycles with a small strain amplitude the densification may become within the measuring accuracy. Some published results that may shed light on this aspect are collected.

The cyclic simple shear tests by Silver and Seed (1971) do not show a real threshold value for the shear strain amplitude. Even for the lowest used shear strain amplitude of 0.01% still a volumetric strain of 0.005% is achieved after 300 cycles. For practical purposes this could be negligible, it is however not zero.

Shamoto et al (1996) describes results of cyclic triaxial tests. Samples are loaded (cyclic, undrained, stress controlled) and than reconsolidated. The volume strain on reconsolidation has been measured. From the test data no threshold shear strain amplitude can be derived. They observed that for a shear strain amplitude of 0.01% still some volume strain occurs.

Tests by Wichtmann et al (2004) show the same tendency. For a shear strain amplitude of 0.5 10^{-4} still a small amount of permanent strain is measured.

Dong-Soo Kim and Stokoe (1995) performed resonant column and torsional shear tests on a.o. dry sand. They defined two threshold values for the strain amplitude: the first is the elastic threshold strain above which deformational characteristics is influenced by strain amplitude. The second is the cyclic threshold above which the characteristics is influenced by the number of cycles. The values found by them are respectively 0.001% and 0.005%. For the permanent deformation the latter is of interest.

Taking all data for the value of the threshold shear strain in consideration one may state that for a shear strain amplitude of 0.5 10^{-4} to 1.10^{-4} the permanent volumetric strain becomes negligible but not zero. For large numbers of load cycles still some densification will occur. If this can be neglected depends on the considered situation.

No firm data on the threshold value for the shear stress amplitude could be traced. Available published data are limited in the number of loading cycles. Extrapolating of the curve through the available data is needed. Three examples are presented.

In (De Alba et al 1976) test data from large scale simple shear tests are presented. The results are shown in figure 4.18.

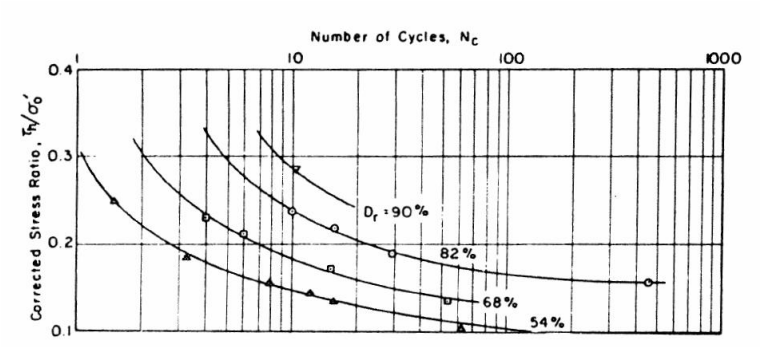

Figure 4.18 Number of cycles to liquefaction as function of relative density and cyclic stress ratio (from (De Alba et al 1976))

No firm value for the threshold shear stress amplitude can be derived from these data. Extrapolating the given curves suggests the following values stress amplitude:

- I_D =0.53 : $\Delta\tau/\sigma'_{v0}$ = 0.08
- I_D =0.68 : $\Delta\tau/\sigma'_{v0}$ = 0.12
- I_D =0.82 : $\Delta\tau/\sigma'_{v0}$ = 0.15.

Oda et al (2001) performed cyclic triaxial tests on sand specimen prepared with different bedding angles. For the samples prepared with a horizontal bedding angle, as is the common situation in preparation of sand samples for triaxial testing, the number of cycles to liquefaction is reproduced as figure 4.19. This figure suggests that for a low relative density (I_D = 34%) the threshold value for the cyclic stress ratio is about 0.1. For higher relative densities the test data suggest a higher value for the threshold value.

D'Appolonia (1970) shows results of vertical vibrated sand samples. For low acceleration levels the loading parameter is the change in vertical stress, expressed as ratio of the initial confining stress. The lowest stress ratio is $\Delta\sigma_v/\sigma_c$ = 0.2. With this load amplitude still some volumetric strain occurs. No threshold value is given. Extrapolating the given data suggests that for $\Delta\sigma_v/\sigma_c$ = 0.1 the permanent volume strain is zero or at least negligible. This can be considered as a threshold shear stress.

As a tentative value for the threshold on shear stress amplitude a value of 0.05 to 0.1 may be given. Possible the threshold value is a function of the relative density.

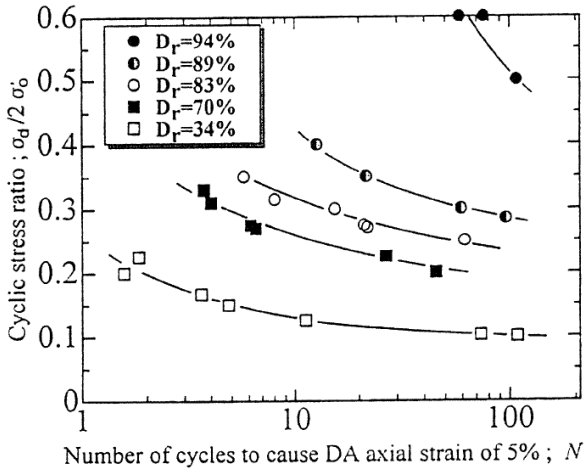

Figure 4.19 Number of cycles to liquefaction as function of relative density and cyclic stress ratio (from (Oda et al 2001)), σ'_0 is the initial confining pressure

4.6 Discussion on sand behaviour during cyclic loading

The behaviour of sand during cyclic loading is an interesting, but complex process. Many factors are of influence. Only a limited number of aspects could be described here.

Most findings are based on the results of cyclic Direct Simple Shear or cyclic triaxial tests. From a theoretical point of view the same loading occurs in these tests and the same results are expected to be obtained. When comparing results from these two types of tests some differences are observed. It is generally accepted to use a correction factor for the load amplitude in a cyclic triaxial test to get comparable results. The published values for the correction factor vary between 0.35 and 1.0.

The possible stress paths in this type of testing are limited. In a cyclic triaxial test the stress path is well defined. In a cyclic DSS test the radial stress, and the variations in the radial stress, are in general not measured. Thus the actual stress path in a cyclic DSS test is not well defined. Some stress rotation may occur in these tests. This may explain the difference in results between the cyclic DSS and the cyclic triaxial testing. Cyclic DSS tests with shearing in two directions shows that this increases the amount of densification.

The actual stress paths in the field will differ from the stress paths in laboratory testing. The use of cyclic torsional tests allows to investigate more complex stress paths. For fundamental research on the behaviour of sand during cyclic loading this type of testing is indispensable. Much research in this field is still needed.

It is often stated that there exists a threshold shear strain amplitude below which no densification occurs. The quoted threshold value is about 1.10^{-4}. This value is based on test results, using a limited number of load cycles. Theoretical considerations, using a simple system of two spheres in contact, confirm the existence of such a threshold value.
It is questionable if for a real soil matrix such a real threshold value exists. Test data with small amplitude loading but large number of loading cycles are scarce. The available data show that for a shear strain amplitude of $0.5\ 10^{-4}$ still some densification may occur after prolonged cycling. It is therefore expected that for smaller shear strain amplitudes some densification will occur. The amount of densification will be small compared to the densification above the threshold value. For situations with a large number of small amplitude loading cycles, and strict requirements with respect to the allowable settlement, densification in this range of shear strain amplitudes may be relevant. For the situation during vibratory sheet piling the concept of a threshold shear strain may be justified from a practical point of view.

Dissipation of excess pore pressure greatly reduces the generation of excess pore pressures. This effect is therefore to be accounted for when considering the soil behaviour during vibratory sheet piling. For large shear strain amplitudes (typically shear strain amplitudes in excess of 1%) the positive effect becomes a negative effect.

4.7 Overview available densification models

4.7.1 General

Models to calculate the densification and/or generation of excess pore pressure can broadly be divided in sophisticated models, aimed at describing the behaviour exactly during each load cycle, and more general models aimed at describing the development of permanent strain and/or excess pore pressure as function of the applied number of cycles.

For large number of applied cycles the first type requires large computational effort. The final accuracy may be low due to the large number of calculation steps (Niemunis and Helm 2001). This type of models is therefore not practical for predicting the densification due to vibratory sheet piling. Therefore the attention is focussed on the second type of models.

4.7.2 Model of Barkan

Barkan (1962) describes a model for assessing the densification of cyclic loaded sand. He states that the main parameter determining the effect of vibrations on compaction is the acceleration amplitude. From experimental investigations Barkan concludes that there is a unique non-linear relation between the void ratio and the acceleration amplitude. This relation is given as:

$$e = e_{min} + C.\exp(-\alpha_B \eta) \quad (4.29)$$

with:

- e : initial void ratio
- e_{min} : minimum void ratio
- α_B : coefficient of vibratory compaction
- η : acceleration amplitude (expressed in g)
- C : a constant.

When the soil is in it's loosest state ($e = e_{max}$) it cannot withstand any acceleration, so η is to be zero. Using $e = e_{max}$ in equation 4.29 the value of C becomes:

$$e = e_{min} + (e_{max} - e_{min}).\exp(-\alpha_B \eta) \quad (4.30)$$

Instead of the void ratio the relative density can be used to express the soil density. This gives:

$$I_D - 1 = \exp(-\alpha_B \eta) \quad (4.31)$$

After some elaboration Barkan arrives at the following expression for the void ratio after vibrating with acceleration η ($\eta > \eta_0$):

$$e = e_{min} + (e_0 - e_{min}).\exp(-\alpha_B(\eta + \eta_0)) \quad (4.32)$$

In this η_0 is the acceleration amplitude needed to arrive at the initial void ration e_0, starting from the loosest state. The parameter η_0 is denoted the threshold acceleration, i.e. the acceleration below which no further densification occurs in sand with a void ratio of e_0.
As may be noticed there is a discrepancy between equation 4.30 and 4.32. No explanation for this difference is given by Barkan.

The densification models described in Engineering Manual EM 1110-1-1904 of the U.S Army Corps of Engineers (USACE 1990) and in MIL-HDBK-1007/3 (Department of Defense 1997) are based on this model. Also the densification model by Hergarden (section 3.7) is based on the model by Barkan.

The first step in the analysis is to estimate the relative density of the soil and the acceleration amplitude. The threshold value for the acceleration amplitude (the acceleration below which no densification occurs) follows from equation 4.31 and is given by:

$$\eta_0 = \frac{-\ln(1 - I_D)}{\alpha_B} \quad (4.33)$$

with:

- η_0 : yield acceleration below which no densification occurs (expressed in g)
- I_D : relative density
- α_B : coefficient of vibratory compaction

The value of α_B, as given by (Barkan 1962), depends on the water content w. At w = 0 the value is $\alpha_B = 0.8$. It drops to $\alpha_B = 0.2$ at w = 4% and rises again to $\alpha_B = 0.85$ at w=17%. For higher values of w the value of α drops again. No value for full saturated sand is given.

The values for α_B, as quoted in MIL-HDBK-1007/3 are nearly equal. In EM 1110-1-1904 the following expressions are given for the value of α_B as function of the water content w (expresses as a percentage):

$$w < 5\%: \quad \alpha_B = 0.2 + 0.12w \tag{4.34}$$

$$5\% \le w < 18\%: \quad \alpha_B = 0.77 + 0.006w \tag{4.35}$$

These expressions differ from the data given in (Barkan 1962). Again the value of α_B for fully saturated sand is not given.

Hergarden (2000) reviewed available laboratory test results and proposes different values for α_B. The value for α_B varies between 0.5 and 5. The lowest value is for high stress levels and the highest value is for sand at low stress levels. In (Hergarden and Tol 2001) the range for α_B is given as 3 to 5.

In MIL-HDBK-1007/3 and EM 1110-1-1904 the following expression for the vertical strain is given:

$$\varepsilon_z = 0.0025 \frac{\Delta I_D}{\gamma_{dry}} \tag{4.36}$$

with:

- ΔI_D : change in relative density
- γ_{dry} : initial dry density of the sand (unit: lb/ft^3).

The change in relative density follows from:

$$\Delta I_D = I_{D,f} - I_{D,0} \tag{4.37}$$

with:

- $I_{D,f}$: final relative density
- $I_{D,0}$: initial relative density.

The values for the final relative density are:

$$\eta_j \le \eta_0 \quad I_{D,f} = I_{D,0} \tag{4.38}$$

$$\eta_j > \eta_0 \quad I_{D,f} = 100 * \left[1 - \exp(-\alpha * (\eta_0 + \eta))\right] \tag{4.39}$$

Equation 4.39 follows from equation 4.32, when expressing the final density as relative density instead of void ratio.

The formula for the vertical strain may seem a little odd at first sight. The correct formula to derive the volume strain from the change in relative density reads

$$\varepsilon_{vol} = \frac{\Delta e}{1+e_0} = \frac{1}{1+e_0} \Delta I_D (e_{\max} - e_{\min}) = (1-n_0) \Delta I_D (e_{\max} - e_{\min}) = \frac{\gamma_{dry}}{\gamma_{solids}} \Delta I_D (e_{\max} - e_{\min}) \tag{4.40}$$

Reasonable values for silica sand are $e_{max} - e_{min} \approx 0.33$ and $\gamma_{solids} = 26.5$ kN/m^3 (168.7 lb/ft^3). Using these values the volume strain becomes (for γ_{dry} expressed in lb/ft^3, as in 4.36):

$$\varepsilon_{vol} = 0.002 \gamma_{dry} \Delta I_D \tag{4.41}$$

This is well in agreement with the previous expression.

Hergarden (2000) does not use equation 4.32. Instead he assumes that the densification follows from the difference between the initial density and the void ratio after vibrating, using equation 4.30.

4.7.3 C/L model, description

Sawicki developed an empirical model for the plastic volumetric strain in cyclic loading (Morland and Sawicki 1985; Sawicki and Sliwinski 1989; Sawicki and Swidzinski 1989a; Sawicki and Swidzinski 1989b; Sawicki et al 1998; Sawicki 2004). The model is called the C/L model (compaction/liquefaction model). The following differential equation for compaction under cyclic loading is used:

$$\frac{d\Phi}{dN} = D_1 J_2 \exp(-D_2 \Phi) \tag{4.42}$$

with:

- Φ : compaction (relative change of porosity, $\Phi = \Delta n/n$)
- J_2 : second invariant of strain amplitudes deviator
- D_1 , D_2 : experimental constants, depending on the relative density
- N : number of loading cycles.

The relation between compaction Φ and the volume strain is:

$$\Phi = -\frac{1-n_0}{n_0}\varepsilon_{vol}^{plas} \tag{4.43}$$

Integrating the differential equation for the compaction gives:

$$\Phi = C_1 \ln(1 + C_2 z) \tag{4.44}$$

with:

- $z = J_2 N$
- C_1, C_2 : constants.

The relation between the parameters C_1 and C_2 with D_1 and D_2 is: $D_1 = C_1 C_2$ and $D_2 = 1/C_1$.

The method is based on results of cyclic simple shear tests. In these tests the second invariant of strain amplitudes deviator is:

$$J_2 = \tfrac{1}{4}.\Delta\gamma^2 \tag{4.45}$$

with:

- $\Delta\gamma$: shear strain amplitude.

In different papers the experimental parameters C_1 and C_2 or D_1 and D_2 are published for different sands. Sometimes the used expression for z differs from the one quoted above. In section 4.7.4 an overview of these data is given in an effort to obtain some guidance for selecting these parameters when using the C/L model.

One feature of the C/L model is that densification will continue forever with increasing number of load cycles. In the long run this will yield unrealistic densities. To overcome this problem Niemunis and Helm (2001) proposed an adjusted expression.

$$\varepsilon_{vol}^{pl} = \frac{a\tilde{N}}{b+\tilde{N}} \tag{4.46}$$

with:

- a, b : material parameters
- Ñ : loading parameter, $\tilde{N} = \int J_2 dN$.

The value of the parameter a follows from the maximum achievable volume strain.

$$a = \frac{e_{\min} - e_0}{1+e_0} \tag{4.47}$$

with:

- e_{min} : minimum achievable void ratio (as will be discussed in section 4.7.4 this value may be smaller as the minimum void ratio from standardised laboratory testing)
- e_0 : initial void ratio.

The value of b is to be derived from the empirical constants C_1 and C_2 by minimizing the difference by the given compaction curve and the curve according to Sawicki for the interval $0 < \tilde{N} < 0.1$.

4.7.4 C/L model, empirical data

The empirical parameters C_1 and C_2 are to be derived from cyclic simple shear testing. Table 4.2 summarises some of the parameters reported in the literature.

In figure 4.20 the empirical data are shown as function of the relative density. For the medium dense sand and the dense sand the relative density is taken as 0.5 and 0.8 respectively. As the value of C_2 for the dense Kozienice sand is out of the range of the other values the parameters for this sand are omitted.

The value of C_2 varies between 0.05 and 0.25, with C_2=0.13 as a best estimate. It is probably independent of the relative density. The value of C_1 seems to be a function of the relative density. Fitting a straight line through the data points gives:

$$C_1 = 13.3 - 7.4 * I_D \tag{4.48}$$

For a relative density of I_D = 1 the value of C_1 is about 5.9. This suggests that sand at the maximum density according to the standard laboratory procedures still will densify under prolonged loading.

sand	relative density	C_1	C_2	D_1	D_2	source
Seymen	0.34	6.54	0.15	1.01	0.153	(Sawicki 2004)
Golcuk	0.41	9.26	0.25	2.28	0.108	
Eregli	0.38	9.52	0.17	1.6	0.105	
Derince	0.48	7.14	0.28	1.97	0.14	
fine sand	0.91	7.52	0.03	0.212	0.133	(Sawicki and Sliwinski 1989)
	0.50	12.35	0.06	0.786	0.081	
	0.30	14.93	0.07	0.99	0.067	
Hostun2 sand	0.72	6.71	0.05	0.339	0.149	
	0.32	8.55	0.10	0.84	0.117	
	0.08	14.50	0.06	0.815	0.069	
Kozienice sand	medium dense	13.18	0.14	1.85	0.076	(Sawicki and Swidzinski 1989a)
	dense	4.87	1.26	6.14	0.205	
silica sand	medium dense	8.7	0.2	1.74	0.14	
Lubiatowo sand	dense	7.52	0.19	1.41	0.133	(Sawicki and Swidzinski 1989b)

Table 4.2 Empirical data C/L model, values are valid for strain unit 10^{-3}

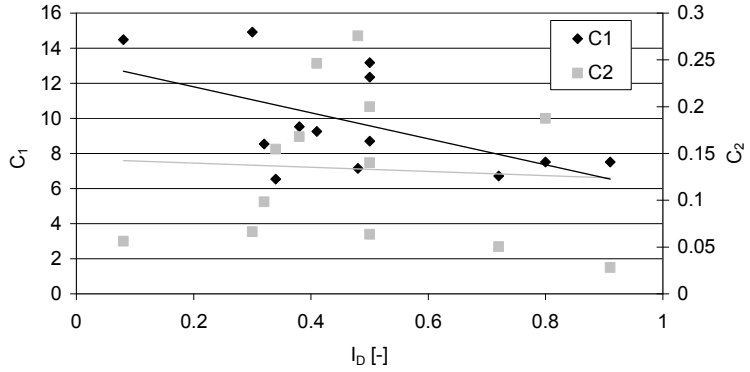

Figure 4.20 Empirical data C/L model (data from table 4.2)

It is tempting to see what the maximum achievable density is, using these empirical data. From the derived empirical expression for C_1 one may conclude that for I_D = 1.8 the value of C_1 becomes zero. This suggests that the real maximum density is achieved at I_D = 1.8. As this value is derived from extrapolating the empirical expression well beyond the tested range of relative densities this value is to be used with care.
Obtaining a relative density above 1 is not impossible. Youd (1972) shows results of cyclic direct simple shear tests where after a large number of loading cycles a kind of maximum achievable density is reached. Using the given values of

minimum and maximum density in his paper the maximum achieved density in his tests corresponds to a relative density of about 1.25.

4.7.5 Cyclic fatigue model

Ibsen (1993, 1994) developed a new densification model, called the cyclic fatigue model. The model is based on the results of a large series of cyclic triaxial tests with varying initial stresses and stress amplitudes. The tests are performed on samples with an H/D ratio of 1 and smooth end platens. In his opinion triaxial tests with H/D = 2 induce inhomogeneities in the sample and therefore do not represent the correct soil behaviour.

In the stress space a CL-line (critical line) is defined. This line represents the 'characteristic state', the p'-q state at which the soil behaviour changes from contraction to dilation.
During undrained cyclic loading the stress point in the effective stress space will move to this line. This implies that soil with a stress point below this line (small initial relative deviator stress) will contract and points above this line will dilate. The CL-line is said to be independent of the relative density of the soil, so even dense sand can contract and densify. Loose sand will not dilate as for this type of soil the failure line will coincide with the CL-line and stress points above the CL-line are not possible.

Ibsen also defines a CSL-line (cyclic stable line) which is located below the CL-line. Figure 4.21 illustrates the concept of the CSL line. This line represents the stress situation where the positive and negative pore pressure generated during a loading cycle neutralizes each other. This represents the situation where prolonged undrained cyclic loading does not result in a change in pore pressure. Figure 4.22 shows the results of his tests. Identical results are obtained by Luong (1981).

For the analysis of the stress situation Ibsen defines a mobilisation index M. This index defined as:

$$M = \frac{q'}{\left|q'_f(p')\right|} \tag{4.49}$$

with:

- q` : deviatoric stress
- $q`_f(p')$: deviatoric stress at failure for an isotropic stress p'.

M=0 is represents an isotropic stress condition, M=1 represents a stress point at the failure line.

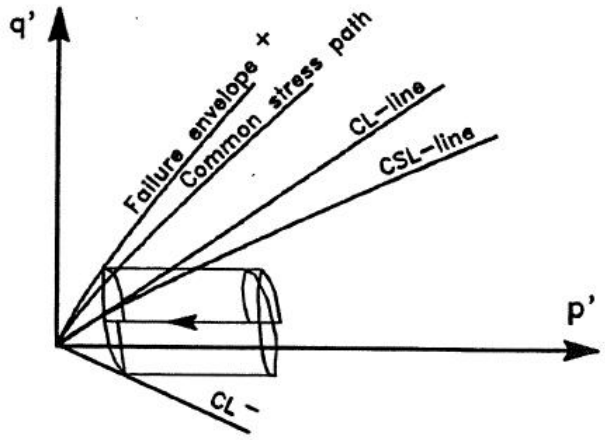

Figure 4.21 Concept of CSL line

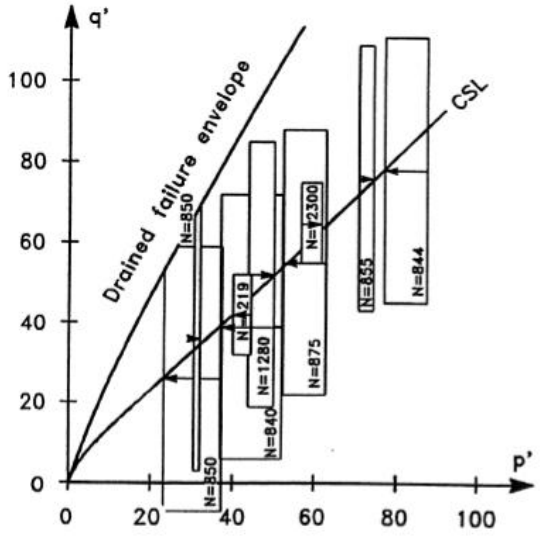

Figure 4.22 Test results by Ibsen

The cyclic fatigue model prescribes the development of M as a function of the number of cycles:

$$M_m = M_m^0 + (M_m^\infty - M_m^0) f(N) \tag{4.50}$$

with:

- M_m : mean value of M
- M_m^0 : value of M at start of the test
- M_m^∞ : end value of M_m.

The value of M_m^{∞} depends on the stress state and deviator amplitude. A yield indicator M_y is defined as:

$$M_y = k_q M_s \tag{4.51}$$

with:

- M_s : value of M for a point at the CSL line.

The parameter k_q is defined as:

$$k_q = \frac{q_m + q_{cyk}}{q_m} \tag{4.52}$$

with:

- q_m : the static (mean) deviator stress
- q_{cyk} : the amplitude of the deviator stress.

If M_y >1 then $M_m^{\infty} = M_m^{max}$. If M_y <1 then $M_m^{\infty} = M_s$.

From the test results Ibsen derived expressions for the different parameters. The relation with the number of cycles is described with:

$$f(N) = \left(\frac{N}{N + N_0} \right)^l \tag{4.53}$$

with:

- N_0 : empirical parameter
- L : empirical parameter.

In this model the value of M can increase or decrease, depending on the value of M_m^0 and M_m^{∞}. This implies that positive or negative excess pore pressures may develop.
From an analysis of performed triaxial tests results the following values for the different parameters are derived:

- l = 1.24
- M_s = 0.5
- $N_0(M_m^0) = 8*(1- M_m^0)/ M_m^0$.

The equation for $N_0(M_m^0)$ is valid for $M_m^0 > 0.2$. No tests have been performed with $M_m^0 < 0.2$.
Extrapolating the equation to $M_m^0 = 0$, so no deviatoric stress at start of the test, yields N_0 = +INF. This implies that no densification at all will occur.

4.7.6 Finn's model

In Finn's model (Molenkamp 1985) the volumetric strain increment is supposed to consist of an elastic and a plastic component:

$$\Delta\varepsilon_{vol} = \Delta\varepsilon_{vol}^{el} + \Delta\varepsilon_{vol}^{pl} \tag{4.54}$$

The plastic volumetric strain during one complete cycle with amplitude $|\gamma|$ amounts:

$$\Delta\varepsilon_{vol}^{pl} = C_1\left[\Delta\gamma - C_2\varepsilon_{vol}^{pl} + \frac{C_3(\varepsilon_{vol}^{pl})^2}{\Delta\gamma + C_4\varepsilon_{vol}^{pl}}\right] \tag{4.55}$$

with:

- C_1, C_2, C_3, C_4 : empirical parameters.
- $\Delta\gamma$: shear strain amplitude
- ε^{pl}_{vol} : plastic volume strain.

The number of empirical constants may be reduced. Molenkamp (1985) has shown that $C_3 = C_2C_4$. Further it has been assumed that the plastic strain can only be positive (contractive). From the last requirement follows that $C_4 \geq C_2$.
For an undrained condition the net volume strain consists of the compression of the pore water and of the soil grains. Assuming that the soil grains are incompressible, the net volume strain is:

$$\Delta\varepsilon_{vol} = \frac{n}{K_w}\Delta u \tag{4.56}$$

with:

- Δu : change in pore pressure
- K_w : bulk moduluswater

The net volume strain can be considered as the sum of an elastic and a plastic volume strain:

$$\Delta\varepsilon_{vol} = \Delta\varepsilon_{vol}^{el} + \Delta\varepsilon_{vol}^{pl} = \frac{\Delta\sigma}{E_{ur}} + \Delta\varepsilon_{vol}^{pl} \tag{4.57}$$

with:

- E_{ur} : elastic unloading/reloading modulus ($E_{ur} = d\sigma_v/d\varepsilon_{vol}$)
- $\Delta\sigma$: change in effective stress ($\Delta\sigma = -\Delta u$)

From this the relation between excess pore pressure and plastic volume strain in undrained condition follows:

$$\Delta u = \frac{\Delta\varepsilon_{vol}^{pl}}{\frac{1}{E_{ur}} + \frac{n}{K_w}} \tag{4.58}$$

It is stated that the empirical parameters can be derived from cyclic tests. As a first indication the following parameters are mentioned:

- C_1 = variable (0.005 to 0.8)
- C_2 = 0.8
- C_3 = 0.64
- C_4 = 0.8.

It is not clear how the influence of the relative density is accounted for in this model. Most likely the parameter C_1 is a function of the relative density.

In order to gain some understanding of the model's behaviour for large numbers of cycles the expression is rewritten as:

$$\Delta\varepsilon_{vol}^{pl} = C_1\left[\Delta\gamma + C_2\varepsilon_{vol}^{pl}\left(\frac{C_4}{\frac{\Delta\gamma}{\varepsilon_{vol}^{pl}} + C_4} - 1\right)\right] \tag{4.59}$$

For large values of ε^{pl}_{vol} ($\varepsilon^{pl}_{vol} >> \Delta\gamma$) the equation becomes:

$$\Delta\varepsilon_{vol}^{pl} = C_1\left[\Delta\gamma + C_2\varepsilon_{vol}^{pl}\left(\frac{C_4}{C_4} - 1\right)\right] = C_1\Delta\gamma \tag{4.60}$$

This implies that, according to this model, densification continues forever and no end value will be reached.

4.7.7 Energy dissipation model, description

In recent years efforts are made to correlate the generation of excess pore pressure to the dissipated energy during cyclic loading.
In cohesionless soil the dominant mechanisms of energy dissipation are frictional sliding at grain-to-grain contact and, in saturated soils, viscous drag of pore fluid moving relative to the soil skeleton. For large strains the energy dissipation due to viscous drag becomes small compared to the frictional energy dissipation (Green 2001). Therefore the energy dissipation due to viscous drag will be neglected. This is further justified considering that in the interpretation of cyclic test results, used for drafting the empirical relation between energy dissipation and excess pore pressure, this mechanism is neglected as well.

The dissipated energy per unit volume is given by:

$$E_{dis} = \int \sigma d\varepsilon^{p} \tag{4.61}$$

For a simple shear test is the energy dissipation described by:

$$E_{dis} = \int \tau d\gamma = \int \tau(t) * \gamma(t) dt \tag{4.62}$$

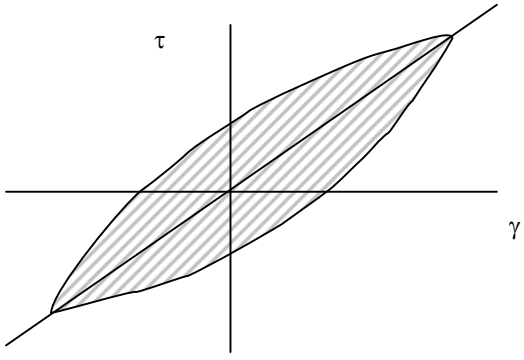

Figure 4.23 Illustration stress-strain behaviour during cyclic loading, the shaded area is the dissipated energy per cycle

Densification itself is a process of re-arranging the soil particles. It does not result in an increase of the energy content (either kinematic, elastic or potential) of the soil. Strictly spoken one can argue that some potential energy is lost in this process due to the vertical movement of the soil. A direct theoretical relation between the dissipated energy and the plastic strain is thus not present.
This dissipated energy is consumed as a rise in temperature. Indeed Luong (1986) shows measurements of the temperature rise are during cyclic testing of sand.

Different researchers have developed empirical equations for the relation between dissipated energy and excess pore pressure. Green (2001) gives an overview of 13 equations from different authors. Most equations are of the type:

$$r_u = \alpha \left(\frac{\Delta E_{dis}}{\sigma'_{v0}} \right)^{\beta} \tag{4.63}$$

or:

$$r_u = 1 - \exp(-\alpha \frac{\Delta E_{dis}}{\sigma'_{v0}}) \tag{4.64}$$

with:
- ΔE_{dis} : dissipated energy
- α : empirical parameter
- σ'_{v0} : initial vertical effective stress.

A version of equation 4.63 is, in their notation, the GMP (Green Mitchell Polito) model.

$$r_u = \sqrt{\frac{\Delta E_{dis}}{PEC}} \tag{4.65}$$

with:
- PEC : Pseudo Energy Capacity, a calibration parameter.

The value of PEC is found to be a function of CSR (cyclic stress ratio, the ratio of the shear stress amplitude and the initial vertical effective stress) and relative density. Test results of PEC for Monterey sand (FC<30%) and Yatesville sand (FC < 30%) are shown by (Green 2001). The value of PEC for these sands differ significantly (e.g. for CSR = 0.2 and I_D = 50% the PEC is respectively 29.8 kNm/m^3 and 5.3 kNm/m^3). For the relative excess pore pressure this implies a difference of a factor 2.3.

Using these models for estimating the development of the excess pore pressure requires an additional model for estimating the energy dissipation per cycle.

4.7.8 Energy dissipation model, empirical data

Before using the energy dissipation model some guidance for selecting the value of PEC is needed. An attempt is made to derive such guidance for clean sand from an interpretation of published test data.

The following data are used:
- data from cyclic tests performed as part of the VELACS project (Arulmoli et al 1992)
- tests performed by Berghe (2001)
- test data from Polito (1999) as presented by Green (2001)
- test data collected by Ostadan et al (1996) as part of an NIST investigation
- data from (Kazama et al 2000) and (Towhata and Ishihara 1985)

For sand the friction at which grains start to slide along each other is proportional to the normal force at the grain interface. It is therefore logical to assume that the dissipated energy is proportional to the effective stress. This approach is commonly used and proved to be reasonable. It will be used here as well.

As part of the VELACS project (VErification of Liquefaction Analyses by Centrifuge Studies) a series of cyclic tests is performed at Nevada sand and Bonnie silt.
In the reports no values for PEC or the dissipated energy are given. Therefore the data are re-analysed. For each test the development of the dissipated energy is determined. The development of the excess pore pressure is plotted as function of the development of the dissipated energy. Through the obtained curve a line is fitted for the average excess pore pressure as function of the dissipated energy, using a square-root function. The value of PEC is determined thus that for r_u=0.8 the correct relation is obtained. From this line the value of for each test PEC is obtained. Unfortunately not for all tests the value of r_u=0.8 could be used. These tests are omitted for the interpretation Figure 4.24 shows the used approach.

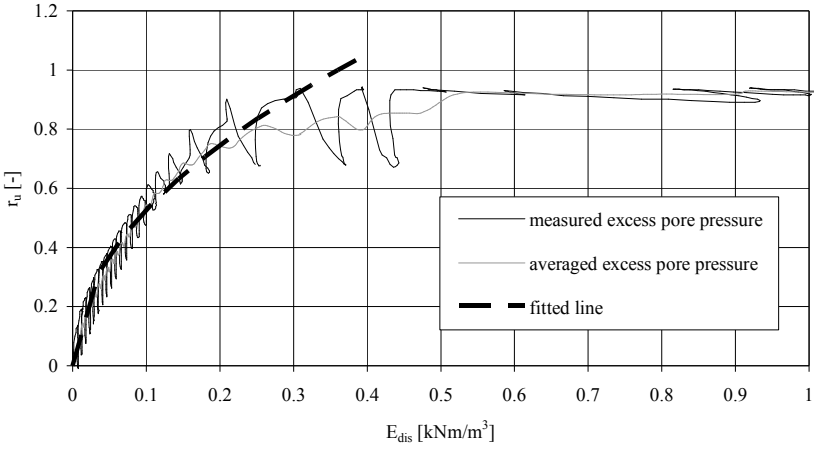

Figure 4.24 Assessment value of PEC (VELACS, test CY60-32)

Test data for Nevada sand are summarised in table 4.3 and figure 4.25. Here also the obtained values for PEC are given.

type of test	test number	effective consolidation pressure (kPa)	void ratio	I_D	static shear stress (kPa)	shear stress amplitude (kPa)	PEC	PEC/σ'_{v0}
cyclic simple shear test	CSS4009	80	0.715	0.459	0	7.4	0.23	0.0029
	CSS4008	80	0.719	0.449	0	14.5	0.82	0.0103
	CSS4007	160	0.725	0.433	0	11.4	0.365	0.0023
	CSS4006	160	0.727	0.426	0	21.5	1.54	0.0096
	CSS4010	160	0.723	0.438	3.1	11.5	0.365	0.0023
	CSS4011	160	0.732	0.414	3.3	11.8	0.41	0.0026
	CSS6005	80	0.652	0.627	0	12.4	0.66	0.0083
	CSS6004	80	0.65	0.63	0	23.6		
	CSS6007	160	0.661	0.601	0	13.4	1.32	0.0083
	CSS6006	160	0.656	0.614	0	26.1	2.34	0.0146
	CSS6008	160	0.655	0.617	0	26.2		
	CSS6009	160	0.654	0.621	5.9	13.7	0.73	0.0046
cyclic triaxial test	40-115	40	0.731	0.416	0	18.6	0.23	0.0058
	40-69	40	0.736	0.403	3.9	18.4	0.82	0.0205
	40-68	40	0.733	0.41	6.3	26.9	0.365	0.0091
	40-114	80	0.728	0.424	0	28.8	1.54	0.0193
	40-71	80	0.729	0.42	17	29.4	0.365	0.0046
	40-73	80	0.725	0.431	25.3	43.1	0.41	0.0051
	40-116	160	0.728	0.423	0	48.8	0.23	0.0281
	40-50	160	0.727	0.428	20.7	48.4	0.82	0.0059
	40-58	160	0.73	0.418	21.5	47.8	0.365	0.0054
	40-65	160	0.729	0.422	29.5	71.3	1.54	0.0191
	60-88	40	0.659	0.606	0	24.4	0.7	0.0175
	60-25	40	0.656	0.656	5.5	17.9	0.57	0.0143
	60-32	40	0.654	0.62	5.8	18	0.63	0.0158
	60-34	40	0.653	0.622	8.6	26	0.94	0.0235
	60-35	40	0.657	0.612	8.3	26.5	1.14	0.0285
	60-86	80	0.656	0.616	0	40.3	1.42	0.0178
	60-87	80	0.656	0.616	0	60.2	1.23	0.0154
	60-36	80	0.656	0.616	7.5	29.6	0.3	0.0038
	60-24	80	0.66	0.605	7.8	29.6	0.38	0.0048
	60-38	80	0.656	0.615	11.2	44.4	1.36	0.0170
	60-37	80	0.65	0.631	11.4	43	0.72	0.0090
	60-29	160	0.663	0.595	33.5	60.5	1.56	0.0098
	60-30	160	0.65	0.63	33	60.3	2.5	0.0156
	60-31	160	0.653	0.624	47.5	90.2	0.7	0.0175

Table 4.3 Tests results VELACS on Nevada sand

The obtained values show a large scatter. The general trend is an increase of PEC with increasing relative density. In general the cyclic triaxial tests show a larger value as the cyclic DSS tests.

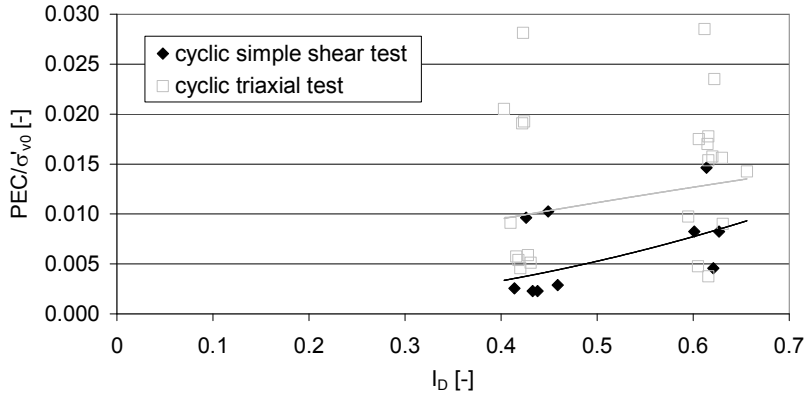

Figure 4.25 Normalised value of PEC as function of relative density, Nevada sand

Berghe (2001) performed both cyclic triaxial tests and cyclic simple shear tests on Brussilian sand. The tests are undrained and strain controlled. The relative density varied between approximately 60% and 85%, the applied shear strain amplitude in general between 0.1% and 5%. Some tests with a small shear strain amplitude (<0.015%) did not show degradation. Figure 4.26 shows the obtained value of dissipated energy at liquefaction for all tests.

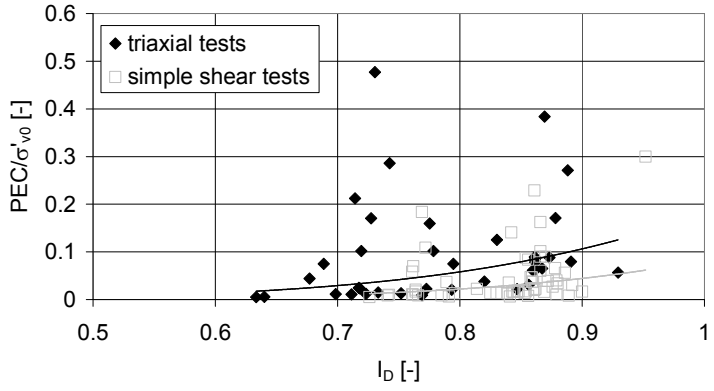

Figure 4.26 Value of PEC from test data by Berghe (2001)

A wide range in obtained values is observed. The general trend is however again that the value increases with increasing relative density.

Green (2001) analysed cyclic tests on Monterey sand-silt mixtures and Yatesville sand-silt mixtures. The cell pressure is 100 kPa. Figure 4.27 shows the obtained values for PEC in their tests. Again a large scatter in values is obtained. The

general trend however still remains an increase in the value of PEC with increasing relative density.

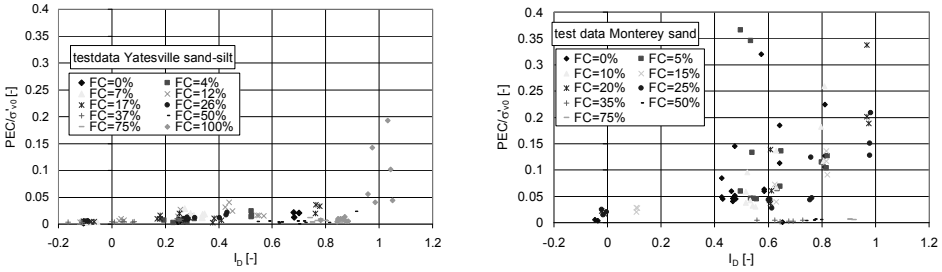

Figure 4.27 Value of PEC for Monterey sand and Yatesville sand, data from (Green 2001)

Two observations can be made from these figures. The first is that there is a large difference between the two types of sand. The second is the influence of the fines content. Soil with a fines content of 35% or more show a noticeable smaller value of PEC as sands with a low fines content. Green (2001) states that the value of PEC is not only a function of the relative density but also of the shear strain amplitude. This aspect is not taken into account in the present analysis.

Ostadan et al (1996) collected, as part of a feasibility study for energy-based liquefaction analyses, a large number of results from cyclic testing of different types of sand. The main results are shown in figure 4.28. Again a wide scatter is found but a general trend of increasing value of PEC with increasing relative density is found.

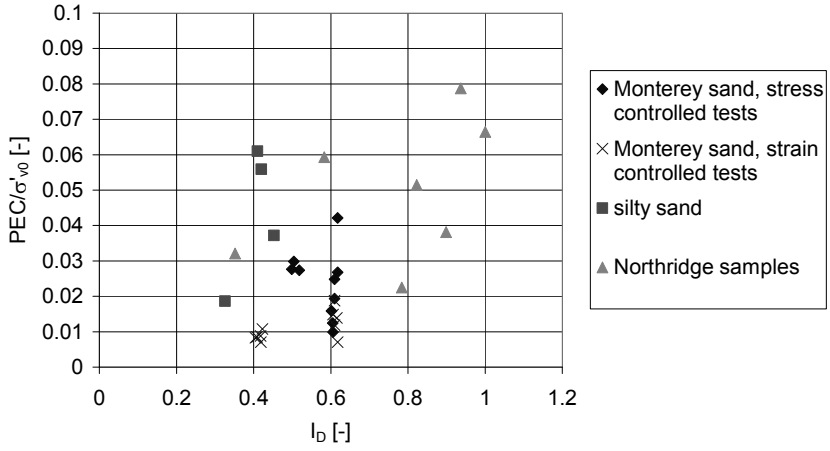

Figure 4.28 Test data from (Ostadan et al 1996)

In addition to these large datasets some additional test data are collected from the literature. These are summarised in table 4.4.

sand	source	I_D [-]	σ'_{v0} [kPa]	PEC [kNm/m^3]	PEC/σ'_{v0} [-]
Toyoura	(Kazama et al 2000)	0.15 0.83			0.003 0.065
Masado		0.49			0.011
Toyoura	(Towhata and Ishihara 1985)	0.5	294	5	0.017

In (Kazama et al 2000) the used stress level is not reported

Table 4.4 Empirical data from literature

It must be concluded that the different data show a large variation. In order to derive an expression that can be used as a first estimate for the dissipated energy at liquefaction (PEC) representative values from the different sources are selected. Table 4.5 and figure 4.29 show shows the selected values as function of the relative density.

sand/source	I_D	PEC/σ'_{v0}
VELACS (Arulmoli et al 1992)	0.4 0.6	0.005 0.009
Brussilian sand (Berghe 2001)	0.7 0.8 0.9	0.03 0.06 0.11
Monterey sand (Green 2001)	0.45 0.8	0.05 0.17
Yatesville sand (Green 2001)	0.3 0.7	0.01 0.018
Monterey sand (Ostadan 1996)	0.5 0.6	0.08 0.02
Northridge samples (Ostadan 1996)	0.35 0.8 1	0.032 0.037 0.07
Toyoura sand (Kazama et al 2000))	0.15 0.83	0.003 0.65
Masado sand (Kazama et al 2000)	0.49	0.011
Toyoura sand (Towhata and Ishihara 1985)	0.50	0.017

Table 4.5 Summary of all data

From figure 4.29 the following empirical relation is derived as estimate for the value of PEC as function of the relative density.

$$\frac{PEC}{\sigma'_{v0}} = 0.07 * I_D^{1.7} \qquad (4.66)$$

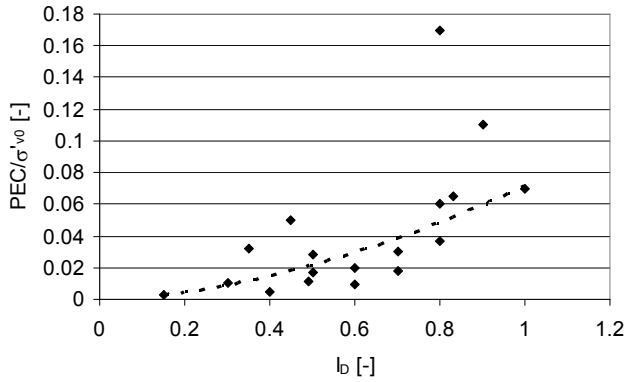

Figure 4.29 Relation between PEC and relative density, summary of all data

It is to be realised that this value is derived neglecting the possible influence of the cyclic stress ratio on the value of PEC. It is therefore to be used as a first estimate for the value of PEC.

4.7.9 Seed and Rahman model

Seed and Rahman (Seed and Rahman 1978) describe a model for assessing the generation of excess pore pressure due to wave loading of the seabed. The principles of this method are implemented in the computer code MCYCLE, developed by GeoDelft (Groot and Meijers 1992). This is a computer program for calculating the development of excess pore pressure in a seabed loaded by waves.

Basis for the model is the observed development of the excess pore pressure in stress controlled cyclic testing. A typical example is shown in figure 4.30.

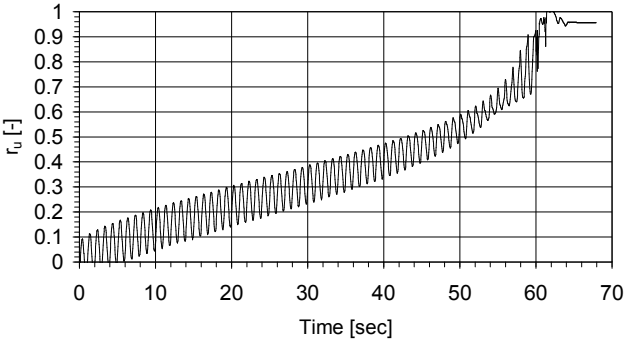

Figure 4.30 Example development relative excess pore pressure during a cyclic triaxial test (VELACS test CYT40-71)

The observed development can be described with the following equation:

$$r_u = \frac{2}{\pi}\arcsin\left(\frac{N}{N_{liq}}\right)^{1/2\theta} \quad (4.67)$$

with:

- r_u : relative excess pore pressure (ratio between excess pore pressure and initial effective vertical stress)
- N : applied number of cycles
- θ : empirical parameter, a reasonable estimate is $\theta = 0.7$
- N_{liq} : number of cycles to liquefaction in an undrained situation.

For the value of N_{liq} the following empirical relation is used (Rahman and Jaber 1986):

$$\frac{\Delta\tau / \sigma'_{v0}}{I_D} = a.N_{liq}^{-b} \quad (4.68)$$

with:

- I_D : relative density
- $\Delta\tau$: shear stress amplitude
- σ'_{v0} : initial effective vertical stress
- a, b : empirical parameters, reasonable estimates are a = 0.48 and b = 0.2.

The continuous generation and dissipation of excess pore pressure results in an adjustment of the grain skeleton (densification and preshearing).
Two options are available. The first is to continuously adjusting the relative density and from that the number of cycles to liquefaction. This approach however does not account for the change in soil fabric. The second method is to adjust the value of $N_{liq,0}$, using an empirical relation e.g. based on the tests by Smits et al (1978), see also section 4.4.

$$N_{liq} = N_{liq,0} * 10^{-X\Delta n} \quad (4.69)$$

with:

- N_{lig} : number of cycles to liquefaction after change in porosity of Δn
- $N_{liq,0}$: number of cycles to liquefaction without preshearing
- X : history parameter
- Δn : change in porosity (in unity).

4.7.10 Accumulation model

Andersen (1976, 1992, 1996) developed a method to determine the pore pressure generation under cyclic loading. The method is based on the use of pore pressure contour diagrams. The diagrams should be site specific. The method consist briefly of applying a number of cycles with a given shear stress amplitude. From the contour diagram the pore pressure is derived. After that some drainage is allowed, which reduces the excess pore pressure. The analysis is continued with the next batch of cycles.

In (Kvalstad and Groot 1999) graphs showing the developed excess pore pressure for medium dense fine sand and dense silty sand are shown. A contour diagram for dense silty sand is reproduced here as figure 4.31.

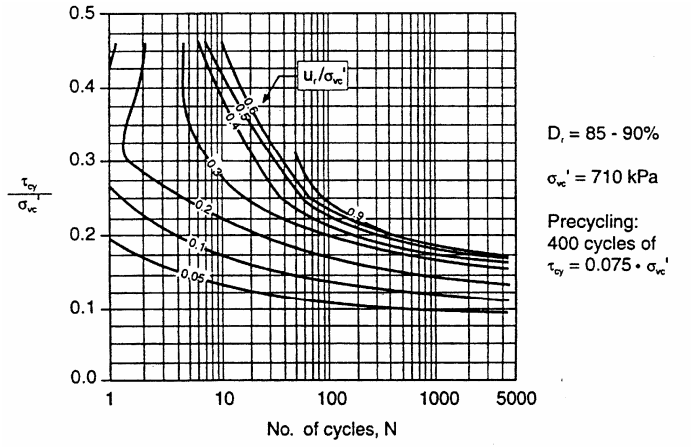

Figure 4.31 Pore pressure accumulation diagram (from Kvalstad and Groot 1999)

The procedure to assess the development of the excess is as follows:

1. construct the pore pressure contour diagram using site specific cyclic direct simple shear tests; if necessary complete the diagram with information from similar soils
2. determine the residual excess pore pressure due to cyclic loading and drainage.

Replotting the data of figure 4.31 yields curves similar to those used in the Seed and Rahman model (see figure 4.32).

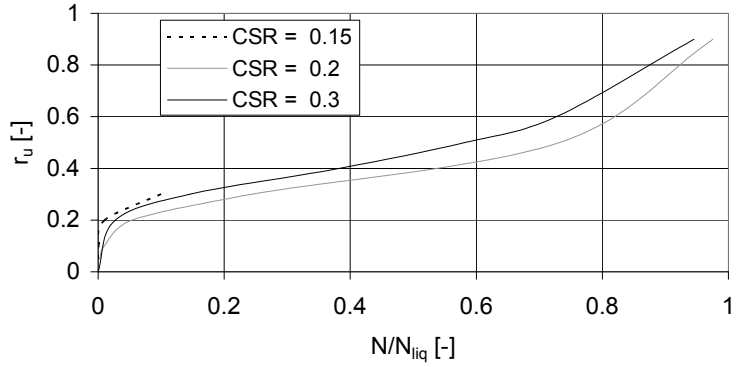

Figure 4.32 Development excess pore pressure according using data from figure 4.31 (accumulation curve Andersen) (CSR is the cyclic stress ratio, CSR = $\Delta\tau/\sigma'_{v0}$)

The method may be considered to be an alternative for the selection of the development of the excess pore pressure in the Seed and Rahman method. The main difference is that Seed and Rahman use mathematical expressions for the pore pressure generation where Andersen uses a graphical representation of the test results.

4.8 Discussion on the densification models

Most of the models use the shear stress amplitude or the shear strain amplitude as loading parameter. These two parameters are uniquely connected through the shear modulus. Thus from a practical point of view they can be considered as the same loading parameter. The model by Barkan is an exception as it used the acceleration amplitude as loading parameter. The relation between the acceleration amplitude and the shear strain amplitude exists is frequency dependent.

When using the acceleration as loading parameter one may conclude that for is that for low frequency cyclic loading the densification is zero, as the acceleration amplitude is nearly zero in such a case. The large amount of published results for cyclic direct simple shear and cyclic triaxial testing clearly show that even for low frequency loading densification and generation of excess pore pressure occurs. Therefore the use of the acceleration amplitude as loading parameter is considered less realistic and not describing the actual physical behaviour.

Different models suffer from a lack of reliable estimates for the empirical parameters in the model. For some of the models (the C/L model and the energy dissipation model) it is possible to derive a correlation between the relative density and the empirical parameters from available test results. These correlations can be used for a first approximation. The Barkan model and the Seed and Rahman model already use the relative density as model parameter. For the cyclic fatigue model and Finn's model no reliable empirical parameters are available for a wide range of relative densities. This restricts the use of these models for practical applications.

The model by Barkan is the only model that takes into account a threshold value below which no densification occurs. For situations with low vibration amplitudes the threshold value may be of relevance and some adjustment of the model is needed. The situation of vibratory sheet piling is such a situation. The shear strain amplitude will decrease with distance the sheet pile and may achieve values well below the threshold value. Neglecting the threshold value will overestimate the area with densification. A practical approach is to define a threshold value and set the densification in ranges where the amplitude is below this value to zero. As postulated before it is anticipated that below the threshold value still some densification may occur. For the situation during vibratory sheet piling this may be marginal compared to the densification close to the sheet pile.

The cyclic fatigue model is considered to be attractive and seems to capture some interesting phenomena. The present version of the model however exhibits some shortcomings. The model is independent of the shear stress amplitude. As Ibsen

already noticed this cannot be correct. The influence of the relative density is not explicitly accounted for. In the tests on which this model is based the influence of the relative density has not been investigated. Most likely the influence of the relative density is to be accounted for in some of the empirical constants. No information on this is presently available.
For an isotropic initial stress condition ($M_m^0 = 0$) the value of N_0 becomes infinite and thus the function f(N) always returns a zero. This implies that, according to this model, for an isotropic stress condition no excess pore pressures are generated.
It is concluded that the present version is not yet suited for use in practical problems. More research and modelling is needed before this model can be used.

The C/L model does not contain an upper limit on the amount of densification. This implies that for large number of cycles and a large strain amplitude the densification may reach unrealistic values. It is clear that for situations with large number of large amplitude loadings the situation is beyond the limits of the model. An alternative formulation for such a situation may be the expression proposed by Niemunis and Helm (2001). This alternative model requires an estimate of the maximum possible densification.
At the other side of the loading spectrum, the situation with small strain amplitudes, no allowance is made for a possible threshold shear strain amplitude.
For most problems these two aspects are of minor concern and the calculated amount of densification with this model will be within acceptable limits.

The practical use of the Finn's model is limited. At present there is no guidance for estimating the empirical parameters without performing laboratory tests. As with most densification models the situation for small strain amplitudes and for a large number of loading cycles is not well described.

The use of an energy dissipation model is at first sight a logical approach. Densification occurs when grains are sliding along each other. The friction in this process results in energy dissipation. Luong (1986) has shown with infrared thermography that the temperature of a sample rises during cyclic loading. The loading parameter in this model is the dissipated energy, which in turn may be represented by the shear stress amplitude and the shear strain amplitude. Depending on the used expression for the relation between energy dissipation and excess pore pressure the relative excess pore pressure may be limited to 1 or may achieve values in excess of 1. It is clear that the latter situation is outside the validity range of the model.

The model of Seed&Rahman is developed for assessing the generation of excess pore pressure. The original model does not take into account the beneficial effect of preshearing. With the extension for taking into account the effect of preshearing on the number of cycles to liquefaction, as proposed by Smit, the model is well suited for use in situations where the combined effect of generation and dissipation is present as e.g. in situations of wave loading and vibratory sheet piling.

The accumulation model is attractive as it can be used graphically. Before the method can be used the relevant graphs are to be constructed from cyclic tests or

selected from databases. The absence of clear mathematical expressions is a disadvantage of the model for use in a computer code.

From the described models a selection is made for possible further use in overall model to be developed. Requirements for the selection are:
- physically sound
- relatively straightforward
- applicable for a wide density range
- capturing the relevant mechanism during vibratory sheet piling (combined effect generation and dissipation of excess pore pressure)
- model parameters are readily available, either by simple testing or from correlations.

This leaves the following models as promising models:
- C/L model
- energy dissipation model
- Seed&Rahman model.

In addition to this the model developed by Hergarden (a version of the Barkan model, see section 3.7) is used as well for comparison purposes. The implementation of these models in the final model is described in chapter 6.

5. Cyclic triaxial tests on sand from Raamsdonksveer

5.1 Testing procedure

5.1.1 Purpose of the testing

The aim of the cyclic triaxial tests is twofold:
- obtain additional insight in the behaviour of sand under cyclic loading
- obtain empirical parameters for the validation of the new model.

These aspects are described further below.

The literature review on cyclic behaviour of sand under cyclic loading shows that an overwhelming amount of literature on this subject is available. Still certain aspects are hardly investigated. Among them are the behaviour for situations of large number of cycles with small loading amplitude, the effect of interim drainage and the effect of interim static loading. These aspects are of importance when considering the situation during vibratory sheet piling. The first aim of the tests is to gain more insight in these aspects.

In chapter 6 a new model is described for determining the amount of settlement during vibratory sheet piling. To check the validity of the model a well instrumented field test has been designed and executed at Raamsdonksveer, the Netherlands. This test and the results will be described in chapter 7. The second aim of the cyclic tests is to obtain the empirical parameters for the used densification models. For this reason the tests are performed on sand obtained from a boring at the site of the Raamsdonksveer sheet pile test.

5.1.2 Selection testing conditions

The test program is focussed on the behaviour of sand during vibratory sheet piling. Some characteristics of this process are:
- large number of cycles (typically in the order of 10,000 to 20,000)
- interim drainage (the duration of sheet piling is thus that it is neither completely drained nor completely undrained, drainage during the process will influence the behaviour)
- complicated stress path, expected to be mainly shearing
- vertical effective stress varies between nearly zero at the top to about 200 kPa at tip of the sheet pile
- shear stress amplitude will vary between zero at large distance to about 0.5*200*tan25° = 47 kPa at tip of the sheet pile; the relative shear stress ratio amounts $\Delta\tau/\sigma'_{v0}$ = 0.24; due to the shape of the sheet pile the shear stress amplitude just outside the wall may be larger (circumference of soil is less as circumference of the sheet pile)
- anisotropic initial stress level.

The following test conditions are selected:
- samples are fully saturated, also for the drained tests; this prevents problems with apparent cohesion/capillary stresses and enables to measure the volume strain from the amount of dissipated water volume
- isotropic stress condition (see below for a motivation)
- an isotropic effective stress of 100 kPa is used; this is well within the range of effective vertical stresses next to the sheet pile; it is also in agreement with the stress level usually used for the cyclic tests reported in the literature
- constant cell pressure (400 kPa) and backpressure 300 kPa
- stress controlled loading; using a strain controlled loading may result in some problems with the applied load amplitude during the test, in strain controlled loading a plastic vertical strain of the sample will result in a change in the vertical loading, it becomes asymmetric
- constant cell pressure, this implies that the loading is not truly a deviatoric loading but that the (total) isotropic stress changes as well
- two types of sand are used in order to gain some insight in the difference in soil behaviour
- some tests are repeated in order to check the reproducibility of the tests
- tests are performed both drained and undrained; the purpose is to check if it is possible to assess the undrained behaviour from the results of drained tests and vice versa; this is relevant as in prototype the behaviour is partly drained so in between fully drained and fully undrained behaviour; an alternative would be to use a slow drainage system during the tests, this complicates the test procedure and introduces another variable
- a few tests are performed with interim drainage to assess the effect of interim drainage on the liquefaction behaviour
- two tests are performed with static loading after dissipation of the excess pore pressure of the first phase, this static loading is to model the effect of excavation and subsequent backfilling of the building pit on the liquefaction behaviour
- height to diameter ratio of the sample is about 1:1 (diameter and height are approximately 6.6 cm and 7.47 cm), with lubricated end platens; this is selected in order to obtain a homogeneous stress field in the sample
- loading frequency 0.2 Hz
- data are logged with a sample frequency of 20 Hz, this gives 100 data points per cycle.

An isotropic initial stress condition is used. This is different from the situation in reality where the horizontal stress is about 0.5 times the vertical effective stress. Previous experience of the author with anisotropic initial stresses showed that this decreases the liquefaction potential significantly. This is also found in the tests by Ibsen. The resulting liquefaction potential is found to be unrealistic low. Therefore an isotropic initial stress is used.

A few tests are performed to mimic the stress history of sand close the sheet pile during the lifetime of a building pit. Excavation of the building pit results in a decrease of the horizontal stress, so a change in the ratio of the vertical to horizontal stress. In the triaxial testing this is imitated by a drained increase of the vertical stress from 100 kPa to 200 kPa and subsequent unloading. The ratio of the

vertical stress to the radial stress thus changes from 1 to 0.5 and back to 1. In this situation the sample is not brought to failure. The effect of failure, or large plastic deformations, on the soil properties is investigated by tests where the samples are subjected to an axial strain of 5% and subsequently unloaded.

5.1.3 General procedure

The samples are prepared inside a latex membrane, supported by a steel mould. A plexiglas cylinder with perforated bottom plate is placed on the lower lubricated end membrane and filled with a known mass of the sand. The required mass of sand is determined from the required relative density. The cylinder is then carefully lifted so creating the lowest possible density. If needed, the density is increased (the volume is decreased) by tapping on the steel mould until the desired density is reached. After reaching the desired density the upper lubricated end plate and the cap is placed. The sample is put under vacuum and the steel mould is removed. The cell is placed, filled with water and put at a low pressure. After removing the vacuum, the sample is flushed with CO_2, followed by de-aired water. The cell pressure of 400 kPa and backpressure of 300 kPa are applied.
After preparation of the sample the test is started. For nearly all tests no waiting time between preparation and testing is used. Therefore some creep and aging effects may have influenced the test results.

The lubricated end platen consists of a circular metal platen lubricated with silicon grease at which a latex membrane is placed (see figure 5.1). A central hole in the latex membrane allows drainage of the sample.

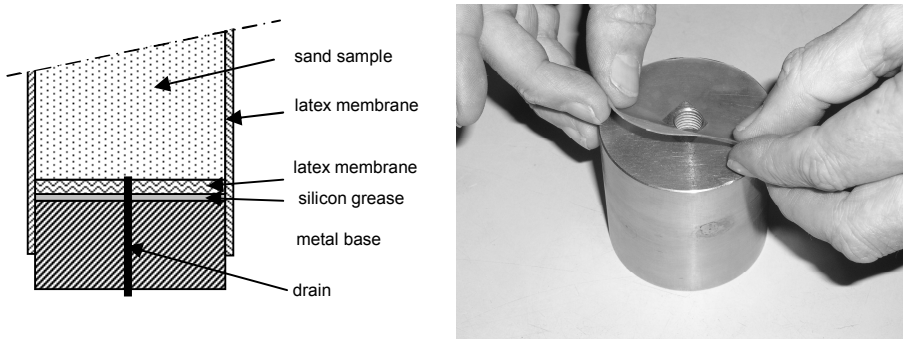

Figure 5.1 Lubricated end platen, left hand figure shows the situation, right hand figure placement of the latex membrane

All tests are performed with a B-factor of at least 0.99.
The B-factor is defined as:

$$B = \frac{\Delta u_1}{\Delta \sigma_c} \tag{5.1}$$

with:

- Δu_1 : change of pore pressure due to an applied change in confining cell pressure
- $\Delta \sigma_c$: change of cell pressure.

The undrained cyclic triaxial tests are continued until liquefaction occurred (excess pore pressure equal to the initial effective stress) or until at least 10,000 cycles are applied. No stop criterion with regard to the strain amplitude is set. In the drained cyclic triaxial tests the drainage valve is open so the sample is allowed to drain. These tests are continued for at least 10,000 cycles and in general for about 15,000 cycles.
For the cyclic triaxial tests with interim drainage the first part is continued until an excess pore pressure of about 70 kPa (excess pore pressure ratio about 70%) or 100 kPa (excess pore pressure ratio about 100%) is reached. After this the excess pore pressure is dissipated. In some tests a drained static loading and unloading is applied. After this the undrained cyclic loading is resumed until liquefaction.

5.1.4 Description of the used sand

The used sand is obtained from a boring at the site of the Raamsdonksveer sheet pile test. Full details of the subsoil conditions are described in section 7.3. From the boring two types of sand are selected, medium sized sand and coarse sand. Main characteristics of the sand, as measured before the cyclic testing, are given in table 5.1. The roundness is determined according to the classification method of Pettijohn, as used by GeoDelft. In section 7.3 the relation between this classification and the more popular classification by Powers is shown.

sand	sample number	depth [m+NAP]	d_{50} [mm]	$C_u = d_{60}/d_{10}$ [-]	e_{min} [-]	e_{max} [-]	ρ_s [g/cm^3]	roundness
medium	12	-10.1	0.222	1.725	0.548	0.894	2.655	0.46
coarse	8A	-5.8	0.664	2.312	0.452	0.817	2.642	0.34
	8B	-6.3	0.559	2.059	0.464	0.802	2.641	0.37

Table 5.1 Properties sand used in the laboratory testing, as measured before the testing

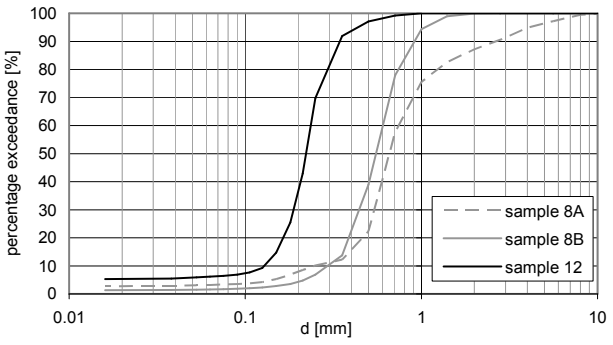

Figure 5.2 Grain size distribution used sand

5.1.5 Test program

Four types of triaxial tests are performed (between brackets the number of tests of each type is shown):
- cyclic, drained (13), the number of cycles is about 15,000
- cyclic, undrained (16), the test is continued till liquefaction
- cyclic, undrained with interim drainage and static drained loading (7).

In the cyclic tests the following parameters are varied:
- grain size and angularity (two types of sand are used)
- relative density, relative densities of 0.2, 0.4, 0.6 and 0.8 are used
- vertical stress amplitude, values of 10 kPa, 20 kPa, 30 kPa, 40 kPa, 60 kPa and 80 kPa are used.

Annex 5.1 gives an overview of the tests.

5.2 Test results and interpretation

5.2.1 Post processing test data

During the cyclic tests relevant data are sampled at a sampling frequency of 20 Hz. With a cycle period of 5 s this gives 100 data points per cycle. Logging of the data started after the cell pressure of 300 kPa is applied.

The raw data are stored in an ASCI file containing the following data:
- time (s)
- vertical force at the plunger (kgf)
- vertical displacement (mm)
- cell pressure (kPa)
- water pressure in sample (kPa)
- volume change (cc).

The data are processed with a special developed program. The program determines the following parameters:
- applied number of cycles
- vertical strain
- volume strain
- shear strain
- vertical stress
- shear stress
- dissipated energy.

Before processing the recorded values are smoothed in order to reduce the noise in the signal. For this smoothing a moving average over 5 data points is used. No correction for membrane penetration is used.

During the consolidation phase the sample already deformed a little. The actual sample size (height and diameter) at start of the cyclic loading are derived from the

values at preparation of the sample and the measured vertical and radial strain just before start of the cyclic loading.

In the post processing the following data are determined:
- number of cycles
- vertical strain
- volumetric strain
- shear strain amplitude
- vertical stress
- shear stress amplitude
- dissipated energy during cyclic loading.

The number of cycles is determined from the applied vertical force. A cycle is considered to be elapsed when the applied force crosses the initial vertical force one time both in a downward and in an upward direction.

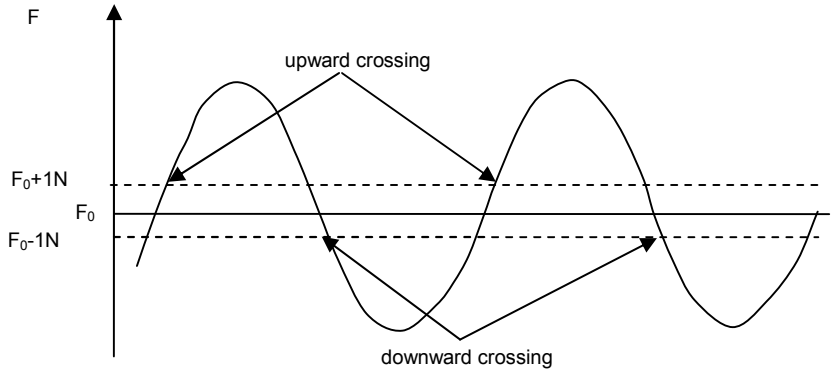

Figure 5.3 Definition of a zero passage

In order to avoid that small undulations during the time of no cyclic loading result in a large number of cycles a small offset is used. An upward crossing is defined as the situation when the vertical force at one time step is below a value 1 N above the value at rest and in the next time step above it. A downward crossing is defined as the situation when the vertical force at one time step is above a value 1 N below the value at rest and in the next time step below it.

The vertical strain follows from the recorded vertical displacement (with respect to the displacement at the start of the cyclic loading) divided by the height of the sample at start of the cyclic loading.
The volume strain follows from the measured volume change divided by the volume of the sample at start of the cyclic loading. The radial strain is not measured but follows from the vertical strain and volume strain:

$$\varepsilon_{rad} = 0.5 * (\varepsilon_{vol} - \varepsilon_z) \qquad (5.2)$$

with:
- ε_{vol} : volume strain
- ε_z : vertical strain
- ε_{rad} : radial strain

The shear strain is:

$$\gamma = \varepsilon_z - \varepsilon_{rad} = 1.5\varepsilon_z - 0.5\varepsilon_{vol} \quad (5.3)$$

The applied vertical stress follows from the applied vertical force divided by the cross section of the sample. The cross section is corrected for the radial strain.

The shear stress follows from:

$$\tau = 0.5(\sigma_z - \sigma_c) \quad (5.4)$$

with:

- σ_z : vertical stress
- σ_c : cell pressure

The dissipated energy E_{dis} in the sample, per unit of volume, during cyclic loading is derived from a summation over all scans using the following expression:

$$E_{dis} = \sum \sigma_z d\varepsilon_z \quad (5.5)$$

In principle the change in radial stress and strain also may result in a contribution to the dissipated energy. As the cell pressure is kept constant the change in stress is zero. The contribution to the dissipated energy thus consists of the net radial strain times the cell pressure. It is assumed that this component is negligible compared to the energy dissipated in the hysteresis loop of the vertical stress-strain.
The measured deformation includes both a plastic and an elastic component. The elastic component is a value varying periodically during each cycle.

For further analysing of the data the extreme values per cycle are determined.
For each interval representing one cycle the following values are determined:

- minimum and maximum value of the pore pressure
- minimum and maximum value of the vertical stress
- minimum and maximum value of the vertical strain
- minimum and maximum value of the volume strain
- minimum and maximum value of the dissipated energy.

The shear stress and shear strain amplitude are set as half the difference between the maximum and minimum value of respectively the shear stress and shear strain. The average volume strain and pore pressure at each cycle is set as the average of the maximum and minimum values of respectively the volume strain and pore pressure. The same holds for the dissipated energy at each cycle.

5.2.2 Results cyclic testing

In annex 5.2 to 5.6 the development of the excess pore pressure (undrained tests) or the development of the volume strain (drained tests) is shown. From the measured data the empirical parameters for the three selected soil densification model are derived. These are the C/L method, the energy dissipation method and the Seed&Rahman method. The models are described in chapter 4. Here the

method used to obtain the empirical parameters in these models from the test results is described first. After this the obtained values are presented.

5.2.3 Method deriving parameters energy dissipation model

The energy dissipation method assumes a relation between the dissipated energy during cyclic loading and the excess pore pressure. In this interpretation a power function is used.

$$r_u = \frac{\Delta u}{\sigma'_{v0}} = \left[\frac{E_{dis}}{PEC}\right]^n \tag{5.6}$$

with:

- r_u : excess pore pressure ratio
- Δu : excess pore pressure
- σ'_{v0} : initial effective vertical stress
- E_{dis} : dissipated energy
- PEC : Pseudo Energy Capacity, dissipated energy at time of liquefaction
- n : empirical parameter.

The method is illustrated with the results of test 12.12. Figure 5.4 shows the measured relation between the dissipated energy and the relative excess pore pressure. The curve is fitted with a power function.

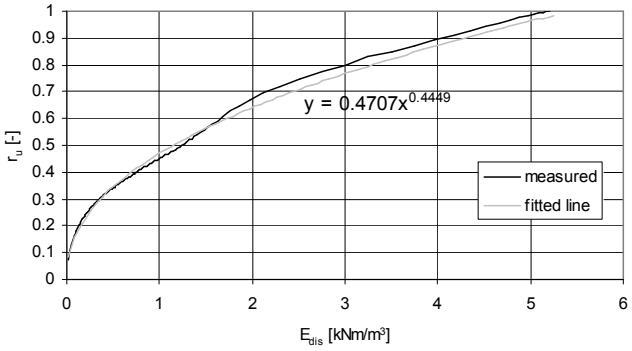

Figure 5.4 Development excess pore pressure as function of the dissipated energy

From this the following empirical parameters are derived:

- n = 0.4449 (1/n = 2.248)
- $PEC^{-n} = 0.4707$, this gives $PEC = 0.4707^{-1/n} = 5.44$.

One of the versions of the mentioned relation uses n = 0.5. Using this value an estimate for PEC is made. Rewriting the expression for the excess pore pressure gives:

$$PEC = \left(\frac{E_{dis}}{r_u^{1/n}} \right) \tag{5.7}$$

For each data point the value of PEC can thus be determined. Figure 5.5 shows the value as function of the applied number of cycles. In the model however the value of PEC is assumed to be a constant, so one single value is to be selected. In this case a value of PEC = 4.5 is selected.

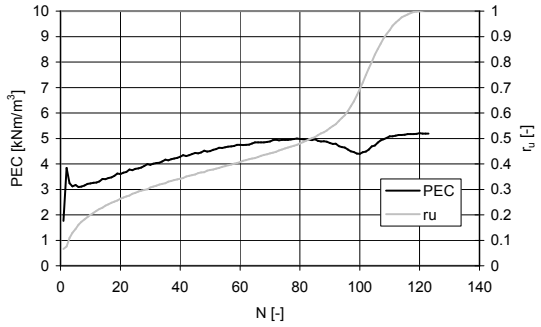

Figure 5.5 Estimate PEC from test data, using n=0.5

Figure 5.6 shows the measured development of the excess pore pressure compared with the fitted line.

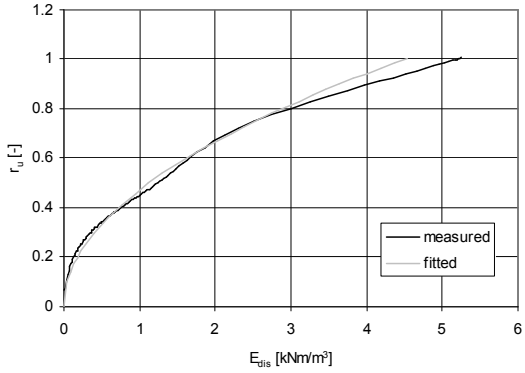

Figure 5.6 Comparison measured and fitted development of the excess pore pressure, using the energy dissipation model

5.2.4 Empirical parameters energy dissipation model from results undrained tests

The obtained empirical parameters for the different tests are given in table 5.2.

test I_D	[-] $\Delta\sigma_z$	[kPa] $\Delta\tau$	[kPa]	PEC [kNm/m^3]	n	PEC [kNm/m^3] (n=2)
8.21	0.18	36.3	18.1	0.887	1.70	1
8.22	0.38	37.2	18.3	2.01	2.33	1.4
8.23	0.58	37.2	19.0	2.19	1.92	2.3
8.24	0.58	27.5	14.0	1.98	2.02	2
8.25	0.58	18.9	9.6	107.64	3.40	30
8.26	0.38	28.55	14.3	1.40	1.86	1.5
8.27	0.38	19	9.6	3.34	1.94	3.75
8.28	0.18	27.5	14.0	0.67	1.56	0.8
8.29	0.18	19	9.6	1.72	1.68	2.5
8.30 UDU	0.18	18.9	9.6	1.39	1.79	1.8
12.10a [1])	0.61	9.4	4.7			
12.11	0.61	18.9	9.6	100.63	2.79	55
12.11h	0.61	18.9	9.6	165.76	3.39	60
12.12	0.61	38	19.0	5.44	2.247	4.5
12.12h	0.61	37.8	19.1	3.12	2.37	2
12.13	0.61	55	27.0	5.01	2.37	4
12.13h	0.61	47	23.5	2.71	2.55	2
12.14 UDU	0.61	37.2	18.8	1.50	1.98	1.2
12.15 UDU	0.61	38.35	18.9	3.04	2.21	2.5
12.16 UDU	0.61	37.7	19.1	5.95	2.55	4
12.17 UDU	0.61	37	19.1	2.10	1.92	2.2
12.18a UDU	0.61		14.9	4.39	2.80	2.0
12.18b	0.61	37	18.5	0.89	2.05	0.8

[1]) test with 4 days waiting time between sample preparation and testing

Table 5.2 Summary results parameter determination undrained cyclic tests

Test 12.10a is performed with a small stress amplitude and resulting small strain amplitude ($\Delta\gamma = 0.8\ 10^{-4}$). After 13,000 cycles the relative excess pore pressure is $r_u = 0.04$. Given this small excess pore pressure no reliable empirical parameters for a pore pressure generation model can be determined from the test results.

The value of PEC as function of the relative density is plotted in figure 5.7. In this plot the results of test 8.25, 12.11 and 12.11h are omitted as they are far outside the range of the other values.

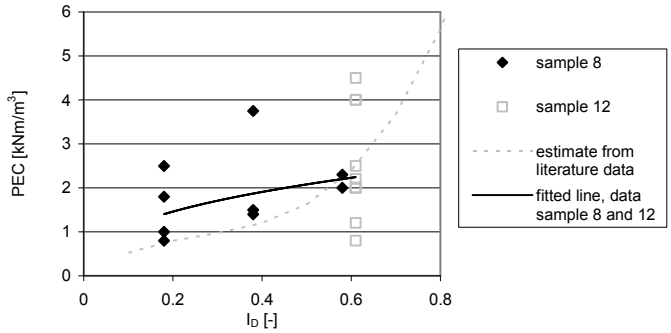

Figure 5.7 Obtained empirical parameter PEC for the energy dissipation model, n=2

The scatter in the obtained values is large. As best estimate of all data the following relation is obtained.

$$PEC = 3.18 I_D^{0.5} \tag{5.8}$$

Based on published test results (see section 4.7.8) the following relation is derived:

$$\frac{PEC}{\sigma'_{v0}} = 0.07 * I_D^{1.7} \tag{5.9}$$

For comparison this relation is plotted in figure 5.7 as well. For low to medium values of relative density (I_D < 0.6) this relation is at the lower bound of the values derived from the laboratory tests.

The power n seems to increase a little with increasing relative density. A value of n=2 is considered a reasonable estimate. The value of PEC increases with increasing relative density. The behaviour in tests 8.25, 12.11 and 12.11h is different from the other tests. The number of cycles to liquefaction is significant higher and the dissipated energy until liquefaction is also significant higher. The tests are common with respect to the relative density (I_D = 0.6) and loading amplitude ($\Delta\tau$= 9.5 kPa). The last is the lowest value used in this series of tests. The reason for this different behaviour is at present unknown. It is possible that for these tests the shear strain amplitude becomes thus low that it approaches the threshold value.

5.2.5 Method deriving parameters Seed&Rahman model

The Seed&Rahman method describes the development of the excess pore pressure as function of the number of cycles as follows:

$$r_u = \frac{2}{\pi} \arcsin\left(N/N_{liq}\right)^{(1/2\theta)} \tag{5.10}$$

with:

- r_u : excess pore pressure ration (ratio between the excess pore pressure and initial effective stress)
- N : number of performed cycles

- N_{liq} : number of cycles to liquefaction, for given stress amplitude
- θ : empirical constant.

For this model two empirical parameters are to be determined from the test results. The first is the number of cycles to liquefaction. The second is parameter θ, used to describe the shape of the development of the excess pore pressure in time.

The determination of the number of cycles to liquefaction seems to be an easy task. Still some problems are present. The measured development of the excess pore pressure does not always fit the mentioned expression. Therefore two approaches are used for deriving the empirical parameters. First a fit is made using the measured value of N_{liq}. This gives the corresponding value of θ. A second estimate is made using only the first part of the measured r_u –N curve is fitted (r_u<0.6). This gives an estimate for both N_{liq} and θ.

For the first estimate the expression for the development of the excess pore pressure is rewritten as:

$$\log\left(\sin\left(r_u\frac{2}{\pi}\right)\right)=\log\left(N/N_{liq}\right)^{(1/2\theta)}=\frac{1}{2\theta}\log\left(N/N_{liq}\right) \tag{5.11}$$

The number of cycles to liquefaction N_{liq} follows from the test results. The parameter θ remains as unknown parameter. Plotting the value of $\log(\sin(r_u*2/\pi))$ against $\log(N/N_{liq})$ the value of θ can be determined from the slop of this line. As an example figure 5.8 shows for test 12.12 the test data plotted this way. In this test the sample liquefied at N_{liq} = 8300.

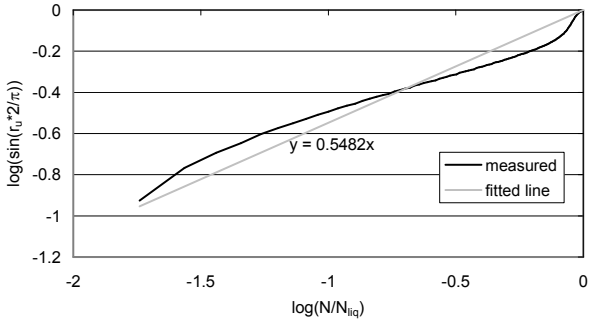

Figure 5.8 Determination parameter θ from test results

From the linear fit through these data points the value for θ follows. In this case the fit gives $1/2\theta = 0.5482$, so $\theta = 0.912$.

For the assessment of the parameters N_{liq} and θ the expression for r_u is rewritten as:

$$\sin\left(r_u\frac{\pi}{2}\right)=\left(N/N_{liq}\right)^{(1/2\theta)}=\frac{N^{(1/2\theta)}}{N_{liq}^{(1/2\theta)}} \tag{5.12}$$

This indicates that, according to the given expression, a linear relation is present between the parameters $\sin(r_u*\pi/2)$ and $N^{1/2\theta}$. Figure 5.9 shows this relation and the fitted power function for test 12.12.

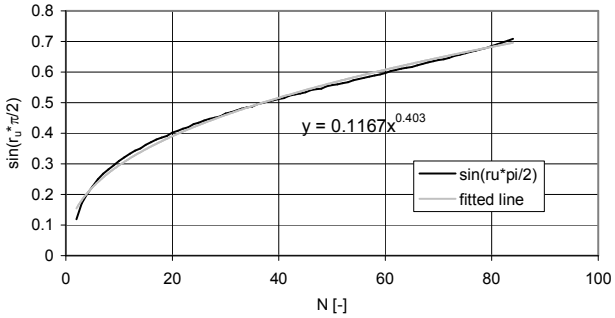

Figure 5.9 Example test result and determination empirical parameter

For high number of cycles the fitted curve deviates from the measured curve. The fitted line can be described with:

$$y=0.1167*x^{0.403} \tag{5.13}$$

From this the parameters N_{liq} and θ are derived. The parameter θ follows from the power in this expression:

$$\frac{1}{2\theta} = 0.403 \Rightarrow \theta = \frac{1}{2*0.403} = 1.24 \tag{5.14}$$

Once the value of θ is known the value of N_{liq} can be determined:

$$\frac{1}{N_{liq}^{1/2\theta}} = \frac{1}{N_{liq}^{0.403}} = 0.1167 \Rightarrow N_{liq} = \left(\frac{1}{0.1167}\right)^{1/0.403} = 206.5 \tag{5.15}$$

With two approaches also two sets of empirical parameters are derived. Figure 5.10 shows the comparison between the measured data and the two fitted lines.

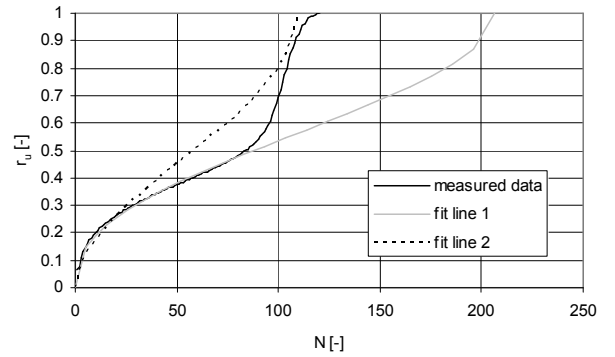

Figure 5.10 Comparison development excess pore pressure using the two sets of empirical parameters

It is observed that none of the two sets gives an acceptable fit with the measured data. For limited values of the excess pore pressure (r_u<0.6) an acceptable fit is obtained when using only the first part of the test data.

5.2.6 Empirical parameters Seed and Rahman model from results undrained tests

From the tests the empirical parameters θ and N_{liq} (a and b) of the Seed&Rahman model will be derived. For each undrained test the derived values of N_{liq} and θ are presented in table 5.3.

test	[-]	[kPa]	[kPa]	full liquefaction		r_u<0.6	
I_D	$\Delta\sigma_v$	$\Delta\tau$		N_{liq}	θ	N_{liq}	θ
8.21	0.18	36.3	18.1	8	0.55	6.4	0.46
8.22	0.38	37.2	18.3	15	0.58	11.7	0.70
8.23	0.58	37.2	19.0	25	0.66	29.5	0.73
8.24	0.58	27.5	14.0	61	0.91	69	0.97
8.25	0.58	18.9	9.6	2390	1.10	9169	1.83
8.26	0.38	28.55	14.3	32	0.74	33	0.75
8.27	0.38	19	9.6	262	0.92	374	1.10
8.28	0.18	27.5	14.0	12	0.61	11	0.57
8.29	0.18	19	9.6	95	0.84	119	0.95
8.30 UDU	0.18	18.9	9.6	85	0.88	120	1.06
12.10a [1])	0.61	9.4	4.7				
12.11	0.61	18.9	9.6	8300	1.10	17838	1.53
12.11h	0.61	18.9	9.6	11000	1.48	18910	1.75
12.12	0.61	38	19.0	110	0.91	207	1.24
12.12h	0.61	37.8	19.1	40	0.87	55	1.04
12.13	0.61	55	27.0	10	0.83	7.1	0.48
12.13h	0.61	47	23.5	6	1.55	4.1	0.65
12.14 UDU	0.61	37.2	18.8	16	0.80	11	0.60
12.15 UDU	0.61	38.35	18.9	--	--	71	0.98
12.16 UDU	0.61	37.7	19.1	96	1.07	143	1.32
12.17 UDU	0.61	37	19.1	--	--	45	0.86
12.18a UDU	0.61		14.9	--	--	269	1.18
12.18b	0.61	37	18.5	--	--	19	0.53

[1]) test with 4 days waiting time between sample preparation and testing

Table 5.3 Summary results parameter determination undrained cyclic tests

For θ two values have been derived, one for the test results until r_u = 0.6 (θ_1) and one for the total test results (θ_2). Figure 5.11 show these values as function of the shear stress amplitude and of the relative density.

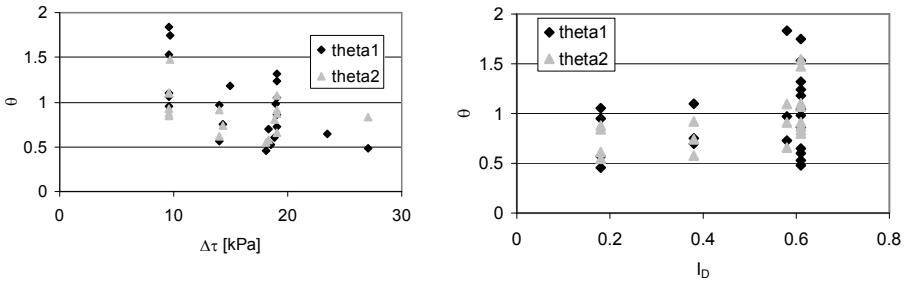

Figure 5.11 Values of θ, as derived from test results

The value of θ (theta) shows a large scatter. The two values of θ are in general equal. No relation with the relative density is present. There however seems to be a relation with the shear stress amplitude. Increasing the stress amplitude results in a lower value of θ.

The number of cycles to liquefaction is a function of the shear stress amplitude and the relative density. A possible expression is:

$$\frac{\Delta\tau / \sigma'_{v0}}{a.I_D} = N_{liq}^{-b} \qquad (5.16)$$

In this a and b are empirical constants.

For cyclic triaxial tests the relative shear stress amplitude is given by $\Delta\sigma_d/2\sigma_{cell}$. Using this expression allows to combine the shear stress amplitude and the relative density to one combined parameter $\Delta\sigma_d/2\sigma_c/I_D$. This parameter is used when further analysing the data.
The relation between the number of cycles to liquefaction and this combined parameter is shown in figure 5.12. Also shown is a line used in the literature for cyclic simple shear loading (a=0.48; b=0.2). In line with the usual presentation in the literature the number of cycle to liquefaction is plotted at the horizontal axis.

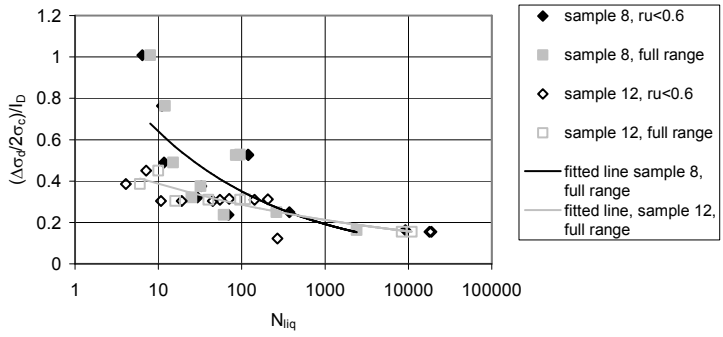

Figure 5.12 Number of cycles to liquefaction as function of the relative shear stress amplitude, as derived from test results

The number of cycles to liquefaction decreases with increasing value of the combined parameter. A wide scatter is present. For small values of the joint parameter (<0.25) the two sands are comparable. For higher values (higher amplitude of the deviator stress $\Delta\sigma_{dev}$ and/or lower relative density I_D) sand 8 gives a larger number of cycles to liquefaction.

From the fitted lines the parameters of a and b can be obtained. The results are presented in table 5.4.

sample	a	b
8	1.166	0.261
12	0.514	0.129

Table 5.4 Derived empirical parameters for estimating number of cycles to liquefaction

5.2.7 Method deriving parameters C/L model

The C/L method is described in section 4.7.3. This model uses a logarithmic relation between the compaction Φ, the second invariant of the strain J and the number of cycles N.

$$\Phi = C_1 \ln(1 + C_2 J_2 N) \tag{5.17}$$

For ease of deriving the values of the empirical constants from the test results the expression is rewritten to a function of the volume strain ε_{vol}^{pl}, the number of cycles N and the shear strain amplitude γ.

$$\varepsilon_{vol}^{pl} = A_1 \ln(1 + A_2 N.\Delta\gamma^2) \tag{5.18}$$

The relation of the parameters A_1 and A_2 with the original empirical parameters C_1 and C_2 is:

$$A_1 = \frac{n}{1-n} C_1 * 0.001 \tag{5.19}$$

$$A_2 = 10^6 * 0.25 * C_2 \tag{5.20}$$

The terms 0.001 and 10^6 comes from the used dimensions in the C/L method.

The objective is to find the values of A_1 and A_2 that best fits with the measured data. First a value of A_2 is assumed. The corresponding value of A_1 is calculated from the following expression, using a least square method.

$$A_1 = \frac{\ln(1 + A_2 N.\Delta\gamma^2)}{\varepsilon_{vol}^{pl}} \tag{5.21}$$

Assuming another value of A_2 will result in another estimate for A_1. The purpose is to find values of A_1 and A_2 that best fits with the measured volume strain. For this the sum of the squared error is used.

$$E = \sum_{i=1}^{N} \left(\varepsilon_{vol}^{pl} - A_1 \ln(1 + A_2 N.\Delta\gamma^2) \right)^2 \tag{5.22}$$

The combination of A_1 and A_2 resulting in the lowest summed error is taken as fit parameter.

Figure 5.13 shows the result of test 5.13. For this test the following fit parameters are obtained: A_1 = 0.000942 and A_2 = 23.6 10^3. When A_1 and A_2 are known the values of C_1 and C_2 can be obtained. For the used example this gives: C_1 = 1.413 and C_2 = 0.0944. The curve showing the volume strain using these parameters is shown as well.

As can be observed from figure 5.13 the fitted line underestimates the volumetric strain at small number of cycles.

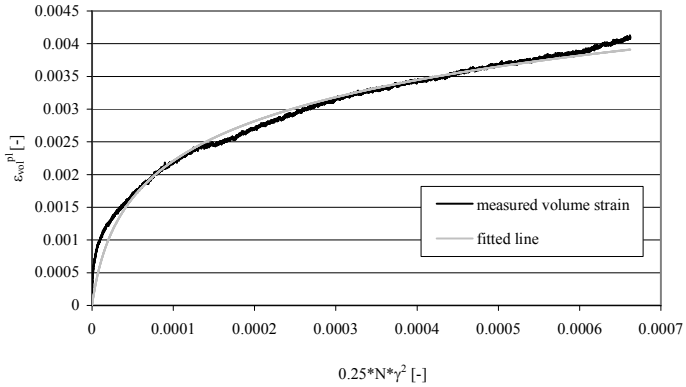

Figure 5.13 Fitting results drained cyclic triaxial test with C/L model

5.2.8 Empirical parameters C/L model from results drained tests

The obtained empirical coefficients for the different tests are given in table 5.5.

In order to check if the behaviour of sample 8 and 12 is different the measured volume strain after about 15,000 cycles in tests with a shear stress amplitude of 19 kPa and relative density of I_D=0.6 is shown in figure 5.14. The densification of sample 8 is in general above the densification of sample 12. In general sample 12 shows a remarkable low volume strain, especially for low relative densities. One test (test 12.7) has been repeated in order to check if a possible error is made during this test. The same results are obtained. Therefore it is concluded that the test result is reliable.

For the undrained test it is found that sample 8 has a higher resistance against liquefaction resistance as sample 12. One may therefore expect that sample 8 will show a lower volume strain in drained testing. The opposite is however observed. No explanation for this difference is known.
The derived values of C_1 and C_2 as function of the relative density are shown in figure 5.15 and 5.16. For comparison also the values derived from literature (see section 4.7.4) are included.

test	I_D	$\Delta\sigma_v$ [kPa]	$\Delta\tau$ [kPa]	C_1	C_2
8.18	0.18	37.2	18.7	8.83	0.0284
8.19	0.38	37.6	18.9	7.125	0.0356
8.20	0.58	37.5	19.1	3.966	0.03
12.2h	0.61	9.1	4.6	3.467	0.046
12.3h	0.61	19.0	9.6	1.378	0.0944
12.4	0.61	37.5	19.1	2.838	0.0468
12.5	0.61	56.8	28.6	2.180	0.1104
12.6	0.61	73.4	36.9	4.126	0.204
12.7	0.21	37.3	18.8	1.850	0.1912
12.7h [1])	0.21	37.2	18.9	2.118	0.21
12.8	0.40	37.3	18.9	1.418	0.0864
12.9	0.80	37.8	19.0	2.600	0.018
12.10b [2])	0.61		4.8	0.066	0.2476

[1]) mentioned empirical parameters are not the combination given the lowest summed error, but nearly the lowest summed error; these values are used in order to be in line with the empirical parameters from the other tests

[2]) test with 4 days waiting time between sample preparation and testing

Table 5.5 Results drained triaxial tests

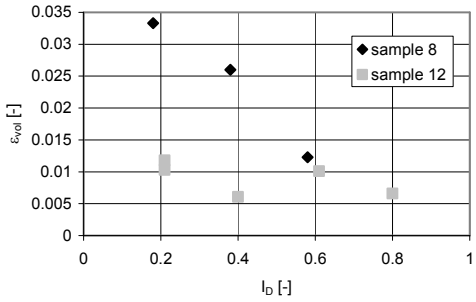

Figure 5.14 Measured volume strain as function of relative density, all tests with $\Delta\sigma'_{v0}$ = 38 kPa

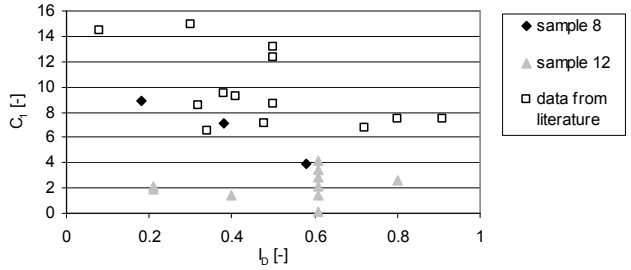

Figure 5.15 Comparison value of C_1 from testing and from literature

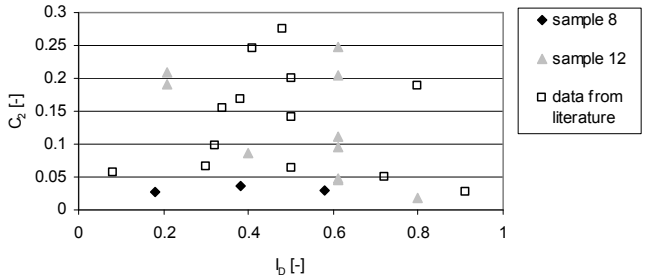

Figure 5.16 Comparison value of C_2 from testing and from literature

There are some striking differences between these two sets of data.
For sample 8 the value of C_1 is in reasonable agreement with the data from literature. The value of C_2 seems to be independent of the relative density. With a value of 0.03 it is below the data from the literature. It should be noted that the data in the literature are derived from simple shear tests. Using a correction factor of 0.7 on the shear strain amplitude (in agreement with the translation used for the shear stress amplitude) the value of C_2 doubles and becomes about 0.06. This value is at the lower side of the data reported in the literature.
For sample 12 the derived value for C_1 is about 2, independent of the relative density. This is far below the data from literature. The obtained value for C_2 varies between 0.03 and 0.2 and is a function of the relative density. For low relative densities the value for C_2 is above the value obtained from literature. For high relative densities the value is below the value from literature. Accounting for the difference between cyclic triaxial testing and cyclic simple shear testing the difference at low relative densities becomes even more. For medium to high relative densities a reasonable agreement is obtained.

The parameters C_1 and C_2 may be not only a function of the relative density but also of the stress amplitude. From the performed cyclic triaxial tests this effect can be assessed using the data for sample 12 and a relative density of $I_D = 0.6$. In figure 5.17 the obtained values of C_1 and C_2 are plotted as function of the vertical stress amplitude.

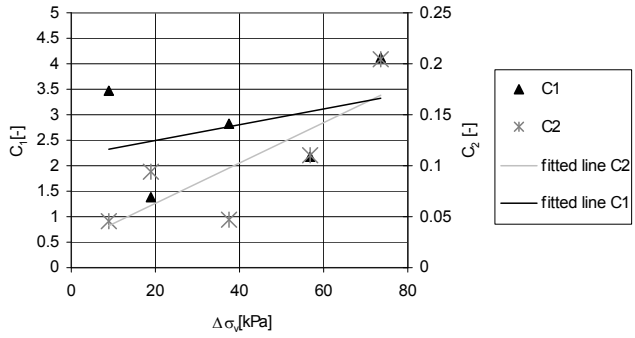

Figure 5.17 Dependency empirical parameters C/L model on applied load amplitude, sample 12, relative density $I_D = 0.6$

An increase of the parameters with increasing load amplitude can be observed. For C_1 the dependency is small and within the range of data. For C_2 the trend may be relevant. However, the scatter in data points is thus that no firm conclusions can be drawn.

5.3 Effect interim drainage

Seven undrained cyclic tests are performed where the sample is drained after a certain amount of excess pore pressure is generated. After this the undrained loading is continued. In some cases a drained static loading is applied between the two undrained cyclic loading stages.

The obtained empirical parameters for the tests with interim drainage are given in table 5.6. The tests are analysed using the measured data for $r_u<0.6$ only, as not always during the first stage the test is continued for $r_u>0.6$. The results for the first stage are already mentioned in table 5.3.

test	I_{D1}	$\Delta\sigma_v$ [kPa]	static loading [kPa]	r_{u1}	ε^{pl}_{vol} due to interim drainage and static loading	I_{D2}	Seed&Rahman model, $r_u<0.6$				energy dissipation	
							before interim drainage		after interim drainage		PEC (n=2)	
							N_{liq}	θ	N_{liq}	θ	before	after
8.30	0.18	18.9	0	1.0	2.7%	0.31	120	1.06	1194	1.80	1.8	6.5
12.14	0.61	37.2	0	1.0	1.6%	0.69	10.7	0.60	10.8	0.47	1.2	2.0
12.15	0.61	38.35	0	0.6	0.25%	0.62	70.8	0.98	5797	1.56	2.5	70
12.16	0.61	37.7	97	1.0	1.3%	0.67	143	1.32	140	1.426	4	6
12.17	0.61	37	98	0.7	0.5%	0.63	45	0.86	2193	1.40	2.2	35
12.18a	0.61		370 [1])	0.6	-0.47%	0.59	269	1.18	?	?	2.0	0.25
12.18b	0.61		370 [1])	0.65	-0.52	0.58	18.9	0.35	?	?	0.8	0.33

[1]) 5% axial strain

Table 5.6 Results undrained tests with interim drainage

Figure 5.18 shows two typical examples. In both cases the sample is drained after the excess pore pressure has reached a value of about 60%. In one case a small drained static loading is applied and in the other case a large drained static loading is applied.

The interim drainage will result in a small compaction of the sand and thus a small increase in the relative density. This increase in relative density will influence the number of cycles against liquefaction. The results (number of cycles to liquefaction) for the second stage are corrected for this change in relative density. For this use is made of the empirical relation between the relative density and the number of cycles to liquefaction. Equation 4.68 gives the relation between stress amplitude, relative density and number of cycles to liquefaction.

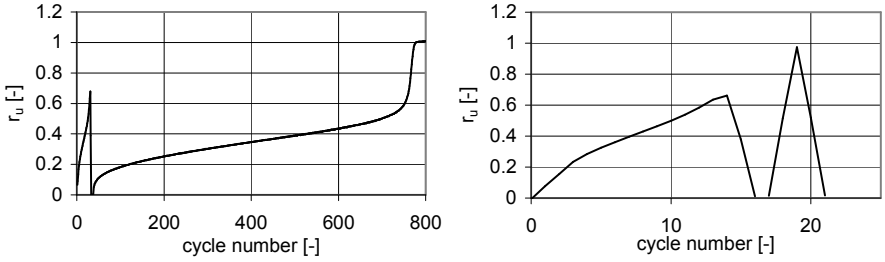

Figure 5.18 Development excess pore pressure test 12.17 (interim drainage, small interim static loading) and test 12.18b (interim drainage, large interim static loading)

Changing only the relative density gives for the ratio of number of cycles to liquefaction:

$$\frac{N_{liq2}}{N_{liq1}} = \frac{\left(\frac{\Delta\tau / \sigma'_{v0}}{a.I_{D2}}\right)^{-1/b}}{\left(\frac{\Delta\tau / \sigma'_{v0}}{a.I_{D1}}\right)^{-1/b}} = \left(\frac{I_{D2}}{I_{D1}}\right)^{1/b} \qquad (5.23)$$

From this follows that the number of cycles may be taken proportional to $I_D^{(1/b)}$. With this relation the number of cycles during the second stage is corrected. The results are shown in table 5.7.

test	I_{D1}	$\Delta\sigma_v$ [kPa]	static loading [kPa]	r_{u1} [-]	I_{D2} [-]	N_{liq1} [-]	N_{liq2} [-]	N_{liq2}/N_{liq1}	N_{liq2}/N_{liq1} after correction for ΔI_D
8.30	0.18	18.9	0	1.0	0.31	120	1194	9.95	0.66
12.14	0.61	37.2	0	1.0	0.69	10.7	10.8	1.016	0.55
12.15	0.61	38.35	0	0.6	0.62	70.8	5797	81.88	75.49
12.16	0.61	37.7	97	1.0	0.67	142	140	0.99	0.62
12.17	0.61	37	98	0.7	0.63	45	2193	48.73	41.47
12.18a	0.61	30	370 (5% strain)	0.6	0.59	268	2	0.007	0.009
12.18b	0.61	37	370 (5% strain)	0.65	0.58	19	1.5	0.079	0.100

Table 5.7 Effect interim drainage on liquefaction potential

More insight is obtained by plotting the relative change in number of cycles to liquefaction as a function of the relative excess pore pressure at start of interim drainage, see figure 5.19.

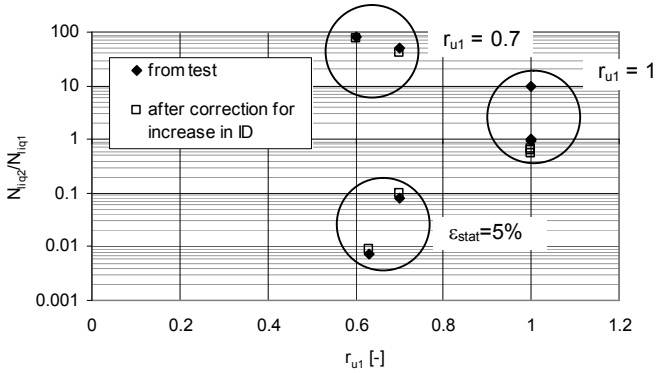

Figure 5.19 Effect interim drainage on the number of cycles to liquefaction

In the test series three situations can be distinguished. The first are tests where drainage is applied when the excess pore pressure is about 70%. In this case the number of cycles to liquefaction greatly increases. The second case is when the drainage is applied when full liquefaction is present. For this situation the number of cycles to liquefaction decreases. The shear strain amplitude at time of first liquefaction is about 1%. The third group of tests is where a large drained static loading (5% axial strain, 4% shear strain) is applied after the interim drainage. During this phase dilation occurred. After unloading the volume has increased with about 1%. When resuming the undrained cyclic loading the sample liquefied in 1 to 2 cycles.

In two tests a moderate drained static vertical loading and unloading of 100 kPa is applied after the interim drainage. With this load the ratio between horizontal and vertical stress is 0.5, which is below failure load of the sample.
The shear strain during this phase is about 0.15%. A small compaction of the sample (about 0.1%) occurred. The effect of this static loading on the liquefaction potential is marginal, if present at all.
In test 12.18a and 12.18b the sample is brought to failure by applying a vertical strain of 5%. The increase in vertical stress is about 370 kPa.

One option to account for the effect of preshearing is to use the findings of Smits (see section 4.4 and equation 4.69). This equation contains an empirical parameter X. The test data can be used for estimating the value of this parameter X. To this end the relation is rewritten. The number of cycles to liquefaction after some preshearing/drainage has occurred van be written as

$$N_{liq} = N_{liq,0}.10^{-X\Delta n} \tag{5.24}$$

Knowing N_l, N_{liq} and Δn the value of X can be calculated.

$$-X\Delta n = \log\left(\frac{N_{liq}}{N_{liq},0}\right) \tag{5.25}$$

$$X = \frac{-\log\left(\frac{N_{liq}}{N_{liq},0}\right)}{\Delta n} \tag{5.26}$$

The obtained values of X are shown in table 5.8.

test	I_{D1}	r_{u1}	I_{D2}	Δn	$N_{liq,0}$	N_{liq}	$N_{liq}/N_{liq,0}$	X
8.30	0.18	1.0	0.31	-0.0159	120	1194	9.95	63
12.14	0.61	1.0	0.69	-0.0097	10.7	10.8	1.016	0.4
12.15	0.61	0.6	0.62	-0.0015	70.8	5797	81.88	1285
12.16	0.61	1.0	0.67	-0.0078	142	140	0.99	-0.8
12.17	0.61	0.7	0.63	-0.0030	45	2193	48.73	565
12.18a	0.61	0.6	0.59	0.0028	268	2	0.007	765
12.18b	0.61	0.65	0.58	0.0031	19	1.5	0.079	359

Table 5.8 Determination of parameter X

It should be noted that in this parameter X also the effect of an increase in relative density is accounted for. For the tests with full liquefaction the value of X is about zero. This implies that there is no effect of preshearing, or even densification. For the tests without full liquefaction during the first phase the value is between 350 and 1300. For the tests 12.18a and 12.18b this may seem odd, as the number of cycles to liquefaction greatly reduces. The porosity n however increases and mathematically a positive value for X results.

5.4 Comparison drained and undrained tests

One of the questions to be answered with these tests is whether the empirical models for drained sand can be used for undrained sand as well and vice-versa. In the model TRILDENS3 the following relation is used:

$$u = M * \varepsilon_{vol}^{pl} \tag{5.27}$$

In comparing the drained and undrained triaxial tests instead of M the stiffness K is to be used. In the actual situation the horizontal strain is zero and the horizontal stress may vary. In the triaxial test the sample is allowed to deform radial. The horizontal stress is constant and the horizontal strain may vary.

First the expressions that may be used to predict the undrained behaviour from a model for drained cyclic loading and vice-versa are derived.

The drained cyclic behaviour is described with the C/L method. Rearranging the expressions for this model gives as expression for the incremental volume strain:

$$\frac{d\varepsilon_{vol}^{pl}}{dN} = \frac{1-n_0}{n_0} C_1 C_2 J_2 \exp(-D_2\Phi) \tag{5.28}$$

As in the undrained test the compaction is zero (Φ=0) this can be expressed as:

$$\frac{d\varepsilon_{vol}^{pl}}{dN} = \frac{1-n_0}{n_0} C_1 C_2 J_2 \tag{5.29}$$

The incremental increase in excess pore pressure follows from the incremental increase in plastic volumetric strain multiplied by the compression modulus.

For the prediction of the drained results (volumetric strain) from the undrained tests two fitting expressions are used. The first is the Seed&Rahman approach, taking into account the preshearing effect according to Smits. As a first approach to estimate the change in volume strain the slope of the relative pore pressure versus number of cycles is used. Differentiating equation 4.67 gives:

$$\frac{dr_u}{dN} = \frac{2}{\pi} \frac{1}{\sqrt{(1-(N/N_l)^{1/\theta}}} \frac{1}{2\theta} N^{-1+1/2\theta} . N_l^{-1/2\theta} \tag{5.30}$$

In a drained test the excess pore pressure is zero ($r_u = 0$), so the slope at N = 0 is to be used. From equation 5.30 follows that, for N=0, the slope is either infinite (for θ>0.5) or zero (for θ<0.5). Neither of these situations is realistic and a different approach is to be used. A more practical approach is to estimate the change in volumetric strain from a linearization of equation 4.76:

$$\frac{dr_u}{dN} = \frac{1}{N_{liq}} \tag{5.31}$$

This gives for the change in volume strain:

$$\frac{d\varepsilon_{vol}^{pl}}{dN} = \frac{1}{K} \frac{\sigma'_{v0}}{N_{liq}} \tag{5.32}$$

with:

- K : compression modulus soil skeleton.

The second approach is the energy-dissipation. The first approach is to use the original expression

$$r_u = \sqrt{\frac{E_{dis}}{PEC}} \tag{5.33}$$

From this follows for the plastic volume strain:

$$\varepsilon_{vol}^{pl} = \frac{u}{K} = \frac{\sigma'_0 r_u}{K} = \frac{\sigma'_0}{K} \sqrt{\frac{E_{dis}}{PEC}} \tag{5.34}$$

The dissipated energy per cycle is estimated from the damping coefficient D according to:

$$E_{dis} = D * 2\pi * \Delta\tau * \Delta\gamma = D * 2\pi * \Delta\tau * \frac{\Delta\tau}{G(u)} \tag{5.35}$$

with:

- D : damping ratio
- G(u) : shear modulus, corrected for the excess pore pressure
- $\Delta\tau$: shear stress amplitude
- $\Delta\gamma$: shear strain amplitude.

In equation 5.34 the preshearing effect is not taken into account. In order to account for this effect the expression is supplemented with a parameter describing

this effect. As first approach the expression derived from the data of Smits (1978) is used. Here this parameter is denoted 'structure parameter' S, and defined as:

$$S = 10^{-X\Delta n} \tag{5.36}$$

This parameter is used to correct the number of cycles to liquefaction. As in the energy dissipation method the parameter PEC determines this value this parameter will be adjusted.
The plastic volume strain per cycle follows from:

$$\Delta\varepsilon_{vol}^{pl} = \frac{\sigma'_0}{K}\sqrt{\frac{\Delta E_{dis}}{PEC * S}} = \frac{\sigma'_0}{K}\sqrt{\frac{E_{dis} + \Delta E_{dis}}{PEC * S}} - \frac{\sigma'_0}{K}\sqrt{\frac{E_{dis}}{PEC * S}} \tag{5.37}$$

with:

- K : compression modulus soil skeleton
- ΔE_{dis} : dissipated energy in the considered cycle
- E_{dis} : dissipated energy in the previous cycles
- S : structure parameter.

Table 5.9 shows the different soil parameters used for the densification models. These parameters are derived from the tests mentioned in the left columns of the table.

The following fixed parameters are used.

- history parameter X = 700
- damping D = 0.1 or 0.11
- compression modulus K = 18 MPa (sample 12) or K = 15 MPa (sample 8)
- shear modulus: G = 22.5 MPa (sample 12) or G = 17 MPa (sample 8).

number drained test	number undrained test	I_D [-]	undrained parameters				drained parameters	
			PEC	a	b	θ	C_1	C_2
8.18	8.21	0.18	0.887	1.165	0.261	0.55	8.83	0.0284
8.19	8.22	0.38	1.4	1.165	0.261	0.58	7.22	0.0356
8.20	8.22	0.58	2.3	1.165	0.261	0.66	4.03	0.03
12.4	12.12 / 12.12h	0.61	4.5	0.51	0.128	0.89	2.84	0.047
12.5	12.13	0.61	4.0	0.51	0.128	0.83	2.18	0.1104
12.3h	12.11 / 12.11h	0.61	60	0.51	0.128	1.3	1.38	0.0944

Table 5.9 Used empirical parameters

As an example of the comparison figure 5.20 shows the measured volume strain in the drained test 12.4 and the predicted volume strain when using the parameters from the undrained tests 12.12. Figure 5.21 shows the measured pore pressure in the undrained test 12.12 and the predicted pore pressure generation when using the parameters from the drained test 12.4. Table 5.10 shows the key results of the comparison.

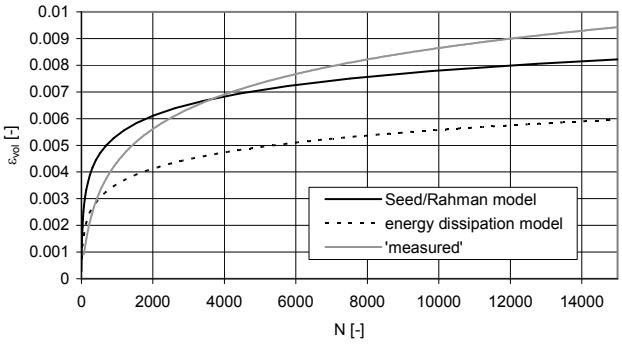

Figure 5.20 Comparison measured volume strain in drained test 12.4 and prediction from results undrained test 12.12

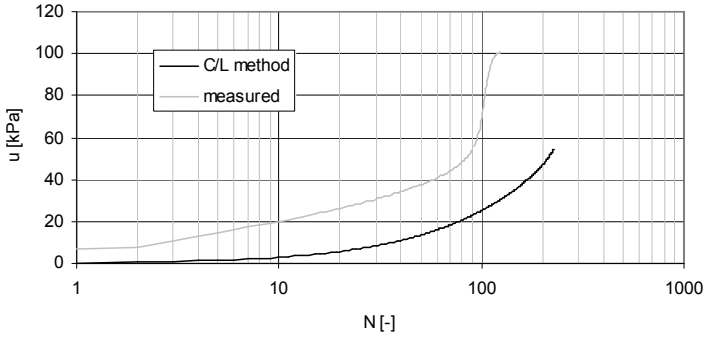

Figure 5.21 Comparison measured development excess pore pressure in undrained test 12.12 and prediction from results drained test 12.4

number drained test	number undrained test	I_D [-]	$\Delta\tau$ [kPa]	ε^{pl}_{vol} [%] (N=15,000)			N_{liq} [-]	
				measured	calculated		measured	calculated
					acc. S&R	acc. E_{dis}		
8.18	8.21	0.18	18	3.19	1.23	0.82	8	53
8.19	8.22	0.38	18.5	2.49	0.90	0.76	14	62
8.20	8.22	0.58	18.8	1.21	0.72	0.69	28	210
12.4	12.12 / 12.12h	0.61	19	0.94	0.83	0.60	120	260
12.5	12.13	0.61	27	0.97	1.11	0.68	17	45
12.3h	12.11 / 12.11h	0.61	9.5	0.39	0.28	0.23	12,300	8,300

Table 5.10 Comparison measured and predicted behaviour cyclic triaxial tests

For sample 8 the predicted number of cycles to liquefaction is in general above the measured value. The difference is a factor 4 to 8. For sample 12 difference between predicted and measured number of cycles to liquefaction is 0.5 to 2.5. The

differences are quite large, but are in line with the scatter in test results already observed during the testing.
The predicted and measured volume strain is in general in fair agreement. For tests 8.18 and 8.19, with measured volume strain of 2% and 3%, the predicted volumes strains are less as the measured values.

5.5 Threshold value shear strain amplitude

One of the questions still to be answered is the threshold shear strain for large numbers of cyclic loading. Figure 5.22 shows the measured volume strain at the end of the drained tests as function of the shear strain amplitude. The test data are not corrected for the possible creep during the testing.
In nearly all tests the shear strain amplitude above 10^{-4}. Only for test 12.10a and 12.10b is the shear strain amplitude below 10^{-4}. In these two tests the measured volume strain is $1.7 .10^{-4}$ for the undrained test and $0.8.10^{-4}$ for the drained test. It should be noted that test 12.10a is performed at a sample that is allowed to creep for 4 days before testing and test 12.10b is performed on a sample that is allowed to creep for 4 days and experienced already about 16,000 small amplitude undrained loading cycles.

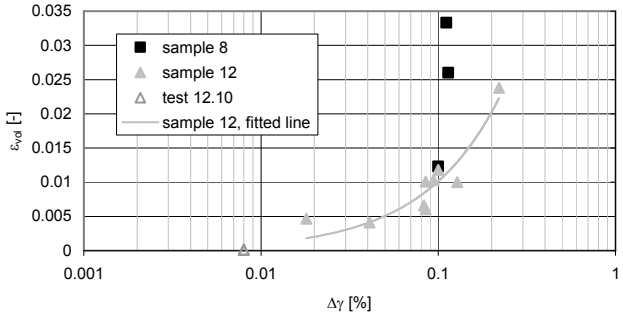

Figure 5.22 Volumetric strain as function of shear strain amplitude

From the available test results no real threshold shear strain amplitude can be derived. The volume strain shows an asymptotic behaviour for low values of the shear strain amplitude. It is concluded that extrapolating the measured volume strain as function of the shear strain amplitude is not justified for low values of the shear strain amplitude. For practical purposes, where the number of applied loading cycles is not excessive, the volumetric strains become almost negligible for shear strain amplitudes below 10^{-4}. High quality testing with extreme accurate measurements of stresses and strains and accounting for creep of the sample and deformations of the testing apparatus is required to get a clear picture for the behaviour of sand during small amplitude cyclic loading.

5.6 Check of sand properties after the testing

Considering the large number of cyclic tests and the limited amount of material it is necessary to re-use the sand during the testing program. This re-use may have altered the sand properties. Therefore the index tests are repeated after the testing program. The tested samples after the laboratory testing are labelled as 8C and 12C.

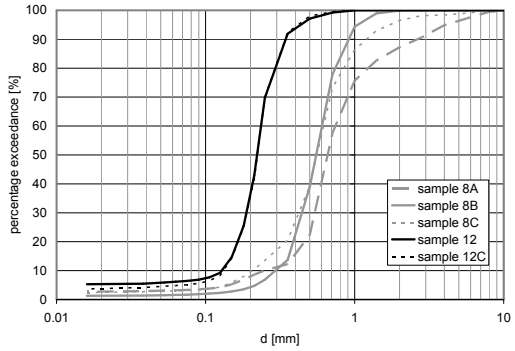

Figure 5.23 Comparison grain size distribution before and after the laboratory testing

The grain size distribution of sample 12 and 12C are nearly equal. This indicates that the grain size distribution did not or hardly change during the testing. For sample 8 there is a small increase of the fraction 0.2 mm to 0.5 mm and a decrease of the fraction 0.5 mm to 1 mm.

sand	sample number	depth [m+NAP]	d_{50} [mm]	$C_u = d_{60}/d_{10}$ [-]	e_{min} [-]	e_{max} [-]	ρ_s [g/cm^3]	roundness
coarse	8A	-5.8	0.664	2.312	0.452	0.817	2.642	0.34
	8B	-6.3	0.559	2.059	0.464	0.802	2.641	0.37
coarse	8C	-5.8/-6.3	0.566	3.04	0.410	0.724	--	0.42
medium	12	-10.1	0.222	1.725	0.548	0.894	2.655	0.46
medium	12C	-10.1	0.223	1.79	0.518	0.877	--	0.47

Table 5.11 Results classification tests before and after the laboratory testing

The sand grains of sample 8 become more rounded during the testing. For sample 12 the roundness of the sand grains hardly changed.

Both the (dry) minimum and maximum void ratio are found to decrease due to the cyclic testing. For sample 12 the change in minimum and maximum void ratio is limited but for sample 8 the change is remarkable. It is noted that the tests 8.28, 8.29 and 8.30 are performed with an initial void ratio of $e_0 = 0.746$, which is above the measured maximum void ratio.

The change in minimum and maximum void ratio will result in a change in the relative density as used in the testing as well. The relative density according to the values measured after the cyclic testing (I_{D2}) can be expressed as a function of the relative density according to the measured values before the cyclic testing (I_{D1}). The result is shown in figure 5.24. The situation of no change is indicated with a dashed line.

For sample 12 the result is a change (decrease) in relative density of 0.05 to 0.08. For sample 8 the change in relative density is 0.256 to 0.16.

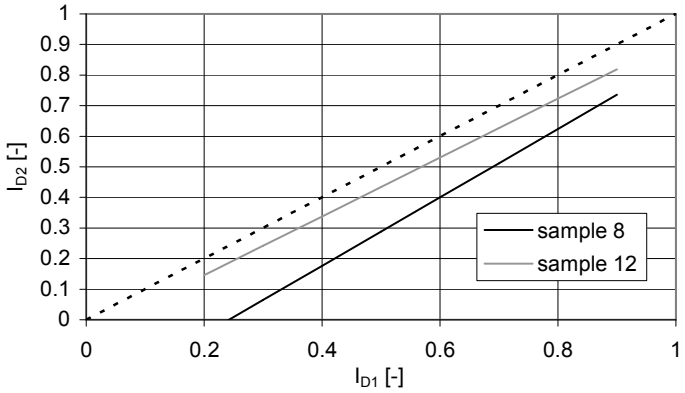

Figure 5.24 Change in relative density due to measured change in minimum and maximum density, the dashed line indicates the situation of no change

When the relative density changes during the test series this may be observed in the test results as well. A decrease in relative density results in an increase in volumetric strain (drained tests) or a decrease in the number of cycles to liquefaction (undrained tests). In order to check this, test results with similar loading conditions (unit weight and load amplitude) are compared. Table 5.12 shows the results. The quoted relative density is the relative density based on the minimum and maximum density as measured before the cyclic testing.

No trend of the test results as function of time of testing is observed. Possible effects are masked by the general variation in test results due to other minor, and not noticeable, changes in the test procedure.

The final result is that the angular coarse sample 8 shows the largest change in properties. The subrounded sample 12 shows only small changes in properties. This is even more remarkable when realising that most tests are performed on sample 12.

test	date of test	I_D	$\Delta\tau$ [kPa]	N_{liq} [-]	ε_{vol} [-[	remarks
12.7	2005-01-07	0.21	18.7	--	0.0103	increase in volume strain
12.7h	2005-02-03	0.21	18.7		0.0118	
12.11	2005-01-03	0.61	9.44	8300	--	increase in N_{liq}
12.11h	2005-02-01	0.61	9.5	11,000		
12.12	2005-01-03	0.61	19	110		
12.14	2005-01-14a	0.61	18.5	16		
12.15	2005-01-17a	0.61	19.15	58		corrected for difference in load amplitude
12.16	2005-01-18	0.61	18.8	96		
12.17	2005-01-21	0.61	18.5	34		
12.12h	2005-01-31	0.61	18.85	45		
12.18a	2005-11-01	0.61	15	108		corrected for difference in load amplitude
12.18b	2005-11-01	0.61	18	19		
12.13	2004-12-24	0.61	27	10	--	decrease in N_{liq}
12.13h	2005-01-28	0.61	23.5	6		
8.29	2005-02-10	0.18	9.45	95	--	decrease in N_{liq}
8.30	2005-02-10	0.18	9.45	85		

Table 5.12 Comparison test results as function of time of testing

5.7 Discussion of the test results

The undrained tests show a behaviour that is more or less in line with expectations from other sources. Reproducibility of the test data is limited. Apparently small differences in soil fabric during sample preparation and during execution of the test influence may have a large influence on the test results. The empirical parameters derived from the test data are in line with empirical data derived from other published tests.

The general trend of the drained test is in line with expectations. Increasing the shear stress amplitude increases the amount of densification. Between preparation of the sample and start of the cyclic loading the sample already shows a decrease in volume. This is attributed to creep of the sample. For the lowest load amplitude used (shear stress amplitude 4.7 kPa, shear strain amplitude 0.8 10^{-4}) the sample shows an ongoing volume decrease. It is hard to distinguish between densification due to creep and due to cyclic loading.

The available test results show an asymptotic decrease of the volume strain with decreasing shear strain amplitude. From the available test results no threshold value for the shear strain amplitude can be derived. Extrapolating the measured volume strain as function of the shear strain amplitude is not justified for low values of the shear strain amplitude. For practical purposes, where the number of applied loading cycles is limited, as for vibratory sheet piling, a threshold value can be defined as the shear strain amplitude showing negligible volume strains. High

quality testing with extreme accurate measurements of stresses and strains and accounting for creep of the sample and deformations of the testing apparatus is required to draw firm conclusions.

An attempt is made to predict the undrained behaviour from drained cyclic tests. It is possible to predict the drained behaviour (densification) from the measured undrained behaviour. The range of results is within the observed variability during the tests. Taking into account the effect of preshearing is necessary to obtain this result.
Predicting the undrained behaviour from the measured drained behaviour did not yet result in an acceptable agreement. The main reason is that it is not possible to differentiate in the drained test results between the contribution of densification and of the preshearing effect.

The undrained tests with interim drainage show interesting results. For tests where the drainage is applied before full liquefaction is reached the resistance against generation of excess pore pressure increases noticeable. For the tests where full liquefaction is reached the resistance during the second load parcel does not increase but remains the same or decreases a little.

A small static loading and unloading of the sample after the drainage stage, but before the undrained loading is resumed, has no influence on the soil behaviour. For a large static loading, till failure, the effect is impressive. The resistance to liquefaction almost vanish. Other researchers observed the same phenomenon (see section 4.4 for examples of research on the effect of combined generation and dissipation of excess pore pressure, see (Tokimatsu and Hosaka 1986) for the effect of static preloading).

This effect cannot be explained from a change in the commonly used geotechnical parameters as relative density. Reason for the large effect must be the soil fabric (structure of the grain skeleton). Apparently the fabric increases with small shear deformations. On large shear deformations the fabric is distorted.
This observation has some major implications. For the cyclic behaviour of sand an important but unknown parameter exists, the fabric of the grain skeleton. This parameter may be influenced by the method of sample preparation (the way the sand is deposited), the preloading (the geologic history of the sand and previous cyclic loading like earthquakes) and possibly aging and creep effects (age of the deposit).

5.8 Application of the results to the situation during sheet piling

The tests show clearly the effect of drainage on the behaviour of sand during cyclic loading. This aspect is therefore to be taken into account. The effect is most likely due to a change in soil fabric. For sand that liquefies, as may be expected close to the sheet pile, the improvement of the soil fabric is lost.
The often advocated value for the threshold shear strain amplitude cannot be justified from the test results. For shear strain amplitudes below and above 10^{-4} it is observed that the amount of densification becomes small. For the situation during

vibratory sheet piling the shear strain amplitude of 10^{-4} can be considered as a threshold value below which the amount of densification can be neglected.
The tests with a drained loading and unloading after the interim drainage mimics the change in stresses in the soil due to excavation and backfilling of a building pit. For the situation on removal of the sheet piles two changes in the subsoil are to be accounted for. The first is the improvement due to the densification during installation. The second is the deterioration due to stress changes during excavation and backfilling of the building pit. At present it is not clear what aspect will dominate the soil behaviour, and thus the amount of densification, during removal of the sheet piles.

6. Development new model

6.1 Introduction

To determine the settlement during vibratory sheet piling a numerical model is developed. The model is called TRILDENS3. The name is a combination of the Dutch word TRILlingen (vibrations) and the English word DENSification. The number '3' indicates that it is the third version of the program since its first coming into existence. In this chapter the basics of the model are described. The sensitivity of the model for certain parameters is shown.

6.2 Outline of the model

In chapter 2 the process during vibratory sheet piling is already described in general terms. This description is the basis for the computational model.

For the modelling of the total process a 'source-path-target' approach is used. In this approach the sheet pile is the source and the surface settlement the target. The program calculates the steps in between. These are the emitted vibrations from the sheet pile, propagation of the vibrations, response of the soil on the vibrations (densification and generation of excess pore pressures) and finally the translation from densification to surface settlement.

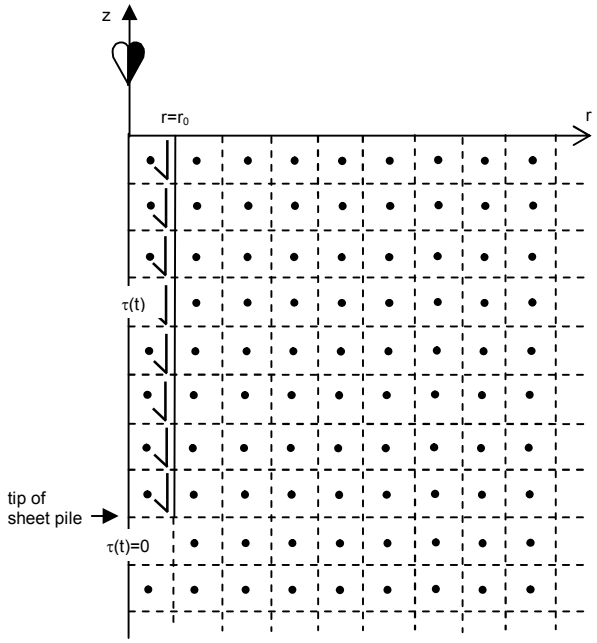

Figure 6.1 Geometry in the calculation, shown are the division in elements and the calculation points

An axial symmetric geometry is used (see figure 6.1). The soil is divided in elements. The behaviour of a point in the centre of an element is considered to be representative for the behaviour of the element.
The modelling of the different steps is discussed in detail in the following sections. In this section first a brief outline of the program is given. The main structure of the program is shown in figure 6.2.
An explicit time integration is used to solve the problem. During a time step the change in these parameters is calculated. The end condition of a time step is the starting condition for the next time step. At start of the calculation the excess pore pressure and the amount of densification is set to zero.
First part of each time step is to determine the embedded length of the sheet pile and the shear stress amplitude at the interface sheet pile – soil. This is called the 'generation model' in the following sections. The model does not calculate the velocity of penetration of the sheet pile. A constant velocity is assumed, the value of it is an input parameter.
The calculation continues with the determination of the vibration amplitude for each calculation node in the mesh. This is called the 'propagation model' in the following sections. The vibration amplitude can be an acceleration amplitude, a velocity amplitude, a shear stress amplitude and a shear strain amplitude.
The response of the soil on these vibrations is determined. For dry sand the response is a change of the volume strain. This is directly calculated for each time step. For saturated sand (sand below the ground water table) generation and dissipation of excess pore pressure occurs simultaneously. For computational reasons a division is made between the generation and dissipation of excess pore pressures. At the start of each time increment the rate of change in pore pressure due to the generation term and due to the dissipation term in an undrained situation and the dissipation of excess pore pressures these two components is calculated. The dissipation of the excess pore pressure is calculated with a finite difference scheme. The calculation of the plastic volume strain and the generation of the excess pore pressure is called the 'generation model'. The dissipation of the excess pore pressures is called the 'dissipation model'. The net outflow of water at an element determines the volume strain of the considered element.
From the requirement that during a single step the change in relevant parameters (excess pore pressure, driving depth of the sheet pile) is limited the value of the time step is selected.

The calculation is continued with the next time step until the end of time of vibrating is reached. The response of the different models is a function of the excess pore pressures, as is explained in the subsequent sections. Starting conditions with respect to the excess pore pressures for the next time step are the end conditions of the previous time step.
At the end of vibrating still some excess pore pressures may be present. This excess pore pressure is allowed to dissipate first. At the end of this step the plastic volume strains in each element are known. Added to this is the effect of the installed or removed volume of the sheet pile. This is called the 'sheet pile volume model'.
Finally the surface settlement is determined from the plastic volume strains in each element. This is called the 'summation model'.

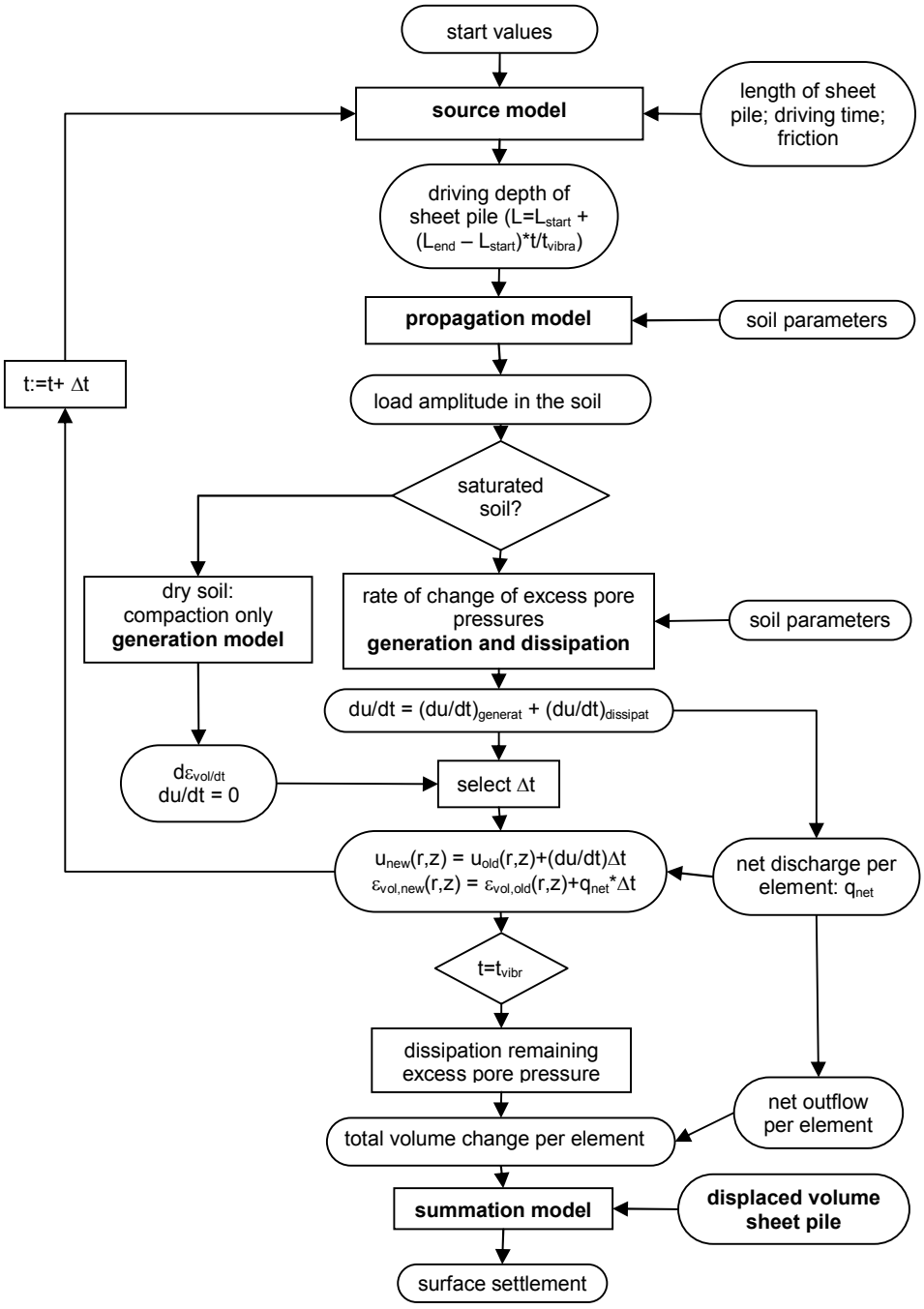

Figure 6.2 Flow scheme TRILDENS3

6.3 Assumptions and simplifications

For the model the following limitations and simplifications are used:

*** geometry**
- axial symmetric situation (horizontal ground level and horizontal soil layering), as a consequence of this simplification the sheet pile is modelled as a tubular pile.

*** source model**
- installation/removal is a continuous operation (the installation/pull is not interrupted, e.g. for connecting or disconnecting a cable)
- constant velocity of installation/pull
- the sheet pile is vibrating in the vertical direction only; possible horizontal vibrations are neglected in the model, but may be accounted for in selecting the values for the model parameters
- vibrations emitted from the tip of the sheet pile are neglected
- the calculation is performed for installing/removing of one sheet pile only
- the external load is applied at a distance r_0 from the symmetry axis, densification in the area r=0 to r=r_0 is accounted for in the generation model.

*** propagation model**
- vibration waves are assumed to expand axial symmetric, vibrations below tip of the sheet pile are neglected
- affect of soil layering on the wave propagation is neglected.

*** generation model**
- the average development of the plastic volume strain and/or the average increase of the excess pore pressure over a number of cycles is calculated, the development during a single cycle is not considered
- influence of stress history and aging of the soil is neglected, this includes the effect of pre-overburden, the effect of installation of previous installed sheet piles and the effect of previous building stages
- the model is intended for densification of sand only, no separate model for densification of clay will be implemented.

*** dissipation model**
- at start of vibrating no excess pore pressures are present
- initial pore water pressure is hydrostatic
- excess pore pressure changes due to piston working of the sheet pile during installation or pull is neglected.

*** summation model**
- for determining the surface settlements the sheet pile wall is assumed to be infinite long in the horizontal direction.

*** sheet pile volume model**
- it is assumed that the effect of densification and the effect of the displaced sheet pile volume can be treated independently.

6.4 Source model

6.4.1 General

The purpose of vibratory sheet piling is to install sheet piles in or remove sheet piles from the soil. This is possible only when the sheet moves vertically with respect to the surrounding soil. Therefore, for the source model it is assumed that at the interface sheet pile – soil slippage occurs. With this starting point the capacity of the vibrator is of less importance for the model, provided it is large enough to overcome the soil resistance. The capacity also determines the speed of installation, but determining this aspect is not in the scope of the proposed model.

Besides this some other assumptions and simplifications are to be made. In the following sections the following aspects will be discussed:
- modelling sheet pile velocity during installation
- modelling the shape of the sheet pile
- shearing at the interface sheet pile-soil (interface friction)
- vertical loading of the soil at the tip (tip resistance)
- horizontal loading of the soil due to out-of-plane movement (e.g. due to out-of-plane bending) of the sheet pile.

External sources of vibrations, and thus possible sources of soil compaction, are:
- vibrations emitted from already (or still) installed sheet piles, as vibrations may be transferred to this sheet pile through the clutch friction
- vibrations from the piling rig and power pack
- external sources (traffic, machinery, other building activities at the site e.g. traffic at the building site and densification of concrete).

For the model it is assumed that the vibrations from these sources are small compared to the vibrations emitted from the sheet pile and can be neglected.

6.4.2 Speed of installation

In the present version of the model a constant speed of installation and removal is assumed. This velocity is derived from the time of vibrating and the length of the sheet pile as prescribed by the user. During installation or removal the velocity of the sheet pile is in general not constant. For installation the velocity is expected to vary with the soil strength encountered. On removal usually some time of vibrating is required before the sheet pile starts to move. Sometimes on removal the sheet pile is first driven a little further in order to decrease the friction at the sheet pile-soil interface and to prevent that lumps of clay are sticking to the sheet pile. After this the velocity gradually increases until a more or less constant value is reached. These aspects can be taken into account by incorporating in the program a model for the forces and movements of the sheet pile itself. This is outside the scope of the present version of the model. For simplicity therefore the actual time of vibrating is an input parameter.

6.4.3 Modelling shape of the sheet pile

In the model an axi-symmetric geometry is assumed. A consequence of this type of modelling is that the sheet pile is in fact modelled as a circular (tubular) pile. In reality it is mostly a double U- or Z-profile. Failure may occur at two possible planes, one is running along the interface sheet pile-soil (the coating area), the other is a straight plane running through the soil. This is illustrated in the figure 6.3.

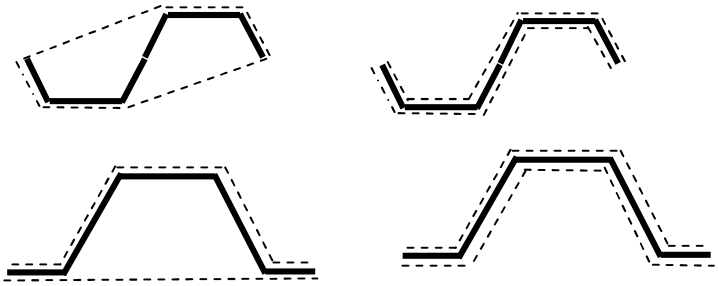

Figure 6.3 Possible shearing planes during sheet pile installation/removal

In practice the shearing planes of the right-hand side in figure 6.3 are observed. A first check on the shearing resistance indicates that for the commonly applied sheet pile profiles this is indeed the plane with the lowest shear resistance.
This actual sheet pile area that transfers vibrations from the sheet pile to the soil is larger as follows from the working width. The difference is in the order of 30%. For a proper calculation this may be taken into account.

The 'equivalent radius' of the 'tubular pile' follows from the width of the sheet pile.

$$2\pi r_{equi} = 2B_{sheet} \tag{6.1}$$

From this follows:

$$r_{equi} = \frac{B_{sheet}}{\pi} \tag{6.2}$$

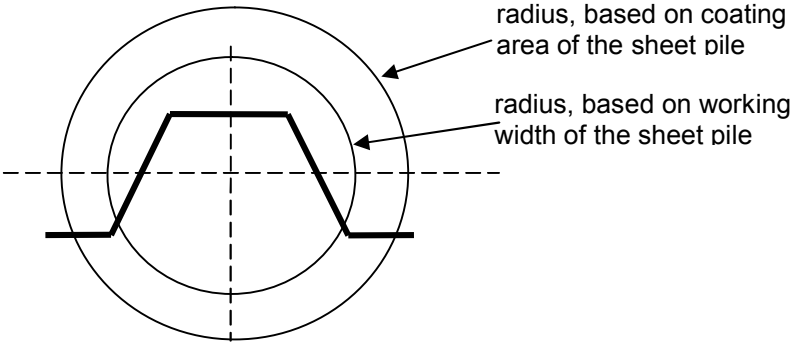

Figure 6.4 Comparison shape of sheet pile and shape as modelled in TRILDENS3

For B_{sheet} two approaches can be used. The first is to take the working width of the sheet pile, the second is to use the actual surface area (coating area). In figure 6.4 both approaches are shown, compared with the actual shape of the sheet pile.

To determine the most appropriate schematisation use is made of the solutions for a vertical vibrating pile in a homogeneous soil (Verruijt 2004). The following situations are considered:
- sheet pile, double Z-profile
- sheet pile, double U-profile
- square tube
- stress attenuation (see section 6.5.2 for a description of this approach).

The sheet pile is modelled as a series of small diameter piles. Figure 6.5 shows the shape of the sheet pile and the used point sources. The different options are compared with respect to the displacement amplitude. The velocity amplitude is proportional to the displacement amplitude.
The actual displacement is a summation of the vertical deformation from the different sources.

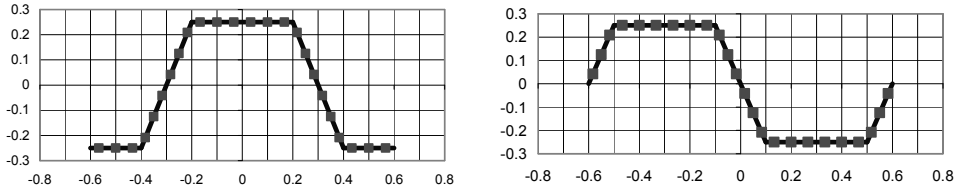

Figure 6.5 Modelling a sheet pile as a set of line loads

As frequency f=33 Hz is used. The results are compared with the stress attenuation model (see section 6.5.2). For this model the start radius is set at r_0 = 0.38 m and the attenuation factor at n= 0.5. The start radius is based on the working width of the considered sheet piles. The stress amplitude at the outer side is taken equal to the value used for the other considered shapes. This implies that the load amplitude transferred to the soil is less as for the actual shape of the sheet pile. Reason for using this combination (radius base on working width and stress amplitude instead of load amplitude) is that it is found to give a better agreement of the amplitude using the different shapes. It is found that the frequency of the vibrator has some influence on the results. Figure 6.6 shows the calculated displacement amplitude for different schematisations of the sheet pile.

The displacement amplitude obtained from the simple ‘stress attenuation’ approach is in acceptable agreement with a more refined approach. The same equation is however to be used for the area of $r < r_0$. It is concluded that modelling the sheet pile as a tubular pile is justified.

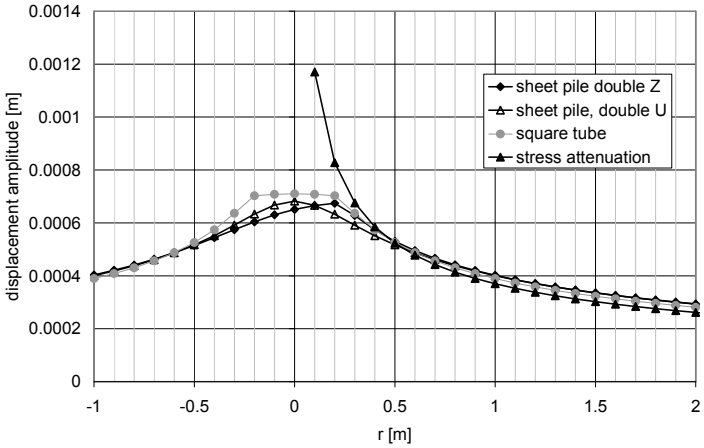

Figure 6.6 Comparison displacement amplitude different shapes of the sheet pile, dimensions sheet pile as in figure 6.5

6.4.4 Interface sheet pile - soil

The purpose of the vibratory sheet piling is that the sheet pile will penetrate into the soil or come out of the soil, depending on the purpose of the vibrating. Therefore it can be assumed that at the interface sheet pile – soil shear failure will occur. This limits the stresses transmitted from the sheet pile into the soil.
Basic assumption in the model is therefore that at the interface sheet pile-soil shear yielding occurs. The maximum friction that can be transferred follows from:

$$\tau_{yield} = \sigma'_h \tan(\delta) = K\sigma'_v \tan(\delta) \tag{6.3}$$

In this δ is the friction angle between sheet pile and soil. It is derived from the angle of internal friction ϕ. A user defined ratio between these two parameters is used.

For K the coefficient of earth pressure at rest is used. For this the empirical relation from Jaky is used:

$$K = 1 - \sin(\phi) \tag{6.4}$$

Possible changes in the value of K during the vibratory process are neglected. For the total force the maximum shear stress is multiplied with twice the working width of the sheet pile (twice in order to account for the front and back side of the sheet pile). The actual surface area of the sheet pile is not accounted for in the present version of the program. If required this can be taken into account by using a higher ratio between angle of interface friction and angle of internal friction, such that the correct amplitude of the friction force is used in the calculation.

With increasing excess pore pressure the effective stress decreases, until it becomes zero at full liquefaction. In this case the shear stress would become zero. In such a case no vibrations can be transmitted from the sheet pile to the surrounding soil. From performed model tests (see section 2.4 and (Meijers and Tol 2002)) it is known that even in fully liquefied sand vibrations are transmitted in

the soil. Apparently some kind of viscous behaviour occurs. The minimum friction can be derived from the following options:

- the concept of 'residual strength', as used in earthquake engineering
- use the empirical formula of Holeyman
- assumed viscous soil behaviour.

In earthquake engineering often the concept of 'residual strength' is used to assess the stable liquefied slope after an earthquake (see e.g. (Stark and Mesri 1972)). This 'residual strength' is derived from back calculating slope failures during an earthquake. The 'residual strength' is the strength required to achieve a stable post-earthquake slope. This concept of 'residual strength' circumvents a quite complex soil behaviour of liquefaction, dilation/compaction during large shearing, dissipation of excess pore pressure during the period of slope instability (slope movement) and acceleration/deceleration of the soil mass during the failure.

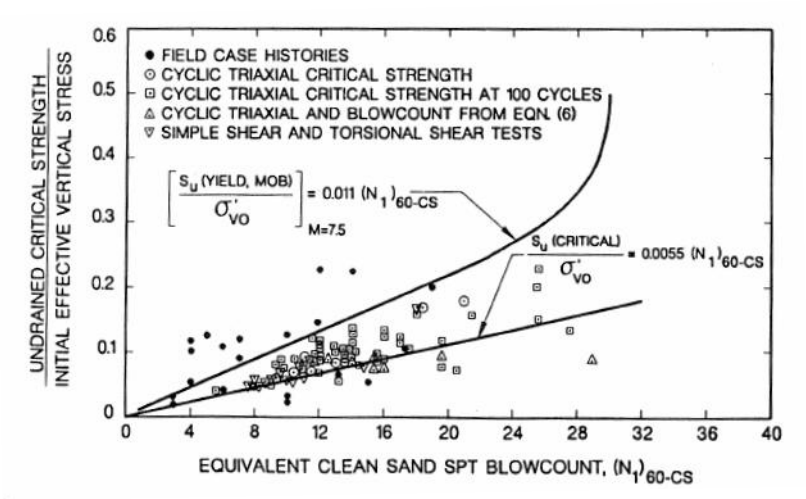

Figure 6.7 Residual strength according to Stark and Mesri (1992)

The 'residual strength' is a function of the initial effective vertical stress and the SPT-value. The last probably represents the initial relative density. The 'residual strength' is in the order of $0.1*\sigma'_{v0}$. For low relative densities the residual strength may be smaller. For high relative densities the residual strength is probably larger.

Holeyman (Holeyman et al 1996) gives the following expressions for the liquefied strength of sand. The background of these expressions is not mentioned in his papers.

$$\tau_{yield} = (\tau_s - \tau_l)e^{-\alpha} + \tau_l \qquad (6.5)$$

$$\tau_l = \tau_s \left[(1 - 1/L).e^{-1/f} + 1/L) \right] \qquad (6.6)$$

with:

- τ_{yield} : driving shaft unit resistance, shear stress at failure
- τ_l : liquefied soil shaft resistance

- τ_s : local friction, in absence of excess pore pressure
- α : acceleration amplitude sheet pile, expressed as fraction of the gravitational acceleration
- L : empirical liquefaction parameter (L = 4 to 10)
- f : friction ratio f_s/q_c, expressed as percentage
- f_s : local friction
- q_c : cone resistance.

It is interesting to compare this expression with the concept of 'residual strength'. Assume as displacement amplitude of the sheet pile 0.005 m and a frequency of 30 Hz. This gives as acceleration amplitude of the sheet pile $\Delta a = 178$ m/s^2 = 18.1 g. For sand the friction ratio is approximately f = 1%. This gives the following residual strength:

L = 4: $\tau_l = \tau_s * 0.525$; $\tau_{yield} = \tau_s * 0.525$ (6.7)

L = 10: $\tau_l = \tau_s * 0.431$; $\tau_{yield} = \tau_s * 0.431$ (6.8)

Assuming Mohr-Coulomb friction the value of τ_s can be estimated using equation 6.3. From this follows that τ_{yield} can be estimated from:

$$\tau_{yield} = K_0 \sigma'_{v0} \tan\delta \tag{6.9}$$

With $K_0 = 0.5$ and $\delta = 20°$ this gives $\tau_d \approx 0.09 * \sigma'_{v0}$. This is the same order of magnitude as with the concept of 'residual strength'.

The third approach is to assume that at the interface sheet pile-soil the soil liquefied and behaves as a viscous fluid. Propagation of vibrations from the sheet pile is thus through a liquefied soil layer. The situation holds only for the soil close to the sheet pile. Here a plane strain situation is present and only 1-dimensional wave propagation of shear waves through a fluid need to be considered.

In a viscous fluid (Newtonian fluid) the relation between stress and velocity is given as:

$$\tau = \eta \frac{dv}{dx} \tag{6.10}$$

with:

- τ : shear stress
- v : velocity (vertical)
- x : horizontal coordinate
- η : dynamic viscosity (dimension Pa.s).

This can also be expressed as:

$$\tau = \eta \frac{d}{dx}\frac{dz}{dt} = \eta \frac{d^2 z}{dxdt} \tag{6.11}$$

with:

- z : vertical displacement.

Figure 6.8 shows the stresses at an element of the liquefied soil.

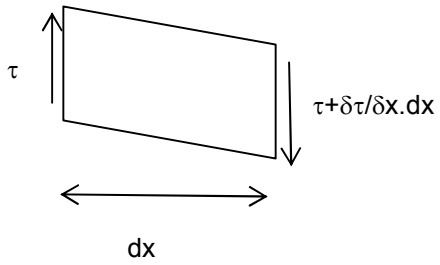

Figure 6.8 Forces at a single liquefied element

From vertical equilibrium of forces (F =m*a) it follows:

$$\rho dx.\frac{d^2z}{dt^2} = \frac{\partial \tau}{\partial x} dx \tag{6.12}$$

This gives:

$$\rho.\frac{d^2z}{dt^2} = \frac{\partial \tau}{\partial x} = \eta \frac{d^3z}{dx^2 dt} \tag{6.13}$$

This differential equation is solved using a complex notation. The displacement is described with:

$$z = A\exp i(\omega t - kx) \tag{6.14}$$

Solving the differential equation gives:

$$z = A\exp i(\omega t \pm (i-1)\sqrt{\frac{\rho\omega}{2\eta}}x) = A\exp(i\omega t)\exp(-\sqrt{\frac{\rho\omega}{2\eta}}x)\exp(-i\sqrt{\frac{\rho\omega}{2\eta}}x) \tag{6.15}$$

From this the shear stress can be obtained.

$$\tau = \eta\frac{dv}{dx} = \eta A\omega\sqrt{\frac{\rho\omega}{2\eta}}(1+i)\exp(i\omega t)\exp(\pm\sqrt{\frac{\rho\omega}{2\eta}}x)\exp(\pm i\sqrt{\frac{\rho\omega}{2\eta}}x) \tag{6.16}$$

As boundary condition it is assumed that at the interface sheet pile-soil the displacement of the soil is equal to the displacement of the sheet pile.
This gives A = z_0, with z_0 the displacement amplitude of the sheet pile.

The problem now is what will be the viscosity of liquefied soil. Only limited data are available in this respect. Meijers (1990) determined the viscosity of a sand-water mixture from back calculating the results of a number of model tests on static soil liquefaction. The liquefied soil has been assumed to behave as a Newtonian fluid. The values for the apparent viscosity are in the range of 100 kg/ms to 1000 kg/ms with extremes values of 50 kg/ms and 7000 kg/ms. The values could not be derived with great accuracy. Given the quite rough approach used to assess the viscosity the mentioned numbers only give an indication of the viscosity.

Using the following values: A=z_0=0.005m, ρ=2000 kg/m^3, ω=188.5, η=500 kg/ms the shear stress amplitude at x=0 amounts about $z_0.\omega\sqrt{(\eta\rho\omega)}$ = 12940 Pa. This is independent of depth, but strongly dependent on the frequency. For an average depth of about 7 m the effective vertical stress will be in the order of 80 kPa. Thus the ratio between shear stress amplitude and vertical effective stress is 0.16. This

is in fair agreement with the value obtained from the concept of 'residual strength' as used in earthquake engineering.
The shear stress amplitude decreases quite fast. At x=0.1 m the shear stress already decreased to only 0.14 times the shear stress amplitude at x=0 (the interface). In general the liquefied zone will be small. For the densification and pore pressure generation models no separate modelling for this zone will be used.

Modelling the interaction sheet pile-soil and the propagation of vibrations in the liquefied soil is complex. The actual behaviour is not yet fully understood. One of the important issues is the rheologic behaviour of the liquefied sand (is it a Newtonian fluid, a Bingham fluid or something else). Another important issue is the numerical value of the relevant soil parameters (e.g. viscosity).

The three approaches used to assess the shear stress amplitude in the liquefied state deliver values that are in fair agreement with each other. Using as liquefied strength of the interface shear stress 5-10% of the initial effective vertical stress is considered, for practical purposes, a reasonable approximation of the actual behaviour.
In the present version of TRILDENS3 the shear stress is taken according to equation 6.3. With increasing excess pore pressure (increasing r_u and decreasing σ'_v), the yield stress at the interface sheet pile – soil decreases. As minimum value 10% of the initial effective vertical stress is used. Equation 6.17 and figure 6.9 show this relation.

$$\Delta\tau = \max(K_0\sigma'_v \tan(\delta), 0.1 * \sigma'_{v0}) \qquad (6.17)$$

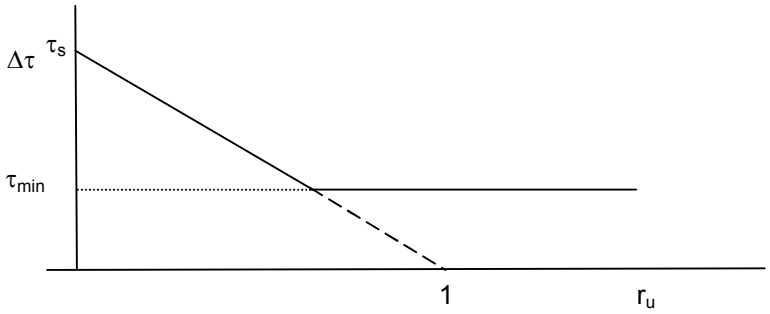

Figure 6.9 Relation between excess pore pressure ratio and shear stress amplitude, as used in TRILDENS3

6.4.5 Tip resistance

One of the sources for vibrations may be the waves emitted from the tip. In order to judge if taking this part into account in the model it is first judged whether this source has a marginal or a significant contribution to the densification.

First the behaviour is qualitatively investigated using videotapes made during a model test at GeoDelft. The test set-up is equal to the model tests described in

section 2.4. In the model test a sheet is placed in a tank filled with saturated sand. One side of the tank consisted of a glass wall, allowing observing the behaviour. The sheet is removed using a small vibrator. A high-speed camera has been used to register the soil movement. Inspecting the videotape of the tests revealed some interesting aspects. It is observed that at the tip of the sheet pile pressure waves are emitted. The amplitude of these body waves is quite high. The amplitude however attenuates fast with the distance. At a few decimetres from the tip the movement is no longer visible. The contribution of this mechanism to the total densification is expected to be limited.

The fast attenuation of the vibrations emitted from the tip of the sheet pile can be explained as follows. The tip of the sheet pile may be considered as a strip. The thickness of a sheet pile is 1 to 2 cm. Propagation of wave emitted from the tip, and close to the tip, is propagation in a 2D situation. With such a small width of the loaded area a fast attenuation with distance close to the sheet pile may be expected.

Apart for the load amplitude also the number of load amplitudes is of relevance for the amount of densification. Assuming a speed of installation of 2 m/minute and an influence area (diameter) of 1 m each soil element is experiencing vibrations from the tip during about 30 s. The number of load cycles is thus about 600 to 1200. This is small compared to the number of load cycles caused by vibrations emitted from the side of the sheet pile.
From this indicative description and estimate it follows that, for the commonly used sheet pile dimensions, neglecting the vibrations emitted from the tip is acceptable.

6.4.6 Out-of-plane bending sheet pile

In the preceding modelling the sheet pile is assumed to vibrate in the vertical direction only. However field experience is that the sheet pile vibrates in the horizontal direction as well. Therefore this aspect needs some attention.
Horizontal vibrations will have two effects. First the horizontal vibration may result in some horizontal compression of the soil. The second effect may be an increase in the shearing deformation of the soil elements next to the sheet pile, as the soil elements are not loaded on shearing but also on compression waves. In order to investigate the last effect an indicative calculation is made with the FEM program PLAXIS. The following modelling is used:

- plane strain situation
- linear-elastic soil, stiffness increases linearly with depth
- the sheet pile is modelled as a line element
- out-of-plane loading is modelled as a moment loading on top of the sheet pile
- amplitude vertical loading, F = 600 kN/m, for the case with moment loading the amplitude of the moment at top is M = 100 kNm/m (eccentricity of the vertical loading is e = 0.16 m).

A plane strain situation has been selected as in an axial-symmetric calculation no horizontal loading can be applied. As the purpose of the calculation is a qualitative

estimate of the effect of out-of-plane loading a plane strain calculation is considered adequate.

Figure 6.10 shows the deformation of the sheet pile under combined vertical and moment loading.

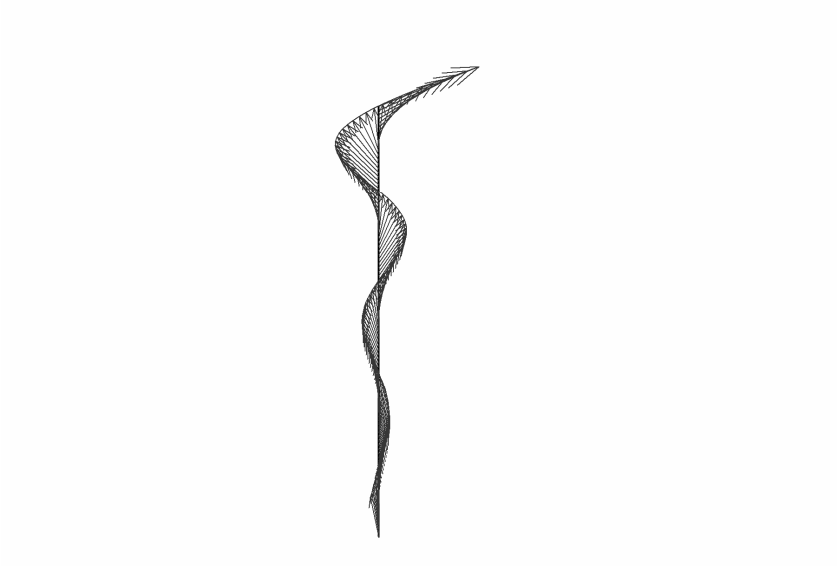

Figure 6.10 Deformation sheet pile under combined vertical and moment loading

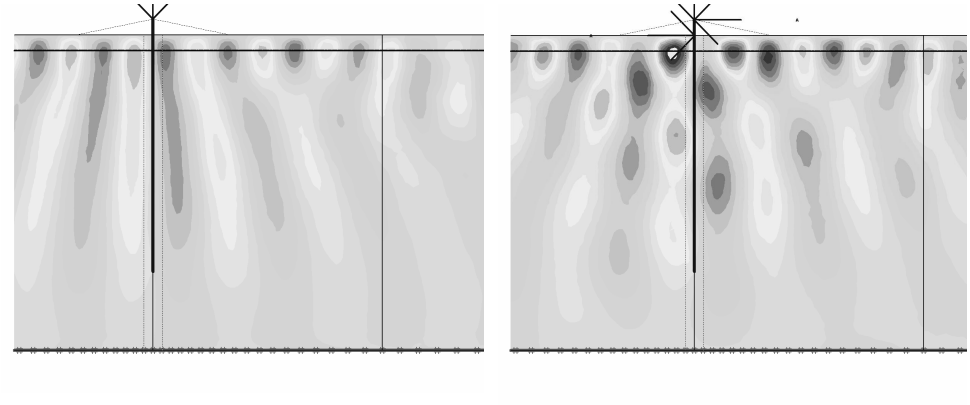

Figure 6.11 Comparison shear strain near sheet pile, for vertical and combined vertical and moment vibratory loading of a sheet pile

Figure 6.11 shows the difference in soil movement (shear strain) for the situation without and with moment loading. Without moment loading the soil movement is more or less a simple shearing of the soil. With moment loading the soil movement is more complex. Also the value of the shear strain is different. For 4 locations near the sheet pile the development of the shear strain in time will be presented. The

considered points are located at about 0.5 m from the sheet pile and at depths of 2m (point K), 5m (point L), 8m (point M) and 14.5 m (point N).

In case of combined vertical and moment loading the shear strain amplitude is found to increase with about 25% to 50% near the sheet pile. This effect cannot be ignored.

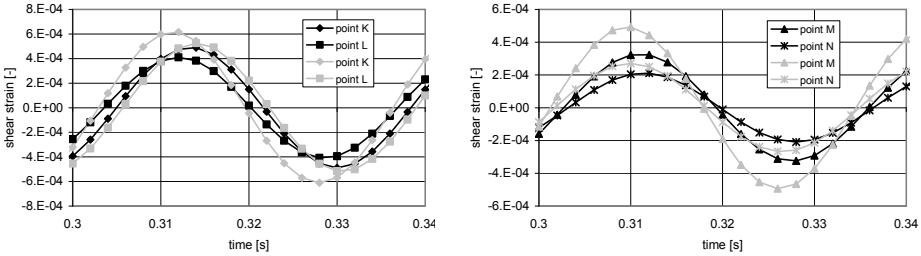

Figure 6.12 Comparison shear strain near sheet pile, black lines are for vertical and grey lines for combined vertical and moment vibratory loading of a sheet pile

6.4.7 Summary modelling source model

From the preceding sections the following conclusions with respect to the modelling of the source model may be drawn.
In the model the source of the vibrations are generated at the interface sheet pile – soil. The stress amplitude drops when the excess pore pressure increases. At large excess pore pressures (for the situation of liquefaction or near liquefaction) the shear stress amplitude does not become zero. The actual physical processes are complex. A practical approach is to use the concept of 'residual strength', as used in earthquake engineering. Equation 6.17 is used to model the effect of the excess pore pressure on the yield shear stress at the interface sheet pile – soil.

Modelling the shape of the sheet pile as a tubular pile gives a displacement field around the sheet pile that is quite similar to the field when using a U sheet pile or a Z sheet pile. The radius of the tubular pile is to be selected from the working width of the sheet pile, rather than the coating area.
Vibrations emitted from the tip may add locally to the densification. Given the relative small thickness of a steel sheet pile the effect is expected to be marginal. More research on this aspect however is needed to asses the contribution.
Moment loading of the sheet pile during vibrating, due to e.g. eccentric placement of the vibrator at the top of the sheet pile, may increases the shear strain amplitude with 25 to 50%. This effect is not accounted for in the model. Instead it is selected to take it into account by changing the parameters describing the stress amplitude at the interface sheet pile – soil.

A logical extension of the program would be to implement a model for installation or removal of sheet piles. Different models are available (see Berghe (2001), Viking

(2002) or Azzouzi (2003)). This has the advantage that a consultant can select directly an appropriate vibrator, capable of installing the sheet piles, that the time of vibrating is modelled correctly, etc. This extension is outside the scope of this study.

6.5 Propagation model

6.5.1 General

The purpose of the propagation model is to determine the relevant loading parameters for the generation model. Depending on the used model the propagation model is to yield the acceleration amplitude, the velocity amplitude, the shear strain amplitude or the shear stress amplitude. Between these parameters the following relations exist.

$$\Delta v = \frac{\Delta a}{2\pi f} \tag{6.18}$$

$$\Delta \gamma = \frac{\Delta v}{C_s} \tag{6.19}$$

$$\Delta \tau = G * \Delta \gamma \tag{6.20}$$

with:

- Δa : amplitude acceleration
- Δv : amplitude velocity
- f : frequency
- $\Delta \gamma$: amplitude shear strain
- C_s : shear wave velocity $C_s = \sqrt{(G/\rho)}$
- G : shear modulus
- ρ : unit mass of the soil
- $\Delta \tau$: shear stress amplitude.

Recent research (Hölscher and Waarts 2003) showed that the accuracy of vibration predictions is low. On average both simple and advanced models give a correct prediction of the vibration amplitude. The accuracy increased only slightly when using advanced models. The gain in accuracy by using advanced methods like a finite element model is therefore considered to be marginal. There will be a significant increase in computational effort as soil condition and driving depth of the sheet pile change during the process. Therefore it is decided to use for the propagation model a simple approach.

The following options for the attenuation of vibrations will be considered:

- attenuation of shear stress amplitude
- attenuation of velocity amplitude
- analytical expression Stokes.

In the next sections these options are described.

6.5.2 Shear stress attenuation

The simplest model for the attenuation of the vibration amplitude is to use a simple relation of the shear stress amplitude with distance.

$$\tau(r) = \tau(r = r_0) * (r / r_0)^n \quad (6.21)$$

with:

- $\tau(r)$: shear stress amplitude at distance r
- $\tau(r=r_0)$: shear stress amplitude at distance r_0
- r : considered distance
- r_0 : reference distance
- n : attenuation parameter, negative for decreasing shear stress amplitude

For the attenuation factor n a value of -0.5 may be used. More sophisticated expressions for determining the amplitude as function of the distance for an infinite long tub in a linear-elastic space are available (Verruijt 2004). Elaborating these expressions yield the same value. The value of n=-0.5 is however for the situation without material damping. Adding some material damping will increase the attenuation. The value of n becomes n = -0.65 to n = -1.0, depending on the used amount of soil damping.

6.5.3 Velocity amplitude attenuation

For assessing the velocity amplitude as function of distance a simple empirical relation as described in (CUR 1993) is used. This relation is a Barkan type relation. The velocity amplitude as function of the distance is:

$$v(r) = v_0 \sqrt{\frac{r_0}{r}} * \exp(-\alpha(r - r_0)) \quad (6.22)$$

with:

- v(r) : the amplitude of the velocity at distance r
- v_0 : amplitude of the velocity at distance r_0
- α : a parameter accounting for the material damping.

The amplitude of the velocity at distance r_0 = 5 m depends on the subsoil conditions and the centrifugal force of the vibrator. For Dutch soils and a centrifugal force of 350 kN the value of u_0 is about 2 mm/s. For vibrators with a higher centrifugal force the velocity amplitude is to be corrected according to:

$$v_{0,coo} = v_0 + 0.002 * (F - 350) \quad (6.23)$$

with:

- F : centrifugal force (in kN)
- v_0 : velocity amplitude (in mm/s)
- $v_{0,cor}$: corrected velocity amplitude (in mm/s).

The mentioned values for the velocity amplitude and its relation with the centrifugal force of the vibrator are purely empirical relations.

The centrifugal force of the vibrator is an input parameter in this expression. Sophisticated models may be used to assess the required capacity of the vibrator. An alternative is to use a simple expression to obtain a first estimate, e.g. the formula derived by Azzouzi (2003). His equation is rewritten as:

$$F = 0.0016 * O \int q_c(z)dz + A_{sheet} * q_{c,tip} \tag{6.24}$$

with:

- F : centrifugal force vibrator
- O : circumference of the sheet pile: O=2*B_{sheet}
- B_{sheet} : coating area, one side
- $q_c(z)$: cone resistance at depth z
- $q_{c,tip}$: cone resistance at tip level
- A_{sheet} : cross section sheet pile.

The mentioned expression is derived for installing sheet piles. In fact in this expression the required capacity of the vibrator is the sum of the shaft resistance and the tip resistance. Possible for removal the last term (tip resistance) may be set to zero.

It should be noted that this approach is valid for the 'far field' situation. Densification is expected to occur relatively close to the sheet pile. Here shear waves will dominate. In view of the length of the sheet pile these will expand as cylindrical waves. For this an attenuation with the square root of the distance can be assumed. The used attenuation curve is therefore considered as representative for this situation as well in case the driving depth of the sheet pile is sufficient large. This is justified in section 6.5.2 (stress attenuation).

The situation where the length of the sheet pile in the soil is small, e.g. at start of installation or end of removal, the previous reasoning is not correct. As this situation is present for a limited time only it will be neglected.
The model uses a fixed soil damping. In reality the soil damping will be a function of the strain amplitude. As the strain amplitude decreases with increasing distance it is expected that close to the sheet pile the soil damping will be larger as at some distance. In the calculations this can be taken into account by using a higher soil damping factor. Due to the nature of the model (with a velocity amplitude at r=5m being independent of the soil damping) this will result in higher velocity amplitudes, and thus more densification, close to the sheet pile.

6.5.4 Stokes

Stokes (Kausel 2006) derived analytical expressions for the Green's function of a point load in an infinite homogeneous space. For a vertical unit point load the Green's functions in the radial and tangential direction are:

$$g_{Rz} = \frac{\psi + \chi}{4\pi GR}\cos\theta \tag{6.25}$$

$$g_{\varphi z} = \frac{\chi}{4\pi GR}(-\cos\theta) \tag{6.26}$$

with:

- g_{Rz} , $g_{\varphi z}$: Green's function
- G : shear modulus
- R : distance to point load
- θ : angle between vertical and line through source and receiver.

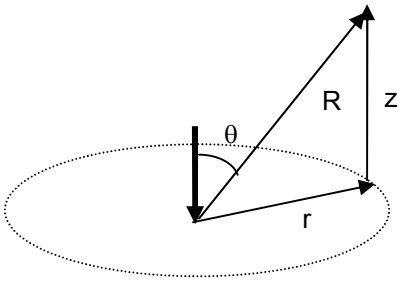

Figure 6.13 Coordinate system for Stokes equations

The parameters Ω_P and Ω_S (dimensionless frequency for respectively P and S waves) are defined as:

$$\Omega_P = \frac{\omega R}{C_P} \tag{6.27}$$

$$\Omega_S = \frac{\omega R}{C_S} \tag{6.28}$$

The functions ψ and χ are:

$$\psi = e^{(-i\omega R/C_P)}\left(\frac{C_s^2}{C_P^2}\right)\left\{\frac{iC_P}{\omega R}+\frac{C_P^2}{\omega R}\right\} + e^{(-i\omega R/C_S)}\left\{1-\frac{iC_S}{\omega R}-\frac{C_S^2}{\omega R}\right\} \tag{6.29}$$

$$\chi = e^{(-i\omega R/C_P)}\left(\frac{C_s^2}{C_P^2}\right)\left\{1-\frac{3iC_P}{\omega R}-\frac{3C_P^2}{\omega R}\right\} - e^{(-i\omega R/C_S)}\left\{1-\frac{3iC_S}{\omega R}-\frac{3C_S^2}{\omega R}\right\} \tag{6.30}$$

For a perfect vertical vibrating sheet pile the deformation is mainly a vertical shearing of the soil. Therefore, for ease of computation, only the vertical component will be considered further. From the Green's functions the Green's function for the vertical displacement is obtained.

The vertical displacement follows from the radial and tangential displacement according to:

$$g_z = g_{Rz}\cos\theta - g_{\varphi z}\sin\theta \tag{6.31}$$

From this follows:

$$g_z = \frac{1}{4\pi GR}\left(\psi + \chi\cos^2\theta\right) \tag{6.32}$$

Elaborating of this expression gives, after some re-arrangement of the different terms, for the vertical displacement:

$$\frac{u_z}{F} = \frac{1}{4\pi\rho R\omega^2} e^{(-i\omega R/C_P)}\left(\frac{1-3\cos^2\theta}{R^2} + \frac{\omega^2}{C_P^2}\cos^2\varphi + \frac{i\omega}{RC_P}(1-3\cos^2\theta)\right) + \frac{1}{4\pi\rho R\omega^2} e^{(-i\omega R/C_S)}\left(-\frac{1-3\cos^2\theta}{R^2} - \frac{\omega^2}{C_S^2}\cos^2\theta - \frac{i\omega}{RC_S}(1-3\cos^2\theta)\right) + \frac{1}{4\pi\rho RC_S^2} e^{(-i\omega R/C_S)} \tag{6.33}$$

The exponential terms can be expresses as:

$$e^{-i\omega R/C_P} = \sin(\omega R/C_P) + i\sin(\omega R/C_P) \tag{6.34}$$

$$e^{-i\omega R/C_S} = \sin(\omega R/C_S) + i\sin(\omega R/C_S) \tag{6.35}$$

Using these expressions equation 6.33 can be rewritten as:

$$u_z = u_{z,P} + u_{z,S} = A_{z,P}\cos(\omega R/C_P) + iB_{z,P}\sin(\omega R/C_P) + A_{z,S}\cos(\omega R/C_S) + iB_{z,S}\sin(\omega R/C_S) \tag{6.36}$$

The terms $A_{Z,p}$, $B_{Z,p}$, $A_{Z,s}$ and $B_{Z,s}$ are:

$$A_{z,P} = \frac{1}{4\pi r\rho\omega^2}\left((\frac{3\cos^2\Theta-1}{r^2} - \frac{\omega^2\cos^2\Theta}{c_P^2})\cos(\omega r/c_P) + \frac{\omega}{c_P r} * (3\cos^2\Theta-1)\sin(\omega r/c_P)\right) \tag{6.37}$$

$$B_{z,P} = \frac{1}{4\pi r\rho\omega^2}\left(-\frac{\omega}{c_P r} * (3\cos^2\Theta-1)\cos(\omega r/c_P) + (\frac{3\cos^2\Theta-1}{r^2} - \frac{\omega^2\cos^2\Theta}{c_P^2})\sin(\omega r/c_P)\right) \tag{6.38}$$

$$A_{z,S} = \frac{1}{4\pi r\rho\omega^2}\left((\frac{3\cos^2\Theta-1}{r^2} - \frac{\omega^2\cos^2\Theta}{c_S^2})\cos(\omega r/c_S) + \frac{\omega}{c_S r} * (3\cos^2\Theta-1)\sin(\omega r/c_S)\right) + \frac{1}{\rho c_s^2}\cdot\frac{1}{4\pi r}\cos(\omega r/c_S) \tag{6.39}$$

$$B_{z,S} = \frac{1}{4\pi r\rho\omega^2}\left(-\frac{\omega}{c_S r} * (3\cos^2\Theta-1)\cos(\omega r/c_S) + (\frac{3\cos^2\Theta-1}{r^2} - \frac{\omega^2\cos^2\Theta}{c_S^2})\sin(\omega r/c_S)\right) + \frac{1}{\rho c_s^2}\cdot\frac{1}{4\pi r}\sin(\omega r/c_S) \tag{6.40}$$

The vibrating sheet pile is modelled as a set of vertical vibrating point loads at the symmetry axis. In the linear elastic system the total response is obtained as a summation of the response of the single sources. The total vertical response follows thus from:

$$u_z = \sum(A_{z,S} + A_{z,P}) + i\sum(B_{z,S} + B_{z,P}) = A_z + iB_z \tag{6.41}$$

Knowing the vertical displacement amplitude the vertical velocity amplitude and the shear strain amplitude can be obtained.

For the assessment of the shear stress and strain amplitude a simple approach will be used. It is assumed that it is governed by the vertical displacement/velocity and

that the contribution of the radial displacement can be neglected. Now the shear strain amplitude follows from equation 6.19.

The equations are derived for a homogenous linear-elastic continuum. The effect of the free surface, the effect of soil layering and the effect of material damping are not taken into account.
In TRILDENS3 the effect of the free surface on the wave propagation is neglected. Soil layering is only partly taken into account. For each location the soil stiffness used in the equations is the soil stiffness at the considered location.
The equations are derived for linear-elastic soil behaviour. Material damping is thus not accounted for, but will be present in reality. A simple method to adjust the derived parameters for this effect is to make use of the well known Barkan relation, see equation 6.22.

$$v(x) = v_0 \sqrt{\frac{r_0}{r}} * \exp(-\alpha(r - r_0)) \tag{6.42}$$

The exponential part describes the 'soil damping'. To account for the soil damping the calculated amplitudes are multiplied with $\exp(-\alpha(r-r_0))$.

In the program the effect of the reduction of the shear modulus on larger strain amplitudes is not taken into account.

6.5.5 Conclusions on the propagation model

For the program three possible expressions for determining the propagation of the vibration amplitude will be considered. Of these two are quite simple and one (Stokes) is more complex. The last may require more computational effort. The attenuation factor of all considered models is -0.5 when the effect of material damping is ignored. Apart from the attenuation, and probably more important, is the actual predicted amplitude. At present no preference to one of the models can be given.

6.6 Generation model

6.6.1 General

In chapter 4 possible models to describe the densification or generation of excess pore pressures in cyclically loaded sand are described. The following models are selected for further processing:

- C/L model
- energy dissipation model
- Seed and Rahman model
- Hergarden (a version of the Barkan model), further referred to as 'Barkan, standard'
- Hergarden, adjusted for time dependent effects, further referred to as 'Barkan/Hergarden, advanced'.

Table 6.1 summarises the features of the different considered generation models.

model / aspect	Barkan, standard	Barkan / Hergarden, advanced	C/L method	energy dissipation	Seed&Rahman
development in time	no	yes	yes	yes	yes
model originally for dry or saturated soil	dry	dry	dry	saturated	saturated
primary result	densification	densification	densification	excess pore pressure	excess pore pressure
driving parameter	acceleration	acceleration	shear strain	shear strain and shear stress	shear stress
preshearing accounted for?	probable implicitly	probable implicitly	probable implicitly	no	yes
loss of preshearing on liquefaction	no	no	no	no	no
stress rotation	no	no	no	no	no
threshold value for densification	yes	yes	no	no	no
upper limit densification	yes, $I_{D,final}$=1	yes	no	no	no

Table 6.1 Overview generation models

The generation models can be grouped in different ways. The first grouping is in models that are derived for assessing the densification of dry soil (Barkan, C/L method) and models that are derived for assessing the generation of excess pore pressure in saturated soil (energy dissipation, Seed&Rahman).
Another division is in the used driving force for the densification. Barkan uses the acceleration as driving force, the C/L method uses the shear strain amplitude as driving force, the Seed&Rahman approach uses the shear stress amplitude as driving force and the energy dissipation method uses a combination of the shear stress and shear strain amplitude as driving force.

A typical situation during vibratory sheet piling can be described by
- frequency of loading 25-50 Hz
- duration of vibrating (per sheet pile) t = 1-5 minutes
- number of cycles (per sheet pile) N $\approx$ 10.000.

The time of vibrating is thus that in saturated sand the situation cannot be considered as fully drained or as fully undrained. Generation and dissipation of excess pore pressure will occur simultaneously. None of the models considered is intended for this situation. Therefore the models will be extended to cope with both generation and dissipation of excess pore pressure. The adjustments to the models are incorporated in the following sections.

6.6.2 Densification model Barkan standard

This model is already described in section 3.7. Densification is assumed to occur only if the acceleration amplitude exceeds a threshold value. After a sufficient number of loading cycles a final density is approached, the value of it depends on the acceleration level. It is argued by Hergarden that during vibratory sheet piling the number of loading cycles is that large that the final density is reached. From the change in relative density the plastic volume strain is calculated.
This model assesses directly the volumetric strain. No development of densification with time and no development of excess pore pressures are determined.
The preshearing effect is not explicitly taken into account. As the empirical parameters are derived from tests on dry sand is can be postulated that this effect is accounted for in the empirical parameters.

6.6.3 Advanced densification model Barkan/Hergarden

The complete expression for the development of the (change in) relative density in time is:

$$\begin{aligned} &\eta > \eta_0 : \ \Delta I_D(\eta,t) = \left[\exp(-\alpha_B \eta_0) - \exp(-\alpha_B \eta)\right] * \left[1 - \exp(-\beta t)\right] \\ &\eta < \eta_0 : \ \Delta I_D(\eta,t) = 0 \end{aligned} \tag{6.43}$$

The last part describes the development in time. In this β is an empirical value and t is the time function. In the version proposed by Hergarden the time effect is excluded. Taking this parameter into account a more advanced version can be developed which takes the development of the volume strain in time into account. This extended version is capable to determine the development of the densification (and excess pore pressure) in time.

Equation 6.43 describes the change in relative density for a constant acceleration amplitude. In reality the acceleration amplitude may vary in time. Therefore for t not the elapsed time can be used. To calculate the change in relative density during the considered time step a fictitious 'starting time' is defined. This fictitious starting time is the vibration time needed to obtain, at the considered point, the same change in relative density with the actual acceleration amplitude as is actually present at the considered point and time. The value is obtained from rewriting expression 6.43 and using a known value of ΔI_D:

$$1 - \exp(-\beta t_{start}) = \frac{\Delta I_D}{\left[\exp(-\alpha_B \eta_0) - \exp(-\alpha_B \eta)\right]} \tag{6.44}$$

From this follows the starting time t_{start}.

The change in relative density during the considered time step follows from:

$$\begin{aligned} &\Delta I_D(\eta,\Delta t) = \Delta I_D(\eta, t_{start} + \Delta t) - \Delta I_D(\eta, t_{start}) = \\ &\left[\exp(-\alpha_B \eta_0) - \exp(-\alpha_B \eta)\right] * \left\{\left[1 - \exp(-\beta(t_{start} + \Delta t)\right] - \left[1 - \exp(-\beta t_{start})\right]\right\} \end{aligned} \tag{6.45}$$

Rearranging this expression yields:

$$\Delta I_D(\eta,\Delta t) = \left[\exp(-\alpha_B \eta_0) - \exp(-\alpha_B \eta)\right] * \exp(-\beta t_{start})(1 - \exp(-\beta \Delta t) \tag{6.46}$$

The (plastic) volume strain follows from the change in relative density.

For the relative density used to determine the threshold acceleration η_0 and change in relative density, the relative density at start of the calculation is used. If the actual calculation would be used the densification would be underestimated as the relative density increases with time.

This model assesses directly the (plastic) volumetric strain. For undrained conditions the change in pore pressure model follows from the change in plastic volumetric strain.

$$\Delta u = M * \Delta \varepsilon_{vol}^{pl} \tag{6.47}$$

with:

- M : constrained modulus.

The method and associated parameters are derived from tests on dry sand, so for a drained condition. The effect of preshearing on the cyclic behaviour is therefore incorporated in the model. In a true undrained situation no preshearing will occur, and the behaviour will be different. No corrections for the preshearing effect are made. During vibratory driven sheet piles dissipation will occur and this aspect is not considered to be a major shortcoming.

In the used expressions the elapsed time is used as parameter for the duration of loading. The change in relative density is expected to be a function of the number of cycles rather than of the elapsed time. Therefore the parameter t is replaced by a parameter describing the number of elapsed cycles. This gives:

$$\Delta I_D(\eta, t) = \left[\exp(-\alpha_B \eta_0) - \exp(-\alpha_B \eta)\right] * \left[1 - \exp(-\beta_1 N)\right] \tag{6.48}$$

The relation with the original expression is:

$$\beta * t_1 = \beta_1 * N = \beta_1 * f * t_2 \tag{6.49}$$

with:

- β : empirical parameter
- β_1 : empirical parameter
- t_1 : time in minutes
- t_2 : time in seconds
- N : number of cycles
- f : frequency.

From this an estimate for the value of β_1 can be obtained.
For the parameter β Hergarden uses β = 1 min^{-1}. This value is derived from results of cyclic tests by Davis. The used frequency is 25 Hz and time t is expressed in minutes.
In the program TRILDENS3 the estimate of Hergarden is used and this value is set to β_1 = 0.04*0.01667 ($\cong 7.10^{-4}$). The value 0.04 is the reciprocal of f=25Hz and the value 0.01667(=1/60) is the translation from minutes to seconds. Using the test data of Leussink and Kutzner (1962) the value is found to be 1 to 2. This is for tests with a frequency of f = 50 Hz and for t in minutes. Using these data the values of about $\beta_1 = 5.10^{-4}$ are derived. The difference with the value of β_1 derived from the test data used by Hergarden is small.

6.6.4 C/L model

This model is described in section 4.7.3. For convenience the main expression is repeated here. The compaction follows from:

$$\Phi = C_1 \ln(1 + C_2 z) \tag{6.50}$$

with:

- z = J_2.N
- J_2 : second invariant of the strain amplitudes deviator, for pure shear strain $J_2 = 0.25*\Delta\gamma^2$
- N : number of load cycles
- $\Delta\gamma$: shear strain amplitude
- C_1, C_2 : empirical constants.

The relation between the compaction Φ and the plastic volume strain ε_{vol}^{pl} is:

$$\Phi = -\frac{1 - n_0}{n_0} \varepsilon_{vol}^{pl} \tag{6.51}$$

with:

- n_0 : initial porosity [-].

This method directly calculates the volumetric strain. The change in pore pressure follows from equation 6.47.

The preshearing effect is not explicitly taken into account. As the empirical parameters are derived from tests on dry sand is can be assumed that this effect is accounted for in the empirical parameters.

The model does not have an upper limit for the amount of densification. For large strain amplitudes and large number of cycles the densification may become unrealistic high. First indications are that for vibratory sheet piling the results stay within acceptable limits. Therefore in the present version of TRILDENS3 no precautions are implemented to prevent an unrealistic high amount of densification. The expression by Niemunis may be used to implement a model that achieves a final density.

6.6.5 Energy dissipation model

This model is already described in section 4.7.7. The model correlates the development of excess pore pressure during undrained cyclic loading to the energy dissipation during cyclic loading. Different researchers published different empirical formulas. In (Green 2001) an overview of the different formulas is given. In TRILDENS3 the expression of Mitchell is used:

$$r_u = \sqrt{\frac{E_{dis}}{PEC}} \tag{6.52}$$

with:

- E_{dis} : dissipated energy
- PEC : Pseudo Energy Capacity, an empirical parameter.

This approach requires that for each soil element the stress-strain behaviour during each cycle be assessed. This is not practical in view of the large number of cycles. Therefore another approach will be used. In soil dynamics it is customary to determine the soil damping as function of the shear strain amplitude. The damping ratio is defined as:

$$D = \frac{1}{4\pi} \cdot \frac{E_{dis}}{0.5.\Delta\gamma \ .\Delta\tau} \tag{6.53}$$

with:

- D : damping ratio;
- E_{dis} : dissipated energy per cycle;
- $\Delta\gamma$: shear strain amplitude
- $\Delta\tau$: shear stress amplitude.

Results of tests where the damping ratio has been measured are widely available in the literature. One well-known example is shown in figure 6.14. From these tests it follows that the damping ratio is a function of the shear strain amplitude.

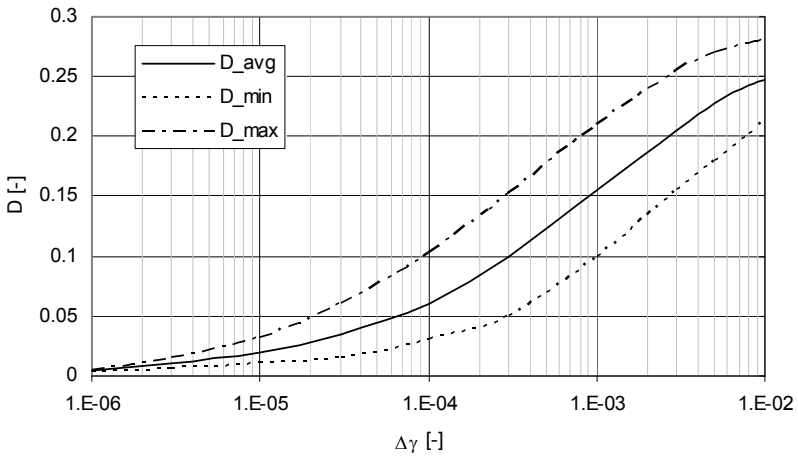

Figure 6.14 Damping as function of shear strain amplitude (after Seed et al. 1986)

Knowing D(γ) the dissipated energy per cycle can be assessed.

$$E_{dis,1} = 2\pi * \tau_{\max} * \gamma_{\max} * D(\gamma) = 2\pi G(\gamma, \sigma')\tau_{\max}^2 D(\gamma) \tag{6.54}$$

Integrating this expression over the number of cycles yields the total dissipated energy.

In TRILDENS3 the damping ratio as function of the shear strain amplitude is described with the following relation, being a fit of the curve in figure 6.14:

$$D = \left(0.75 + 0.125\log(\Delta\gamma)\right)^2 \tag{6.55}$$

This gives for $\Delta\gamma = 10^{-6}$ D = 0 and for $\Delta\gamma = 10^{-2}$: D = 0.25.

The (undrained) change in relative pore pressure during a time step Δt (with $f\Delta t$ cycles) follows from:

$$\Delta r_u = \sqrt{\frac{E_{dis,0} + E_{dis,1} * f\Delta t}{PEC}} - \sqrt{\frac{E_{dis,0}}{PEC}} \tag{6.56}$$

with:

- $E_{dis,1}$: dissipated energy per cycle
- $E_{dis,0}$: dissipated energy at start of considered time step.

This method assesses the change in pore pressure.
Using this expression the relative excess pore pressure may exceed $r_u = 1$. This is not corrected as the value is only used to assess the rate of pore pressure generation.
In the model the stiffness becomes almost zero at liquefaction and thus the shear strain amplitude becomes quite large (if the shear stress amplitude does not change). The shear stress amplitude will decrease as well, but a lower bound of $0.1*\sigma'_{v0}$ is used. This gives large energy dissipation per cycle. The model thus allows for energy dissipation in the liquefied zone.

The preshearing effect is not explicitly taken into account. Implicitly some kind of preshearing is used. The rate of pore pressure generation amounts:

$$\frac{dr_u}{dE_{dis}} = 0.5\left(PEC * E_{dis}\right)^{-0.5} \tag{6.57}$$

From this follows that the generation rate of excess pore pressure (dr_u/dt) drops when the amount of dissipated energy E_{dis} increases. This is a kind of preshearing effect. If this accounts for the preshearing in a correct way still needs to be investigated.
The complete loss of preshearing on reaching liquefaction is not accounted with this expression.

For dry and unsaturated soil no excess pore pressures will be generated. Instead densification will occur immediately. The plastic volume strain is determined from the change in pore pressure if the soil would be saturated.

$$\Delta\varepsilon_{vol}^{pl} = \frac{\sigma'_{v0}}{M}\left(\sqrt{\frac{E_{dis,0} + E_{dis,1} * f\Delta t}{PEC}} - \sqrt{\frac{E_{dis,0}}{PEC}}\right) \tag{6.58}$$

From the analysis of the cyclic triaxiaal tests (see section 5.4) it is observed that a correction to this value is to be applied in order to account for the preshearing effect. A parameter that accounts for the change in ‘structure’ has been introduced:

$$S = 10^{-X\Delta n} \tag{6.59}$$

with:

- X : empirical parameter, the value is found to vary between 333 to 1000
- Δn : change in porosity.

This gives the following expression for the change in volumetric strain during time step Δt:

$$\frac{\Delta\varepsilon_{vol}^{pl}}{\Delta t} = \sigma'_0 \, m_v \left(\sqrt{\frac{E_{dis,0} + E_{dis,1} * f\Delta t}{PEC * S}} - \sqrt{\frac{E_{dis,0}}{PEC * S}} \right) \tag{6.60}$$

6.6.6 Seed&Rahman model

This model is already described in section 4.7.9. The method is developed for saturated undrained soil behaviour. The equations for this situation are given in the mentioned section. The effect of partial drainage on the pore pressure generation is described there as well.

To use this method for calculating the volumetric strain in dry or drained soil some adjustments are required. For this the empirical relation will be linearised. First the number of cycles to liquefaction, in case of saturated soil, is determined. During N_{liq} cycles the change in pore pressure, and thus in effective vertical stress, is σ'_{v0}. This gives an average change in pore pressure per cycle. The number of cycles during a time step Δt is $f\Delta t$. Using the compression modulus M the volumetric strain for the considered time step follows from:

$$\Delta\varepsilon_{vol}^{pl} = \frac{\sigma'_{v0} \Big/ N_{liq}}{M} f\Delta t \tag{6.61}$$

6.6.7 Threshold value vibration amplitude

For low vibration levels the densification will be negligible. In the model by Hergarden a threshold value for the acceleration level is already used. For the other densification models described in this chapter it is assumed in TRILDENS3 that no densification or generation of excess pore pressure occurs for shear strain amplitudes below a threshold value of 10^{-4}. For locations and times where this situation is present the increase in plastic volumetric strain is set to zero. A consequence of this approach is that there is a discontinuity in the densification for shear strain amplitudes just below and just above the threshold shear strain amplitude.

6.7 Dissipation model

Dissipation of the excess pore pressure is calculated using the combined dissipation in vertical and radial direction (Verruijt 2006).

$$\frac{\partial u}{\partial t} = c_v \frac{\partial^2 u}{\partial z^2} + c_h \left(\frac{\partial^2 u}{\partial r^2} + \frac{1}{r} \frac{\partial u}{\partial r} \right) + A(t) \tag{6.62}$$

with:

- c_v : coefficient of vertical consolidation

- c_h : coefficient of horizontal consolidation
- u : excess pore pressure
- z : vertical coordinate
- r : radial coordinate
- A(t) : generation term.

The generation term A(t) is the result if the generation model. In the flow scheme this term is mentioned as $(du/dt)_{generat}$.

The coefficient of vertical consolidation is defined as:

$$c_v = \frac{k}{(\alpha + n\beta)\gamma_w} \tag{6.63}$$

with:

- k : permeability
- α : compressibility of the soil
- β : compressibility pore water
- γ_w : unit weight water.

The used boundary conditions for the consolidation equation are:

- axis of symmetry: closed
- outer boundary: open (at sufficient distance it should not matter if this boundary is open or closed as the excess pore pressure at this boundary is expected to be almost zero)
- lower boundary: closed
- groundwater level: free draining.

The change in volume per time step follows from the net outflow of water during the considered time step. This is equal to the change in pore pressure due to dissipation divided by the constrained modulus.

$$\Delta\varepsilon_{vol}^{pl} = \frac{1}{M}\frac{\sigma'_{v0} * \Delta r_{u,dissipat}}{\Delta t}\Delta t \tag{6.64}$$

At the end of vibrating still some excess pore pressure may be present. Dissipation of this excess pore pressure results in an additional settlement. This can be conveniently assessed from:

$$\varepsilon_{vol}^{pl} = \frac{u}{M} \tag{6.65}$$

with:

- u : excess pore pressure.

The value of M is stress dependent and so a function of the excess pore pressure. Equation 6.65 is numerically solved by decreasing the excess pore pressure at the end of vibrating in 10 steps to zero. For each step the correct value of M is used.

6.8 Contribution volume of sheet pile

During installation a certain volume of steel, the volume of the sheet pile, is inserted into the soil. During removal the same volume, increased with the soil sticking to the sheet pile, is removed.

This effect is accounted for as an adjustment of the volume change of the soil elements next to the sheet pile (positive for installation and negative for removal of the sheet pile).

$$\Delta\varepsilon_{vol}^{pl} = \pm\frac{0.5 * D_{sheet}}{r_0} \tag{6.66}$$

with:

- D_{sheet} : average thickness sheet pile (cross section divided by working width of the sheet pile)
- r_0 : width first element mesh.

6.9 Summation model

Three options are used to translate the plastic volume strain to a surface settlement:

- vertical integration
- volumetric spreading
- equation of Peck.

For the summation a plane-strain situation is considered. The plastic volume strains are calculated in an axial-symmetric geometry. After installing or removing a large number of sheet piles the situation with respect to the plastic strains a plane strain situation. For this situation the surface settlement is calculated. The difference in plastic volume strain from installing or removing a single sheet pile and a row of sheet piles is treated in section 6.11.

The easiest option is a vertical integration of the volume strains. For each vertical the surface settlement follows from:

$$\Delta z_i = \sum h_j \varepsilon_{vol,ij}^{pl} \tag{6.67}$$

with:

- Δz_i : settlement for column i
- h_j : height of sublayer j
- $\varepsilon^{pl}_{vol,ij}$: volume strain of element ij

This approach is however not realistic. An approach where some spreading of the settlement is taken into account is more realistic.

The second approach is to assume the presence of a sliding plane. The situation is illustrated in figure 6.15. The volume change of element ij is:

$$\Delta V = \varepsilon_{vol,ij}^{pl} * h_j * b_i \tag{6.68}$$

with:
- $\varepsilon^{pl}_{vol,ij}$: volume strain of element ij
- h_j : thickness sublayer j
- b_i : width of element ij.

The width of the area at surface over settlement occurs is:

$$B_{ij} = (GL - z_j)\tan\beta + b_i + (GL - z_j)\tan\theta \tag{6.69}$$

with:
- GL : ground level
- z_j : level of centre of element ij
- b_i : width of element ij
- θ : angle of volume spreading.

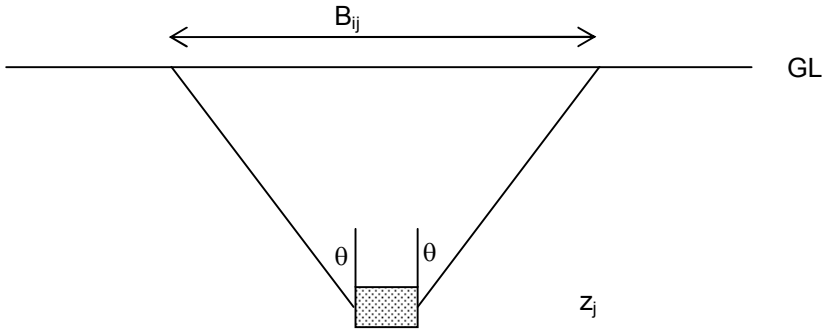

Figure 6.15 Method of assessing the surface settlement from local densification

The settlement Δz_{ij} due to the densification of element ij follows from:

$$\Delta z_{ij} = \frac{\varepsilon^{pl}_{vol,ij} * h_j * b_i}{b_i + 2(GL - z_j) * \tan\theta} \tag{6.70}$$

If the considered point at the surface is within the range B_{ij} this point is considered to settle with Δz_{ij}. If it is outside this range the additional settlement is taken as zero. The total surface settlement Δz_i follows from summation of the contribution of all volume elements:

$$\Delta z_i = \sum \sum \frac{\varepsilon^{pl}_{vol,ij} * h_j * b_i}{b_i + 2(GL - z_j) * \tan\theta} \tag{6.71}$$

The third considered approach is applying the method used for assessing the surface settlement during tunnelling. In (CUR/COB 1996) an inventory of empirical formulas for the settlement trough due to tunnelling is given. From this report the expression of Peck is taken to assess the surface settlement.

$$S(x) = S_{\max} \exp(\frac{-x^2}{2i^2}) \tag{6.72}$$

with:
- x : distance considered point to tunnel centre line

- S_{max} : settlement at tunnel centre line
- i : width parameter (distance centre to point of maximum inclination).

The parameter i is a function of the distance z between tunnel and surface. Mostly a linear relation is assumed:

$$i = K * z \tag{6.73}$$

For the parameter K different values are reported in the literature. In general the value range from 0.2 to 0.7, with K=0.5 as most popular value.
The relation between the maximum settlement S_{max} and the volume change of the considered soil element is:

$$S_{\max} = 0.4 \frac{\varepsilon_{vol}^{pl} \Delta z \Delta r}{i} \tag{6.74}$$

For the surface settlement it is assumed that superposition of the different components is allowed.
In the present version of TRILDENS3 the value of K is calculated from the input parameter θ (angle of volume spreading). The following relation is used:

$$K = \sin\theta \tag{6.75}$$

The default values for the parameter describing the spreading are θ = 30° and K = 0.5. Using a lower value of θ or K (which may be relevant for a sandy soil) results in a smaller and deeper settlement trough.

Figure 6.16 shows a comparison of the surface settlement using both the method with vertical spreading and the formula of Peck. For the calculation the following is assumed:

- volumetric strain 0.1 over 1 m width
- θ = 30°
- i/z = 0.5 (K=0.5).

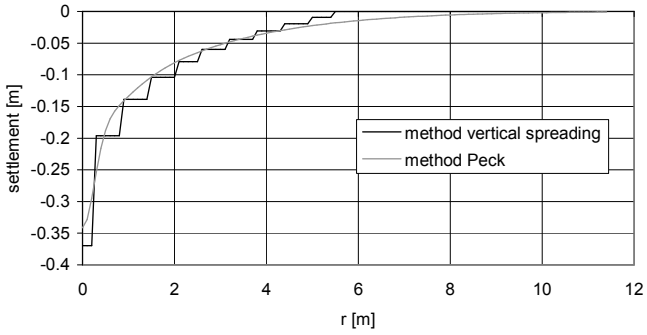

Figure 6.16 Comparison surface settlement using an angle of volume spreading and using Peck's equation

The two methods yield comparable settlement troughs. The stair like curve for the method with vertical spreading is a result of the used discretisation.

6.10 Adjustment shear modulus during the calculation

The stiffness (shear modulus) is a function of the effective stress and the shear strain amplitude. Both effects are accounted for in the program TRILDENS3.

It is assumed that the stiffness is proportional to the square root of the effective stress. From this assumption it follows:

$$G = G_{ref}\sqrt{\frac{\sigma'_{v0}-u}{p_{ref}}} = \sqrt{\frac{\sigma'_{v0}}{p_{ref}}(1-r_u)} \tag{6.76}$$

with:

- G : shear modulus
- G_{ref} : shear modulus at reference stress p_{ref}
- p_{ref} : reference stress
- σ'_{v0} : initial vertical effective stress
- u : excess pore pressure
- r_u : excess pore pressure ratio.

In the propagation model of Stokes a slightly different expression is used for determining the shear wave velocity, as the above expression yielded unrealistic results.

$$G_i = G_{ref}(0.5 + 0.5\frac{\sigma'_{v0}-u}{p_{ref}}) \tag{6.77}$$

The difference between the two approaches is small, as illustrated in figure 6.17.

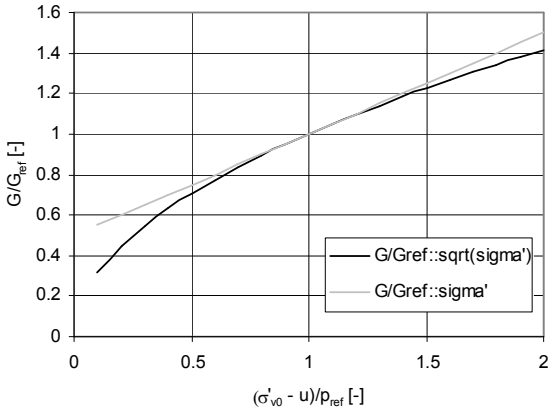

Figure 6.17 Comparison shear modulus, as function of effective stress

For the propagation model according to Barkan and stress attenuation the shear modulus is corrected for the actual strain amplitude. In the propagation model according to Stokes at present no correction for the actual strain amplitude is used. The reason for this is that the shear modulus is needed to perform the calculation. Using a strain dependent shear modulus requires an iterative procedure. This will increase the computational time to an unacceptable level.

The shear modulus is corrected for the strain amplitude. For this the Hardin-Drnevich approach is used. A hyperbolic relation between stress and strain is used.

$$\tau = \frac{\gamma}{\frac{1}{G_{\max}} + \frac{\gamma}{\tau_{yield}}} \tag{6.78}$$

with:

- G_{max} : initial (small strain) shear modulus
- τ_{yield} : shear stress at failure
- γ_r : reference shear strain.

From this follows for the actual shear modulus G:

$$G = \frac{\tau}{\gamma} = \frac{G_{\max}}{1 + \frac{\gamma}{\gamma_r}} \tag{6.79}$$

The reference shear strain is defined as

$$\gamma_r = \frac{\tau_{\max}}{G_{\max}} \tag{6.80}$$

The value of τ_{yield} is the value at which failure occurs in a Mohr-Coulomb approach:

$$\tau_{yield} = \left[\frac{\{(1+K_0)\sigma'_v \sin\phi + c.\cos\phi\}^2}{2} - \frac{\{(1-K_0)\sigma'_v\}^2}{2} \right]^{0.5} \tag{6.81}$$

For the situation the shear stress amplitude is assumed to be known (as in the stress attenuation propagation model) the expression for the actual shear modulus can be rewritten as:

$$G = \frac{G_{\max}}{1 + \frac{\tau / G}{\gamma_r}} \tag{6.82}$$

From this follows:

$$G = G_{\max} - \frac{\tau}{\gamma_r} \tag{6.83}$$

The shear strain amplitude becomes:

$$\gamma = \frac{\tau}{G} = \frac{\tau}{G_{\max} - \frac{\tau}{\gamma_r}} = \frac{\tau\gamma_r}{G_{\max}\gamma_r - \tau} = \frac{\tau\gamma_r}{\tau_{yield} - \tau} \tag{6.84}$$

This relation is of course only valid when $\tau < \tau_{yield}$.

For the situation that the shear strain amplitude is known the shear stress amplitude follows from:

$$\tau = G\gamma = \frac{G_{\max}}{1 + \gamma/\gamma_r}\gamma = \frac{G_{\max}}{1/\gamma + 1/\gamma_r} = \frac{G_{\max}}{1/\gamma + G_{\max}/\tau_{yield}} \tag{6.85}$$

The used relation can be compared with the empirical known shear degradation curves. The following parameters are used:

- σ'_v = 100 kPa

- c = 0
- ϕ = 35°
- K_0 = 1-sinϕ = 0.43.

Compared to empirical degradation curves the used approach shows less degradation.

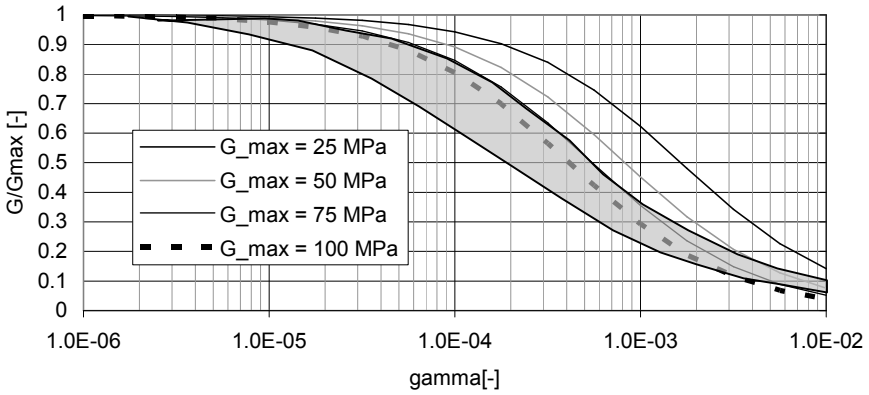

Figure 6.18 Shear degradation according to Hardin&Drnevich approach, for comparison also the empirical data from (Seed 1986) are included (the shaded area)

6.11 Effect additional sheet piles on amount of densification

The present model is not capable for predicting the effect of multiple sheet piles. Here a first estimate of the effect of installing more sheet piles on the settlement is made. According to the C/L model the densification is a function of the parameter z = $J_2N = \Sigma¼.\Delta\gamma^2$. The shear strain amplitude is a function of the distance to the sheet pile. This allows considering the effect of additional sheet piles as an increase in the parameter z.

Figure 6.19 shows the situation. The densification at the considered spot is a result of the summation of the load cycles from all sheet piles.

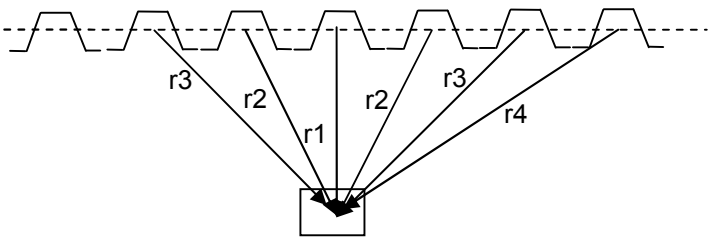

Figure 6.19 Summation of effect of multiple sheet piles

The summation of the multiple sheet piles follows from:

$$J_2N = \sum fT\,¼.\Delta\gamma^2(r) = ¼fT\sum\left((\Delta\gamma(r=r_0))^2 * \left(\frac{r_0}{r}\right)^{2n}\right) = ¼\,fT.(\Delta\gamma(r=r_0))^2\sum\left(\frac{r_0}{r}\right)^{2n} \quad (6.86)$$

with:

- r : distance between considered point and centre of considered sheet pile ($r = \sqrt{(x-x_0)^2 + (y-y_0)^2}$)
- r_0 : reference distance
- γ : shear strain amplitude
- γ_0 : shear strain amplitude at $r=r_0$
- n : power in attenuation relation.

This value can be compared with the value present when only one sheet pile is installed. From this follows a multiplication factor. The value of which turns out to be dependent on the distance from the sheet pile wall and the attenuation factor n. Figure 6.20 shows the relation.

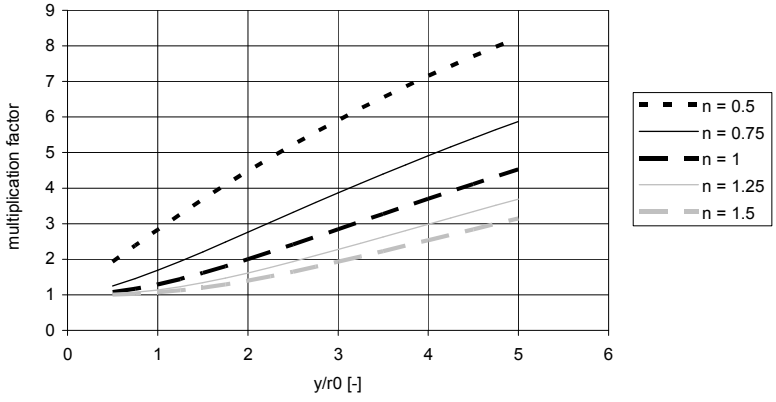

Figure 6.20 Effect multiple sheet piles on parameter z, as function of distance to sheet pile wall and attenuation factor

Close to the sheet pile (y/r_0 = 1 to 2), where most of the densification is expected, the factor is in the order of 2. This indicates that using in the calculation a time of vibrating which is twice the expected time for a single sheet pile may serve as a first approach. Future research may refine this approach.

6.12 Sensitivity of the model

6.12.1 General

In this section the sensitivity of the calculated settlement for a number of parameters is investigated. The purpose is to check whether the model shows some unexpected trends for some of the parameters and to obtain some insight in the sensitivity of the results for these parameters. This allows focusing on these parameters for predictive calculations.

First a reference situation is defined with the following characteristics:
- homogenous subsoil
- relative density ID = 50%
- length of sheet pile 15 m
- time of vibrating 300 s (v = 3 m/minute)
- frequency f = 25 Hz
- ratio δ/ϕ = 1
- stress attenuation factor n = -0.75
- vibration attenuation according to the stress attenuation model with n = -0.75
- C/L densification model
- centrifugal force vibrator F = 1000 kN, vref = 2 mm/s (v(r = 5m) = 3.3 mm/s)
- remaining parameters default values and correlations with relative density are used.

An example of the input file is shown in annex 6.1. Figure 6.21 shows the calculation result for this reference case.

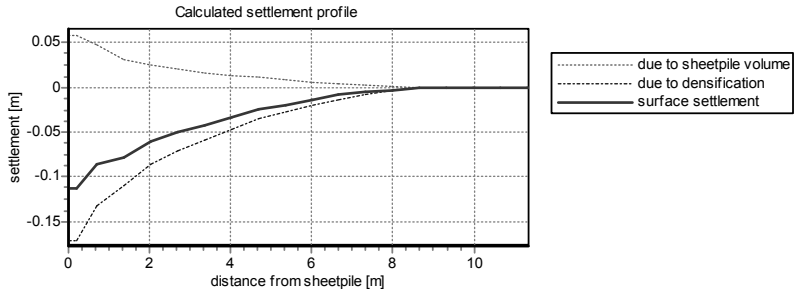

Figure 6.21 Result calculation reference case

The contribution of the volume of the sheet pile is equal for all considered variations in this section. Therefore this contribution will be omitted in the

comparison and only the contribution of the densification on the settlement is shown.

6.12.2 Influence densification and propagation models

The considered situation is installation of the sheet pile. Table 6.2 shows the calculated settlement close to the sheet pile (r = 2m) for the different combinations of propagation model and densification model. For the stress attenuation model also the effect of the attenuation parameter n is investigated.

densification / propagation	Barkan, standard	Barkan / Hergarden, advanced	C/L model	energy dissipation	Seed& Rahman
velocity attenuation	0.0399	0.0326	0.0161	0.0028	0.0204
stress attenuation, n=-0.75	0.6777	0.1905	0.0863	0.0279	0.0575
stress attenuation, n=-1	0.4334	0.1898	0.0750	0.0220	0.0483
Stokes	0.5432	0.1355	0.0329	0.0118	0.0440

Table 6.2 Comparison calculated settlement at 2 m from the centre line of the sheet pile

Using the velocity attenuation propagation model predicts settlements that are below the values obtained when using the other options. This model underestimates the vibration level close to the sheet pile, as will be demonstrated below with a comparison of the estimated shear stress amplitude at r = 1 m, using both the stress attenuation model and the velocity attenuation model.
The yield shear stress at the interface sheet pile-soil (r_0=0.38m) follows from $\tau=K_0*\sigma'_v*\tan\alpha$ = 0.441*75*tan34° = 22.3 kPa. Using the stress attenuation model the shear stress amplitude at r = 1 m becomes 10.8 kPa.
From the velocity attenuation model the shear stress amplitude at this location can be estimated as well. At r = 5 m the velocity amplitude is 0.0033 m/s. From this follows for the velocity amplitude at r=1 m v = 0.0077 m/s. The small strain shear modulus at reference stress is 68743 kPa. For an average vertical stress of 75 kPa the average small strain shear modulus becomes 59533 kPa. This gives a shear wave velocity of 173 m/s. The corresponding shear strain amplitude is 4.410^{-5} and the shear stress amplitude (in case of no excess pore pressure) 2.6 kPa.
It is found that the velocity attenuation model predicts much lower shear stress amplitudes and thus much lower settlements.
The largest settlements are predicted with the 'Barkan, standard' densification model. The difference in settlement calculated with the 'Barkan, standard' and 'Barkan/Hergarden, advanced' model is attributed to the time of vibrating and the reduction in shear stress amplitude at the interface sheet pile soil when excess pore pressures are generated. In section 6.12.7 the effect of time of vibrating on the settlement is shown.

6.12.3 Influence installation and removal

The different densification models are compared with respect to the difference in settlement during installation and removal. As propagation model the stress attenuation model is used. The difference in the calculation is that during installation the tip of the sheet pile starts at ground level and ends at the desired tip level. For removal the tip is at the installed level at start of the calculation and at ground level at the end of the calculation. It should be noted that in this comparison the effect of vibrations emitted from the tip are neglected. Also the effect of the volume of the sheet pile is neglected here.

densification / propagation	Barkan, standard	Barkan / Hergarden, advanced	C/L model	energy dissipation	Seed& Rahman
stress attenuation installation	0.6777	0.1905	0.0863	0.0279	0.0575
stress attenuation removal	0.6777	0.1364	0.0819	0.0277	0.0580

Table 6.3 Comparison difference in calculated settlement at installation and at removal

The model predicts in general a slightly larger settlement (densification) during installation as during removal. A relative large difference between installation and removal is found when using the 'Barkan/Hergarden advanced' model for the densification. It should be noted that in the mentioned figures the effect of the volume of the sheet pile is omitted. Also it should be noted that in the used model the effect of the pile tip is not accounted for.

6.12.4 Influence frequency vibrator

One of the parameters that can be influenced by the piling operator is the frequency of the vibrator. Table 6.4 shows the predicted surface settlement when using a normal frequency or a high frequency vibrator. The time of vibrating is considered independent of the used frequency.

densification / propagation	Barkan, standard	Barkan / Hergarden, advanced	C/L model	energy dissipation	Seed& Rahman
stress attenuation f=25Hz	0.6777	0.1905	0.0863	0.0279	0.0575
stress attenuation f=50Hz	1.1532	0.1863	0.0977	0.0329	0.0632
ratio	1.70	0.98	1.13	1.18	1.10

Table 6.4 Difference in settlement due to different frequencies of the vibrator

Almost all densification models predict an increase in settlement when using a high frequency vibrator. This increase is attributed to the increased number of cycles. In general the difference is limited.

Using the 'Barkan, standard' densification model however a large difference is observed. This can easily be understood as this model uses the acceleration as driving force. Using a high frequency vibrator increases the acceleration level significantly. For 'Barkan/Hergarden, advanced' a small decrease in the settlement is predicted when using a high frequency vibrator. A possible explanation may be the influence of the excess pore pressure on the shaft friction. In the calculation with high frequency vibrator the excess pore pressures reaches its maximum a little earlier as with the normal frequency vibrator.

6.12.5 Influence tip resistance

As mentioned only the Stokes propagation model is capable to take into account the tip resistance. To check the influence the cross section of the sheet pile is varied. Table 6.5 shows the results.
It is found that the contribution of the tip resistance on the settlement profile is limited in case of normally used cross section areas. For extremely large cross section areas the influence increases, as is expected. The effect of the volume of the sheet pile on the settlements dominates the effect of the tip resistance.

tip area [m^2]	settlement due to displaced volume sheet pile [m]	settlement due to densification [m]				
		Barkan, standard	Barkan / Hergarden, advanced	C/L model	energy dissipation	Seed& Rahman
0.0	0.0	0.4854	0.1210	0.0279	0.0100	0.0386
0.024	0.0252	0.5432	0.1355	0.0329	0.0118	0.0440
0.2	0.2099	1.003	0.1740	0.0755	0.0370	0.0870
1.0	1.0497	1.8271	0.2194	0.1418	0.1046	0.1449

Table 6.5 Influence of tip area on surface settlement

6.12.6 Influence relative density

Three different relative densities are used to check the influence of the relative density on the surface settlement. Calculation results are given in table 6.6.

As is to be expected all models predict a decreases in surface settlement when increasing the relative density.

relative density	Barkan, standard	Barkan / Hergarden, advanced	C/L model	energy dissipation	Seed&Rahman
0.3	1.4119	0.2826	0.1371	0.0651	0.1148
0.5	0.6777	0.1905	0.0863	0.0279	0.0575
0.7	0.2269	0.1083	0.0486	0.0120	0.0353

Table 6.6 Difference in settlement due to different relative densities

6.12.7 Influence time of vibrating

An increase in time of vibrating is expected to result in an increase in densification, and thus an increase in surface settlement. Three times of vibrating (5 minutes, one quarter of an hour and one hour) are used. Calculation results are shown in table 6.7.

time of vibrating [s]	Barkan, standard	Barkan / Hergarden, advanced	C/L model	energy dissipation	Seed&Rahman
300	0.6777	0.1905	0.0863	0.0279	0.0575
900	0.6777	0.3267	0.1284	0.0383	0.0829
3600	0.6777	0.5136	0.1877	0.0537	0.1150

Table 6.7 Difference in settlement due to different relative densities

As is expected increasing the time of vibrating increases in general the surface settlement. In the model ‘Barkan standard’ no time function is present. Therefore the result of this model is not a function of the time of vibrating. The results of the densification model ‘Barkan/Hergarden advanced’ tend towards the results of ‘Barkan, standard’ for large times of vibrating, as might be expected.

The settlement is not proportional to the time of vibrating. The rate of settlement is largest at the early time of vibrating and decreases with time of vibrating..

6.12.8 Conclusions from the sensitivity analysis

The predicted amount of settlement depends on the used combination of the densification model and the propagation model. From the densification models the standard model of Barkan shows the largest settlements. When using this model in combination with the stress attenuation model or the Stokes model the calculated settlements are unrealistic high. In combination with the propagation model according to Barkan (in this study called the velocity attenuation model) more realistic values are obtained. This is also the combination used by Hergarden (2000).
When the attenuation of the vibration amplitude increases the amount of densification decreases.

There is hardly any difference in the situation of installation and removal, at least for the case that during removal the effect of installation on the soil properties can be neglected.
The effect of frequency is limited. Doubling the frequency increases the densification with about 20%.
Vibrations emitted from the tip increase the amount of densification. For cross sections representative for steel sheet piles the effect is limited (10% to 20%). For larger cross sections, and equal time of vibrating, the contribution to the densification increases.
The influence of the relative density on the settlement is large. The effect of the time of vibrating is limited. The densification approximately doubles when the time of vibrating is increased by a factor 10.
The final conclusion is that the observed trends are in line with expectations. No conclusion with regard to the preferred densification model can be drawn.

7. Execution and results Raamsdonksveer sheet pile test

7.1 Purpose of the test

In chapter 6 a new model is described to assess the settlements during vibratory sheet piling. In order to check and improve the developed model well documented cases with measured settlements during vibratory sheet piling are needed. These data are rare. Known cases for which data on measured surface settlements are available only contain data on the subsoil conditions, the type of sheet piles and the surface settlement. These data are useful for checking the overall behaviour of the method, but do not allow checking the different processes leading to the surface settlement. In case of discrepancies between predicted and observed settlement it cannot be investigated what part of the model needs to be improved. In case of good agreement between predicted and observed settlement it remains a question whether the model is correct or if this is just by chance.
For this reason a well instrumented field test has been initiated and executed. Prime purpose of the test is to provide all necessary data to validate the model. In case of discrepancies between predicted and measured settlement the data are to show the reason for the mismatch, thus allowing improving the developed model on that part. The second purpose of the test is to check if no important mechanisms are neglected.

This chapter describes the test and the main obtained data. The data are used in the chapter 8 for validation of the model.

7.2 Test location

The test is performed at the yard of WoudWormer. This yard is located at the industrial quarter Dombosch of Raamsdonksveer, The Netherlands. To the north of this quarter the river Bergsche Maas is flowing and to the south-west the river Donge, a tributary of the Bergsche Maas. The test location is at a distance of about 50 meters from the river Donge. The Bergsche Maas has a small tidal variation (the amplitude is 0.1 to 0.15 m). It is not expected that this tidal variation will influence the test.

The area used to be a meadow. Some 30 years ago the area has been raised with about one meter of sand and put into use as stockyard by WoudWormer. It is used for storing steel sheet piles and steel planking since. The preloading of the area due to storage of sheet piles is estimated to be approximately 20 kPa (4 bundles of 5 sheet piles with a weight of 100 to 150 kg/m^2). According to the yard manager no other activities have been performed in the past at the test location.
The ground level of the test location is at approximately 1.3 m above NAP (Dutch Ordnance Datum).
For the test an area of about 15*25 m^2 is cleared of stored sheet piles. Beams used to store the sheet piles and other objects on or just below ground level are removed as well.

Figure 7.1 Test site before the test

At the side of the test location a drain is present for dewatering the site.

7.3 Subsoil conditions

Preceding the installation phase 7 CPT's are performed at the test site (CPT1-01, 1-02, 1-03, 1-04, 1-07, 1-09 and 1-10). During and after the installation of the transducers the CPT's 1-05, 1-06 and 1-08 to 1-15 are performed. Results of the CPT's at the centre line of the sheet pile wall are shown in figure 7.2.
A discussion of the measured values, and in particular on the deviant behaviour of CPT 1-06, will be given later in this section.

After the test one boring is made. The purpose of this boring is to obtain material for the calibration of the electrical density probe and for cyclic triaxial tests. The type of boring is a Begemann boring with a diameter of 66 mm. A photograph and of the boring and a bore log is given in annex 7.1.

In the boring 9 different sand layers are discerned. From each layer a sample is taken and the following properties are determined:
- grain size distribution
- porosity of the sample n_0
- minimum and maximum porosity n_{min}, n_{max}
- specific grain mass ρ_s
- angularity.

The porosity of the sample is the porosity of a sample taken carefully from the boring. The boring is a high quality boring and therefore the obtained value may be considered as an indication of the in-situ porosity.

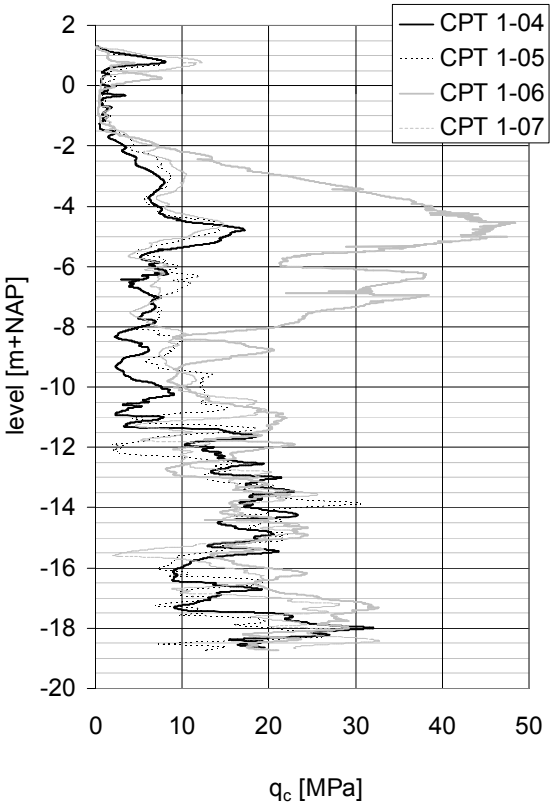

Figure 7.2 Results CPT testing at centre line of sheet pile wall

The grain size distribution is shown in figure 7.3. Other results are shown in table 7.1. The determination of the roundness is according to Pettijohn. This procedure differs slightly from the roundness according to Powers. The relation is shown in figure 7.4. Sand with roundness between 20 and 40 is classified as subangular and sand with roundness between 40 and 60 as subrounded.

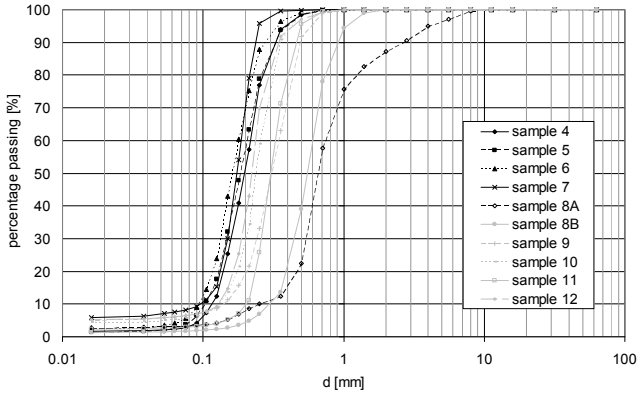

Figure 7.3 Grain size distribution

sample	level [m+NAP]	n_0 [-]	n_{min} [-]	n_{max} [-]	ρ_s [g/cc]	d_{50} [mm]	d_{60}/d_{10} [-]	roundness
4	-2.2	0.38	0.32	0.44	2.639	0.116	1.87	52
5	-3.1	0.36	0.32	0.43	2.643	0.103	1.99	52
6	-4.0	0.36	0.31	0.44	2.647	0.093	1.93	48
7	-5.25	0.44	0.38	0.52	2.655	0.100	1.88	27
8a	-5.8	0.38	0.31	0.45	2.642	0.322	2.32	34
8b	-6.3	0.4	0.32	0.45	2.641	0.298	2.06	37
9	-7.2	0.4	n.a.	n.a.	2.643	0.141	2.45	45
10	-7.9	0.41	0.34	0.47	2.649	0.137	1.86	45
11	-8.95	0.37	0.34	0.45	2.650	0.209	1.57	53
12	-10.1	0.42	0.35	0.47	2.656	0.137	1.73	46

for sample 9 no minimum and maximum density is determined in view of the amount of clay in the sample

Table 7.1 Results index testing

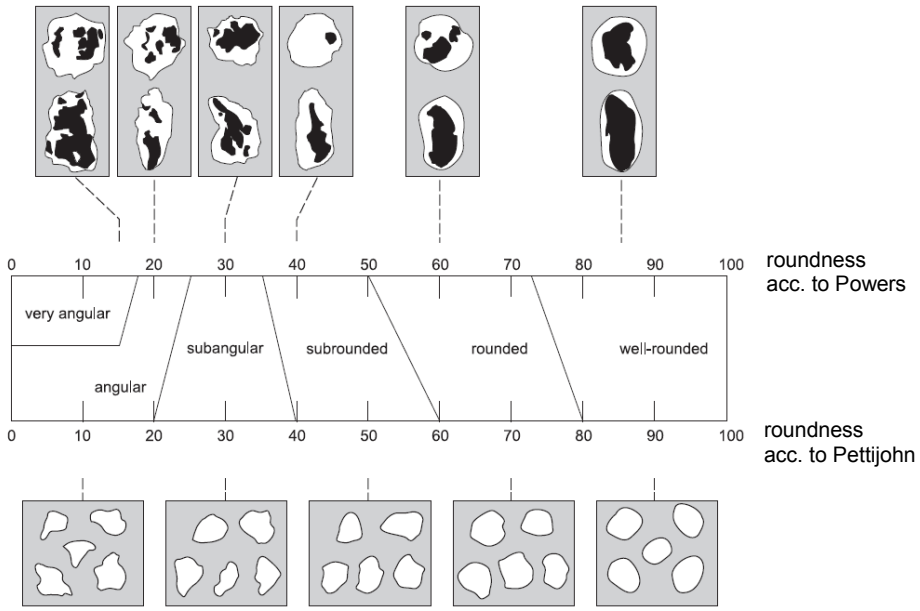

Figure 7.4 Relation roundness according to Powers and according to Pettijohn (from (CROW 2004))

From the performed CPT's and the boring the following description of the subsoil is derived. In general the CPT's show in horizontal direction a homogeneous subsoil condition. The top is clean sand of antropogene origin. During a rainy period it becomes a little slickly. Below this, a layer of clay with a thickness of about 1.5 m is present. At a depth of 6 m below ground level (NAP – 4.7m) a thin layer with a high cone resistance (10 to 15 MPa) is encountered. In some of the performed CPT's gravel is detected (audible during penetration as a grinding noise) at this depth.

The friction ratio of the sand is about 0.8% for the soil above NAP – 4.7m and about 0.6% for the sand below NAP – 4.7m. This indicates medium sand for the top layer and medium coarse sand for the sand below GL-6m. From the boring no such difference could be detected, apart from one layer between NAP – 5.6 m and NAP – 6.7 m.

At CPT 1-06 a remarkable high cone resistance (30 to 50 MPa) is encountered between 4 m and 9 m below ground level. These high cone resistances is also encountered in one of the additional CPT's performed after discovering this feature (CPT1-14) and during the installation of the transducers ED-4 (some 3 m apart) and ED-1 (0.6 m apart). Combining all the available information it is inferred that the size of this spot is about 2*5 m^2. Available information is that no former construction activities have been performed at this spot. The reason for this locally high cone resistance is not clear.
The measured pore pressure indicates a nearly hydrostatic water pressure. A small difference in piezometric head is sometimes observed for the soil above and below NAP – 5 m. The difference is small (a few decimetres at the most). The change in measured pore pressure seems to coincide with the change in friction ratio and with the depth of the gravel layer. From the results of the piezocone testing it is determined that the water table is at approximately NAP +0.5 m to NAP + 0.8 m.

7.4 Test program

The test consisted of installing and removing 10 steel double sheet piles. Five of them are AZ26 profiles and the five are Larssen 605 profiles. Details of the used sheet piles are given in table 7.2. At the same location also three concrete elements (Spanwand SPW600) are installed and removed. Results of this part of the test are not described here. Reference is made to (Meijers and Tol 2007).

pile	type	number in test	length [m]	width [m]	height [m]	W [cm^3]	cross section [cm^2]	cross section [cm^2/m]	coating area [m^2 per meter length]
double Z	AZ26	6 – 10	15	1.26	0.427	3280	249	198	3.56
double U	Larssen 605	1 - 5	15.5	1.2	0.42	2424	213	177	3.74

Table 7.2 Dimensions used sheet piles

Before a sheet pile is installed a set of two vibration transducers is mounted at the top of the sheet pile, using a specially designed clamp. These transducers measure the vibrations in the vertical direction and the horizontal direction perpendicular to the wall. Unfortunately one transducer was damaged during installation of the first sheet pile. After this it has been decided to use the other transducer alternately for measuring the vibrations in the vertical and horizontal direction. After installation of the fourth sheet pile this transducer ran out of order as well.

A PVE 2323 VM vibrator is used to install and remove the steel sheet piles. The operating frequency of the vibrator is 38 Hz. During installation the clamp is placed at the middle clutch of the double sheet piles. This implies that for the Z-profile the vibrator is located eccentric from the centre line. It is expected that this will introduce bending moments in the sheet pile. For the U-profile the vibrator is located at the centre line.
During removal of the Z-profiles and of sheet pile 1 (U-section) the clamp is also placed at the middle clutch of the double sheet pile. For removal of sheet pile 2 to 5 (U-section) the clamp is placed at the flange of the sheet pile, at the side of the test field and closest to the sheet pile still in place.

When discovering the spot with local hard soil near CPT1-06 it was not feasible anymore to change the location of the test. As far as reasonably possible the test program is adjusted such that the influence of this spot on the test results is as small as possible. This is achieved by selecting an installation sequence where the last sheet piles to be installed are installed at this spot. Therefore installation starts with the Z-profile and proceeds with the U-profile. The sequence of installation is: 6-7-8-9-10-1-2-3-4-5.
When all sheet piles are installed a series of CPT's is performed (series 2). After this the sheet piles are removed. The same sequence as for installation is used, so 6-7-8-9-10-1-2-3-4-5. A third series of CPT's is performed after the sheet piles are removed in order to check if the soil condition has changed. Sounding depth of all CPT's is 20 m below ground level.

CPT number	phase during the test	purpose
1-01 to 1-15	before start	characterise subsoil
2-01 to 2-10	after installation steel sheet piles	effect installation of sheet piles and extend of influence
3-01 – 3-08	after removal steel sheet piles	effect removal of sheet piles and extend of influence

Table 7.3 Overview performed CPT's

7.5 Used instrumentation

The selection of the used transducers follows the process outlined in section 6.2 (outline of the model). The following list gives an overview of the identified sub processes and the transducers to measure this sub process. For completeness also the sub processes for which no instrumentation is used are mentioned.

- source
  - 2 acceleration transducers at top of sheet pile
  - 1 wire extensometer (to measure speed of installation and removal)
- interface behaviour sheet pile-soil
  - no instrumentation
- propagation of vibrations
  - acceleration transducers (8 at surface and 9 at depth)

- generation excess pore pressures and densification
  - 4 pore pressure transducers
  - 4 electrical density probes
  - CPT's before installation, after installation and after removal sheet piles
- dissipation of excess pore pressures
  - 4 pore pressure transducers
- displaced soil volume due to sheet pile volume
  - no instrumentation
- settlement at surface
  - 30 settlement points at surface
  - 8 settlement points at depth.

It is not possible to check all identified sub processes with the used instrumentation. Measuring the interface behaviour between sheet pile and soil requires instrumentation of the sheet pile. This has been omitted in view of the associated costs. The displaced volume due to the installed volume of the sheet pile is determined from the embedded length and the cross section of the sheet pile. The first is determined from levelling the top of the sheet pile after installation, combined with the known length of the sheet pile and ground level. The last is taken from the documentation of the manufacturer of the sheet piles.
A list of all transducers and their location, as actual present during the test, is shown in annex 7.2. A description of some of the transducers is given in the next section, when describing the measured data.

Figure 7.5 Instrumented test site, just before start of installation of the sheet piles

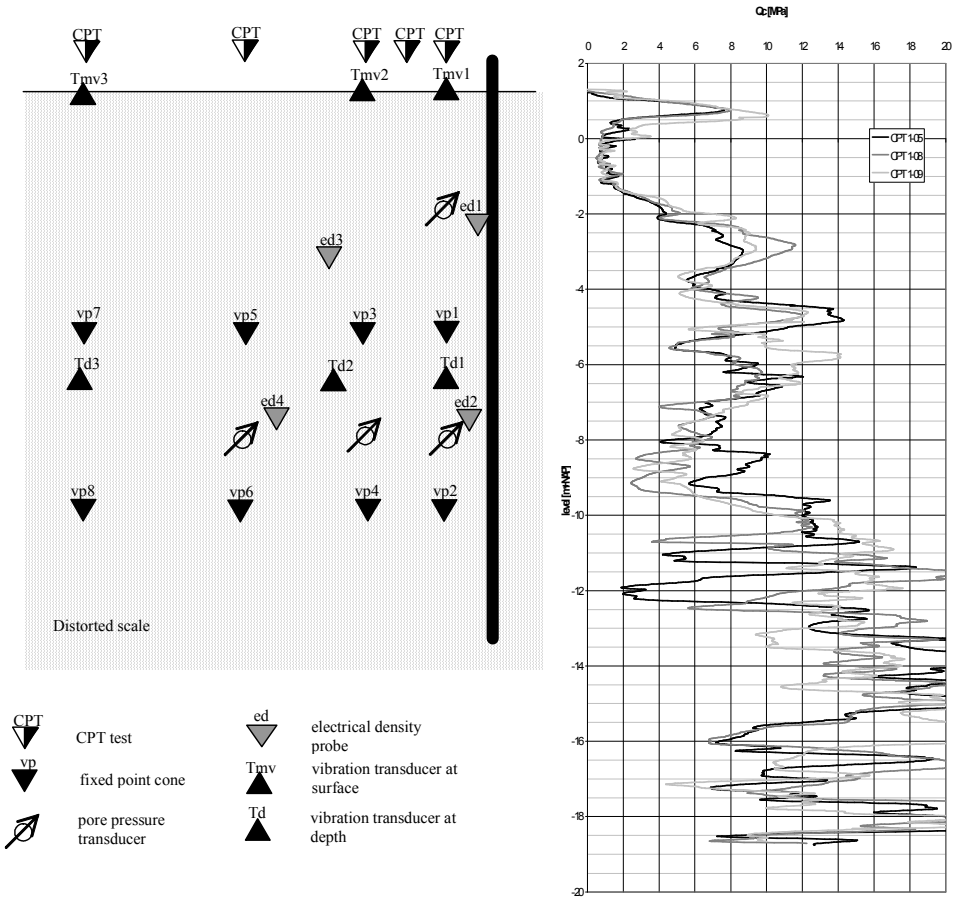

Figure 7.6 Cross section with indication depth of the transducers

7.6 Test results

7.6.1 Driving depth sheet piles

The driving depth of the installed elements will be used to determine the displaced soil volume during installation and removal. After installation of all steel sheet piles the level of the top is measured. The top level is shown in figure 7.7.

From the value of the top level the level of the tip is derived. Each single pile is measured. This implies that each double pile is measured twice. For determining the driving depth of the sheet pile a ground level of NAP + 1.3 m is used. Table 7.4 shows the results.

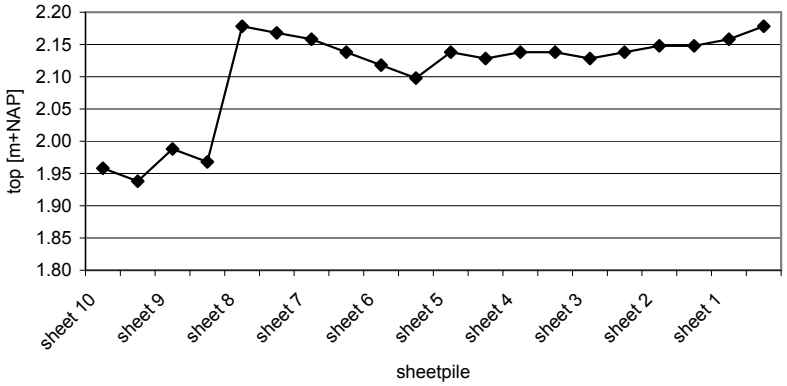

Figure 7.7 Top of sheet pile

The driving depth is also derived from the measurements with the wire extensometer. Two values are given, one for the installation phase and one for the removal phase. The driving depth according to the wire extenso meter differs from the value obtained from the levelling of the top of the sheet pile. In general lower values are obtained. The values derived from the wire extenso meter refer to the period of vibrating. It is observed that the sheet piles penetrated a little into the soil before vibrating started due to its own weight and the weight of the vibrator. During the removal phase the vibrator is switched off and disconnected from the sheet pile before the sheet pile is completely out of the soil. The last part is lifted using the hoist of the crane. Therefore the correct driving depth of the sheet pile cannot be determined from the measurement with the wire extenso meter.

7.6.2 Speed of installation and removal

Table 7.5 shows the length of time of installation for the sheet piles. This time is derived from the vibration time. The steel sheet piles are removed in one continuous operation. From the time of installation or removal and the driving depth the average speed of installation and removal can be derived. Values are presented in table 7.5 as well.

Time of installation a sheet pile is approximately 4 minutes. For sheet pile 3, 4 and 5 longer times of installation are found. These sheet piles are located at the hard spot. Time of removal of a sheet pile is approximately 2.5 minute. For this operation no effect of the stiff spot is found.

sheet pile number	type	top level [m+NAP]	tip level [m+NAP]	driving depth [m]	driving depth acc. to wire extensometer
1	U	2.178 2.158	-13.322 -13.342	14.65	14.45 / 14.65
2	U	2.148 2.148	-13.352 -13.352	14.65	14.45 / 13.20
3	U	2.138 2.128	-13.362 -13.372	14.65	14.40 / 14.00
4	U	2.138 2.138	-13.362 -13.362	14.65	14.35 / 14.40
5	U	2.128 2.138	-13.372 -13.362	14.65	14.35 / 14.80
6	Z	2.098 2.118	-12.902 -12.882	14.20	-- [1])/ 14.00
7	Z	2.138 2.158	-12.862 -12.842	14.15	13.85 / 13.70
8	Z	2.168 2.178	-12.832 -12.822	14.15	13.70 / 13.65
9	Z	1.968 1.988	-13.032 -13.012	14.30	13.80 / 13.70
10	Z	1.938 1.958	-13.062 -13.042	14.35	13.50 / 13.75

[1]) First part of installation not measured, on detecting the problem with the data logging the test was halted and the problem solved

Table 7.4 Top and tip level of the sheet piles

sheet pile number	driving depth [m] [1])	time of installation [s]	time of removal [s]	speed of installation [m/s]	speed of removal [m/s]
1	14.44 / 14.66	299	164	0.05	0.09
2	14.45 / 13.21	263	132	0.05	0.10
3	14.41 / 14.02	341	139	0.04	0.10
4	14.35 / 14.40	439	162	0.03	0.09
5	14.34 / 14.78	293	156	0.05	0.09
6	11.62 / 13.98	220	210	0.05	0.07
7	13.83 / 13.71	223	205	0.06	0.07
8	13.71 /13.63	194	167	0.07	0.08
9	13.81 / 13.69	223	213	0.06	0.06
10	13.49 / 13.74	208	151	0.06	0.09

[1]): length of installation/removal according to wire extensometer

Table 7.5 Velocity installation and removal

7.6.3 Vibration level sheet piles

Vibrations of the sheet pile are measured in the vertical direction and in the horizontal direction. The vibration transducers are connected to the top of the sheet pile using a special designed clamp. Figure 7.8 shows the mounting of the vibration transducers at the top of the sheet pile.

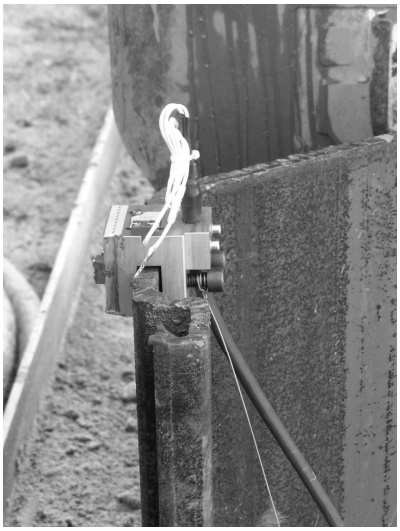

Figure 7.8 Vibration transducers at top of Z-profile

Only during the installation of the first four sheet piles the vibration level of the sheet pile itself could be measured in one direction. The direction of measurements is:

- sheet pile 6 and 7: vertical
- sheet pile 8 and 9: horizontal perpendicular to the wall

Figure 7.9 and 7.10 show the measured values. Presented is the amplitude of acceleration. Shortly after start of vibrating of sheet pile 6 it was discovered that the vibration transducer was out of order. After noticing the installation is stopped and the problem fixed. For this reason for sheet pile 6 only data for a free standing length less than 13 m are available.

At start of the installation the vibrations exceeded the measurement range of the transducer (50g according to the specifications, 65g according to the recorded data). The vibration level and shape show different patterns for the vertical and horizontal vibration. The vertical amplitude is nearly constant during the installation phase. The mode is nearly a sine function. The horizontal amplitude varied during the installation. Eigen modes of the free standing length of the sheet pile are expected to be responsible for this behaviour. A Fourier analyse of the measured signal shows that the vertical mode consists of one component while the horizontal vibration contains higher modes as well. The amplitude of these modes changed during the installation.

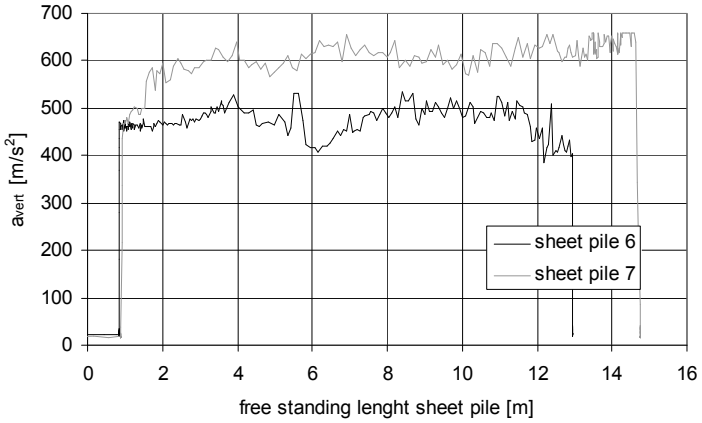

Figure 7.9 Vertical vibrations sheet pile as function of the free standing length

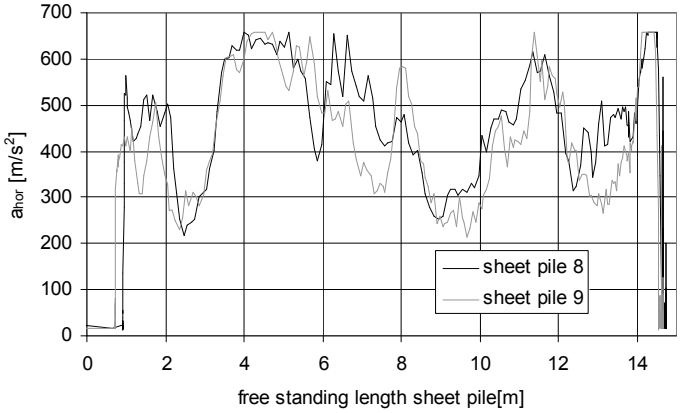

Figure 7.10 Horizontal vibrations sheet pile as function of the free standing length

7.6.4 Vibration levels surrounding

The vibration level next to the sheet piles will be analysed using the velocity amplitude. As the accelerations are measured, integration of the measured signal is needed. The following procedure is used.
First a general offset of the accelerations is determined so the net velocity at the end of the measurement is zero. The measured accelerations are corrected with this offset during further processing of the data.

For each second the development of the velocity is determined by integrating the signal. The acceleration is corrected for the average offset. At start of each period

the velocity is set to zero. In reality the velocity will not be zero but an unknown value. The velocity amplitude is determined for each second as half the difference between the minimum and maximum velocity. With this approach an offset of the velocity does not influence the obtained velocity amplitude.

It is known that small errors in the acceleration may influence the velocity. In general a small systematic error in the acceleration will result in a continuous increasing or decreasing trend of the velocity. This will increase the derived velocity amplitude per cycle. It is expected that the described adjustment of the acceleration will correct this error. Assumptions in this respect are that the systematic error is constant during the measurement period and that the random error cancels during the integration interval. This assumption is checked by performing the processing for one data file using different lengths of the time interval and comparing the results. It is found that the maximum amplitude is hardly influenced by the length of the used time interval. From this it is concluded that no continuous change of the zero level of the velocity is present in the calculation.

An example of the velocity amplitude is shown in annex 7.3. This is the situation for installation of sheet pile 3, situated close to the location of the vibration transducers. The velocity amplitude varies during the process of installation. For further processing only the maximum value of the velocity amplitude found at each transducer and each sheet pile is used. Annex 7.4 and 7.5 shows this velocity amplitude as function of the distance to the sheet pile for each sheet pile.

In order to distinguish between the vibrations due to the Z-profiles and the U-profiles the first are indicated with a cross. From these annexes it can be observed that for the steel sheet pile the horizontal and vertical vibrations are of the same magnitude. The velocity amplitudes show a large scatter. The ratio between upper and lower bound of the measured velocity amplitude at a given distance from the sheet pile wall is about 4.
For comparison of the different situations a trend line for the vertical velocity amplitude is derived for each situation. These lines are shown in figure 7.11.

As expected the velocity amplitude decreases with distance. The attenuation with distance is about $r^{-1.5}$. In general the soil vibrations at depth are less as the soil vibrations at the surface. The ratio of the velocity amplitude is approximately 0.5 to 1.0 with an average of about 0.8.
During removal the vibration is in general below the vibration level during installation, the ratio is about 0.85. It is to be realised that in the test the sheet pile did not experience any deformations as there is no building stage and possible cementation of the clutches due to corrosion etc. Therefore this observation may not be valid for a situation where sheet piles used for a building pit are removed.

For the vibrations at surface and at depth also a comparison is made between the U- and Z-section. For this figure 7.12 shows the vertical and horizontal vibration amplitude at surface near the sheet pile wall during installation.

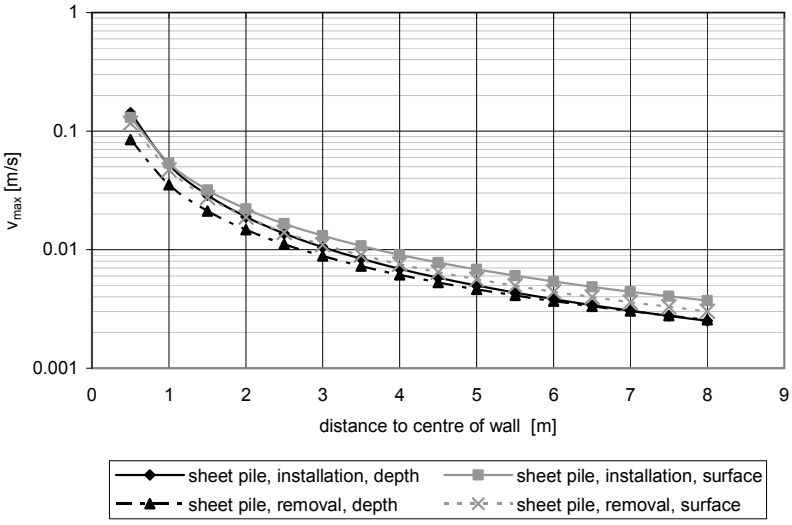

Figure 7.11 Comparison vertical velocity amplitude for different situations

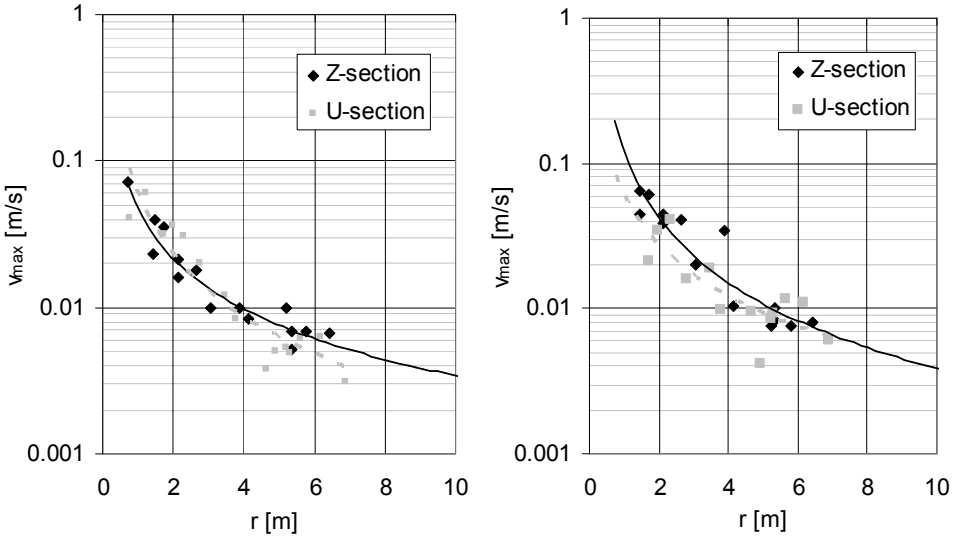

Figure 7.12 Comparison vibration amplitude at surface during installation Z-section and U-section; at left the vertical amplitude and at right the horizontal amplitude perpendicular to the sheet pile wall

From this figure follows that, for the vertical vibrations, there is in general no difference between the two types of sheet piling. For the horizontal vibrations the U-sections shows on average smaller vibrations as the Z-section.
It is expected that this difference is not caused by the type of sheet piles but by the location of the vibrator at the top of the sheet pile. When installing the Z-section the

vibrator is placed eccentrically. For installing the U-section the vibrator is placed at the centre line of the sheet pile wall. It is expected that eccentric placement of the vibrator will result in larger horizontal vibrations of the sheet pile itself.
Unfortunately the vibration transducer at the sheet pile was out of order during installation of the U-section, so this cannot be verified.

7.6.5 Excess pore pressure

The pore pressure as measured with the transducers may fluctuate due to the following reasons:
- water level variations (tidal influence) from the river Donge
- precipitation/evaporation
- generation of excess pore pressure due to vibrating sheet piles.

For this investigation only the last component is of interest. The first two components are expected to have a small influence on the ground water level. The influence during the period of vibrating (a few minute) can be considered as negligible. Therefore no correction for the first two aspects is made.

During post processing of the data file it is found that the measured pore pressures shows on top of the variation with the frequency of the vibrator more or less regularly high variation in recorded pore pressure. This is present not only during the time of vibrating but also when the vibrator is switched off. The reason for this variation could not be determined. This variation is believed to be an error in the reading or the recording of the data and not a physical mechanism. During processing of the data this variation has been removed as far as possible. For this a check is made on the difference in recorded pore pressure during subsequent scans. In case of a difference exceeding a prescribed value the recorded scan is neglected. This procedure yields results useful for analysing the mechanisms.

An example of the development of the excess pore pressure during installation is shown in figure 7.13.

During removal an interesting behaviour is observed. This is illustrated in figure 7.14, showing the development of the excess pore pressure in time during the removal of a sheet pile. In this figure the tip level of the sheet pile is indicated with a dashed line. As can be seen at pr-2, pr-3 and pr-4, located close to the removed sheet pile 8, at first the pore pressure increases rapidly and then starts to decrease. After some time even a small underpressure develops. For pr-1, located at some distance from the removed sheet pile 8, the development is more even, but shows the same behaviour.
This behaviour can be explained as follows. The excess pore pressure during removal will be the combined effect of soil densification, suction due to the removal of the sheet pile and possible dilation of the sand flowing in the void left by the sheet pile. The removed volume per time can be considered as a local discharge. This ‘discharge’ is the product of the cross section and the speed of removal. For the steel sheet pile this amounts 0.0249*0.08 = 0.00199 m^3/s. For pr-1 the contribution of the suction to the excess pore pressure suction is apparently larger

as the contribution of the densification. For the other transducers the contribution of the suction and the densification to the excess pore pressure are more or less equal.

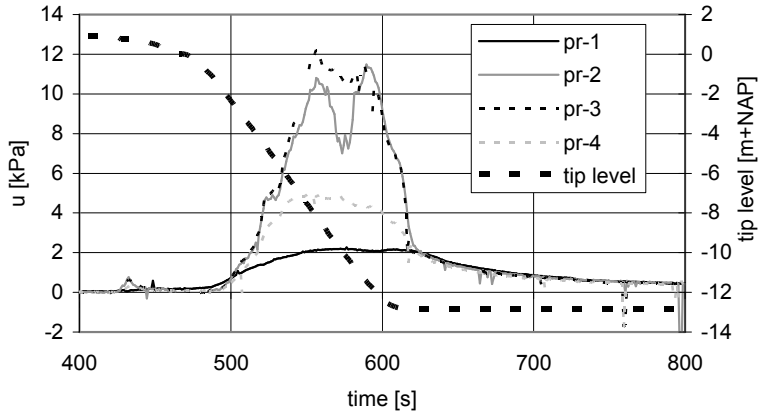

Figure 7.13 Measured excess pore pressure during installation sheet pile 8

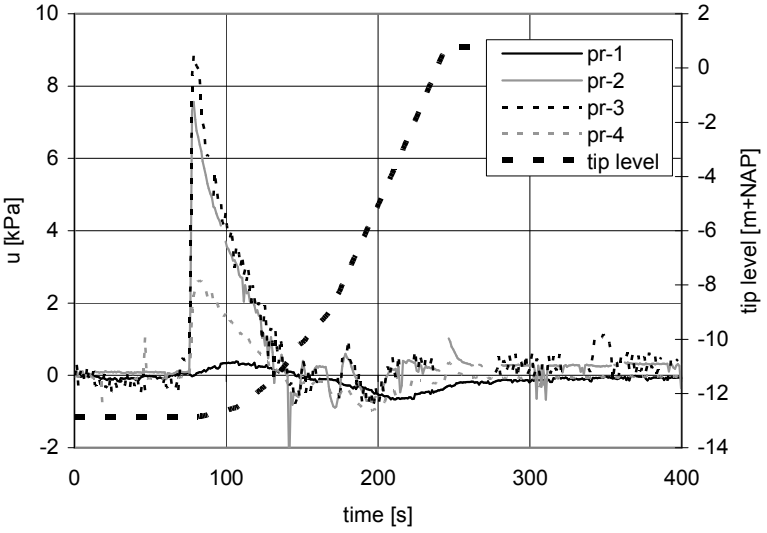

Figure 7.14 Development of excess pore pressure during removal sheet pile 8.

The extreme values of the excess pore pressure, as measured during installation and removal, are plotted as function of the distance to the considered sheet pile. For the phase of removal not only the high extreme but also the low extreme (the underpressure) is plotted as well. Figure 7.15 and 7.16 show these extremes.

The excess pore pressures measured during installation and removal of the steel sheet piles show a decrease with distance. At a distance of about 3 m (pr-1) or 6 m (pr-2, pr-3 and pr-4) the excess pore pressure is negligible. At pr-1 the excess pore pressures close to the sheet pile are higher as for pr-2, pr-3 and pr-4. Extrapolating the values for pr-1 to the centre line of the sheet pile suggests that here complete liquefaction may have occurred. For pr-1 the underpressure shows a relation with distance. For pr-2, pr-3 and pr-4no clear relation of the (small) underpressure with distance is present.

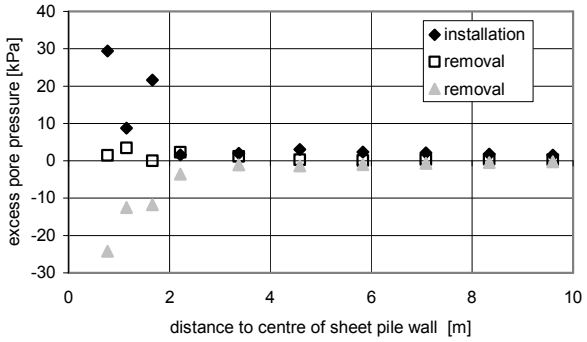

Figure 7.15 Excess pore pressure at pr-1 during installation and removal

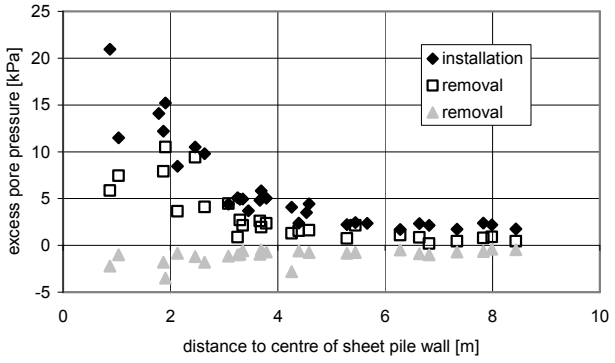

Figure 7.16 Excess pore pressure at pr-2, pr-3 and pr-4 during installation and removal

7.6.6 Local densification

The local densification is measured using an electrical density probe. A short description of this device will be given first.

The measurement principle of the electrical density probe is that water will conduct electricity well and silica will act as an electrical isolator. Decreasing the amount of voids decreases the electrical conductivity and increases the electrical resistance.

During the measurement an electrical current is applied between two drive electrodes. In between these electrodes the resistance is measured between two measuring electrodes. A photo and drawing of the electrical density probe are given in figure 7.17 and 7.18. It contains two sets of electrodes, the A-electrodes and the B-electrodes. Each set consists of four electrodes, two drive electrodes for supplying the electrical current and two measuring electrodes for measuring the electrical potential. The last are located between the drive electrodes. The distance between the A-electrodes is 0.50 m. The resistance is measured over 0.25m. The distance between the B-electrodes is 0.1 m. The resistance is measured over 0.03 m. The diameter of the probe is 0.036 m.

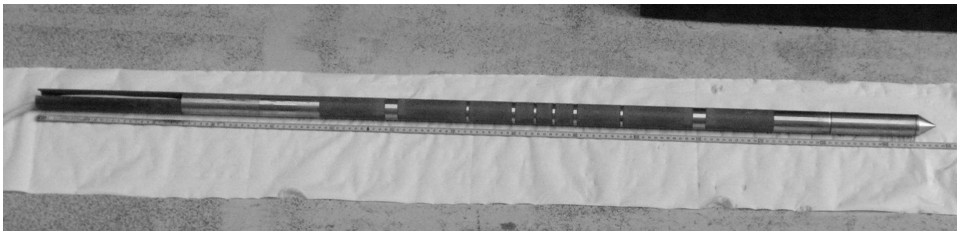

Figure 7.17 Electrical density probe

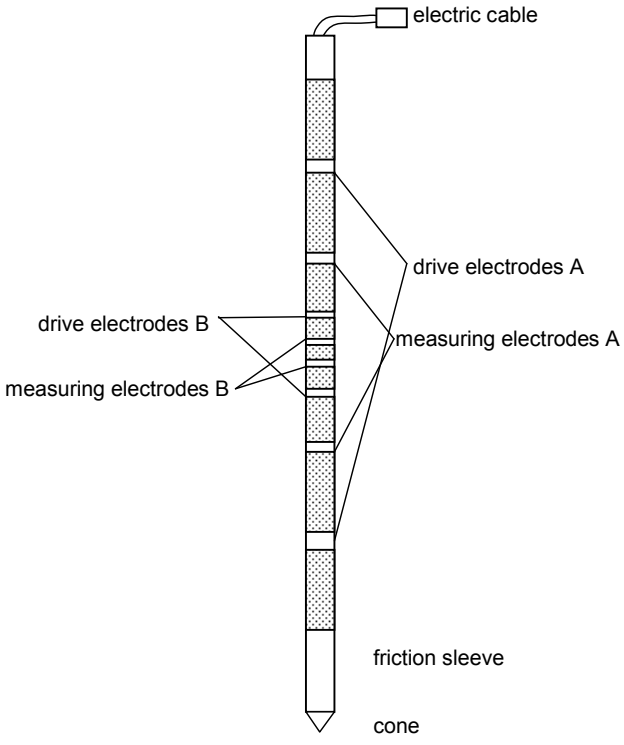

Figure 7.18 Electrical density probe

Before the start of the test two questions have been identified that required special attention. One is the possible influence of the steel from sheet pile on the measured electrical resistance. The second question is the possible influence of long term behaviour (e.g. corrosion of the electrodes) on the measurement.
Before installation of the probes therefore tests are performed in the laboratory. In this test the electrical density probe and a steel sheet are installed in a tank. The distance between electrical density probe and steel sheet is varied and the electrical resistance is measured. The tank is filled with water or with saturated sand. Results are reported in (Meijers 2004c). Figure 7.19 shows the test set-up and figure 7.20 the measured electrical conductivity as function of the distance to the steel plate.

Figure 7.19 Test set-up for checking the influence of a steel plate on the measured conductivity with the electrical density probe

From the results of that test it is concluded that the steel sheet plate will not noticeable influence the measurements when it is located at a distance in excess of the distance between the driving electrodes.
In the same test the electrical density probe is left in place in a water filled tank for about one week. During this week the electrical resistance is regularly measured. No change in measured value is found. From this it is concluded that the time between installation of the transducers and performing the test will not influence the measurement results.

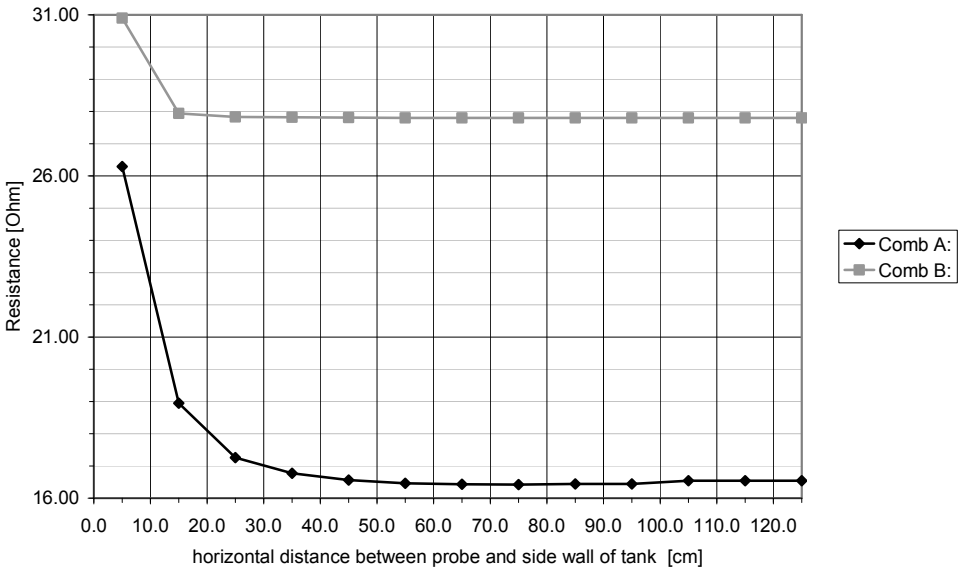

Figure 7.20 Measured electrical conductivity, sand filled tank

In the field test four electrical density probes are used. Two of them (ed-1 and ed-2) are installed close to the sheet pile wall (intended distance to the front of the sheet pile is 0.1 m) and two (ed-3 and ed-4) at a distance of about 2 m from the wall. During the installation and removal of the sheet piling the electrical conductivity is continuously monitored. This enables to measure the change in porosity during the vibratory operation and subsequent dissipation of excess pore pressure.

The electrical density probes located close to the sheet pile have distance between the driving electrodes of 0.10 m. Close to the sheet pile a strong variation of densification with distance is expected. Using a small distance between the driving electrodes implies that only a small amount of soil is measured and that the measurement is more or less a point measurement. Therefore, for this location a probe with a small distance between the driving electrodes is selected. A disadvantage is that the initial density of the measured volume may be influenced during the installation of the probe (push in of the rod). The main objective of this measurement is to record changes in porosity, rather than measuring the actual porosity. Therefore the disturbance during installation of the probes is considered acceptable.
The probes close to the sheet pile are installed with an inclinometer attached to it in order to determine the exact distance between probe and sheet pile. To this end the inclination of the nearby sheet piles after installation is also measured. During installation of ed-2 it is found that the probe moved towards the location of the sheet pile wall. Therefore the rod is rotated 180 degrees when the tip was at a depth of 1.8 m below ground level. With this correction the probe is forced to move in the opposite direction.

From the measured inclination during installation of probe ed-1 and ed-2 the horizontal dislocation of these transducers is determined. From the measured inclination of sheet pile 4 and 9 after installation the horizontal deviation from the vertical of these sheet piles is determined.
Transducer ed-1 is dislocated about 0.005 m. Sheet pile 4 is inclining backward (the tip is displaced towards the test field). At 3 m below the top the displacement towards the test field is 13 mm. At ground level the distance between rod and sheet pile is 0.15 m. The actual distance between the front of the sheet pile and transducer ed-1 is thus 0.15 + 0.005 – 0.016 = 0.14 m.

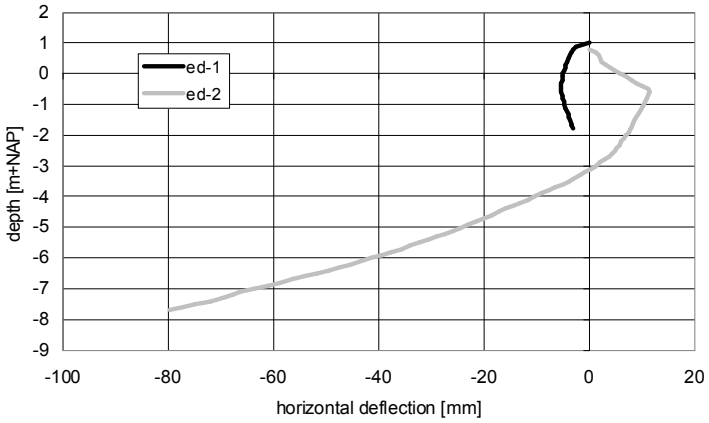

Figure 7.21 Horizontal deflection electrical density probe during installation, positive is towards the sheet pile wall

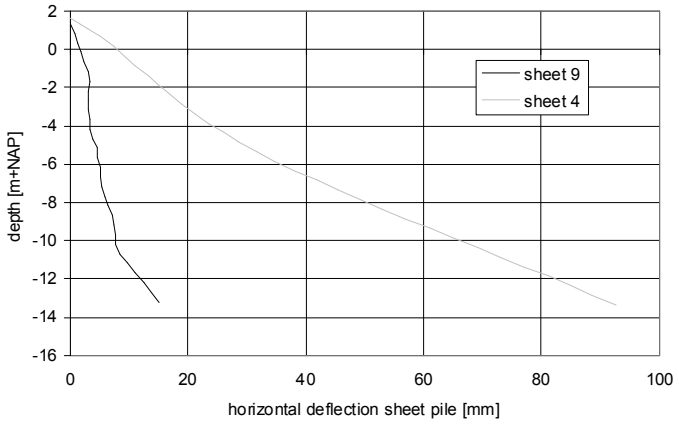

Figure 7.22 Inclination sheet pile 4 and 9, positive is towards the instrumented side

The horizontal dislocation of transducer ed-2 is about 0.08 m. Sheet pile 9 is also inclining backward. The displacement at the level of ed-2 (NAP – 7.46 m) is 6 mm. The actual distance between the front of the sheet pile and the probe is thus 0.15 + 0.08 – 0.006 = 0.22 m.
It is concluded that the distance between electrical density probe and sheet pile is in excess of the minimum required distance of 0.1 m for preventing influence of the steel on the measurements.

For the electrical density probes located at 2 m from the sheet pile as distance between the driving electrodes 0.50 m is used.

The porosity of the sand is derived from the quotient of the measured electrical resistivity of the water and of the soil.

$$n = A + B\frac{\rho_{water}}{\rho_{soil}} \tag{7.1}$$

with:

- n : porosity
- A, B : empirical non-dimensional parameters for the specific soil type
- ρ_{water} : specific electrical resistance of water (Ωm)
- ρ_{soil} : specific electrical resistance total mass of sand and water (Ωm).

For the calibration (determination parameter A and B) soil and water samples are taken at the site. The soil samples are taken from the performed boring at level NAP – 3.1m and NAP – 8.0 m. These are the depths at which the density probes are located. The water samples are taken at NAP – 3.8m and NAP – 7.8m. The discrepancy for the level at which the water is collected is caused by an error in instructing the field crew.
The empirical parameters A and B are determined in the laboratory. Table 7.6 shows the relevant data.

sample	depth [m + NAP]	ρ_{water} [Ωcm]	A	B
5	- 3.1	1429	0.1309	1.0406
10	- 8.0	1786	0.1072	1.1075

Table 7.6 Empirical parameters for determining the change in porosity

For measuring a known electrical current is applied through the drive electrodes. The difference in voltage between the measuring electrodes is measured. The quotient of voltage and current gives the apparent electrical resistivity R. This is a function of the geometry and distance between the electrodes. In the past the geometry factor of the cones has been measured by placing them in a large water tank (in fact a swimming pool). This factor is called ‘characteristic length’. Multiplying the measured electrical resistivity R with this length yields the electrical resistivity of the soil. For the used electrical density probe the characteristic lengths are given in table 7.7.

transducer	number of probe	characteristic length A-electrodes	characteristic length B-electrodes
ed-1	B-54, cone 293	0.742	--
ed-2	B-44, cone 309	0.741	--
ed-3	8-218	0.736	1.297
ed-4	8-216	0.736	1.316

Table 7.7 Parameters used electrical density probes

The probes are measured sequential, in order to avoid cross currents between the different electrodes. After starting the measurement at a particular probe a time of about 10 to 15 seconds is required to get a stable value. From this follows a time interval between subsequent measurements of at least 1 minute. During the test one measurement per transducer is made every 90 seconds.
The results of the density measurements are shown in annex 7.6. Close to the sheet pile the measured volume strain during installation (compaction) is 4 – 5 %. During removal some additional densification occurred here (about 1%). The transducers at 2 m from the sheet pile wall show no or marginal volume strains, both during installation and during removal. From this it may be concluded that the area with densification next to the sheet pile wall is limited, about 0.5 m to 1 m.

7.6.7 Settlement at surface and at depth

The surface settlement is measured using the installed pickets. For the installation phase measurements are taken at the start of each day and after installation of each sheet pile. For the removal phase measurements are taken at start of the day and after removal of sheet pile 7, 10, 2 and 5.
The settlement of the 30 surface settlement points is shown in annex 7.7. For the 8 fixed point cones (subsurface settlement points) the development is shown in annex 7.8.

In order to gain some more insight in the development of the surface settlement the settlement as function of the distance to the wall is shown in annex 7.9 and 7.10 for respectively the situation after installation and after removal of the sheet piles. Figure 7.23 and 7.24 show the settlement at depth after installation and removal of the sheet pile. For the settlement at the surface the average settlement of the 5 arrays is shown.

More insight in the settlement profile is obtained by shifting the settlement profiles to get the settlement profiles with respect to both distance and depth. For the situation after removal only the change in settlement between end of installation and end of removal is shown. The resulting graphs are shown as figure 7.25 and 7.26. With a solid line the driving depth of the sheet pile is indicated.

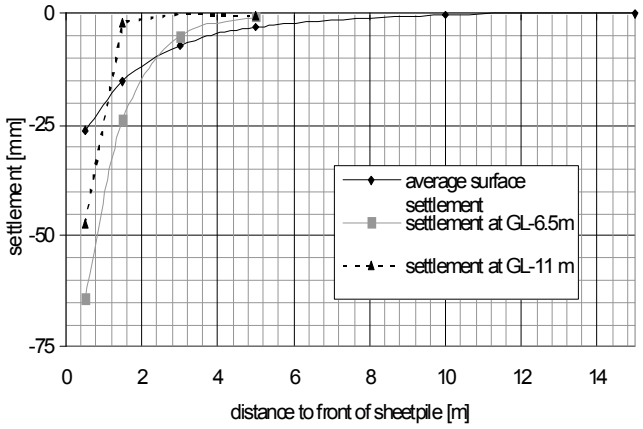

Figure 7.23 Average settlement profile at surface and at depth, after installation of the sheet piles

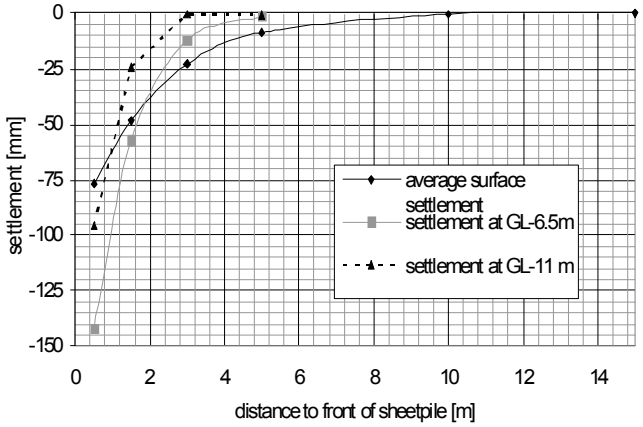

Figure 7.24 Average settlement profile at surface and at depth, after installation and removal of the sheet piles (note that this is the combined effect of installation and removal)

At surface the width of the settlement trough is between 5 and 10m. As there are no surface settlement points between 5 m and 10 m the exact distance can only be estimated from the shape of the settlement trough. A best estimate is 7 to 8 m, which is about half the driving depth. The distance seems to increase a little during removal. The distance from the sheet pile at which no or negligible settlement occurs decreases with increasing depth. Drawing a line between the estimated points of negligible settlement (the straight dashed line in figure 7.25 and 7.26) shows that the settlements occur within in a zone bounded by the sheet pile and a line at an angle of about 30 degrees with the vertical from the tip of the sheet pile or from a point located about 1 m next to the sheet pile.

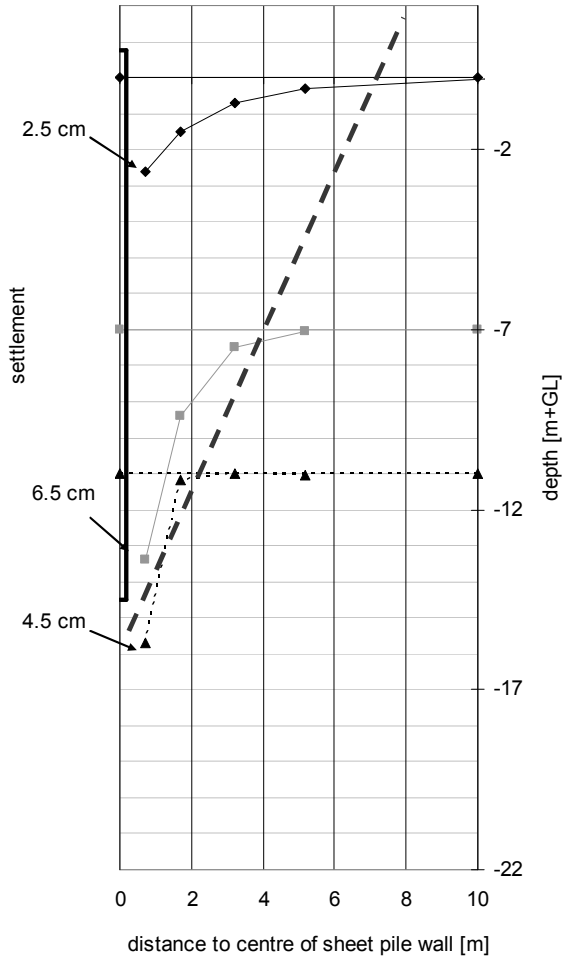

Figure 7.25 Settlement profile as function of distance and depth, after installation of the sheet piles

It was anticipated that at depth the settlement would be less as at the surface. The opposite however occurred for the points close to the sheet pile. It is expected that for the fixed cone VP1 the measured values during and after removal are influenced by the free stroke of the cone. Inspecting photographs made during the test indicate that the length of the rod extending above the outer tube did not change during this phase. This indicates that the inner rod and outer tube exercised the same settlement. This may be an indication of reaching the free stroke of 5 cm for the larger settlement at depth.

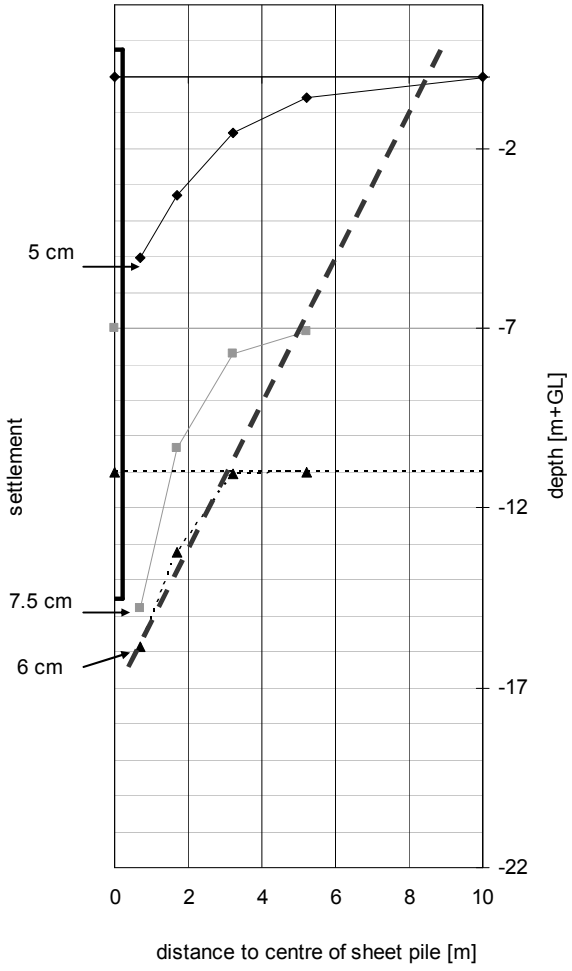

Figure 7.26 Settlement profile as function of distance and depth, due to removal of the sheet piles

7.6.8 Net volume change

From the measured surface settlement the actual loss of volume of the soil is determined. From the measured settlement through it can be concluded that the measured settlement justify to assume a 2D behaviour. As settlement line the average line is used. During the test no reliable measurements are made at the centre line of the wall. Therefore, first the measured settlements are extrapolated to the centre line. From the obtained full profile the volume of the settlement trough at surface is calculated. The following values are obtained.

- volume of half the trough after installation: V = 0.078 m^3/m

- volume of half the trough after removal (including effect of installation): V = 0.234 m^3/m
- volume (average of the Z- and U section) of the embedded sheet pile: V = 0.27 m^3/m.

From this follows that due to installation the net volume change is: V = 2*0.078 + 0.27 = 0.43 m^3/m. The net volume change due to removal amounts: V = 2*(0.234 – 0.078) – 0.27 = 0.04 m^3/m.

From this follows that during removal some additional densification occurs. The amount of densification is only 10% of the densification during installation.

As these results may be influenced by the 'stiff spot' at CPT1-06 the same exercise is repeated for the Z-section only. The surface settlement is taken as the average of the settlement in the arrays through MV1, MV2 and MV3. The following values are obtained:

- volume of half the trough after installation: V = 0.090 m^3/m
- volume of half the trough after removal (including effect of installation): V = 0.279 m^3/m
- volume (Z-section only, A=198cm2/m, L=14.2m) of the embedded sheet pile: V = 0.28 m^3/m.

From this follows that due to installation the net volume change is: V = 2*0.090 + 0.28 = 0.46 m^3/m. The net volume change due to removal amounts: V = 2*(0.279 – 0.090) – 0.28 = 0.10 m^3/m.

The net volume change during removal is small in this test. According to the measured local densification the increase in local density is about 1%, or about 0.25 to 0.5 times the densification during installation. From the measured volume change a value of 0.1 to 0.2 is obtained. Possible locally, at the former place of the sheet pile, the soil becomes loose due to flowing of soil towards this place.
In the calculation no correction for the soil sticking to the sheet pile on removal is made. This volume is not measured but will be small. On removal the sheet piles appeared to be nearly clean.

An attempt is made to see whether Z-shaped sheet piles or U-shaped sheet piles are more profitable with regard to settlements. A difficulty for this comparison arises from the hard spot at CPT1-06. It is expected that this spot will influence the settlements. Therefore the comparison is made for the part of the test where this spot is expected not to influence the test results. From this requirement follows that the comparison is made for the settlements due to the installation of sheet 6, 7 and 8 (Z-section) and sheet 1 and 2 (U-section). The arrays with surface points used are the array at surface settlement point MV2 and at surface settlement point MV5. Figure 7.27 shows the measured surface settlement. The corresponding CPT's (CPT 1-05 and CPT 1-07) are nearly equal so any difference in observed settlement does not originate from a difference in subsoil conditions.

Not only the number of installed sheet piles will influence the settlement. The location of the measurement array with respect to the installed sheet piles may be of influence as well. In order to use comparable arrays and situations for the settlement due to installing the Z-section the total settlement after installation of sheet pile 8 minus the settlement after installation of sheet pile 6 will be used.

The test data show that close to the sheet pile the U-section shows more settlement. At distances in excess of 1 m the surface settlement at the U-section is below the surface settlement at the Z-section. The settlement at the U-section is drops to values between 40% and 80% of the settlement at the Z-section. This is despite the longer time of vibrating during installation of the U-section.

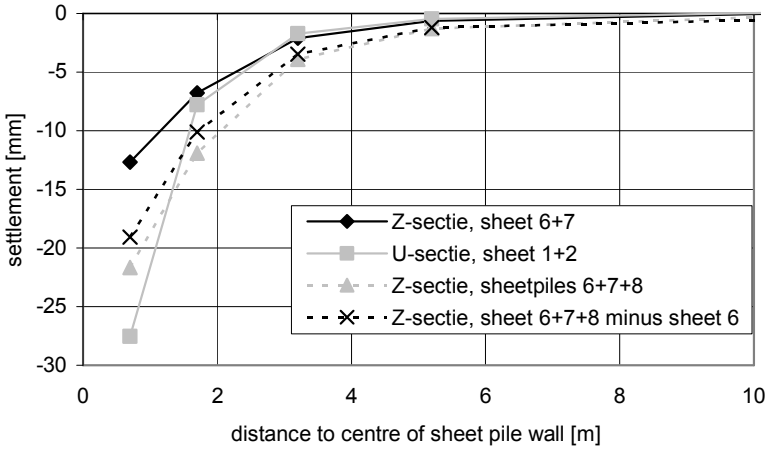

Figure 7.27 Comparison settlement at Z-section and at U-section

When analysing the vibration measurements (see figure 7.12) it is found that at surface the horizontal vibrations during installation of the U-section are on average smaller as during installation of the Z-section. For the vibrations at depth the same may be concluded, but this is less conclusive. The transducers at depth are not relocated during the test, so the distance to the sheet pile for which data are available is different (about 0 to 7m for the U-section and 5 to 12m for the Z-section). The reason for the more favourable settlement behaviour at the U-section is therefore attributed to the position of the vibrator and not so much to the used shape of the sheet piles.
It is realised that the available data is limited. The observed differences are within the scatter found for the vibration amplitude. Still it may be concluded that the observed behaviour is in accordance with expectations.

7.6.9 Creep

Measuring the creep of the soil is not part of the measurement plan. Still an indication of the possible creep can be acquired from the measured data. To this end the vertical deformation of the settlement points during periods without installation or removal of sheet piles are used. The following periods can be used:

- from October 18, 16.30 hr till October 19, 8.00 hr
- from October 19, 14.30 hr till October 21, 8.30 hr
- from October 21, 16.40 hr till October 25, 9.30 hr.

Figure 7.28 shows the summed creep as function of the distance to the sheet pile wall for two moments. The first (October 21) is just before removal of the sheet piles. The second (October 25) is after removal of the sheet piles and a few days rest. Not all surface settlement points are measured on October 25.

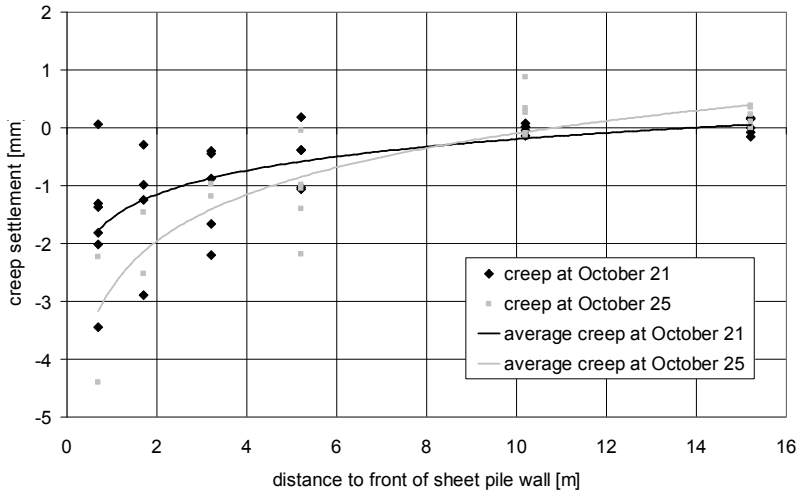

Figure 7.28 Creep as function of distance to the sheet pile wall

The creep data show a large scatter. In general the creep at surface amounts a few millimetres near the sheet pile. At large distance the obtained values suggest a heave of 0.5 mm.
A relative large part of the time period used for assessing the creep occurred is at night time. This introduces the question whether the creep is a consequence of other factors e.g. temperature effects (cooling down of the earth and measurement points during night time). The zero creep or small heave at large distance indicates that these effects are not responsible for the measured settlement close to the sheet pile.
One may argue that the observed vertical settlement between October 19 and October 21 and between October 21 and October 25 is not creep but (partly) irrecoverable compression of the sand due to the weight of the CPT-rig and the crane mats used for performing the CPT's of series 2 and 3. This is considered less likely as the area has been preloaded with sheet piles prior to the test and also preloaded with a CPT-rig during installation of the transducers and performing the CPT's of series 1.

The measured creep during the indicated periods amounts 5 – 10 % of the total settlement. It should be noted that this value is not necessarily the final creep as the measurements have not been continued for a long time after finishing the test.

7.6.10 Horizontal displacements

At four times during the test the horizontal distance between the guiding beam and the surface settlement point near the guiding beam is measured. The measurement is done using a normal measuring tape. The accuracy will be a few millimetres. This data is supposed to give some information on the horizontal deformation of the soil due to vibratory sheet piling. The measured distances are shown in table 7.8.

	horizontal distance [mm]			
	before start of installation	after installation Z-section	after installation U-section	after removal sheet piles
MV1	193	180	184	180
MV2	221	199	205	178
MV3	212	203	189	164
MV4	253	247	235	207
MV5	194	184	165	148

Table 7.8 Measured horizontal distance between surface level point and guiding beam

From these data the horizontal displacements after installing the Z-section, after installing the U-section and after removal of all sheet piles can be derived. Results are shown in figure 7.29.

During the installation phase visually no horizontal deformations of the surface have been noticed. After removal of the sheet piles cracks in the soil surface could be observed up to a distance of 5 m from the sheet pile wall. The width of the cracks is limited to a few millimetres. The cracks appear to be running through the points where measurement transducers or pickets are installed.
The measurement could be influenced by a horizontal displacement of the (not fixed) guidance beam. Support for this hypothesis is that it is possible to draw a more or less straight line through the measured displacements due to installation.

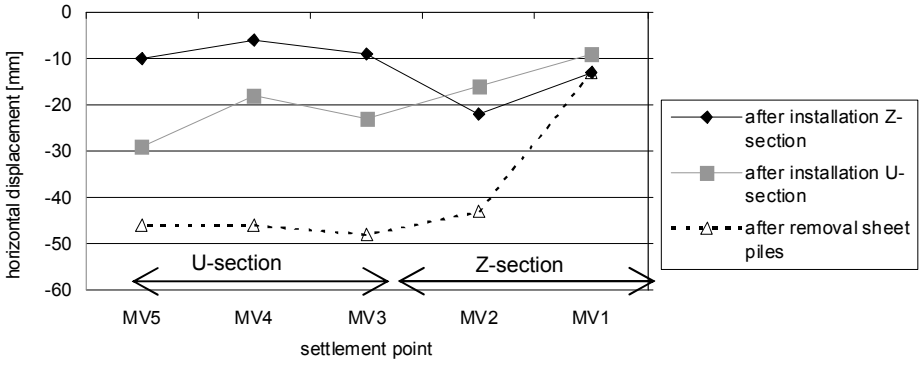

Figure 7.29 Horizontal displacements near the sheet pile wall

Support for the hypothesis that the beam did not displace can be found from the deformation pattern. The deformation pattern show clearly that most horizontal displacements occur at the location of the installed section. After the test and removal of the guidance beam the surface was carefully inspected for signs of horizontal displacement of the beam like shovelling of the top layer. The absence of any such signs suggests that the beam did not or hardly displace.

7.6.11 Change in cone resistance

The purpose of performing CPT's at different stages of the test is to see the change in cone resistance due to installation and removal of the sheet piling. For this purpose combination plots are prepared where the measured cone resistance at different stages and different arrays is plotted in one graph. The following combinations are made:

- Z-section, after installation steel sheet pile (series 2)
- U-section, after installation steel sheet pile (series 2)
- Z-section, after removal steel sheet pile (series 3)
- U-section, after removal steel sheet pile (series 3).

The combined CPT profiles are shown in annex 7.11. For comparison the measured cone resistance before the test is shown as well. For the original CPT's black and grey lines are used. The coloured lines in the graphs show the cone resistance after installation or removal. The colours used for the other CPT's are chosen according to the colours of the rainbow. This means that the CPT closest to the wall is red. With increasing distance the colour changes to orange, yellow, green and blue. Not all colours are used in all plots. This depends on the number of CPT's performed in the considered array.

In order to get a better insight in the change in cone resistance the ratio between the cone resistance after and before the test is determined. For this the cone resistance over a number of depth intervals is determined. Figure 7.30 shows the results for the CPT's at the U-section and figure 7.31 for the Z-section.

For the Z-section a remarkable decrease in cone resistance due to installation of the sheet piles is observed. Careful inspection of the CPT-records shows that the lowest cone resistance is encountered at 1 m in front of the sheet pile. At 0.5 m in front of the sheet pile the cone resistance is still below the original cone resistance but a little higher as at a distance of 1 m.
Due to removal of the sheet piles the cone resistance close to the wall increases. At 1.5 m from the sheet pile the cone resistance decreases.
In all cases the cone resistance at about 5 m from the sheet pile is about equal to the cone resistance before the test.
For the U-section the cone resistance close to the sheet pile decreases due to the installation for the soil below NAP -5 m. The cone resistance above NAP – 5m seems to increase. It is however expected that the apparent increase in cone resistance in CPT2-01 between NAP-2m and NAP-5m may be due to the 'stiff spot' as mentioned in the description of the subsoil conditions. During removal the cone resistance decreases.

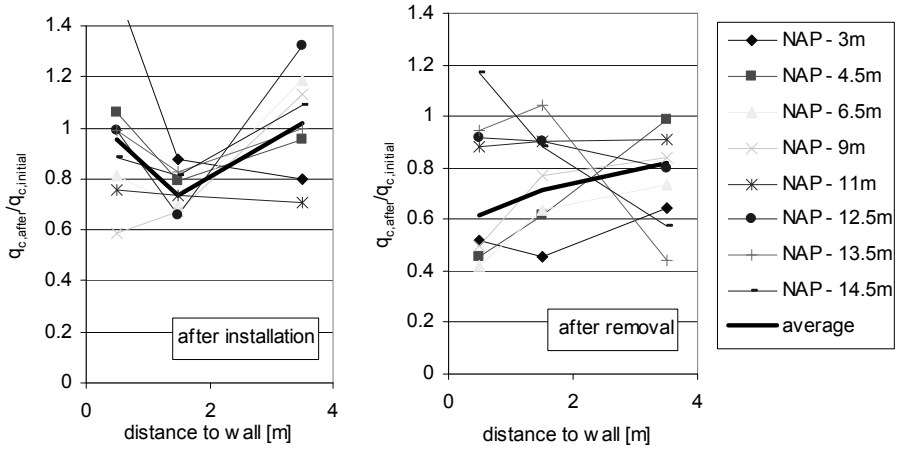

Figure 7.30 Change of cone resistance at U-section

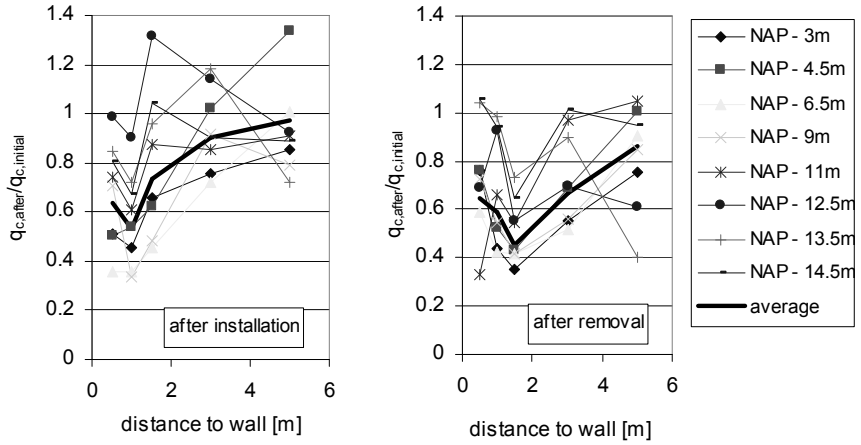

Figure 7.31 Change of cone resistance at Z-section

The vertical stress, the horizontal stress and the relative density of the soil determine the cone resistance. All measurements (surface settlement and electrical density measurements) show that densification has occurred and thus the relative density has increased during installation and removal. This increase in relative density will result in an increase in cone resistance. The excess pore pressure is found to dissipate rather quickly and is no longer present when the CPT's are performed. The decrease in cone resistance therefore cannot be attributed to a decrease in vertical effective stress. The only parameter left that may explain the observed decrease in cone resistance is a decrease in horizontal stress. This decrease may be explained from the volumetric strain. For small strains the volumetric strain is the sum of the strain in three orthogonal directions. Assuming that the volumetric strain is isotropic the soil wants to contract in horizontal direction as well. This is however not possible, so instead a reduction in

horizontal stress occurs. This may explain the reduction in cone resistance on installation of sheet piles.

7.7 Summary main results

From the measured data some interesting conclusions may be drawn.

The measured vibrations at the sheet pile show that the horizontal vibrations are not negligible. Above ground level the horizontal amplitude of the flange is of the same magnitude as the vertical amplitude. This is in conformance with the data of Viking (2002). For the part of the sheet pile below ground level no data are measured. It is expected that for this part the horizontal vibrations are limited, due to the horizontal constraints. Instead horizontal vibrations/stresses may be emitted.

In the soil the amplitude of the horizontal and vertical vibrations is about the same. At surface the amplitude is a little higher as at depth.

From the local density measurements it is concluded that the zone with densification is limited, between 0.5 m and 2 m.

The measured settlement profile at surface and at depth allows assessing the size and location of the area where vertical settlement occur. The area is more or less restricted by a plane at 30 degrees with the vertical from the tip of the sheet pile. The settlement at surface is not necessarily the maximum settlement. At depth the vertical settlement may be larger.
In the area enclosed by the web and flange of the sheet pile large vertical settlements occur. The reason for this is not clear from the measurements.

The measured data on horizontal movement suggest that the soil not only settles (vertical movement) but also show a horizontal movement. The performed measurements are not high quality measurements and are therefore only indicative. This aspect will not be elaborated further in this study.

The area with excess pore pressure is found to be limited, about 5 to 10 m from the sheet pile. During the test the excess pore pressure is found to dissipate rather quickly, usually within 5 minutes. During installation the excess pore pressure is no overpressure, during removal it is at first an overpressure, but changes quickly to an underpressure. The last mechanism is attributed to the suction at the tip of the sheet pile being removed.

From the performed CPT's after installation and after removal it is noticed that close to the sheet pile wall the cone resistance decreases, at least for the short term. At distances of about 5 m from the sheet pile wall the cone resistance is not or only marginal influenced by the installation and removal process. This change in cone resistance is attributed to a change in horizontal stress. Due to the vibrating the soil wants to densify. It is still not clear what will be the preferred direction for this volume strain. Assuming that it is isotropic the soil wants to shrink in the horizontal direction. As this is not possible a horizontal elongation, resulting in a

decrease in the horizontal stress, counteracts this shrinkage. As the stresses in the soil are not measured during the test this hypothesis cannot be verified with the present data.
No CPT's are made some time after the test. It is therefore not known if the decrease in cone resistance will last or if the cone resistance will increase with time due to e.g. creep effects.

From a check on the loss of volume during installation and during removal it is concluded that most of the densification occurs during installation. The settlement is limited as the inserted volume of the sheet pile counteracts the effect of densification. During removal the loss of volume is mostly due to the removed volume of the sheet piles. Some additional densification occurs. It is quite well possible that near the tip of the sheet pile the soil loosens when flowing to the void left by sheet piles.

In the course of time the settlement increases due to some creep phenomena. During the test period the amount is about 10% of the settlement due to densification. The available test data do not allow determining a more exact figure for the amount of creep after installation and removal.

8. Validation of the model

8.1 Introduction

In chapter 6 a new model for estimating the amount of surface settlement due to vibratory sheet piling is presented. Before it can be used the model needs to be validated. The purpose of the validation is to show that the model described the actual behaviour sufficiently accurate. For this predictions with TRILDENS3 are compared with measured data.

For this validation first the results of the Raamsdonksveer sheet pile test are used. The availability of the large number of data allows not only comparing the final result (the surface settlement) but also the correctness of the different sub models. In addition to this, a number of cases are selected where the settlements during vibratory sheet piling are measured or can be estimated from the available data. The relevant data are made available by different people and organisations. All cases are situated in The Netherlands.

8.2 Raamsdonksveer sheet pile test

8.2.1 General

Details of this test are described in chapter 7, together with a first interpretation of the results. In this section some of the assumptions made during the development of the model are checked. For the following aspects a comparison is made between the model and the measured data:

- attenuation of the velocity amplitude
- attenuation of the shear strain amplitude
- local densification
- amount and attenuation of the excess pore pressure
- surface settlement during installation and removal of the steel sheet piling.

These aspects are related to the different sub models. The attenuation of the velocity amplitude and the shear strain amplitude are related to the sub model propagation. The development of the local densification and the excess pore pressure are related to the densification model. The excess pore pressure is also related to the dissipation of excess pore pressures and as such the dissipation model is checked. The development of the surface settlement is related to the summation model. The source will not be checked as no appropriate measurements at the interface sheet pile – soil are available.

8.2.2 Selection of the relevant soil parameters

The relative density of the sand is estimated using the correlation by Lunne and Christoffersen (1983). The measured values of C_1, C_2 and PEC are derived from the results of the performed cyclic triaxial testing (see chapter 5). The empirical

parameters are taken from the previous derived correlations (see section 4.7.4). The values for the small strain shear modulus $G_{i,ref}$ is for a reference stress of 100 kPa. The value of PEC (Pseudo Energy Capacity) is normalised for a vertical effective stress of 100 kPa.

top of layer [m+NAP]	soil type	q_c [MPa]	I_D [-]	measured values				empirical values			
				$G_{i,ref}$ [kPa]	C_1 [-]	C_2 [-]	PEC/σ'_{v0} [-]	$G_{i,ref}$ [kPa]	C_1 [-]	C_2 [-]	PEC/σ'_{v0} [-]
1.3	sand	5	0.9	125000	1.5	0.1	0.035	220164	6.64	0.13	0.059
0.1	clay	1	--	not used [1])	0 [2])	0.1	1000	not used [1])	0 [2])	0.13	0.069
-1.4	sand	7	0.72	92500	3	0.1	0.029	130396	7.972	0.13	0.04
-4.2	sand	12	0.82	96000	2	0.1	0.031	174439	7.232	0.13	0.05
-5.2	sand	7	0.57	78000	4.5	0.1	0.026	84274	9.082	0.13	0.027
-8	sand	7	0.55	74000	5.5	0.1	0.024	79509	9.23	0.13	0.025
-9.5	sand	12	0.65	83000	3.5	0.1	0.028	106365	8.49	0.13	0.034
-11	sand	14	0.67	86000	3.5	0.1	0.028	112739	8.342	0.13	0.035

[1]): value of shear modulus in clay layer is not relevant for the calculation
[2]): C_1 = 0 is used in order to model zero densification in clay

Table 8.1 Soil profile and selected soil parameters at Raamsdonksveer

For the ratio between the angle of interface friction δ and the angle of internal friction φ a value of $\delta/\varphi = 1$ is used. In selecting this value the effect of the larger interface area of the folded shape of the sheet pile profile is accounted for.

8.2.3 Comparison measured and calculated velocity amplitude

Three options are available for describing the vibration attenuation. These are the stress attenuation, the Barkan method (velocity attenuation) and the Stokes method. All three options will be considered, starting with the stress attenuation model.
The stress attenuation model contains an empirical parameter describing the attenuation:

$$\tau(r) = \tau(r = r_0) * (r / r_0)^n \qquad (8.1)$$

The theoretical value for the velocity attenuation of the radial expanding vibration waves is n = -0.5. Close to the sheet pile effects of excess pore pressure, shear strain dependency of the shear modulus and soil damping will increase the attenuation. In order to account for these aspects the first validation calculation is performed using as stress attenuation parameter n=-0.75. Figure 8.1 shows a comparison of the measured vertical maximum velocity and the calculated maximum velocity amplitude at NAP – 6.7 m.

The measured and calculated values are in good agreement with each other. The measured values however show a larger attenuation with distance. In order to increase the fit of the attenuation the calculation is repeated using as attenuation parameter n = -1. Figure 8.2 shows the result. The attenuation of the calculated

wave velocity is larger as the attenuation of the shear stress amplitude. Responsible for this effect is the excess pore pressure and the shear strain amplitude. Both aspects result in an increasing shear modulus with increasing distance to the sheet pile and thus a decreasing velocity amplitude.

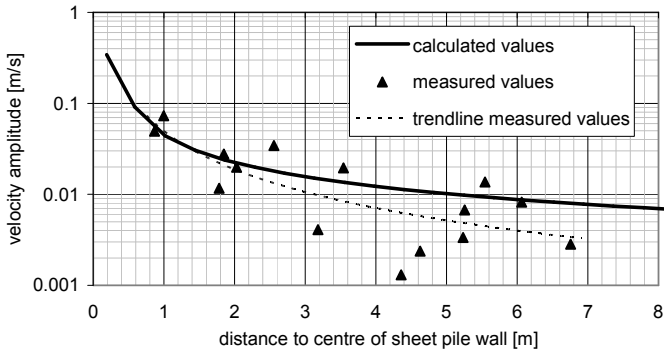

Figure 8.1 Comparison measured and calculated velocity amplitude using stress attenuation n = -0.75

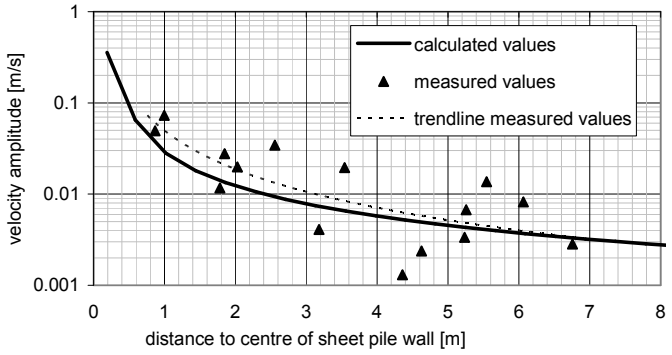

Figure 8.2 Comparison measured and calculated velocity amplitude, using stress attenuation n=-1 and soil parameters from correlation

Changing the stress attenuation parameter from n = -0.75 to n = -1.0 results in a better fit between measured and calculated velocity amplitudes. The absolute value of the velocity amplitude may be increased by increasing the shear stress amplitude at the interface sheet pile – soil. This may be achieved by increasing the ratio δ/φ from 1.0 to 1.25.

The measured velocity amplitude is compared with the calculated velocity amplitude using the other described options for the propagation model. In all cases the densification model is the C/L model. For the Barkan model a centrifugal force of the vibrator of 1350 kN is used.

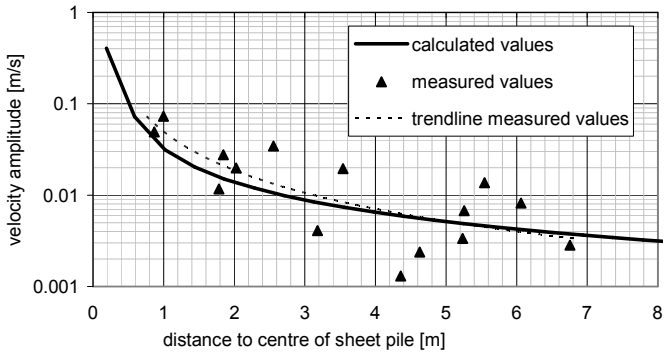

Figure 8.3 Comparison measured and calculated velocity amplitude, using stress attenuation n=-1 and soil parameters from laboratory testing

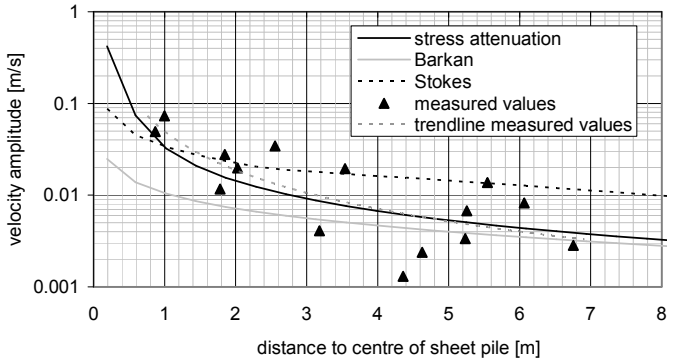

Figure 8.4 Comparison measured and calculated velocity amplitude, using different propagation models

From this comparison follows that, amplitude at distances of 5 m or more from the sheet pile, the velocity attenuation model slightly underestimates the vibration. For smaller distances this model greatly underestimates the vibration amplitude. The velocity attenuation model is intended for a first prediction of the vibration amplitude at distances in excess of 5 m from the sheet pile. This is confirmed with the test results. For the area close to the sheet pile the model is not correct. For assessing the amount of densification the area close to the sheet pile is of most interest.
The model of Stokes shows an attenuation that differs significantly from the other models and from the measured attenuation. Further use of this model is less attractive in view of the large calculation time.

From this comparison it follows that the stress attenuation model best describes the development of the vibration amplitude, especially in the area close to the sheet pile.

For completeness also a comparison of the vibration amplitude at or near ground level is made. The result is shown in figure 8.5 and 8.6.

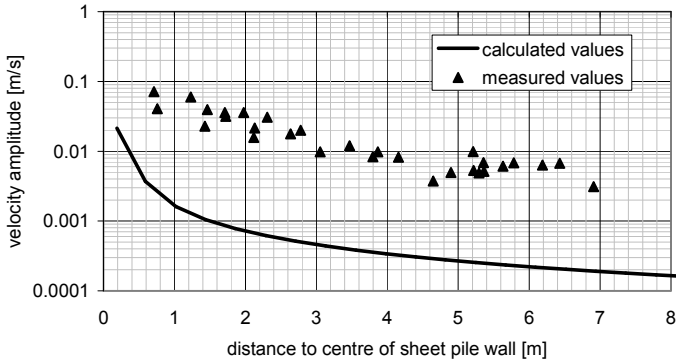

Figure 8.5 Comparison measured and calculated velocity amplitude at ground level, using n=-1 and soil parameters from correlation

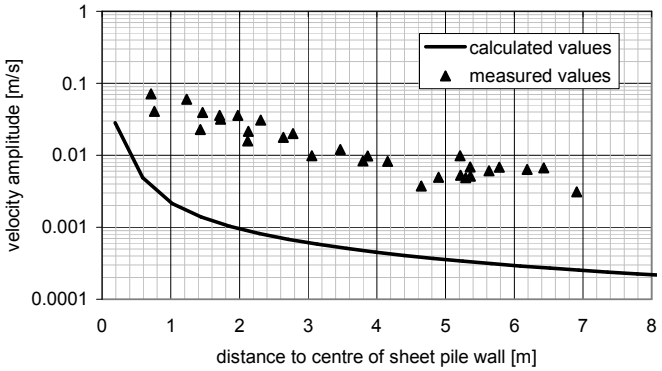

Figure 8.6 Comparison measured and calculated velocity amplitude at ground level, using n=-1 and soil parameters from laboratory testing

For ground level there exists a large difference between the measured and the calculated velocity amplitude. This difference can be explained form the presence of Rayleigh waves in practice, a type of waves not accounted for in TRILDENS3. The influence depth of the Rayleigh waves will be small. Assuming C_R = 150 m/s and f = 38 Hz the wave length is about 4 m.
As the purpose of TRILDENS3 is to assess the surface settlements, and not to predict the vibration amplitude, the discrepancy between the measured and calculated velocity amplitude at surface is considered acceptable.

8.2.4 Comparison measured and calculated attenuation shear strain amplitude

The loading parameters considered responsible for cyclic densification in the C/L model is the shear strain amplitude. This parameter is not directly been measured. An attempt is made to derive this parameter from the measured vibrations.

The shear strain is (assuming vertical deformation only):

$$\gamma = \frac{dz}{dr} \tag{8.2}$$

with:

- z : vertical deformation
- r : radial coordinate.

For the vibration transducers Td1 and Td2 the measured accelerations are integrated twice in order to obtain the displacement. A problem with this approach is that small errors in the measured acceleration result in large errors in the calculated displacements. Therefore a different approach is used.
First the velocity is obtained by integrating the acceleration record. The offset in the acceleration is obtained by postulating that at the end of the considered time interval the net velocity is zero.
The vertical displacement is obtained from integration of the vertical acceleration.

$$z(t+\Delta t) = z(t) + v(t) * \Delta t + 0.5 * 0.5(a(t) + a(t+\Delta t)) * \Delta^2 t \tag{8.3}$$

The shear strain is determined from difference in vertical displacement of the two used transducers, divided by the difference in distance between the two used transducers. Small errors in the used acceleration record may result in a large error in the calculated shear strain. As the interest is in the amplitude of the shear strain the value is corrected with the average shear strain over two cycles. The result is an estimate of the shear strain. The amplitude is taken as half the difference between the minimum and maximum value.

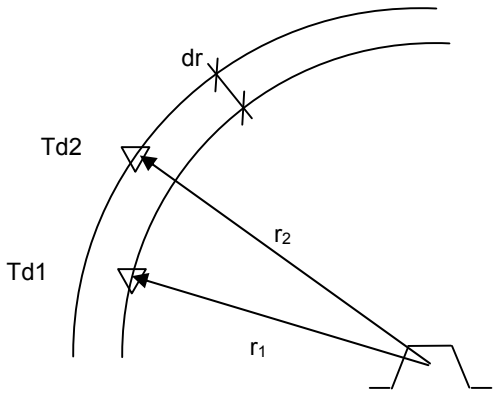

Figure 8.7 Determination difference in distance

For determining the distance between the transducers radial wave propagation is assumed. The distance dr is thus dr = $r_2 - r_1$. For the difference in vertical displacement the momentary difference in vertical displacement is used. Considering part of the record with the highest vibration level the maximum difference is obtained.

The analysis is performed only for installing and removing the U-section, as this is the section close to the used vibration transducers at depth. Results are shown in figure 8.8 and 8.9. For comparison also the development of the vertical velocity as function of distance is plotted, as well as general trend lines.

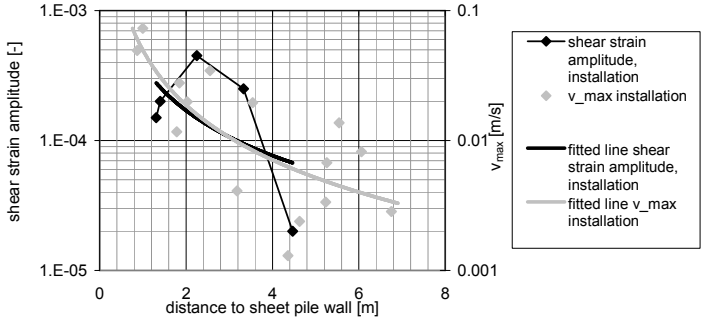

Figure 8.8 Results determination shear strain amplitude during installation of steel sheet piling

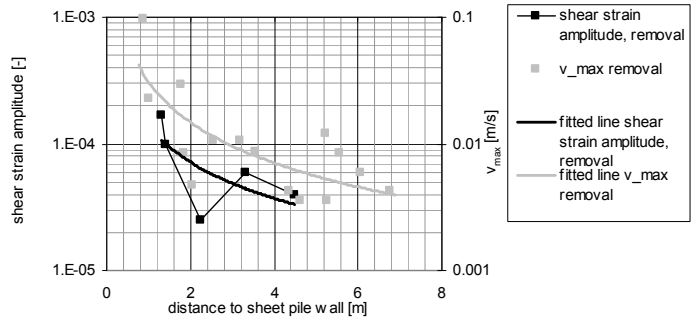

Figure 8.9 Results determination shear strain amplitude during removal of steel sheet piling

The scatter in data points is quite large. Only some indicative observations can be made. From figure 8.8 and 8.9 it is concluded that the attenuation of the shear strain amplitude and the vertical velocity are in reasonable agreement. In general the attenuation of the shear strain amplitude is a little less as the attenuation of the velocity amplitude. On installation the ratio between velocity amplitude and shear strain amplitude is about 100 m/s, for removal it is about 200 m/s. Theoretical this ratio should be equal to the shear wave velocity. The initial, small strain, shear modulus at the depth of the vibration transducers (NAP – 6.7 m) is estimated to be 70 MPa. For a shear strain amplitude of 10^{-4} the degradation of the shear modulus

is limited, to about 80% of the initial value. This gives G = 56 MPa. From this follows as estimate of the shear wave velocity C_s = 167 m/s. The estimated values are in the same order of magnitude.

Table 8.2 summarises the attenuation parameter (for the velocity and the shear strain) for installation and removal of the steel sheet piling.

action	strain attenuation parameter	
	vertical velocity amplitude	shear strain amplitude
installation	-1.40	-1.15
removal	-1.07	-0.95

Table 8.2 Comparison measured velocity and strain attenuation parameter

From table 8.2 follows that the attenuation of the shear strain amplitude is a little below the attenuation of the velocity amplitude. Given the inaccuracies for determining the shear strain amplitude the agreement is considered reasonable.

Having determined the shear strain amplitude, a comparison with the calculated values can be made. For the validation calculation a value of n = -1.0 will be used. The used soil parameters are from the measured values. Figure 8.10 shows the comparison.

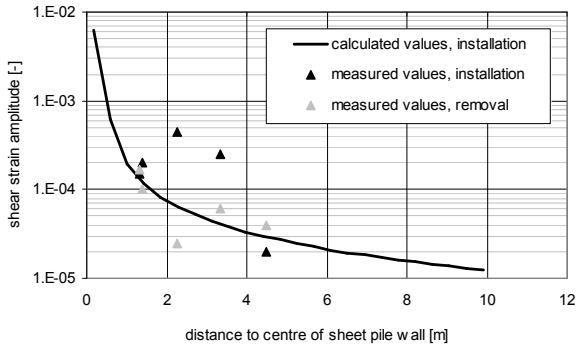

Figure 8.10 Comparison measured and calculated shear strain amplitude at depth during installation, using n=-1 and soil parameters from laboratory testing

The calculated values of the shear strain amplitude for the installation phase are at the lower bound of the measured values. The determination of the shear strain amplitude is not very accurate. The measured values also show a large scatter. From this result it cannot be concluded that the model is not correct. It is however an indication that the actual loading parameter may be larger as used in the program TRILDENS3.

8.2.5 Comparison measured and calculated local densification

In the Raamsdonksveer sheet pile test the local densification is measured at four points. For the calculation model still three densification models are under consideration. When taking 'Barkan, standard' and 'Barkan/Hergarden, advanced' in account as well five densification models are present. The program TRILDENS3 is run with all five models. The calculated densification (volume strain) for the two depths where the local densification is measured are shown in figure 8.11.

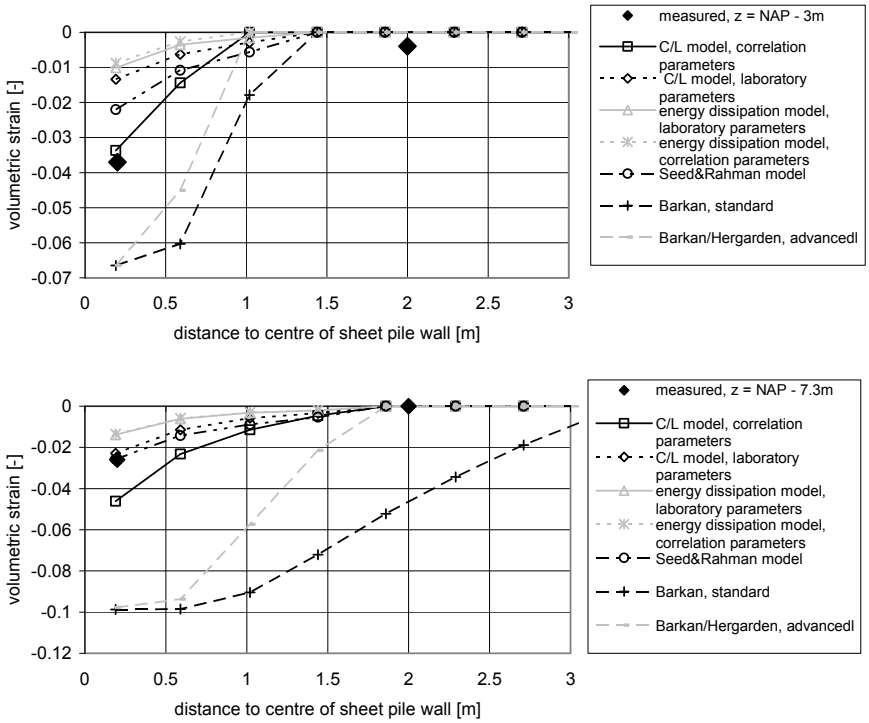

Figure 8.11 Comparison measured and calculated plastic volume strain, different densification models

The model by Barkan predicts volume strains that are in excess of the measured values. It is expected that the use of a high frequency vibrator, and thus high acceleration amplitudes, is responsible for this large difference.
The energy dissipation model predicts volume strains that are well below the measured values.
The two other options (C/L model and Seed&Rahman model) yield for a depth of NAP – 7.3 m volume strains that are in reasonable agreement with the measured values. The C/L model with parameters from laboratory testing and the Seed&Rahman model yields for this depth values that nearly perfectly match the measured values.
For the depth of NAP – 3 m similar conclusions can be drawn.

8.2.6 Comparison measured and calculated excess pore pressures

The development of the excess pore pressure has been measured at two different depths. For the validation the maximum excess pore pressure at each point and each installed sheet pile is used. For the postdiction the used densification model is the C/L model. The empirical parameters in this model are assessed both from the correlation and from the performed laboratory testing. The used propagation model is the stress attenuation model with n = -1.

Figure 8.12 and 8.13 show the comparison between the measured and the calculated values.
For level NAP – 8 m the agreement between measured and calculated excess pore pressure is good. Using the parameters from the correlation yields a better fit as using the parameters from the laboratory testing. For level NAP – 3 m the agreement close to the sheet pile wall is less, the measured values are much higher as the calculated values. This difference is consistent with the observed difference in measured and predicted local volume strain.

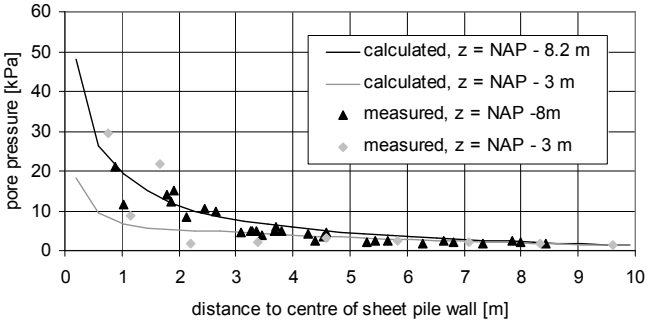

Figure 8.12 Comparison measured and calculated excess pore pressure at depth during installation, using n=-1 and soil parameters from correlation

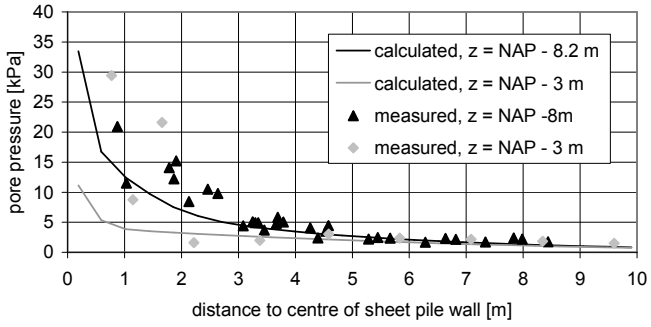

Figure 8.13 Comparison measured and calculated excess pore pressure at depth during installation, using n=-1 and soil parameters from laboratory testing

When using the Seed&Rahman model an excess pore pressure is predicted that is much in line with the values predicted with the C/L model and parameters from correlation, see figure 8.14.

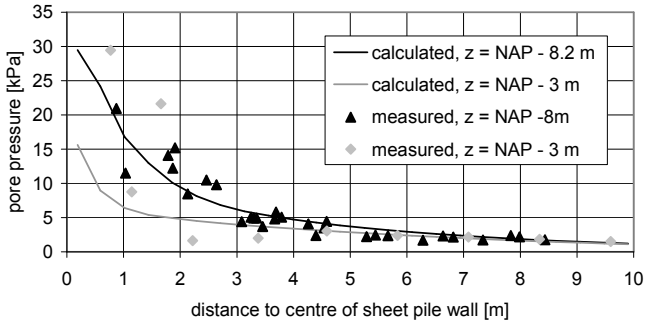

Figure 8.14 Comparison measured and calculated excess pore pressure at depth during installation, using Seed&Rahman model and n=-1

8.2.7 Comparison measured and calculated surface settlement due to installation

Finally a comparison is made between the measured and calculated surface settlement. After all this is the purpose of the model. Figures 8.15 and 8.16 show the results.

The model of Barkan predicts surface settlements that are far in excess of the measured values. It has already been noticed that local densification predicted with this model are in excess of the measured values. In this respect the results are consistent. For a better comparison of the measured settlement with the result when using the other models these data are removed.
The energy dissipation method predicts a heave of the surface whereas the measurements indicate a settlement. It has been noticed already that the energy dissipation method predicts local densification below the measured values. The heave is caused by the inserted volume of the sheet pile.

The best agreement between measured and predicted surface settlement is obtained with the C/L model and the Seed&Rahman model. For the C/L model there is a difference when using the parameters from the correlation and from the laboratory testing. The first gives the best results close to the sheet pile but overestimates the settlement at some distance. The last gives a good fit for the settlement at some distance of the sheet pile but underestimates the settlement close to the sheet pile.
Most models predict that settlements occur to a distance of 8 m from the sheet pile wall. The model ‘Barkan standard’ predicts a somewhat wider settlement trough; settlements are predicted to occur to a distance of 9 m from the sheet pile wall.

This is consistent with the larger area (about 1 m more, see section on local densification) over which it is predicted that densification will occur.

A peculiar result of all models is a heave or reduction of the settlement close to the sheet pile. Responsible for this is the inserted volume of the sheet pile. In practice this effect is not observed. This aspect will be discussed in the next section.

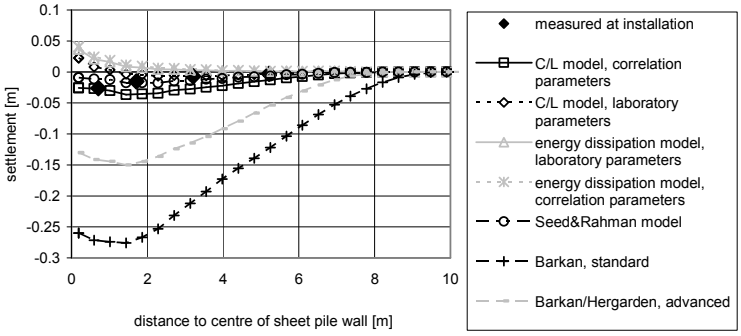

Figure 8.15 Comparison measured and calculated settlement after installation, using all models

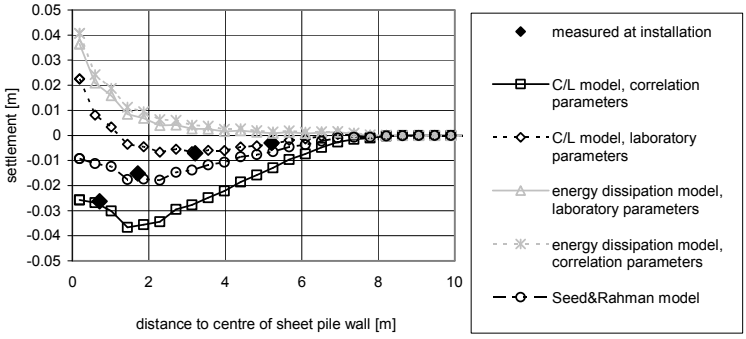

Figure 8.16 Comparison measured and predicted settlement after installation

8.2.8 Comparison measured and calculated surface settlement due to removal

The settlement due to removal is calculated as the sum of the settlement due to removal of the volume of the sheet pile and the settlement due to the additional densification during vibratory pull. To determine the last item the densification is calculated for a time of vibrating of 500 s (to model the installation phase) and 750 s (to model the installation plus removal phase). Figure 8.17 shows the calculated and measured surface settlement due to removal of the steel sheet piles for one densification model (the C/L model and empirical parameters derived from correlation).

The calculation result indicates that the additional densification hardly contributes to the settlement. This is in agreement with the observation that in the Raamsdonksveer sheet pile test hardly any densification occurred during removal. Using other densification models also show that hardly any additional densification occurs during removal. Nearly all settlement is a result of the removal of sheet pile volume.

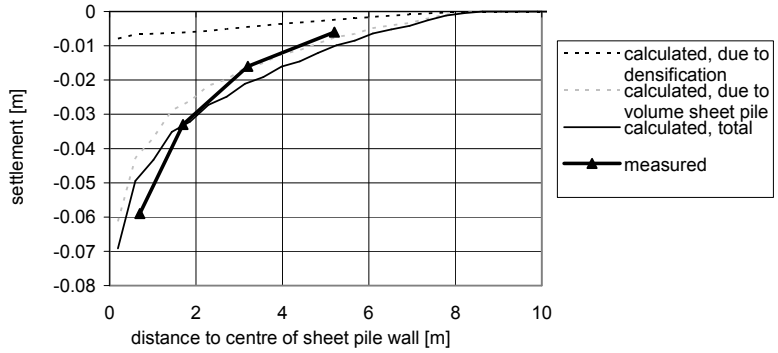

Figure 8.17 Comparison measured and calculated surface settlement due to removal, using n=-1, soil parameters from correlation

8.2.9 Discussion results comparison measured and calculated values

In this section some of the findings from the comparison are summarised and discussed. These findings are the angle of interface friction to be used, the attenuation of the velocity amplitude, the large settlement close to the sheet pile,

*** angle of interface friction**
For the interface friction between sand and steel usually about 0.66 times the angle of internal friction is used. A reasonable agreement between the measured and calculated velocity amplitude and wave attenuation is obtained when the angle of interface friction is taken equal to the angle of internal friction. The larger ratio to be used can be motivated from the difference in shearing area between a sheet pile and the circular pile used in the calculation.

*** velocity attenuation**
For a close fit between measured and predicted velocity amplitude the parameter describing the velocity attenuation is to be set at unity as well. This is in excess of the expected value of -0.75. In order to understand this discrepancy first some attention is paid to the factors influencing the attenuation. The wave attenuation is caused by the following aspects:
- axial symmetric expansion of waves
- shear strain dependent shear modulus
- effect excess pore pressure on the shear modulus
- energy dissipation in the soil (material damping)
- interference of waves.

The first three aspects are incorporated in the model. The last two aspects are not accounted for in the model. Instead a wave attenuation parameter larger than the theoretical value of n = -0.5 is used. Energy dissipation in the soil alone does not explain the value of n = -1. Interference of S- and P-waves emitted from flange and web are considered to be responsible for the larger value of n.

*** settlement close to the sheet pile wall**
A peculiar aspect of the calculated surface settlement during installation is rise in surface close to the sheet pile. This results from the inserted volume of the sheet pile. In reality a large settlement is observed close to the sheet pile. This indicates that close to the sheet pile mechanisms are present that will increase the amount of densification, but are still not or not fully understood.

Some possible mechanisms are listed below.
- vibrations from the tip
- multi directional shearing/rotation of principle stresses
- horizontal vibrations sheet pile
- velocity amplitude near ground level is underestimated
- net downward friction at interface sheet pile – soil.

A short description of these aspects will be given.

In the present model it is assumed that loading of the soil is predominately a vertical shearing. Vibrations from the tip are neglected. These may result in a local stronger densification.

It is found that the stress attenuation model underestimates the velocity amplitude near the surface. As a consequence the local densification near the surface, in case of fully saturated sand, will be underestimated as well. The top meters of the soil consist mainly of moist sand and clay. These layers are expected to show less densification as dry or saturated sand. The error due to underestimating the velocity amplitude near the surface is therefore expected to be limited.

Observations during the test show that the surface settlement between the flanges of the sheet pile is far in excess of the surface settlement next to the sheet pile. A possible explanation for this is that the net downward friction at the interface sheet pile –soil results in some kind of plugging of the sand and thus a large downward movement. No proof for this explanation is yet available.

For improving the present model attention is to be paid to these aspects.

8.3 Nijverdal sheet pile test

In 2005 the Dutch Public Works Department ordered to perform a sheet pile test at Nijverdal, The Netherlands. The purpose of the test is to assess the environmental aspects during vibratory and impact sheet piling at that location. In total 12 sheet piles are installed and subsequently removed. Vibratory driving, vibratory driving

with flushing/jetting and vibratory driving with predrilling of the soil at the location of the clutches are used. For two of the sheet piles impact driving has been used for the last two meters.
The used sheet piles are double AZ26 profiles with a length of 17 m. The driving depth is about 16.5 m. The soil is mainly sand with a relative high cone resistance. As vibrator is a leader mounted PVE 2335VM (maximum frequency 38 Hz, maximum eccentric force 2000 kN) has been used.

One of the parameters measured during the test is the surface settlement. To this end 10 settlement plates are installed at different distances to the sheet pile wall. Figure 8.18 shows the surface settlement at three arrays after the following phases:
- installation of all sheet piles
- impact driving of 2 sheet piles over the last 2 m.

Figure 8.19 shows the difference in surface settlement after the test and after installation of the sheet piles, so the surface settlement due to removal only.

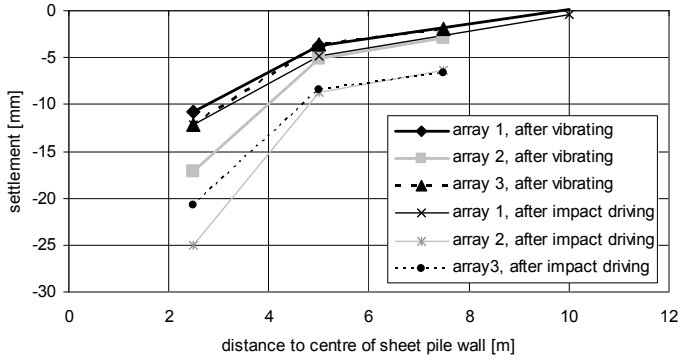

Figure 8.18 Measured surface settlement after installation, Nijverdal sheet pile test

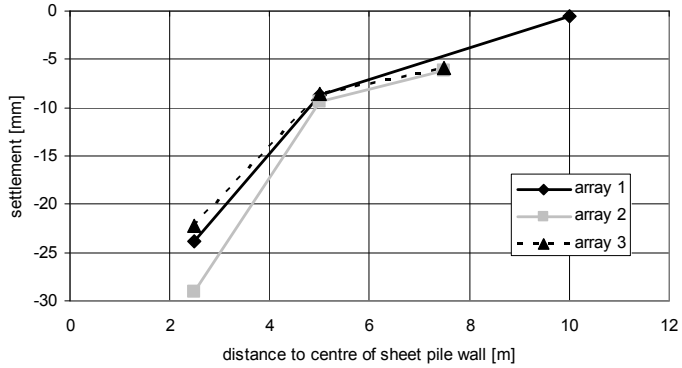

Figure 8.19 Settlement due to removal of the sheet piles, Nijverdal sheet pile test

Indications are that fluidisation during installation of sheet pile 7, 8 and 9 (closest to array 2) may have contributed to the total settlement. It is obvious from figure 8.18 that impact driving greatly increased the amount of settlement in this test. The width of the settlement trough cannot be assessed from the measurements.

A postdiction of the settlement is made with the program TRILDENS3. Calculations are made using the C/L model, the energy dissipation model and the Seed&Rahman model. Table 8.3 shows the used soil profile and soil parameters. As illustration the calculated settlement when using the C/L model is shown in figure 8.20.

top of layer [m+NAP]	I_D	C_1	C_2	PEC/σ'_{v0} [-]
9.2	--	0	0.13	0.022
8.7	0.94	6.344	0.13	0.063
7	0.8	7.38	0.13	0.048
5	0.75	7.75	0.13	0.043
4	0.55	9.23	0.13	0.025
3	0.65	8.49	0.13	0.034
0	0.9	6.64	0.13	0.059
-4	0.8	7.38	0.13	0.048

Table 8.3 Soil profile at Nijverdal

For 2.5 m and 5 m from the sheet pile the measured surface settlement agrees well with the calculated total surface settlement. The actual width of the settlement trough is however larger as results from the calculation. Also in this postdiction the peculiar behaviour of the surface settlement close to the sheet pile can be observed.

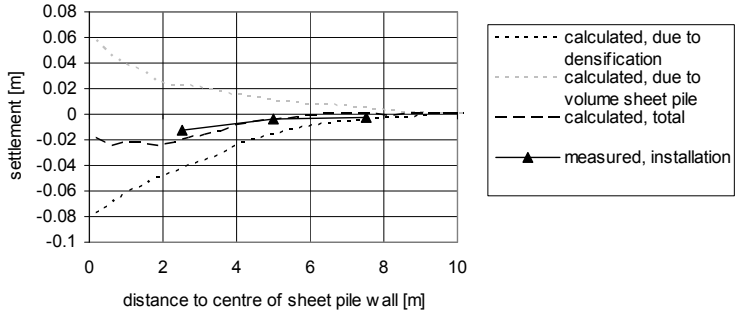

Figure 8.20 Postdiction Nijverdal sheet pile test

The settlement due to removal of the sheet piles is assessed from the settlement due to removal of the volume of the sheet piles and the difference in densification between a time of vibrating of 360 s and 540 s. The result is shown in figure 8.21.

The densification contributes marginal to the total settlement. Therefore the result of one calculation (C/L densification model) is shown.

The settlement during removal seems to originate mainly from the removal of the sheet pile volume. As with the installation the width of the trough is more as is in general expected.

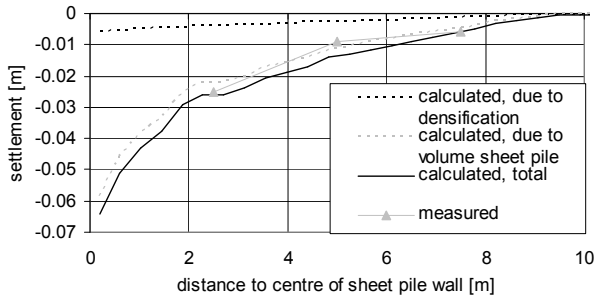

Figure 8.21 Settlement due to removal of the sheet piles, Nijverdal sheet pile test

8.4 The Hague sheet pile test

In (Nijs 2003) results of a sheet pile test are reported. Purpose of the test is to check the drivability of the sheet piles and the consequences for the surrounding, for a situation comparable to the test location.
Sheet piles PU20 with a length of 15 m are installed into the subsoil. The driving depth is about 14.5 m. A Tünkers Pe180.18 vario vibrator is used at 80% of its capacity (frequency 25-30 Hz, maximum eccentric force 1800 kN). Five sheet piles are installed using vibratory driving only, four sheet piles are installed using vibratory driving and fluidisation. The reported time of vibrating per sheet pile is 10 to 15 minutes. Surface settlements are measured after installation of each sheet pile. Close to the sheet pile the measurements are considered less reliable due to activities close to the sheet pile. The closest distance at which reliable measurements are present is at 2.9 m from the centre line of the sheet pile.

The surface settlement turned out to vary not only with respect to the distance of the sheet pile wall, but also with respect to the location parallel to the wall. Figures 8.22 and 8.23 show the surface settlement at the end of installation for array 1, 2 and 3, located respectively at the start, the middle and end of the section installed with vibratory driving only. The measured values close to the sheet pile (within 2 m from the sheet pile) are considered less reliable by the author.
Measured surface settlements at the section where fluidisation has been used indicate that fluidisation may reduce the surface settlement. The fluidisation process however could not be considered as robust.

The subsoil is mostly a sandy soil. Cone resistances differ over the depth. Interesting is that both before and after the test CPT's are made. Figure 8.24

shows a representative CPT profile before the test, after installation and after removal of the sheet piles. The CPT's are made at or close to the centre line of the sheet pile wall. Therefore it cannot be excluded that the results of the CPT test after installation are influenced by the proximity of the sheet piles.

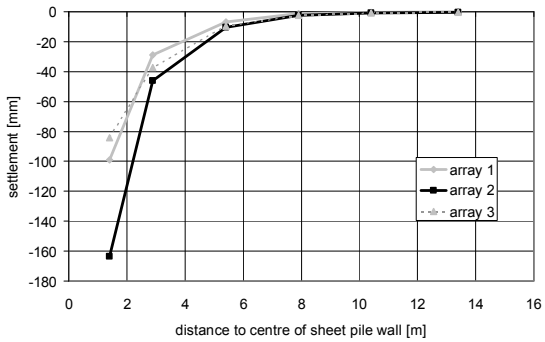

Figure 8.22 Settlement after installation of all sheet piles, The Hague sheet pile test

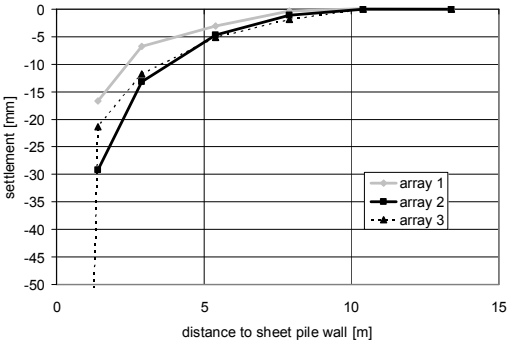

Figure 8.23 Settlement due to removal of sheet piles, The Hague sheet pile test

The measured surface settlements are far in excess of the calculated values, especially close to the sheet pile wall. When the effect of the volume of the sheet pile is neglected a better agreement is obtained. Still the calculated settlements are below the measured values. Also the measured width of the settlement trough is in excess of the calculated one. The relative long duration of the vibrating is taken into account in the calculation. The limited length of the test wall may result in an underestimate of the surface settlements. This indicates that the proposed method is optimistic for this case.

The settlement due to removal is assessed from the settlement due to removal of the volume of the sheet pile and the difference in densification between an installation time of 1200 s and 1800 s. The result is shown in figure 8.26.

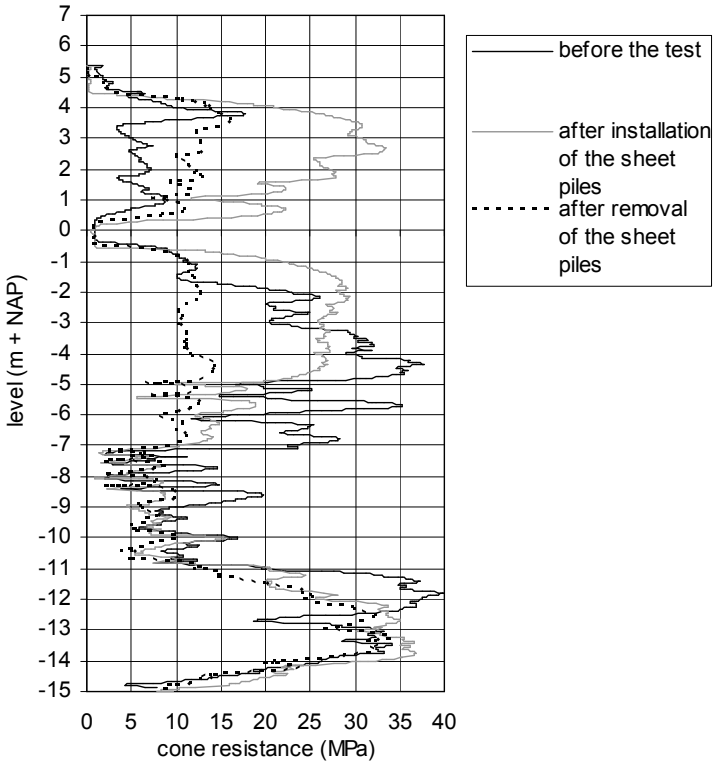

Figure 8.24 Measured CPT profile at The Hague sheet pile test

The soil profile used for the postdiction is given in table 8.4.

layer	top of layer [m+NAP]	I_D [-]	k [m/s]	C_1	C_2	PEC/σ'_{v0} [-]
sand	5.4	0.7	10^{-4}	8.12	0.13	0.038
sand	4.4	0.85	10^{-4}	7.01	0.13	0.053
sand	3.4	0.65	10^{-4}	8.49	0.13	0.034
clay	0.5	--	10^{-8}	0	0.13	0.069
sand	-0.5	0.72	10^{-4}	7.972	0.13	0.04
sand	-1.5	0.9	10^{-4}	6.64	0.13	0.059
sand, clayey	-7	0.55	10^{-4}	4.6 [1])	0.13	0.025
sand	-8.5	0.53	10^{-4}	9.378	0.13	0.024
sand	-11	0.85	10^{-4}	7.01	0.13	0.053

[1]) : adjusted for clayey soil

Table 8.4 Soil profile used for postdiction The Hague sheet pile test

Figure 8.25 shows the result of the postdiction, using the C/L densification model. The measured values in this figure are the average of the settlement at array 1, array 2 and array 3.

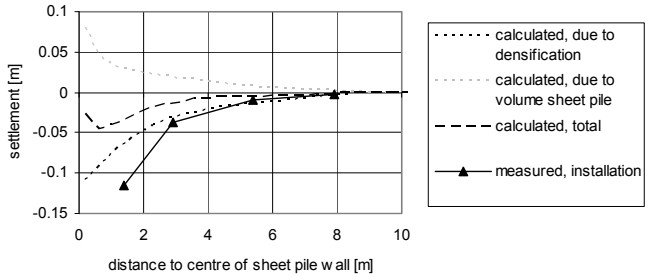

Figure 8.25 Postdiction The Hague sheet pile test (time of vibrating 1200 s)

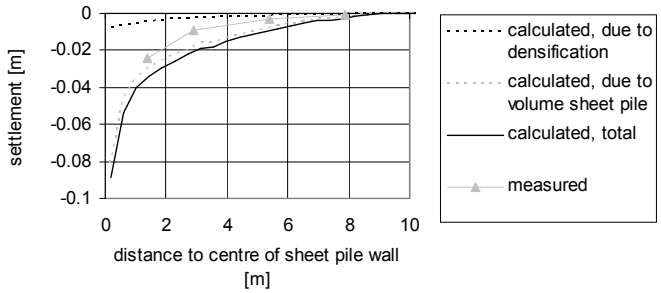

Figure 8.26 Settlement due to removal, The Hague sheet pile test

The measured settlements due to removal are less as would be predicted from removal of the volume of the sheet pile only. One explanation is that the limited extend of the test wall influences the measurement, as the situation during the test is not a pure plane strain situation.

8.5 Settlement at A15

During installation of sheet piles at the centre of the road embankment of highway A15 large settlements occurred. The amount of settlement was thus that two lanes of the highway needed to be temporarily closed for traffic. As this occurred during morning rush hours the consequence was a major traffic jam.

The embankment was constructed using the displacement method. Big amounts of sand were supplied at the existing ground level or in a shallow ditch. The supplied sand pushed the underlying clay and peat downwards and sideward until a stable situation is reached.
CPT testing in the embankment shows a low cone resistance, about 2 MPa. The relative density of the embankment, as estimated from the measured cone resistance, is about 20-25%.
The actual surface settlements due to vibrating are not measured. First priority was to reopen the closed traffic lanes. Eyewitness reports are that the settlement close

to the sheet pile was in the order of 0.8 – 1 m. From available photographs the width of the settlement trough is estimated to be in the order of 5 m. An accurate estimate cannot be given due to the limited area covered by the available photographs and the effect of the asphalt layer covering the settlement trough.
The driving depth of the sheet piles is about 10 m. Table 8.5 shows the soil profile, as used for the postdiction.

layer	I_D [-]	C_1	C_2	PEC/σ'_{v0} [-]
sand	0.2	11.82	0.13	0.005

Table 8.5 Soil profile at A15

The groundwater level is assumed to be well below the tip of the sheet pile. As time of vibrating in the calculation 500 s is used. Figure 8.27 shows the result of the postdiction.
The calculated settlement close to the sheet pile is 0.4 m. This is about 50% of the reported settlement. The calculated width of the settlement trough is 8 m. This is in reasonable agreement with the observed width of the settlement trough.

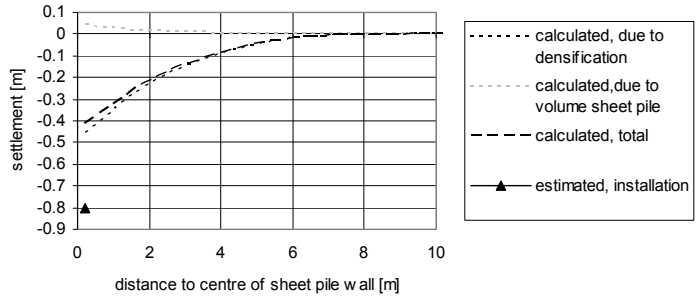

Figure 8.27 Results calculation settlement A15

8.6 Sewage line Haarlem

As part of his M.Sc study Hergarden (2000) measured the settlement during removal of sheet piling for a sewerage project in Haarlem, The Netherlands.
The sewage line is constructed between two sheet pile walls. The distance between the sheet piles is 2.75 m. Sheet piles Larsen 25, with a length of 11 m, are used. The tip of the sheet pile is at NAP - 10 m. The bottom of the sewage line is at NAP – 5 m. The measured settlement of the sewage line after removal of the sheet piles is 4 to 5 cm. Specifications of the used leader mounted vibrator are a frequency of 40 Hz and an eccentric force of 500 kN.
The surface settlement outside the trench is measured as well. It was noticed that driving of the piling rig along the settlement points already resulted in some deformations. These data are therefore considered unreliable.

Below the excavation depth of NAP – 5 m and tip of the sheet pile (NAP – 10 m) the subsoil consists of sand wit a varying cone resistance. Two soil profiles are

used for the postdiction, one at the location of CPT 11 and the other at the location of CPT 8. Table 8.6 shows the used soil profiles.

layer	top of layer [m+NAP]	I_D [-]	C_1	C_2	PEC/σ'_{v0} [-]
fictitious top layer	-4.5	--	0	0.13	0.059
sand	-5	0.55	9.23	0.13	0.025
sand	-5.5	0.35	10.71	0.13	0.012
sand	-6.8	0.52	9.45	0.13	0.023
clayey sand	-8.8	--	2 [1])	0.13	0.001

[1]) Assumed value for clayey sand

Table 8.6 Soil profile at sewage line Haarlem, CPT 11

In order to account for the volume of two sheet piles being removed the thickness of the sheet pile is set at twice the thickness of a single wall. For the calculation the 'surface' is set at NAP – 4.5 m. The weight of the layers above NAP – 5 m is taken into account as a fictitious layer of 0.5 m thickness and a wet volume weight of 110 kN/m^3.
Analysing this case is not straightforward for two reasons. First the settlement of the sewage line is influenced by removal of two walls. The second reason is that during installation already some densification occurred and the soil cannot be considered as virgin soil.

The first aspect is taken into account by summing the settlement due to removal of both sheet piles. As the considered point is at equal distance to the wall at one side and at the other side this is for this case equal to doubling the settlement due to removal of one sheet pile wall. The latter aspect is taken into account by considering as settlement due to densification the difference in settlement during a time of vibration representing the time of installation and the settlement due to a time of vibrating representing the time of installation plus removal. Figure 8.28 shows the result of the postdiction.
The best estimate for the settlement of the sewage line becomes 0.053 m.

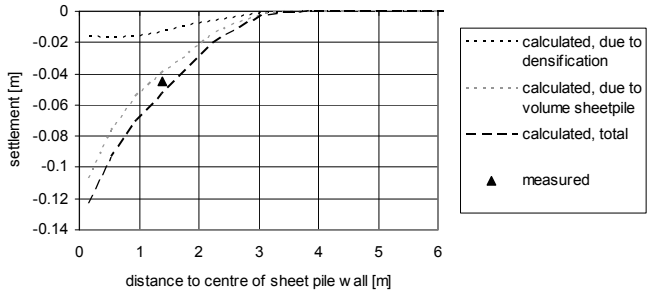

Figure 8.28 Result postdiction settlement due to removal of two sheet pile walls, soil profile CPT 11

8.7 Pettemer Zeedijk

In 2004 the crest of the Pettemer Zeedijk has been raised using sheet piles. The used sheet piles are Hoesch 1700 profiles with a length of 8 m. Top of the sheet piles is about 0.75 m above crest level, resulting in a driving depth of 7.25 m. The vibrator used for the installation is a PVE 2315VM (frequency 2300 rpm, centrifugal force is 870 kN).

The dike consists of sand with varying density. The groundwater table is at approximately NAP + 0m, so well below the tip of the sheet pile.

Surface settlements during installation are measured at the crest and seaward slope of the dike. Figure 8.29 shows the results.

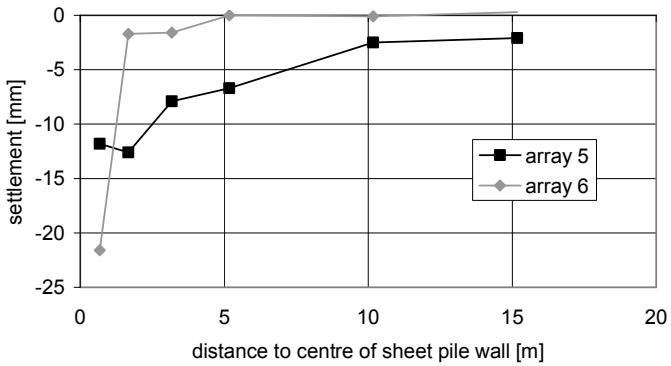

Figure 8.29 Measured settlement at Pettermer Zeedijk, to front of wall

A large difference in settlement between array 5 and array 6 is observed. As the measurement points are situated at the slope it is possible that the measured settlement is caused both by densification and by some downward movement of the slope.

With TRILDENS3 a postdiction of the settlements is made. The following soil stratification is used.

layer	top of layer [m+NAP]	q_c [MPa]	I_D [-]	C_1	C_2	PEC/σ'_{v0} [-]
sand	12.8	4	0.85	7.01	0.13	0.053
sand	11.5	10	0.88	6.788	0.13	0.056
sand	10	6	0.56	9.156	0.13	0.026
sand	8.5	2.5	0.2	11.82	0.13	0.005
sand	6	5	0.34	10.784	0.13	0.011
sand	5	4	0.22	11.672	0.13	0.005

Table 8.7 Soil profile Pettemer Zeedijk used for the postdiction

The estimated time for installing one sheet pile is taken as 3 minutes. Figure 8.30 shows the calculated surface settlement.

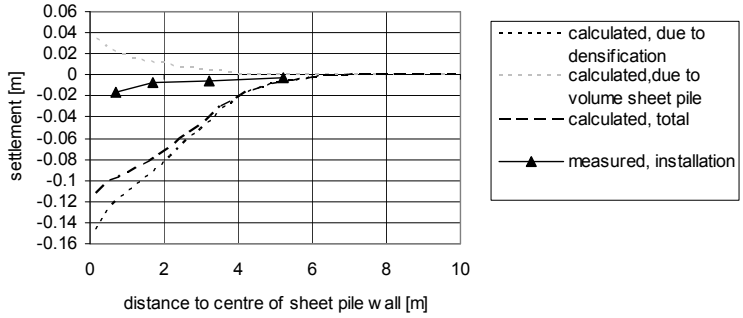

Figure 8.30 Results postdiction settlement at Pettemer Zeedijk

The measured settlements are far below the calculated values. The sheet piles are installed in sand above the ground water table. The rainy days preceding the installation may have influenced the degree of saturation of the sand. It is expected that the difference between measured and calculated settlement is caused by the apparent cohesion of the subsoil.

8.8 Building pit Wassenaar

For a building project in Wassenaar sheet piles with a length of 16 m are driven into the soil. The type of sheet pile is a PU20 and the used vibrator an ICE 23RF. Specifications of this vibrator are a frequency of 2300 rpm and a maximum centrifugal force is 1334 kN. Time of driving is not recorded but is estimated to be approximately 5 minutes per double sheet pile. At one side of the building pit the surface settlements in two arrays are measured. Figure 8.31 shows the measured settlements.

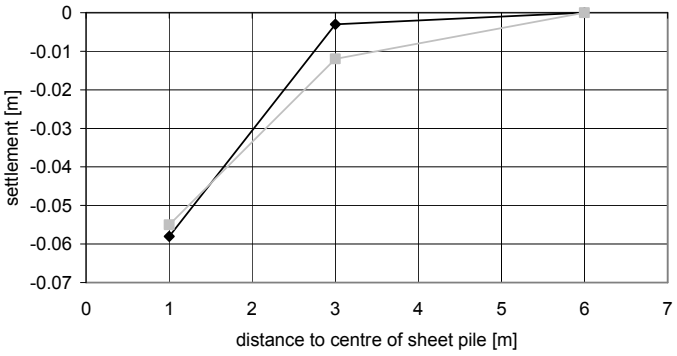

Figure 8.31 Settlements at building pit Wassenaar

The subsoil consists mainly of sand, interbedded with some tiny clay layers, especially between NAP – 11 and NAP – 14.5 m.

For the postdiction the soil layering as given in table 8.8 is used. The relative density is based on correlations with the cone resistance. The relevant parameters for the densification model are determined using the previously derived correlations, as implemented in TRILDENS3.

layer	top of layer [m+NAP]	I_D [-]	k [m/s]	C_1	C_2	PEC/σ'_{v0} [-]
sand	0.76	1	10^{-4}	5.9	0.13	0.07
sand	-1.2	0.8	10^{-4}	7.38	0.13	0.048
sand	-5	0.67	10^{-4}	8.342	0.13	0.035
sand	-7.4	0.48	10^{-4}	9.748	0.13	0.02
sand	-9.4	0.6	10^{-4}	8.86	0.13	0.029
clay	-10.2	0.99	10^{-8}	0	0.13	0.022
sand	-13.4	0.7	10^{-4}	8.12	0.13	0.038
clay	-13.8	0.99	10^{-8}	0	0.13	0.022
sand	-14.6	0.75	10^{-4}	7.75	0.13	0.043

Table 8.8 Soil profile Wassenaar used for the postdiction

Figure 8.32 shows calculated settlement. When ignoring the effect of the sheet pile volume the calculated settlement close to the sheet pile wall matches with the observed settlement. At 3 m distance from the sheet pile the calculated settlement is in excess of the measured value. The wide of the trough is in good agreement or a little more as the observed width.

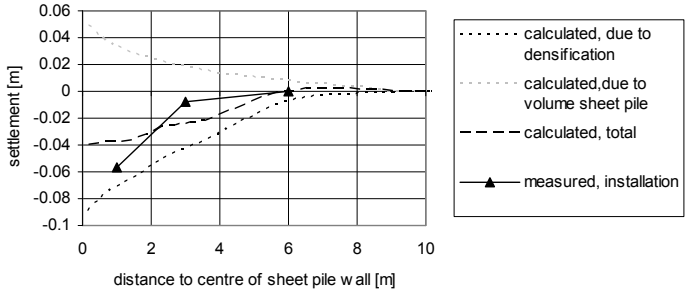

Figure 8.32 Calculated surface settlement at Wassenaar

8.9 Summary of validation calculations, installation

For a comparison of the measured and calculated settlement all data are plotted. For a clear insight the data are plotted in two different ways. The upper graphs in figure 8.33 to 8.35 show at the horizontal axis the calculated settlement and at the vertical axis the measured value. Points belonging to the same case are connected

with a solid line. In the graphs three straight lines are plotted as well. The solid line represents the case where the measured and calculated settlements are in perfect agreement. The dotted lines represent the cases where the measured value is half or twice the calculated value. The difference between the figures is the used densification model.

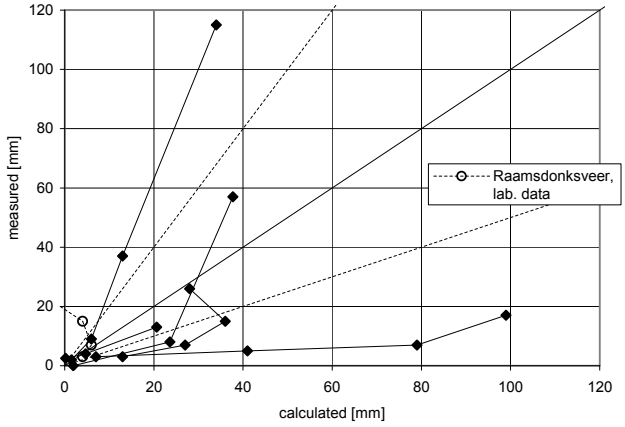

Figure 8.33 Comparison measured and calculated settlement due to installation, C/L densification model

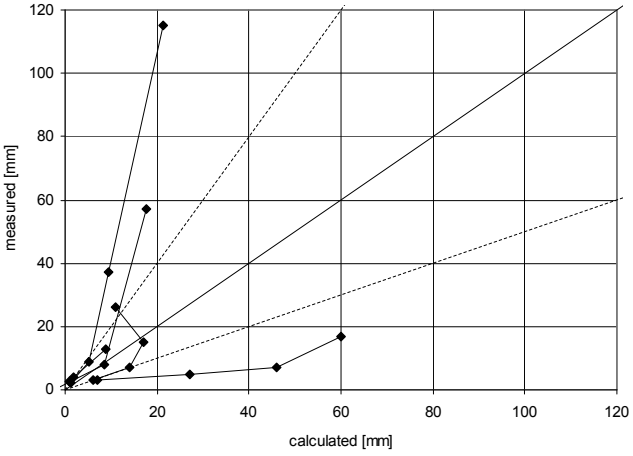

Figure 8.34 Comparison measured and calculated settlement due to installation, Seed&Rahman densification model

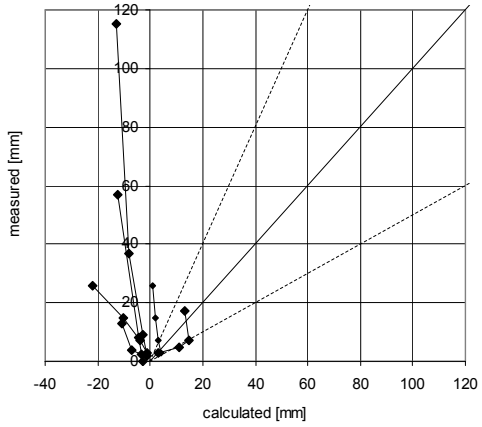

Figure 8.35 Comparison measured and calculated settlement due to installation, energy dissipation densification model

These graphs give insight in the accuracy, but do not provide information on the behaviour with distance. Therefore the results for the C/L densification model and the Seed&Rahman densification model are also presented in a different way, see figure 8.36 and 8.37. There the ratio between measured and calculated settlement as function of the normalised distance to the sheet pile wall is shown. For normalising the distance the driving depth of the sheet pile is used.

The C/L model and the Seed&Rahman model yield more or less consistent values. For the installation phase the ratio between measured and predicted values may vary between 1/3 and 3. A general aspect of all models is that they tend to underestimate the settlement close to the sheet pile wall. This confirms the opinion that close to the sheet pile wall some still unknown mechanisms may be present, which influence the amount of settlement.

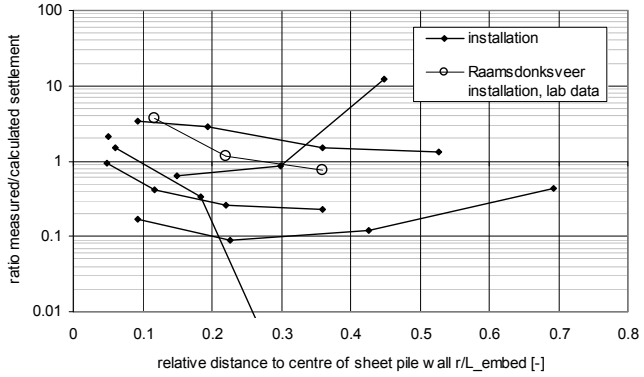

Figure 8.36 Comparison measured and calculated settlement due to installation, C/L densification model

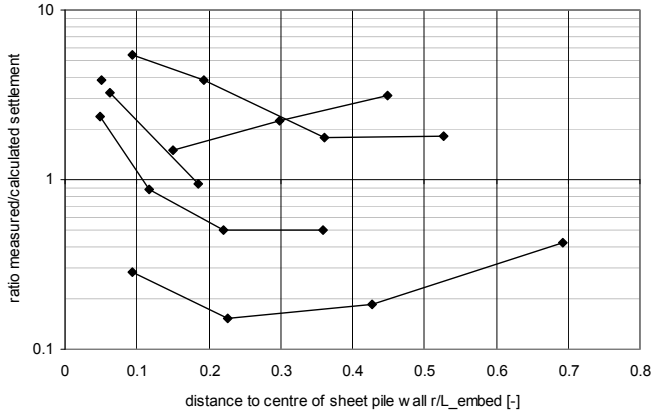

Figure 8.37 Comparison measured and calculated settlement due to installation, Seed&Rahman densification model

For the phase of installation TRILDENS3, using the C/L model as generation model, in general gives more cases with an underestimation as an overestimation of the settlement. When the case Pettemer Zeedijk is removed from the dataset the number of case where the settlements are underpredicted and overpredicted are nearly equal.
Using the Seed&Rahman model as generation model the predicted settlement tends to be lower as the measured value.

Using the energy dissipation model as densification model the predicted surface settlements are far outside the range of measured values. In many cases even a heave is predicted where in reality a settlement is measured. The present implementation of this model is therefore considered a less reliable method of predicting the densification during vibratory sheet piling. More research is needed before this model can be used for this type of problems.

The results of the comparison between model and field data can be presented in a different way. The settlement is attributed to two mechanisms, densification and installation of a volume of sheet piles. For the installation phase the two mechanisms counteract.

$$\Delta z = \Delta z_{densification} - \Delta z_{volume} \tag{8.4}$$

Thus far the sum of these mechanisms has been compared. This implies that a small relative error in one of the components may results in a large relative error in the summation. In order to get a better understanding of the accuracy of the densification a comparison is made of the contribution of this part to the total settlement. The calculations yield directly this contribution. The measured values are corrected for the contribution of the sheet pile volume to the total settlement. For this the measured settlements are corrected with the settlement due to the volume of the sheet pile, as predicted by TRILDENS3. In some cases this results in a negative settlement due to densification. This may be the case when soil loosens during removal.

Figure 8.38 to 8.40 shows for three densification models the calculated settlement due to densification only, compared to the measured settlement due to densification only. The dashed lines indicate the situation where the ratio between measured and calculated settlement is 0.5 or 2.

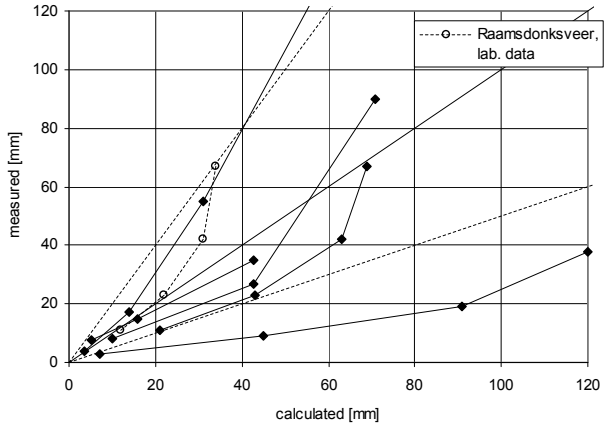

Figure 8.38 Comparison measured and calculated settlement due to densification only, densification model is the C/L model

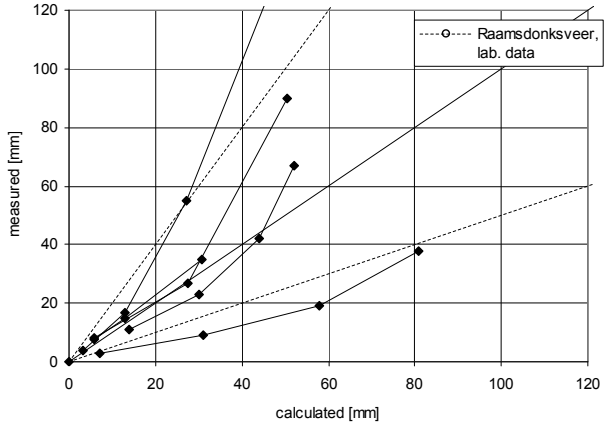

Figure 8.39 Comparison measured and calculated settlement due to densification only, densification model is the Seed&Rahman model

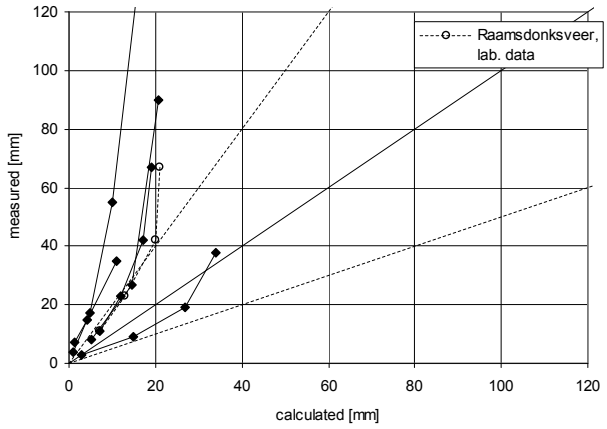

Figure 8.40 Comparison measured and calculated settlement due to densification only, densification model is energy dissipation model

When using the C/L densification model or the Seed&Rahman model nearly all cases give a settlement due to densification that is within the range of 0.5 to 2 times the calculated settlement. There is one exception, the case of the Pettemer Zeedijk. It was noted before that for this case the calculated settlements for this case are far above the measured values.

8.10 Summary validation calculations, removal

For a number of projects data are available for the stage of removal. These projects are Raamsdonksveer, Nijverdal, The Hague and Haarlem. Only the results of the C/L densification model are presented (figure 8.38). The other models yield comparable results.

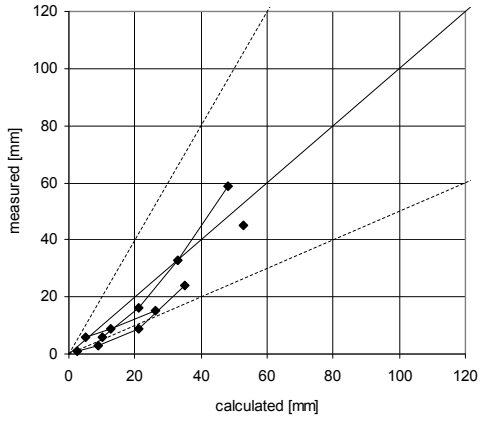

Figure 8.41 Comparison calculated and measured settlement during removal, C/L densification model

For the phase removal of the sheet piles the measured surface settlement is in good agreement or a little below the calculated values. For this situation the settlement during removal is dominated by the removal of the volume of the sheet pile. The general trend is that close to the sheet pile the actual settlement is reasonable while at larger distances the actual settlement is less. This suggest that the used angle of volume spreading may be a little less than the used value of β=30°.

For this situation no firm conclusions can be drawn as three out of four cases are situations where no excavation and/or backfilling of a building pit is applied.

8.11 Conclusions

It is found that the C/L and Seed&Rahman model gives the best prediction of the surface settlement. The general trend is that the calculated settlements are less as the measured values. The energy dissipation model largely underpredicts the settlements. This model, in it's present formulation, is not suitable for predicting the settlements.

During installation the settlement is the result of two counteracting mechanisms, the densification of the soil and the insertion of a sheet pile volume. The accuracy of the densification model only is about a factor 2. Combining this model with a model for the displaced soil volume due to the insertion of the volume of the sheet pile reduces the accuracy of total model to a factor of about 3.

Especially close to the sheet pile the measured settlement is above the calculated value. It is expected that close to the sheet pile mechanisms are present, not incorporated in the present model, which cause these larger settlements.

According to the model the settlement during removal is mainly caused by the removed volume of the sheet pile. Nearly all cases with removal of sheet piles are test situations. In these situations no excavation and backfilling of the building pit is performed. Only one case is available with removal of sheet piles after excavating and backfilling of a building pit. This case could be well predicted assuming that preshearing is not lost during excavation.

9. Conclusions and recommendations

9.1 Conclusions

In this section the main conclusions from this thesis are summarised. The conclusions are grouped as ‘existing experience’, ‘existing models’, ‘behaviour of sand under cyclic loading’, ‘results full scale test’, ‘model development’ and ‘validation of the model’.

*** existing experience**
Settlements due to vibratory installation of sheet piles close to the sheet pile wall, as reported by various sheet piling contractors, vary between zero and nearly 1 m. In most cases the reported settlements are based on visual observations. Most likely in many cases the settlements due to sheet piling remain unnoticed, as they are outshined by other disturbances at the working area. There are no reports on surface heave. For about 50% of the sheet piling projects the settlement close to the sheet pile wall exceeds 0.1 m.
At a distance of about half the driving depth the surface settlements become negligible.

*** existing models**
In the literature a series of models is described that are intended for or may be used for predicting the surface settlement. Some of the models do not describe the relevant mechanisms during vibratory sheet piling. Other models show unrealistic trends when varying some of the parameters (e.g. the frequency or the density of the sand). None of the models is considered to correctly describe the actual behaviour. A more sophisticated model, which takes into account in a physically correct way the different mechanisms, is necessary for as a more reliable prediction method.
At present the use of FEM models is hardly pursued and to date no methods based on this approach are known.

*** behaviour of sand under cyclic loading**
The behaviour of sand during cyclic loading is a complex process. An important aspect during vibratory sheet piling is the combined effect of generation and dissipation of excess pore pressure. Cyclic triaxial tests show that, when the soil is allowed to drain, the resistance to liquefaction greatly increases. This increase is known as ‘preshearing’ or ‘history’. It is erased on complete liquefaction.
Static loading with a limited shear strain increase (well below the failure of the sample) has hardly or no influence on the behaviour during following cyclic loading. Static loading with a large (plastic) shear strain however has a ruinous effect; the resistance against liquefaction almost disappears. This behaviour cannot be explained from a change in relative density only. Other parameters, as the fabric of the grain skeleton, are of importance when dealing with cyclic behaviour of sand.

Predicting the behaviour of a drained cyclic test (densification) from the results of an undrained test (excess pore pressure) or vice versa gives the correct order of

magnitude, but large discrepancies exist. This indicates that predicting the densification with great accuracy may not be possible.

For shear strain amplitudes below 10^{-4} the densification becomes small but not zero. This is in contradiction with the often stated value of a threshold shear strain amplitude of 10^{-4} below which no densification occurs. For situations with a limited number of loading cycles, as with vibratory sheet piling, the densification becomes negligible for shear strain amplitudes below the quoted value.

*** results full scale test**
During the Raamsdonksveer sheet pile test many interesting observations are made. Main observation is that most densification occurs during the installation phase. The area with densification during vibratory sheet piling is limited to 0.5 to 2 m. During removal only limited additional densification occurs. The settlement is mainly caused by the removed volume of the sheet pile. The surface settlements due to removal are larger as during installation, despite the smaller amount of densification. This apparently contradictionary result can be explained from the influence of the installed or removed volume of the sheet pile on the settlements.

The area with settlement is bounded by a line at an angle of about 30 degrees with the vertical from the tip op the sheet pile. Settlements occur to a distance from the sheet pile of about half the driving depth of the sheet pile. The largest settlements do not necessarily occur at the surface. It is possible that the largest settlements occur at some depth.

To a distance of about 3 to 5 m from the sheet pile the cone resistance decreases, at least for the period shortly after the installation. This effect may be explained by a reduction of the horizontal stresses as a consequence of the volumetric strain of the sand. If this explanation is true it must be concluded that during vibrating the effective horizontal stress at the sheet pile not only reduces due to an increase in pore pressure but also due to a reduction of the horizontal earth pressure coefficient. In this study the development of the cone resistance with time is not investigated.

During vibrating the sheet pile not only vibrates in the vertical direction but also in the horizontal direction. Above ground level the vibration amplitude in the horizontal direction may be of the same order of magnitude as the vibration in the vertical direction.
The vibration amplitude attenuates with distance. For apparently the same conditions still relative wide margin (a factor 4 between upper and lower bound) is found. The variation must be attributed to small and not noticeable variations in the situation as the quality of the sheet pile being vibrated, the tuning of the vibrator, small variations is soil layering etc. This indicates that prediction of the vibration level with great accuracy is not possible.

*** model development**
From an analysis of the processes during vibratory sheet piling the processes leading to settlement are identified: vibration of the sheet pile, interface behaviour at the interface sheet pile – soil, propagation of vibrations into the soil, densification

and/or generation of excess pore pressures due to cyclic loading of the soil, dissipation of excess pore pressures, settlement due to local densification and deformations due to the displaced soil volume by the sheet pile. The settlement during vibratory sheet piling is mainly caused by two mechanisms. The first is the densification of the soil. The second is the displaced soil volume due to the volume of the sheet pile. For the installation phase the two mechanisms counteract each other. For the removal phase both densification and removal of the sheet pile volume contribute to the surface settlement.

A model is developed to predict the settlement. The model follows the sub processes mentioned above. Different options for the propagation model and densification model are considered. A selection between the different options is made during validation of the model.

*** validation of the model**
Postdictions with the model are compared with measured surface settlements from different projects. The best results are obtained with a propagation model that assumes an attenuation of the shear stress amplitude with the reciprocal of the distance and the C/L or Seed&Rahman densification model. A general trend is that close to the sheet pile the settlements are underestimated.
The actual accuracy for the installation phase is a factor 3. When the data are corrected for the effect of the displaced volume of the sheet pile the contribution effect of densification only on the surface settlement can be determined. For this contribution only the accuracy of the model is found to be a factor 2.

Only limited data are available to check the accuracy of the model for the phase of removal. For situations where no excavation of a building pit is present the settlement at removal is dominated by the contribution from the removed volume of the sheet pile. Most of the densification occurred during the installation phase. Only limited additional densification occurs during the removal phase, at least for situations without excavating or backfilling. For situations with excavation and backfilling shear deformations of the soil next to the sheet pile may destroy the soil fabric. This may result in more densification and thus larger settlements. This however could not be verified with the available data.

*** final conclusion**
The final conclusion is thus that a model that is a combination of a series of relative simple sub models is capable of predicting the total process. The accuracy of the model for predicting the surface settlement due to vibratory installation of sheet piles is a factor 3. Taking into account only the contribution of the densification the accuracy becomes a factor 2. The model still posses some simplifications, in particular with respect to the used stress path and the response of the soil to the actual stress path.

The presently developed model does not predict the large settlements often observed close to the sheet pile, and especially in the area enclosed by the flange and web of the sheet pile. It is therefore expected that close to the sheet pile still an unidentified process is present that contributes to the total settlements.

From the performed research no firm conclusions with respect to the effect of vibration frequency, used eccentric force of the vibrator, location of the vibrator at the top of the sheet pile, jetting and fluidisation on the vibration amplitude and the amount of settlement can be drawn.

9.2 Recommendations for further research

Still many questions remain unanswered. In this section a list of topics for more in-depth further research is given in order to increase our understanding of the processes and increase the reliability of the perdition of settlements during vibratory sheet piling. A subdivision is made in subjects relating to the (fundamental) understanding of the behaviour of sand during cyclic loading, the behaviour of the sheet pile and surrounding soil during vibrating and in the effect of possible mitigating measured.

*** fundamental research on the behaviour of sand during cyclic loading**
Close to the sheet pile stress rotation is expected to occur. It is known that stress rotation increases the densification of the sand. No practical and validated models are available to quantify this aspect. For improving the prediction of the settlement such a model is required.

It is found that the history of the sand influences its behaviour. Most laboratory testing is on reconstituted samples. This implies that the (geologic) history of the sand and possible cementation effects are erased. Also the method of preparation of the samples may differ from the process during the actual sedimentation. This introduces uncertainties with respect to the actual soil behaviour. Therefore the best practice would be to measure the behaviour of the sand on cyclic loading in-situ and derive the model parameters from those tests. For this a new test device is to be developed and interpretation methods are to be derived.

*** behaviour sheet pile and surrounding soil**
The behaviour of the sheet pile determines the stress variations in the soil. Understanding of the behaviour is relevant for the prediction of the settlements. The following investigations can be distinguished.

The horizontal movement of the sheet pile in the soil will contribute to the stresses and stress variations in the soil. Horizontal vibrations will results in the emission of pressure waves from the sheet pile. The purpose of the investigation is to quantify these stress waves. Variables are the type of sheet piling, the location of the vibrator at the top of the sheet pile, the use of one or two clamps, the used frequency and the length (both free standing and embedded) of the sheet pile. The result will be a quantification of the possible stress variations and stress rotation in the soil close to the sheet pile. This is an input parameter for the more advanced soil densification model for predicting the amount of densification.

Visual observations are that at the area enclosed by web and flange of the sheet pile locally large settlements may occur. The mechanism responsible for this behaviour and its influence on the settlement is not yet clear. This aspect is to be

investigated in order to understand the mechanism and judge the relevance for the settlement prediction.

The present model excludes the contribution of vibrations emitted from the tip. When using thicker walled elements this contribution may become relevant.

At removal of the sheet pile the soil close to the sheet pile has experienced two loading conditions. The first is the densification and possible sideward pushing during installation. The second is the change in stress during excavation and backfilling of the building pit. Both loading conditions will influence the behaviour of the soil. Purpose of the proposed research is to quantify the stress history of the soil and to quantify its effects on the cyclic behaviour. Part of the research will be cyclic tests to define and quantify a structure parameter.

*** effect mitigating measures**
Different possible measures to limit the amount of densification may be identified. A non exhaustive list is to prevent horizontal vibrations of the sheet pile, adjustment of the frequency, used centrifugal force of the vibrator, jetting or fluidisation at the tip of the sheet pile, impact driving instead of vibratory driving and injection at the tip of the sheet pile on removal.
The purpose of the research will be to identify all possible mitigating measures, to quantify the effectiveness and to quantify possible adverse effects as a reduction on the capacity of the sheet pile.

References

ABI 2004. The “directional vibrator” – an innovative vibrating technology. Abi News, March 2004, pp 4-5

Andersen K.H., 1976. Behaviour of clay subjected to undrained cyclic loading. Int. conf. Behaviour of Offshore Structures, BOSS'76. Trondheim 1976. Proceedings, Vol. 1, pp. 392-403

Andersen, K.H., Dyvik, R., Kikuchi, Y., Skomedal, E., 1992. Clay behaviour under irregular cyclic loading. Proc. 6th int. conf. Behaviour of Offshore Structures BOSS’92, pp 937–950

Andersen, K.H., 1996. Description of the pore pressure accumulation procedure. Norwegian geotechnical institute, publication 198, vol. 2, appendix V

Azzouzi, A., 2003. Intrillen van stalen damwanden in niet-cohesieve gronden (vibratory installation of steel sheet piles in non-cohesive soils). Master thesis, Delft University of Technology (in Dutch)

Arulmoli, K., Muraleetharan, K.K., Hossain, M.M., Fruth, L.S., 1992. VELACS, Verification of liquefaction Analyses by centrifuge studies, laboratory testing program, soil data report. Earth Technology Corporation project 90-0562, March 1992

Barkan, D., 1962. Dynamics of bases and foundations. New York: McGraw-Hill Book Cy Inc. (original publication in Russian 1948)

Bement, R.A.P., Selby, A.R., 1997. Compaction of granular soils by uniform vibration equivalent to vibrodriving of piles. Geotechnical and Geological Engineering, 15, 1997, pp 121-143

Berghe, J-F. vanden, Holeyman, A., Juaristi, E., Schmitt, A., 2001. Interlock friction in a sheet pile wall: laboratory tests. 15th Int. Conf. Soil Mech. and Foundation Engineering, pp 1273-1276

Budhu, M., 1985. Lateral stresses observed in two simple shear apparatus. Journal of Geotechnical Engineering, Vol. 111, No. 6, June 1985, pp 698-711

Castro, G., 1975. Liquefaction and cyclic mobility of saturated sands. Journal of the Geotechnical Engineering Division, Proceedings of the American Society of Civil Engineers, Vol. 101, No. GT6, June 1975, pp 551–569

Clough, G.W., Chameau, J., 1980. Measured effects of vibratory sheetpile driving. Journal of Geotechnical Engineering Division, Proceedings of the American Society of Civil Engineers, Vol. 106, No. GT10, October 1980, pp 1081-1099

CROW 2004. Verdichting van de zandbaan (densification of the earth embankment), CROW report 04-04, April 2004 (in Dutch)

CUR 1993. Damwandconstructies (sheet pile structures). CUR publication 166, 669 pp, (in Dutch)

CUR/COB 1996. Inventarisatie ontwerpmethoden boortunnels voor weg- en railverbindingen (Inventory of design methods bored tunnels for road- and rail connections). CUR/COB report L510-01 (in Dutch)

Dalmatov, B.I., Ershov, V.A., Kovalevsky, E.D., 1986. Some Cases of Foundation Settlement in Driving Sheeting and Piles. Proceedings International Symposium on Wave Properties of Earth Materials, 1968, pp. 607-613

D’Appolonia, D.J., Whitman, R.V., D’Appolonia, E.D., 1969. Sand compaction with vibratory rollers. Journal of the Soil Mechanics and Foundations Division, Proceedings of the American Society of Civil Engineers, SM 1, January 1970, pp 263-284

D'Appolonia, E.D., 1970. Dynamic loadings. Journal of the Soil Mechanics and Foundations Division, Proceedings of the American Society of Civil Engineers, SM 1, January 1969, pp 263-284

De Alba, P., Seed, H.B., Chan, K., 1976. Sand liquefaction in large-scale simple shear tests. Journal of the Geotechnical Engineering Division, Proceedings of the American Society of Civil Engineers, Vol. 103, GT9, September 1976, pp 909-927

Department of Defense 1997. Soil dynamics and special design aspects. Department of defense handbook MIL-HDBK-1007/3, November 1997

Deresiewicz, H., 1953. Mechanics of granular matter. Advances in applied mechanics, vol. 5, Academic Press Inc.

Dong-Soo Kim, Stokoe II, K., 1995. Deformational characteristics of soils at small to medium strains. Proc. First Int. Conf. Earthquake Geotechnical Engineering, Tokyo 1995, pp 89-94

Drabkin, S., Lacy, H., Kim, D.S., 1996. Estimating settlement of sand caused by construction vibration. Journal of Geotechnical Engineering, November 1996, pp 920-928

Finn, W.D.L., Bransby, P.L., Pickering, D.J., 1970. Effect of strain history on liquefaction of sand. Journal of the Soil Mechanics and Foundation Division, Proceedings of the American Society of Civil Engineers, vol 96, no. SM6, proc. paper 7670, November 1970, pp 1917-1934

Fujita, K., 1994. Soft ground tunnelling and buried structures. Proceedings XIII ICSMFE, New Delhi 1994, pp89-108

Green, A.R., 2001. Energy-based evaluation and remediation of liquefiable soils. Ph.D thesis Virginia Polytechnic Institute and State University, August 2001

Glatt, J., Roboski, J., Finn, R.J., 2004. Sheetpile-Induced Vibrations at the Lurie Excavation Project. Geotechnical Engineering for Transportation Projects, M.K. Yegian & E. Kavazanjian, Eds. Special Geotechnical Publication #126, ASCE, July 2004, pp 2130-2138

Grabe, J., Mahutka, K.-P., 2005. Finite-Elemente-Analyse zur Vibrationsrammung von Phählen. Bautechnik 82 (2005), Heft 9, pp 632–640

Green, R.A., 2001. Energy based evaluation and remediation of liquefiable soils. Ph.D. thesis Faculty of the Virginia Polytechnic Institute and State University, August 2001

Groot, M.B. de, Meijers, P. 1992. Liquefaction of trench fill around a pipeline in the sea bed. Proceedings 6th Int. Conf. Behaviour of Offshore Structures, London, BPP Tech. Serv., pp 519-527

Heckman, W.S., Hagerty, D.J., 1978. Vibrations associated with pile driving. Journal of the Construction Division, Proceedings of the American Society of Civil Engineers, Vol. 104, No. C04, December 1978, pp 385-394

Hemmen, B.R., 2005. The synergy between theory and practice in geo-engineering. Proceedings 16th International Conference on Soil Mechanics and Geotechnical Engineering, Osaka 2005, pp 2809-2811

Hergarden, R.H., 2000. Gronddeformaties tijdens het trillend trekken van damwanden (Ground deformations during vibratory pull of sheet piles). M.Sc. thesis Delft University of Technology, December 2000 (in Dutch)

Hergarden, R.H., Tol, A.F. van, 2001. Zakkingen tijdens het trillend trekken van damwanden (Settlements during vibratory pull of sheet piles). Geotechniek, July 2001 pp 85–90 (in Dutch)

Holeyman, A.E., Legrand, C., Rompaey, D. van, 1996. A method to predict the drivability of vibratory driven piles. "Proc. 5th Int. Conf. Appl. Stress-Wave

Theory to Piles, Orlando, Sept. 1996, Gainesville, Univ. Florida, Dep. Civ.Eng., 1996, pp. 1101-1112
Holeyman, A., Berghe, J.F. vanden, Cock, S. de, 1999. Toe resistance during pile vibratory penetration. Proc. 12th Eur. Conf. Soil Mech. Geotech. Eng., Amsterdam, June 1999, pp 769-776
Hölscher, P., Waarts, P.H., 2003. Reliability of vibration predictions and reducing measures, final report on the project. Delft Cluster report 01.05.02-20, June 2003
Hsu, C.C., Vucetic, M., 2004. Volumetric threshold shear strain for cyclic settlement. Journal of Geotechnical and Geoenvironmental Engineering, January 2004, pp 58–70
Ibsen, L.B., 1993. Poretryksopbygning i sand (Pore pressure build-up in sand). Ph.D thesis, Aalbog University, soil mechanics Laboratory, Department of Civil Engineering, 1993 (in Danish)
Ibsen, L.B., 1994. The stable state in cyclic triaxial testing on sand. Soil Dynamics and Earthquake Engineering 13, 1994, pp 63-72
Kazama, M., Yamaguchi, A., Yanagisawa, E., 2000. Liquefaction resistance from a ductility viewpoint. Soils and Foundations, Vol. 40, No. 67, December 2000, pp 47-60
Kausel, E., 2006. Fundamental Solutions in Elastodynamics, a Compendium. Cambridge University Press.
Kim, D.S., Drabkin, S., Rokhvarger, A., Laefer, D., 1994. Prediction of low level vibration induced settlement. Proc. Spec. Conf. Settlement '94, College Station, June 1994, New York, ASCE, 1994, Vol.1, pp. 806-817.
Kim, D.S., Drabkin, S., 1995. Investigation of vibration-induced settlement using multifactorial experimental design. Geotechical Testing Journal, 18(1995)4, pp 463-471
Kvalstad, T.J., Groot, M.B., 1999. Degradation and residual pore pressures. In: Groot, M.B. de, 1999 (ed.). MAST III/PROVERBS, Probabilistic design tools for vertical breakwaters, final report, volume IIb geotechnical aspects. Report MAS3-CT95-0041, April 1999
Lacy, H.S., Gould, J.P., 1985. Settlement from pile driving in sand. Proc., ASCE Symposium on Vibration Problems in Geotech. Eng., Detroit, Michigan, October 1985, pp 152-173
Lee, K.L., Focht, J.A., 1975. Liquefaction potential at Ekofisk Tank in North Sea. Journal of the Geotechnical Engineering Division, Proceedings of the American Society of Civil Engineers, Vol. 101, No. GT1, January 1975, pp 1-18
Leussink, H., Kutzner, C., 1962. Laboratoriumversuch zur Feststellung der dichtesten Lagerung körniger Erdstoffe. Veröffentlichungen des Institutes für Bodenmechanik und Grundbau der Technischen Hochschule Fridericana in Karlsruhe, Heft 8.
Li, X.S., Yang, W.L., 1989. Effects of vibration history on modulus and damping of dry sand. Journal of Geotechnical and Geoenvironmental Engineering, November 1998, pp 1071-1081
Lineham, P.W., Longinow, A., Dowding, C.H., 1992. Pipe response to pile driving and adjacent excavation. Journal of Geotechnical Engineering, Vol. 118, No. 2, February 1992, pp 300-316
Lukas, R.G., Gill, S.A., 1992. Ground movement from piling vibrations. Proceedings Conference Piling: European practice and worldwide trends, London 1992 pp 163-169

Luong, M.P., 1981. Mechanical performance of granular materials subjected to cyclic and transient loading. In: Mech. of structured media, Vol B, pp 269-282, 1981

Luong, M.P., 1986. Characteristic Threshold and Infrared Vibrothermography of Sand. Geotechnical Testing Journal, Vol. 9, No. 2, June 1986, pp 80-86

Lunne, T., Christoffersen, H.P., 1983. Interpretation of cone penetrometer data for offshore sands. Proc. 15th Offshore Technology Conference, pp 181-192

Mahutka, K., Grabe, J., 2006. Numerical prediction of settlements and vibrations due to vibratory pile driving using a continuum model. Proc. TRANSVIB2006, Paris, September 2006, pp 243-252

Massarsch, K.R., 1992. Static and dynamic soil displacements caused by pile driving. Proceedings 4th Int. Conference Application of Stress-wave Theory to Piles, The Hague 1992, pp 15-24

Massarsch, K.R., 2000. Settlements and damage caused by construction-induced vibrations. Proceedings Intern. Workshop Wave 2000, Bochum, December 2000, pp 299-315

Massarsch, K.R., 2004. Vibrations caused by Pile Driving. The Magazine of Deep Foundations institute, Fall 2004, pp 39-42

Meijers, P., 1990. Viscositeit van zand-water mengsels (Viscosity sand-water mixtures). GeoDelft, internal report SE-702492, September 1990 (in Dutch)

Meijers, P., Tol, A.F. van, 2002. Settlement due to sheetpile extraction, results of experimental research. Proc. Int. Conf. on Vibratory pile driving and deep soil compaction-TRANSVIB2002, Louvain-la-Neuve, 9-10 September 2002, pp 141-145

Meijers, P., Tol, A.F. van, 2004a. Densification of sand caused by vibratory sheetpiling Proc. Cyclic behaviour of sand and liquefaction phenomena, CBS04, Bochum 2004, pp 523-532

Meijers, P., 2004b. Invloed inbrengen en verwijderen van damwanden op omgeving (Influence of installation and removal of sheet piles on the surrounding). Geotechniek 8, 2004, pp 8-13

Meijers, P., 2004c. Effect steel sheet pile on measurements with an electrical density probe. GeoDelft, internal report 525250-2, December 2005

Meijers, P., Tol, A.F. van, 2005. Observations on densification of soil during vibratory sheetpiling. Proc. 16th Int. Conf. Soil Mech. Geotech. Eng. Osaka 2005, Vol 4, pp 2153-2156

Meijers, P., Tol, A.F. van, 2006. The Raamsdonksveer sheet pile test: observed settlements due to installation of vibratory driven sheet piles. TRANSVIB2006, Paris, 2006, pp 353-362

Meijers, P., Tol, A.F. van, 2007. The Raamsdonksveer sheet pile test, measured surface settlements during vibratory sheet piling. Proc. 14th Eur. Conf. Soil Mech. and Geotech. Eng. Madrid 2007, pp 603-609

Mitchell, R.J., Dubin, B.I., 1986. Pore pressure generation and dissipation in dense sands under cyclic loading. Canadian Geotechnical Journal, Vol. 23, August 1986, pp 393-398

Molenkamp, F., 1985. Liquefaction parameters of the seafloor for earthquake analysis, part of the report 'DESRA-SPASM, analysis of earthquake loading of pile-supported offshore-platforms. Report by by LGM and Aquater, job no. 539700

Morland, L.W., Sawicki, A., 1985. A model for compaction and shear hysteresis in saturated granular materials. J. Mech. Phys. Solids, Vol. 33, No. 1, 1985, pp 1-24

Niemunis, A., 2000. Akkumulation der Verformung infolge zyklischer Belastung des Bodens – numerische Strategien. Beitrage zum Workshop 'Boden unter fast zyklischer Belastung: Erfahrungen und Forschungsergebnisse', 2000 (in German)

Niemunis, A., Helm, J., 2001. Settlement of a strip foundation due to cyclic loading. Centrifuge model and FE-calculations. Proc. XV ICSMFE, Istanbul, 2001, pp 761-764

Nijs, R.E.P., 2003. Het trillen van damwanden in granulaire bodem (Vibratory installation of sheet piles in granulair soil). Geotechniek, October 2003, pp 56-64 (in Dutch)

NVAF, PSD, 2002. Schadevrij installeren van stalen damwand in Nederland (damage free installation of sheet piles in The Netherlands), report of NVAF and PSD, 246 pp, 2002 (in Dutch)

Oda, M., Kawamoto, K., Suzuki, K., Fujimori and H., Sato, M. 2001. Microstructural inerpretation on reliquefaction of saturated granular soils under cyclic loading. Journal of Geotechnical and Geoenvironmental Engineering, May 2001, pp 416-423

O-Hara, S., Kotsubo, S., Yamamoto, T., 1985. Pore pressure developed in saturated sand subjected to cyclic shear stress under partial-drainage conditions. Soils and Foundations, Vol. 25, No. 2, June 1985, pp 45-56

Ohara, S., Yamamoto, T., 1990. Stress induced in sand during cyclic shear. Proc. 8th Japan Earthquake Engineering Symposium, Tokyo, December 1990, pp 765–770

Ostadan, F., Deng, N., Arango, I., 1996. Energy-based method for liquefaction potential evaluation, phase I – feasibility study. Report NIST GCR 96-701, August 1996

Peacock, W.H., Seed, H.B., 1968. Sand liquefaction under cyclic loading simple shear conditions. Journal of the Soil Mechanics and Foundation Division, Vol. 94, No. SM 3, May 1968

Picornell, M., Del Monte, E., 1985. Pile driving induced settlements of a pier foundation. Vibration problems in geotechnical engineering, ASCE, October 1985, pp 174-186

Polito, C.P. 1999. The effect of non-plastic fines on the liquefaction of sandy soils. Ph.D thesis Virginia Polytechnics Institute, December 1999

Pyke, R., Seed, H.B., Chan, C.K., 1975. Settlement of sands under multidirectional shaking. Journal of the Geotechnical Engineering Division, Vol. 101, No. GT4, April 1975, pp 379-398

Rahman, M.S., Jaber, W.Y., 1986. A simplified drained analysis for wave-induced liquefaction in ocean floor sands. Soils and Foundations. Vol. 26. No. 3, pp 57-86

Sassa, S., Sekiguchi, H., 1999. Wave-induced liquefaction of beds of sand in a centrifuge. Géotechnique 49, No. 5, 1999, pp 621-638

Sato, K., Yasuhara, K., Yoshida, N., 1997. Effect of drainage with preshearing on undrained cyclic shear behaviour of dense sand. Proc. 8th Int. Conf. Behaviour of Offshore Structures, Boss'97, Delft, July 1997,pp. 85-97

Sawicki ,A., Sliwinski, P., 1989. Compaction due to a cyclic force acting in the inside of a sandy subsoil. Computers and Geotechnics 7 (1989), pp 223-237

Sawicki, A., Swidzinski, W., 1989a. Mechanics of a sandy subsoil subjected to cyclic loadings. Int. Journal for Numerical and Analytical Methods in Geomechanics, Vol. 13, 1989, pp 511-529

Sawicki, A., Swidzinski, W., 1989b. Pore pressure generation, dissipation and reconsolidation in a saturated subsoil. Soils and Foundations, Vol. 29, No. 4, December 1989, pp 62-74
Sawicki, A., Swidzinski, W., Zadroga, B., 1998. Settlement of shallow foundation due to cyclic vertical force. Soils and foundations Vol. 38, No. 1, 1998, pp 35-43
Sawicki, A., 2004. Modelling earthquake-induced phenomena in the Izmit Bay coastal area, Proc. Cyclic behaviour of sand ands liquefaction phenomena, CBS04, Bochum 2004, pp 431-440
Seed, H.B., Idriss, I.M., 1971. Simplified procedure for evaluating soil liquefaction potential. Journal of the Soil Mechanics and Foundation Division, September 1971
Seed, H.B., Peacock, W.H., 1971. Test procedures for measuring soil liquefaction characteristics. Journal of the Soil Mechanics and Foundation Division, Vol 97, No. SM8, August 1971, pp1099-1119
Seed, H. B., Silver, M. L. 1972. Settlements of dry sand during earthquakes. Journal of the Soil Mechanics and Foundation Division, Proceedings ASCE, Vol. 98, pp. 381-396
Seed, H.B., Rahman, M.S., 1978. Wave-induced pore pressure in relation to ocean floor stability of cohesionless soils. Marine Geotechnology, Vol. 3, No. 2, pp 123-150
Seed, H.B., 1979. Soil liquefaction and cyclic mobility evaluation for level ground during earthquakes. Journal of the Geotechnical Engineering Division, proceedings ASCE, Vol 105, No, GT2, February 1979, pp 210-255
Seed, H.B., Wong, R.T., Idriss, I.M., Tokimatsu, K., 1986. Moduli and damping factors for dynamic analyses of cohesionless soils. Journal of Geotechnical Engineering, Vol. 112, No. 11, November 1986, pp 1016-1032
Shamoto, Y., Sato, M., Zhang, J.M., 1996. Simplified estimation of earthquake-induced settlements in saturated sand deposits. Soils and Foundations, Vol. 36, No. 1, March 1996, pp 39-50
Silver, M.L., Seed, H.B., 1971. Volume changes in sands during cyclic loading. Journal of the Soil Mechanics and Foundation Division, Proceedings of the American Society of Civil Engineers, Vol. 97, No. SM9, September 1971, pp 1171-1182
Smits, F.P., Andersen, K.H., Gudehus, G., 1978. Pore pressure generation. Proceedings Int. Symposium on Soil Mechanics Research and Foundation Design for the Oosterschelde Storm surge Barrier, Foundation aspects of Coastal Structures, The Netherlands, October 9-12, 1978
Stark, T.D., Mesri, G., 1992. Undrained shear strength of liquefied sands for stability analysis. Journal of Geotechnical Engineering, Vol. 118, No. 11, November 1992, pp 1727-1747
Sumer, B.M., Fredsøe, J., Christensen, S., Lind, M.T., 1999. Sinking/flotation of pipelines and other objects in liquefied soil under waves. Coastal Engineering 38, 1999, pp 53–90
Tokimatsu, K., Hosaka, Y., 1986. Effect of sample disturbance on dynamic properties of sand. Soils and Foundations, Vol. 26, No. 1 March 1986, pp 53-64
Towhata, I., Ishihara, K., 1985. Shear work and pore water pressure in undrained shear. Soils and Foundations, Vol. 25, No. 3, September 1985, pp 73-84
USACE 1990. Engineering and Design, settlement analysis. Engineer Manual No. 1110-1-1904 September 1990

USACE 1998. Pile driving equipment. Technical instruction TI 818-03, Headquarters U.S. Army Corps of Engineers, Engineering Division, Directorate of Military Programs, August 1998
Verruijt, A., 2004. Elastic solutions for soil dynamics. Delft University of Technology, 2004
Verruijt, A., 2006. Offshore soil mechanics, Delft University of Technology, March 2006
Viking, K., Bodare, A., 1999. Laboratory studies of dynamic shaft resistance of a vibro-driven model pile in granular soil by varying the relative density. Proc. 12th Eur. Conf. Soil Mech. Geotech. Eng., Amsterdam, June 1999, Vol.2, pp. 863-869.
Viking, K., 2002. Vibro-driveability, a field study of vibratory driven sheet piles in non-cohesive soils. Ph. D. thesis Royal Institute of Technology (KTH), Stockholm May 2002
Viking, K., 2006. The vibratory pile installation technique. Proc. TRANSVIB2006, September 2006, Paris, pp 65-82
Vucetic, M., 1994. Cyclic threshold shear strains in soils. Journal of Geotechnical Engineering, Vol. 120, No. 12, December 1994, pp 2208-2228
Whang, D.H., 2001. Seismic compression of compacted soils. Ph.D thesis University of California, Los Angeles, 2001
Wichtmann, T., Sonntag, T., Triantafyllidis, T., 2001. Über das Erinneringsvermögen von Sand unter zyklischer Belastung. Bautechnik 78, Heft 12, 2001, pp 852-865 (in German)
Waarts, P.H., Wit, M.S. De, 2004. Does more sophisticated modelling reduce model uncertainty? A case study on vibration predictions. Heron, Vol. 49, No. 2, 2004, pp 119-137
Yoshimi, Y., Tokimatsu, K., Ohara, J., 1994. In situ liquefaction resistance of clean sands over a wide density range. Géotechnique 44, No. 3, 1994, pp 479-494
Youd, T.L., 1970. Densification and shear of sand during vibration. Journal of the Soil Mechanics and Foundation Division, Vol. 96, No. SM 3, May 1970 pp 863-880
Youd, T.L., 1972. Compaction of sand by repeated shear straining. Journal of the Soil Mechanics and Foundation Division, Vol. 98, 1972, pp 709-725
Youd, T.L., 1977. Packing changes and liquefaction susceptibility. Journal of the Geotechnical Engineering Division, Proceedings of the American Society of Civil Engineers, Vol. 103, No. GT8, August 1977, pp 918-922

Curriculum vitae

Piet Meijers was born in Utrecht, The Netherlands, on August 8, 1959.
After attending the Christelijk Lyceum in Veenendaal he started his study Civil Engineering at Delft University of Technology in 1977, where he graduated in 1984.
After a short stay at Haskoning he joined in 1985 GeoDelft (at that time named LGM, Delft Soil Mechanics Laboratory). In 2008 GeoDelft will form, together with other institutes, Deltares.
He has been engaged in a large number of research and consultancy projects on geotechnical and foundation engineering. The main line in those projects deals with the behaviour of soil during cyclic and dynamic loading, such as vibration prediction, behaviour of soil during wave loading and behaviour of soil during earthquake loading.

ANNEX 5.1 Cyclic triaxial tests, overview

test	sample	I_D	$\Delta\sigma_v$ [kPa]	remark
8.21	8	0.18	36.3	
8.22	8	0.38	37.2	
8.23	8	0.58	37.2	
8.24	8	0.58	27.5	
8.25	8	0.58	18.9	
8.26	8	0.38	28.55	
8.27	8	0.38	19	
8.28	8	0.18	27.5	
8.29	8	0.18	19	
12.10a	12	0.61	9.6	test after 4 days of consolidation
12.11	12	0.61	18.9	
12.11h	12	0.61	18.9	
12.12	12	0.61	38	
12.12h	12	0.61	37.8	
12.13	12	0.61	55	
12.13h	12	0.61	47	

Testing program undrained cyclic triaxial tests

test	sample	I_D	$\Delta\sigma_v$ [kPa]	remarks
8.18	8	0.18	37.2	
8.19	8	0.38	37.6	
8.20	8	0.58	37.5	
12.2h	12	0.61	9.1	
12.3h	12	0.61	19.0	
12.4	12	0.61	37.5	
12.5	12	0.61	56.8	
12.6	12	0.61	73.4	
12.7	12	0.21	37.3	
12.7h	12	0.21	37.2	
12.8	12	0.40	37.3	
12.9	12	0.80	37.8	
12.10b	12	0.61	9.5	continuation of test 12.10a

Testing program drained cyclic triaxial tests

test	sample	I_D	$\Delta\sigma_v$ [kPa]	remarks
8.30	8	0.18	18.9	
12.14	12	0.61	37.2	
12.15	12	0.61	38.35	
12.16	12	0.61	37.7	
12.17	12	0.61	37	
12.18a	12	0.61	29.8	5 % axial strain
12.18b	12	0.61	37.0	5 % axial strain

Testing program undrained cyclic triaxial tests with interim drainage and static loading

ANNEX 5.2 Cyclic triaxial tests, results undrained tests sample 8

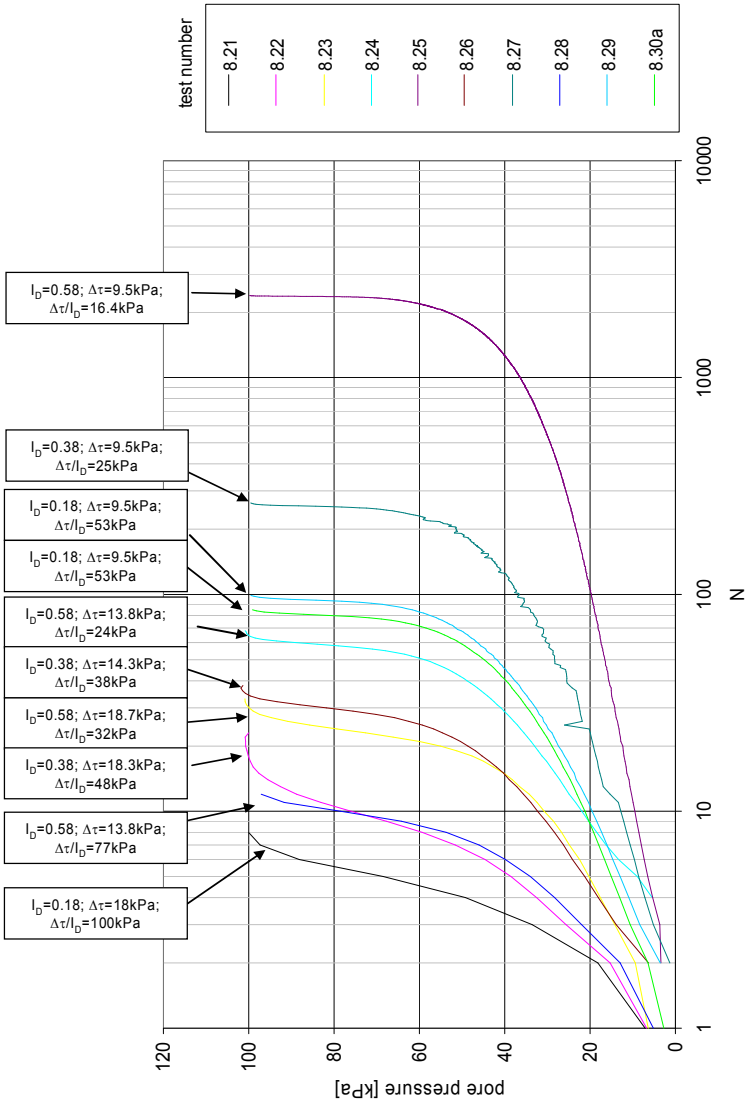

ANNEX 5.3 Cyclic triaxial tests, results undrained Tests sample 12

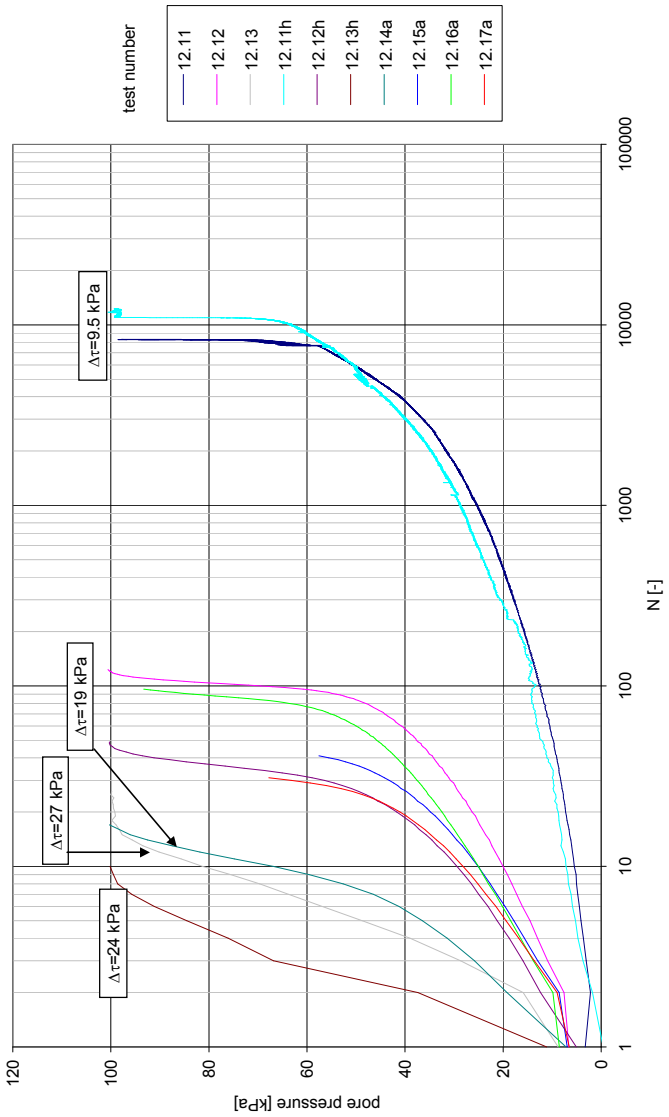

ANNEX 5.4 Cyclic triaxial tests, results drained tests sample 8

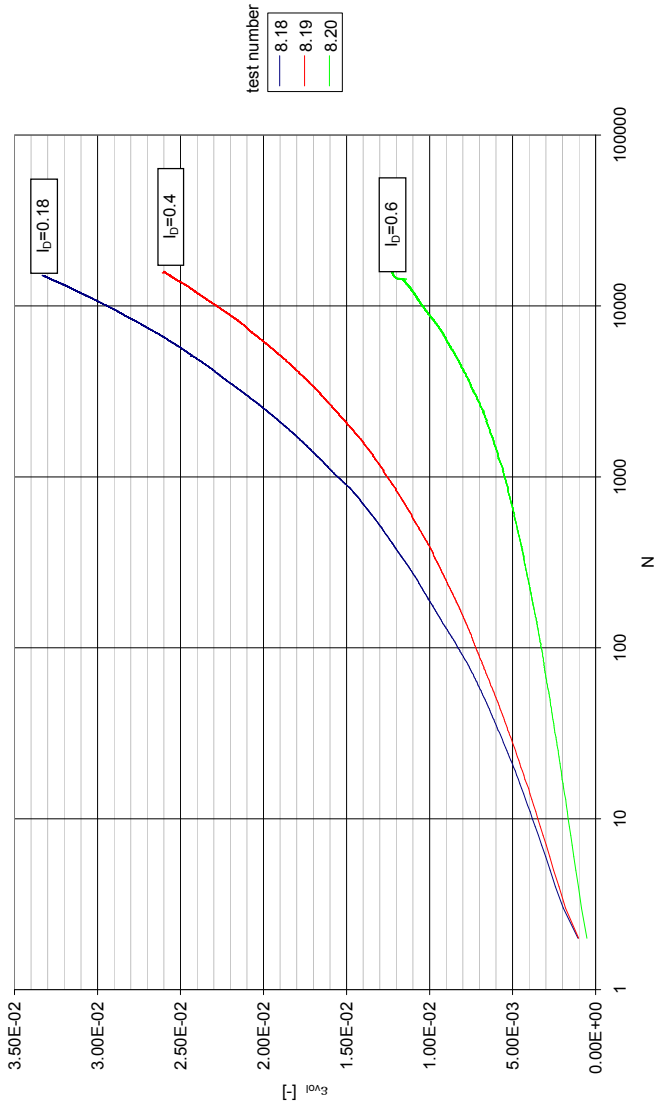

ANNEX 5.5 Cyclic triaxial tests, results drained tests sample 12, relative density is 0.6

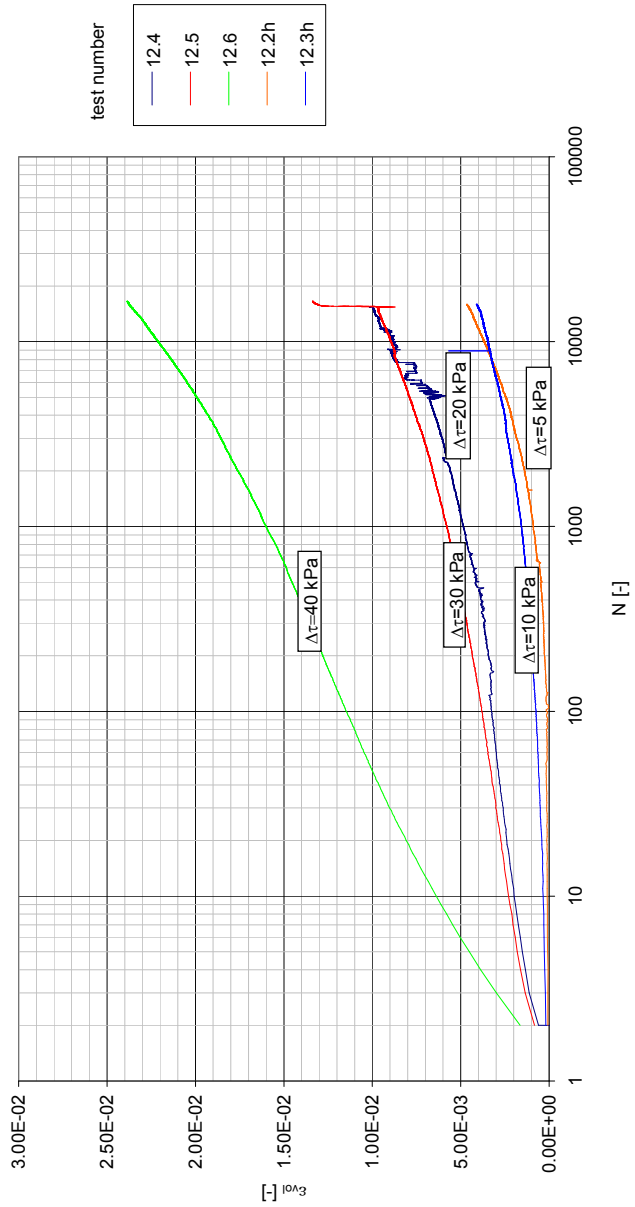

ANNEX 5.6 Cyclic triaxial tests, results drained tests sample 12, shear stress amplitude is 19 kPa

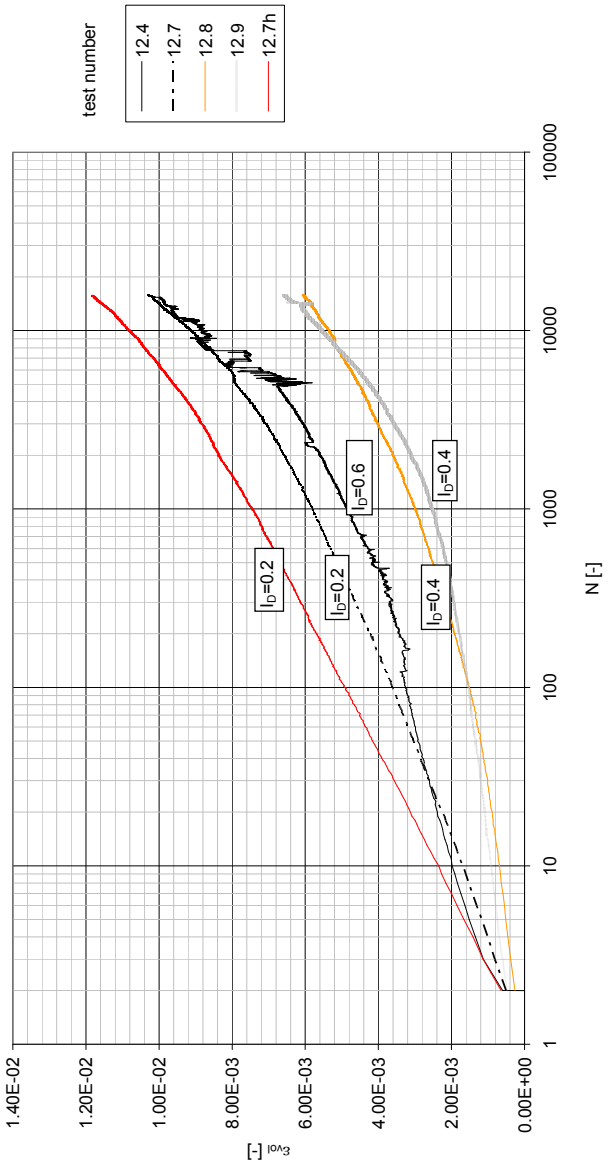

ANNEX 6.1 Example inputfile for validation calculations TRILDENS3

```
**************************************************
*                                                *
* calculation settlement during sheetpile extraction*
*           axial symmmetrix, 2-dimensional      *
*             layered subsoil                    *
*                                                *
**************************************************
file name: sensitivity
date:      16/10/2007
time:      08:09:44

check sensitivity TRILDENS3
---

- - - - - - - - - - - - - - - - - -

subsoil parameters
- - - - - - - - - - - - - - - - - -
number of soil layers:               1
power in attenuation relation: -0.7500
reference stress is:          100.0000
unit weight water is:          10.0000

layer number top  I_D  g_dry g_wet nmin nmax  Gref   mv0        phi   k
layer   1    0.00 0.50 16.00 20.00 0.31 0.45 68743 3.637E-0005 34.00 1.0E-4
layer adamp aBarkan history  amcycle bmcycle THETA     C1      C2      PEC
 1    0.010  4.000   333.00  0.480   0.200   0.700   9.6000  0.1300   0.022

properties sheetpile
- - - - - - - - - - - - - - - - - - -
embedment sheetpile, start:       0.00
embedment sheetpile, end:       -15.00
width of sheetpile:               1.20
cross section of sheetpile:      0.024
time of vibrating:            300.0000
frequency of vibrator:         25.0000
reference velocity at r0=5m:    0.0020
force of vibrator:            1000.00
vibration velocity at r0=5m:    0.0033
ratio delta/phi:                1.0000

properties geometry
- - - - - - - - - - - - - - - - - - -
inner and outer radius:         0.3820  50.0000
depth of mesh:                -20.0000
groundwaterlevel is:            0.0000
no.of elements radial:        75
no.of elements depth:         40
minimum number of steps       3000
width of element:               0.6616

calculation options
- - - - - - - - - - - - - - - - - - -
source model:                    1  standard model
propagation model:               2  stress attenuation
densification model:             5  C/L method
summation model:                 2  vertical with spreading

angle volume spreading:  30.00
```

ANNEX 7.1 Raamsdonksveer sheet pile test, boring at the test site

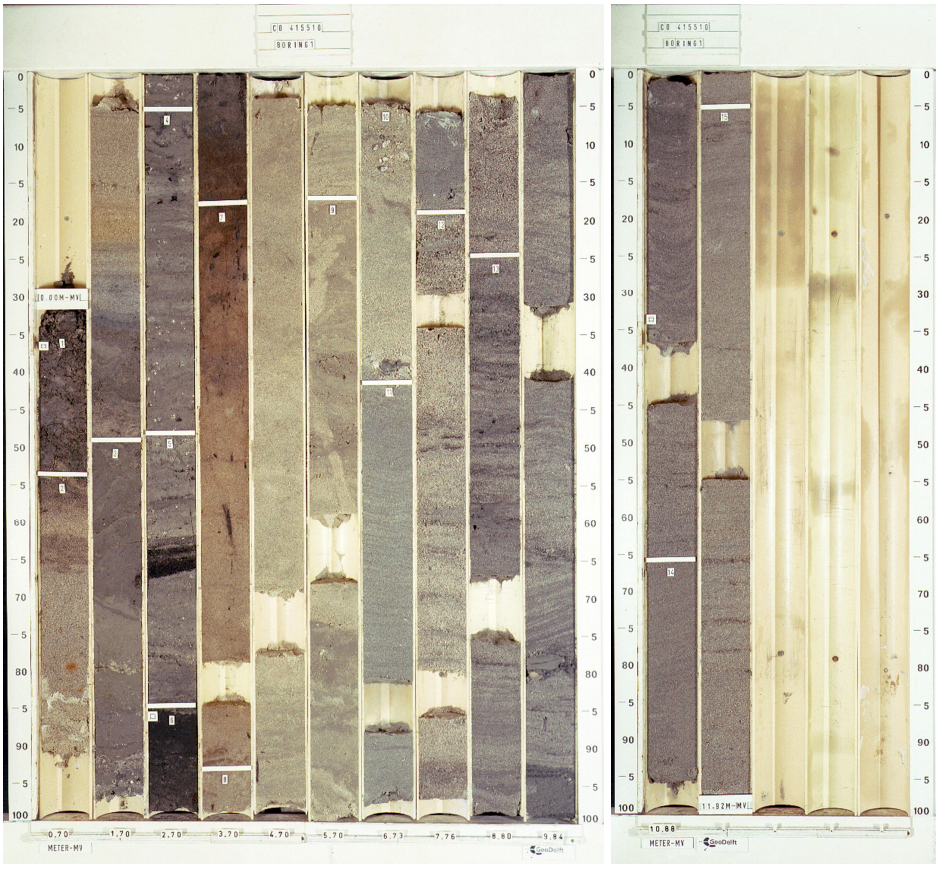

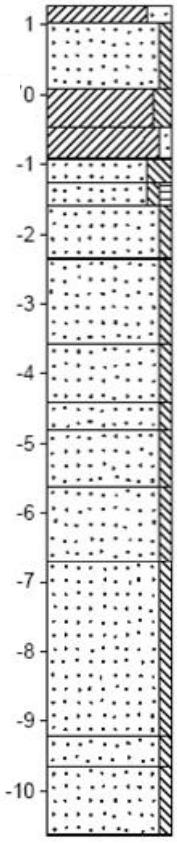

layer	top [m+NAP]	bottom [m+NAP]	description
1	1.28	1.03	clay, very sandy
2	1.03	0.08	sand, slightly silty, ZM = 0.30 mm
3	0.08	-0.47	clay, sandy
4	-0.47	-0.92	clay, slightly sandy
5	-0.92	-1.27	sand, strongly silty, ZM = 0.125 mm
6	-1.27	-1.60	sand, slightly silty, slightly organic, ZM = 0.21 mm
7	-1.60	-2.35	sand, slightly silty, ZM = 0.21 mm
8	-2.35	-3.57	sand, slightly silty, ZM = 0.175 mm
9	-3.57	-4.42	sand, slightly silty, ZM = 0.15 mm
10	-4.42	-4.82	sand, slightly silty, ZM = 0.25 mm gravel from NAP - 4.78 to NAP - 4.82
11	-4.82	-5.62	sand, slightly silty, ZM = 0.175 mm
12	-5.62	-6.70	sand, slightly silty, ZM = 0.50 mm
13	-6.70	-9.22	sand, slightly silty, with some clay, ZM = 0.35 mm
14	-9.22	-9.65	sand, slightly silty, ZM = 0.21 mm
15	-9.65	-10.64	sand, slightly silty, with some clay, ZM = 0.25mm

ZM: average of sand fraction

end of boring at NAP - 10.64 m

ANNEX 7.2 Raamsdonksveer sheet pile test, location transducers

transducer	number in test	brand	type	level [m+NAP]	sample frequency
fixed point cone	reference point	--		-14.35	once per sheet pile during installation; 4 times during removal
fixed point cone	VP-1	--	--	-5.46	ditto
fixed point cone	VP-2	--	--	-9.94	ditto
fixed point cone	VP-3	--	--	-5.47	ditto
fixed point cone	VP-4	--	--	-9.93	ditto
fixed point cone	VP-5	--	--	-5.43	ditto
fixed point cone	VP-6	--	--	-9.92	ditto
fixed point cone	VP-7	--	--	-5.37	ditto
fixed point cone	VP-8	--	--	-9.88	ditto
electrical density probe, with inclinometer	ed-1	GeoDelft	GeoDelft number 293	-2.37	1/90 = 0.011
electrical density probe, with inclinometer	ed-2	GeoDelft	GeoDelft number 309	-7.46	1/90 = 0.011
electrical density probe	ed-3	GeoDelft	GeoDelft number 8-218	-3.58	1/90 = 0.011
electrical density probe	ed-4	GeoDelft	GeoDelft number 8-216	-7.33	1/90 = 0.011
vibration transducer	Td-1	Sundstrand	800	-6.68	500 Hz
vibration transducer	Td-2	Sundstrand	800	-6.64	500 Hz
vibration transducer	Td-3	Sundstrand	700 and 800	-6.64	500 Hz
vibration transducer	Tmv-1	Sundstrand	700	G.L.	500 Hz
vibration transducer	Tmv-2	Sundstrand	700	G.L.	500 Hz
vibration transducer	Tmv-3	Sundstrand	700	G.L.	500 Hz
pore pressure transducer	pr-1	GeoDelft	GeoDelft number 361	-2.21	500 Hz and 1/90 = 0.011
pore pressure transducer	pr-2	GeoDelft-	GeoDelft number 470	-8.04	500 Hz and 1/90 = 0.011
pore pressure transducer	pr-3	GeoDelft	GeoDelft number 495	-8.04	500 Hz and 1/90 = 0.011
pore pressure transducer	pr-4	GeoDelft	GeoDelft number 293	-8.03	500 Hz and 1/90 = 0.011
vibration transducer		RDP Electronics	JTF screw 060-F482-05	mounted on sheet pile	500 Hz
wire extensometer		Boart Longyear Interfels	420A	G.L.	500 Hz
inclinometer	sheet pile 4 and 9				once, after installation sheet piles

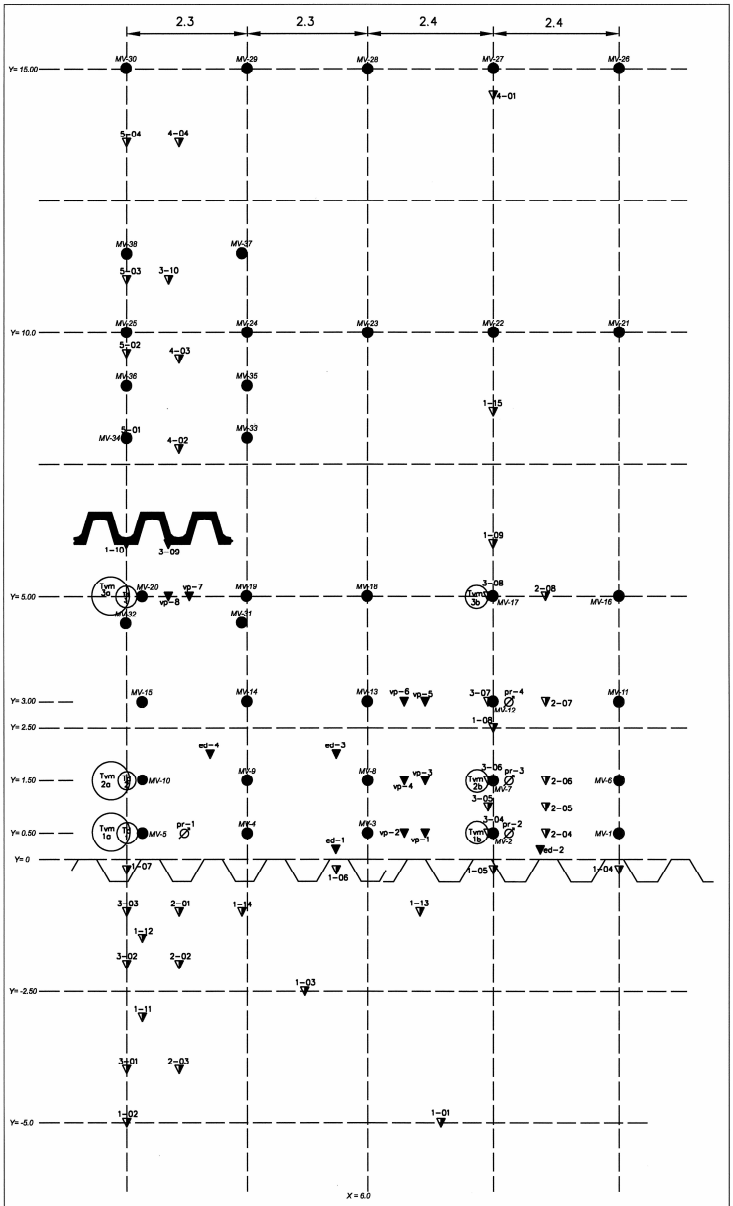

LEGEND

- 1-01 CTP before test
- 2-01 CTP after installation sheet pile
- 3-01 CTP after removal sheet pile
- 4-01 CTP after installation SPANWAND
- 5-01 CTP after removal SPANWAND
- vp-1 subsurface settlement point
- pr-1 pore pressure transducer
- Td 1 vibration transducer at depth
- Tvm 3a vibration transducer at surface
- MV-1 surface settlement point
- ed-1 electrical density rod

schaal 1.50

GeoDelft	POSTBUS 69 2600 AB DELFT	TELEFOON (015) 269 35 00 TELEFAX (015) 261 06 31	date 2005-10-06	dwn. BAL
RAAMSDONKSVEER SHEET PILE TEST			CO-415510	ppn.
LOCATION TRANSDUCERS AND CPT'S			ANNEX. 3.1	form. 40 / 60

ANNEX 7.3 Raamsdonksveer sheet pile test, example development velocity amplitude

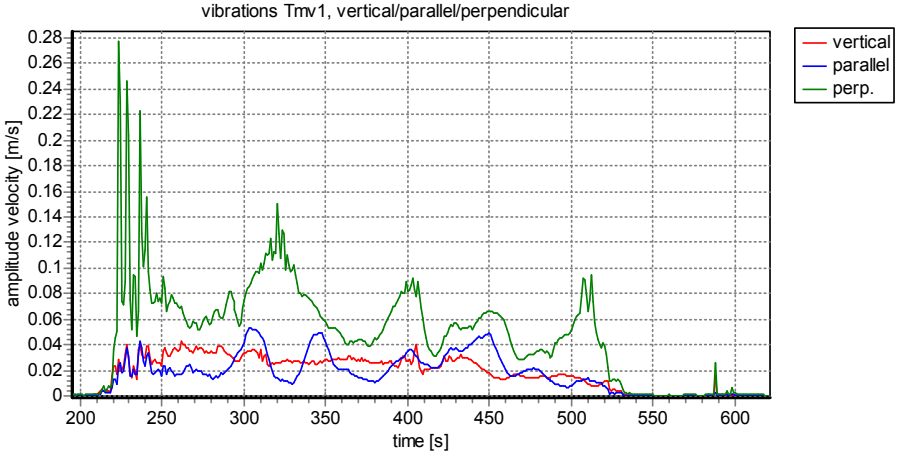

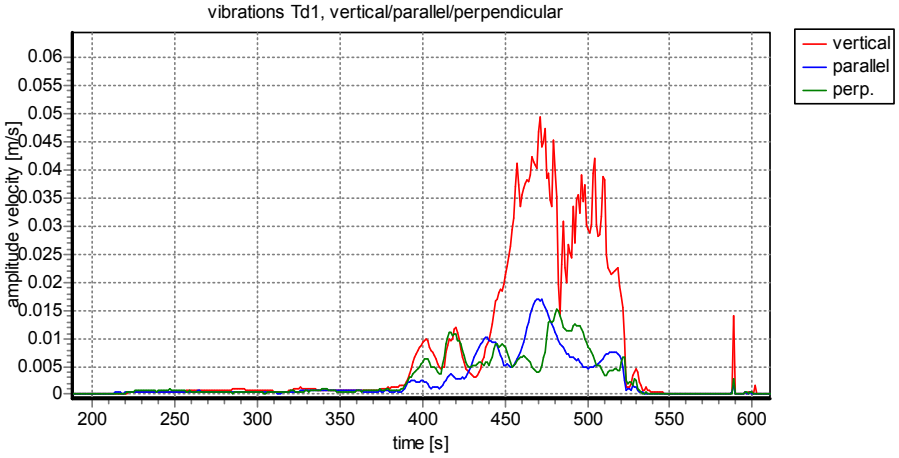

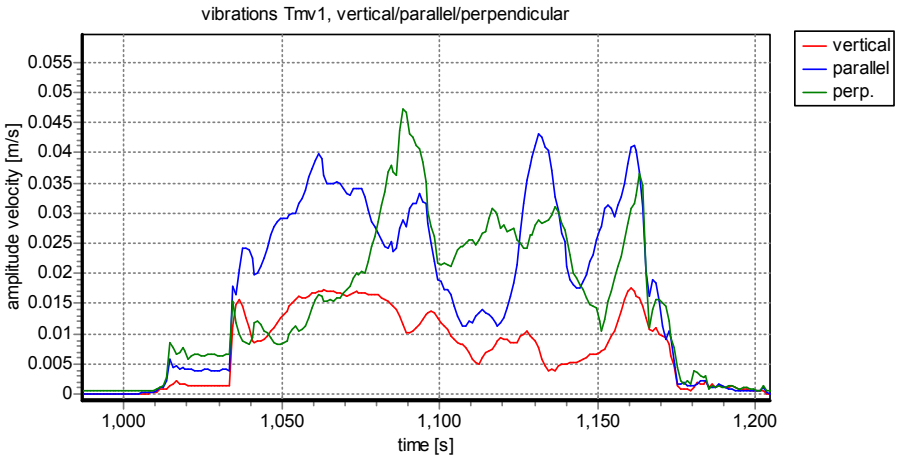
vibrations Tmv1, vertical/parallel/perpendicular
vertical
parallel
perp.
amplitude velocity [m/s]
0.055
0.05
0.045
0.04
0.035
0.03
0.025
0.02
0.015
0.01
0.005
0
1,000
1,050
1,100
1,150
1,200
time [s]

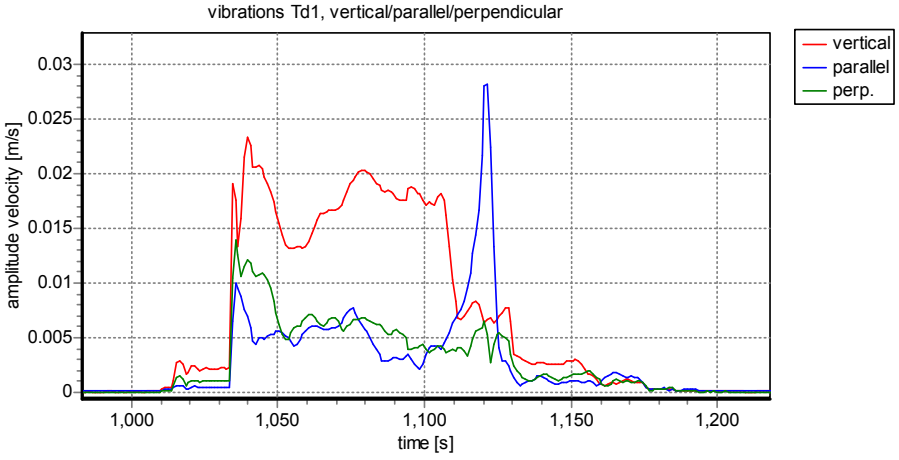
vibrations Td1, vertical/parallel/perpendicular
vertical
parallel
perp.
amplitude velocity [m/s]
0.03
0.025
0.02
0.015
0.01
0.005
0
1,000
1,050
1,100
1,150
1,200
time [s]

ANNEX 7.4 Raamsdonksveer sheet pile test, velocity amplitude as function of distance, installation of sheet piles

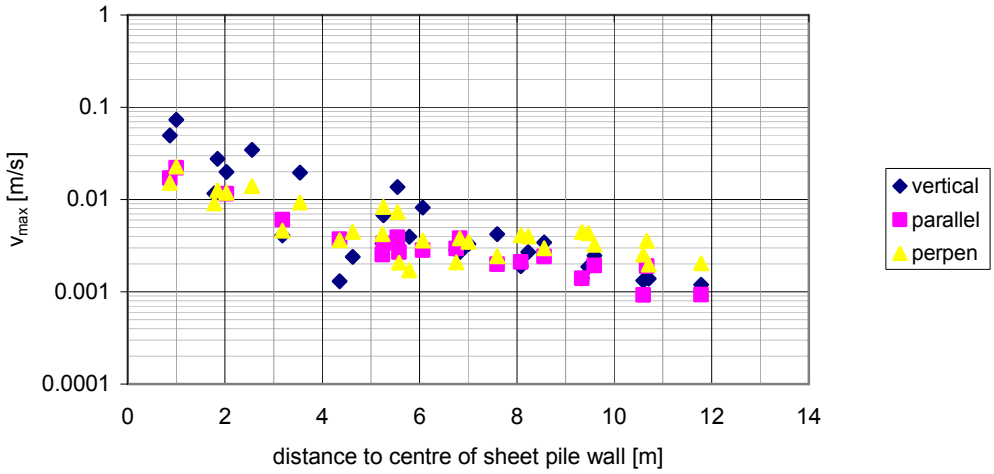

Vibration amplitude at depth

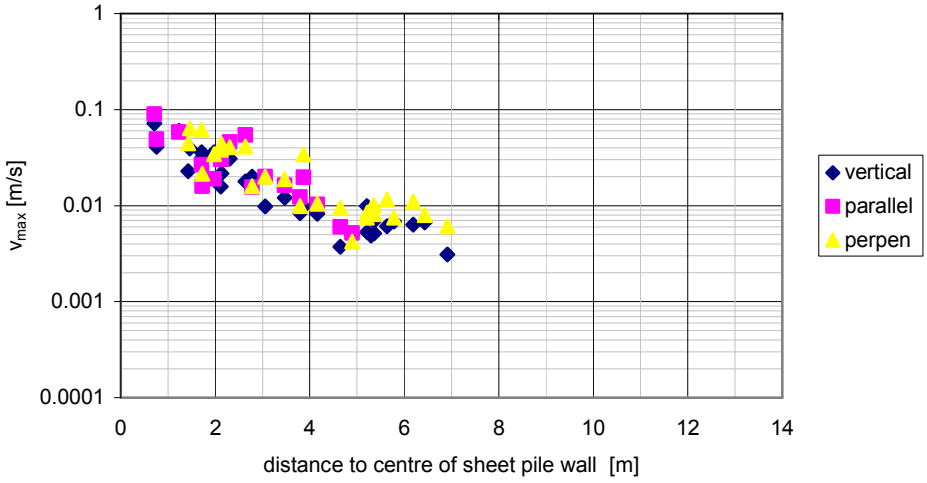

Vibration amplitude at surface

ANNEX 7.5 Raamsdonksveer sheet pile test, velocity amplitude as function of distance, removal of sheet piles

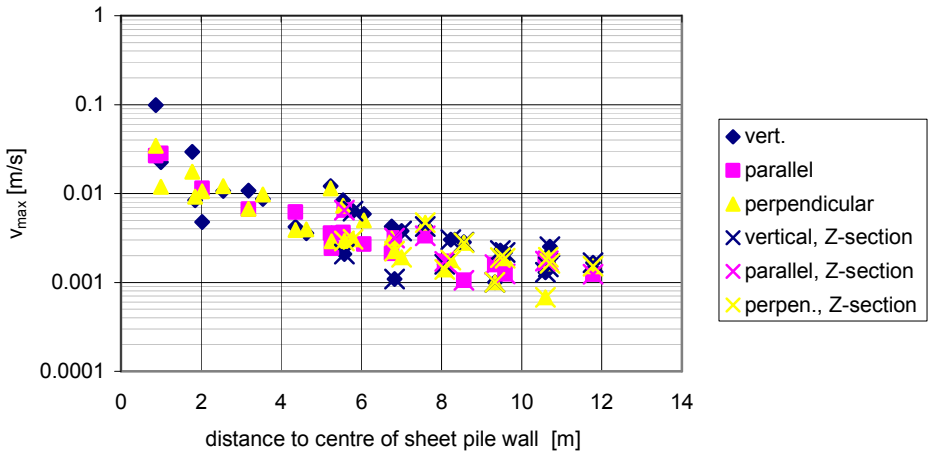

Vibration amplitude at depth

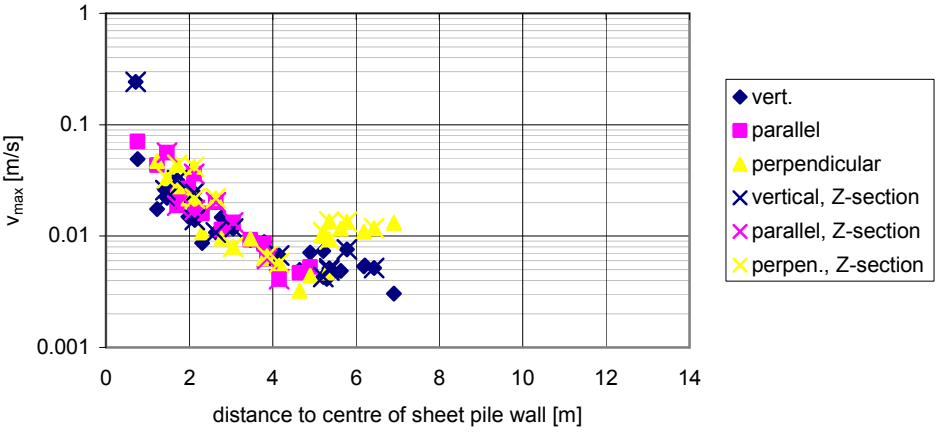

Vibration amplitude at surface

ANNEX 7.6 Raamsdonksveer sheet pile test, Results local densification Measurements

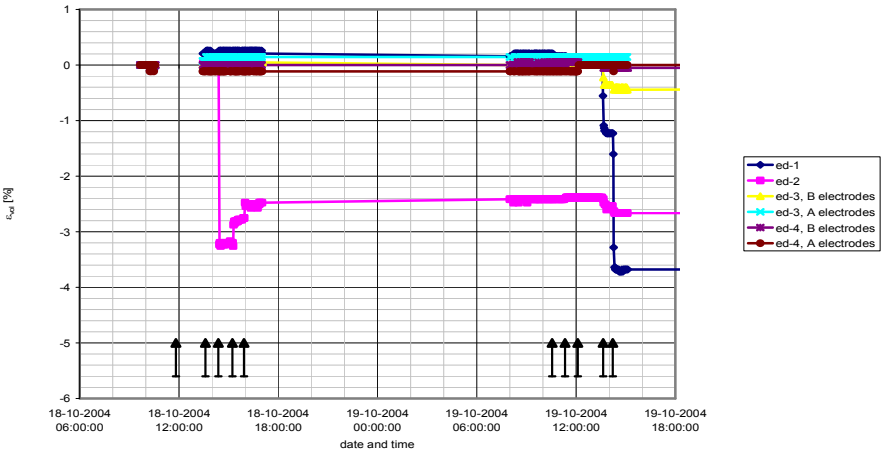

Densification during the installation phase

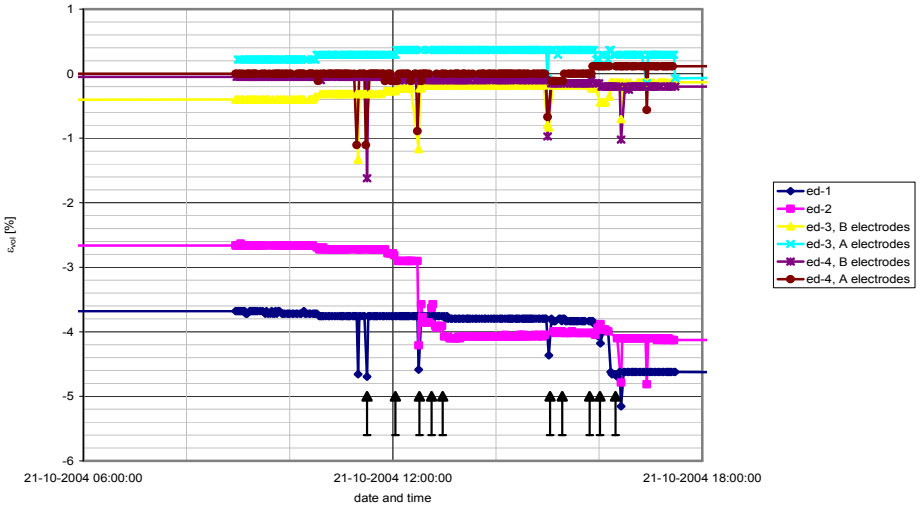

Densification during the removal phase

Note: arrows indicate time of installation or removal of a sheet pile

ANNEX 7.7 Raamsdonksveer sheet pile test, development surface settlement

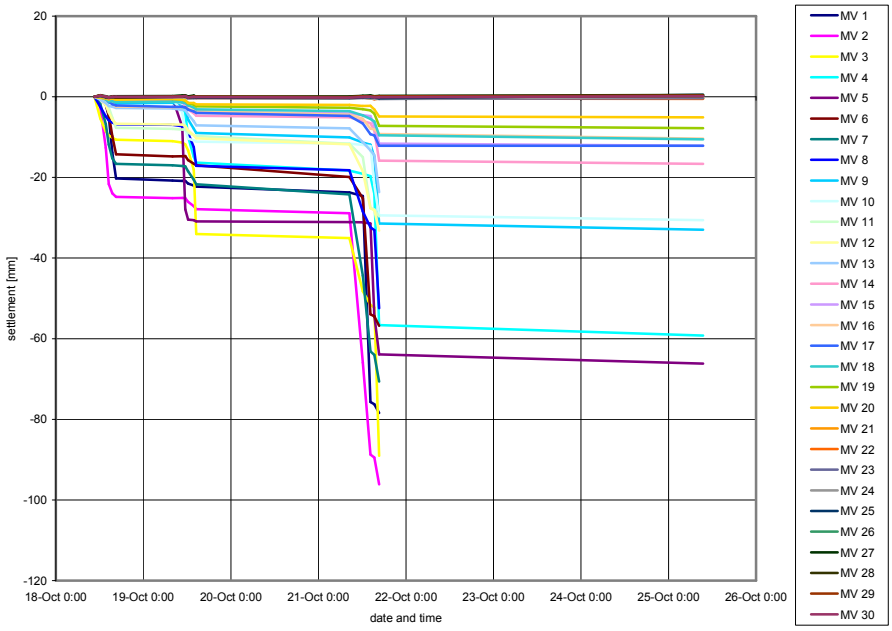

ANNEX 7.8 Raamsdonksveer sheet pile test, development settlement at depth

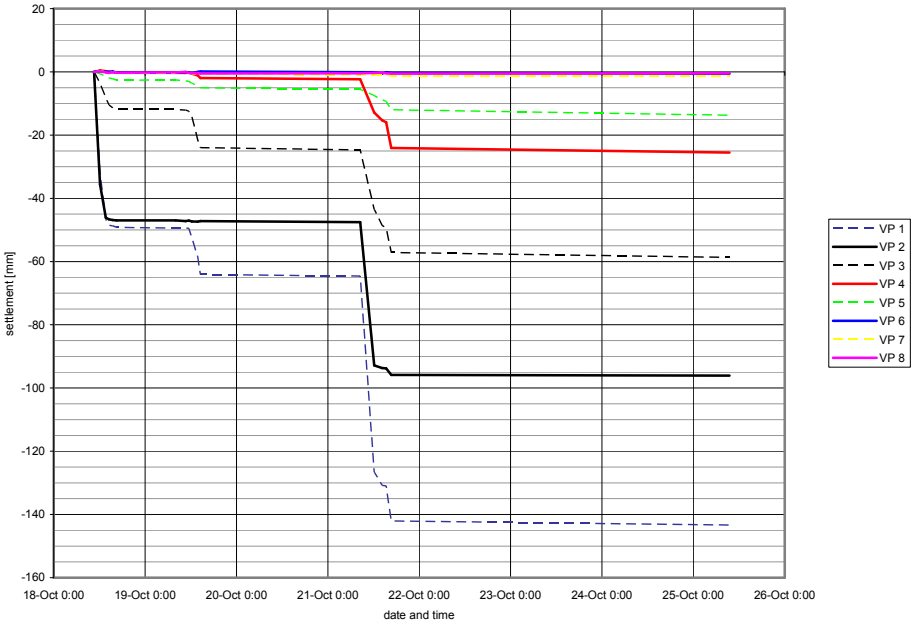

ANNEX 7.9 Raamsdonksveer sheet pile test, surface settlement trought after installation

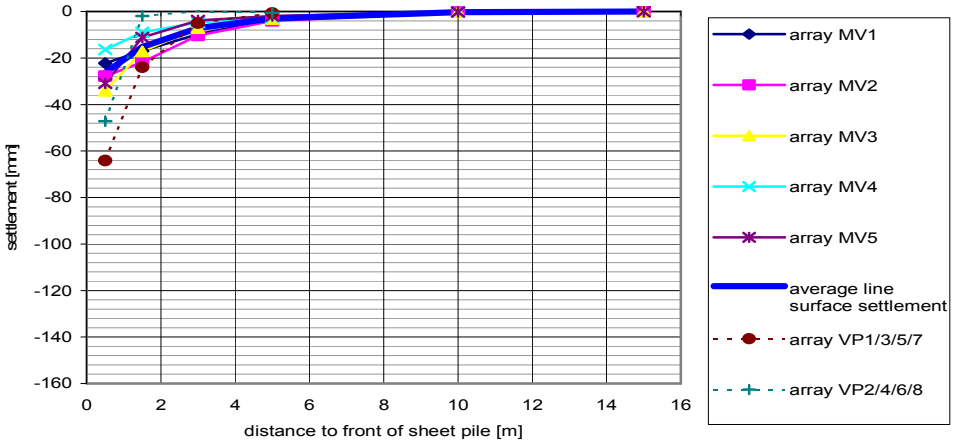

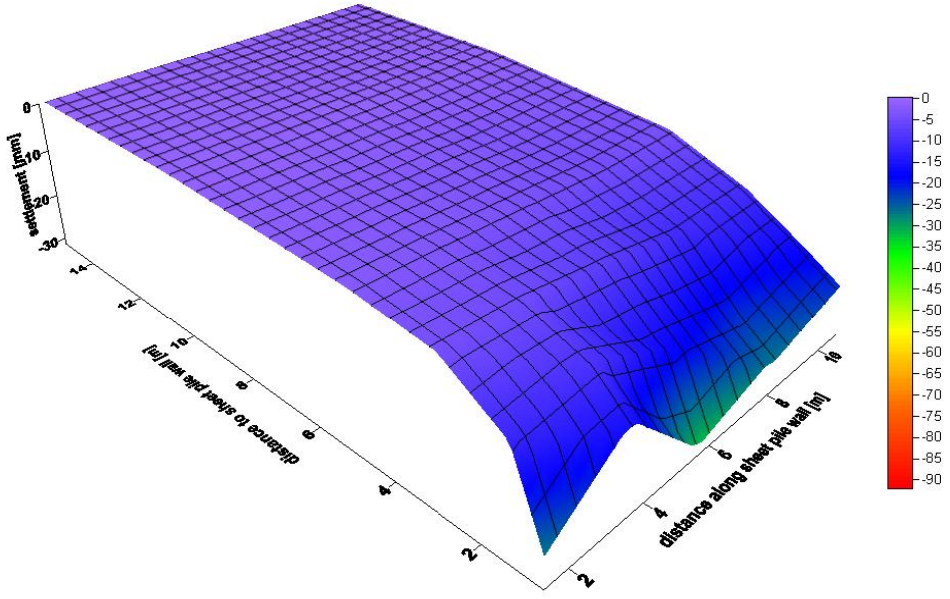

ANNEX 7.10 Raamsdonksveer sheet pile test, surface settlement trough after installation and removal

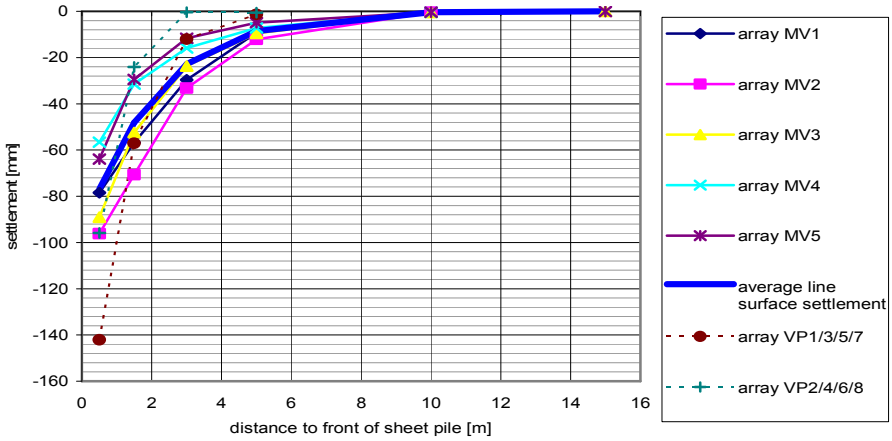

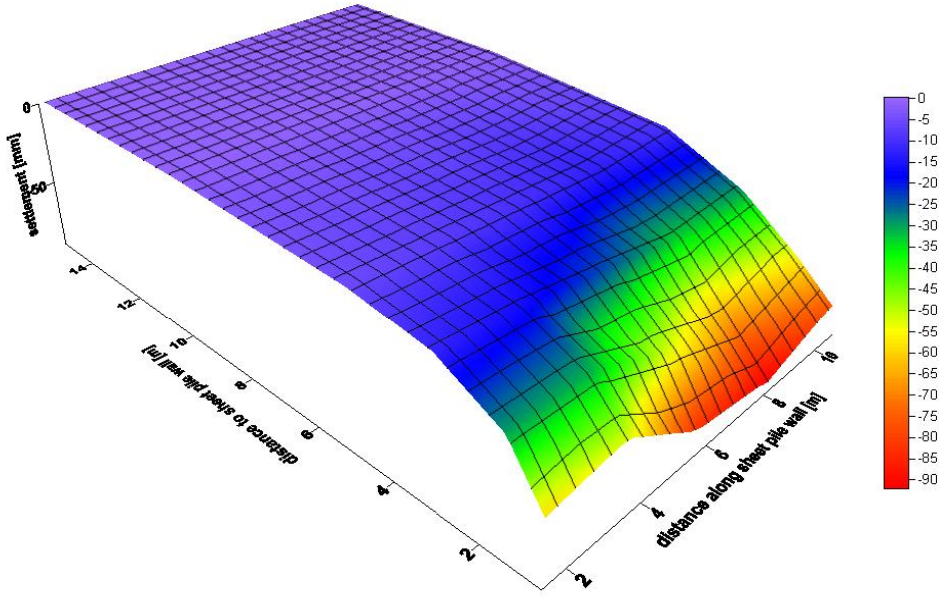

ANNEX 7.11 Raamsdonksveer sheet pile test, change in cone resistance

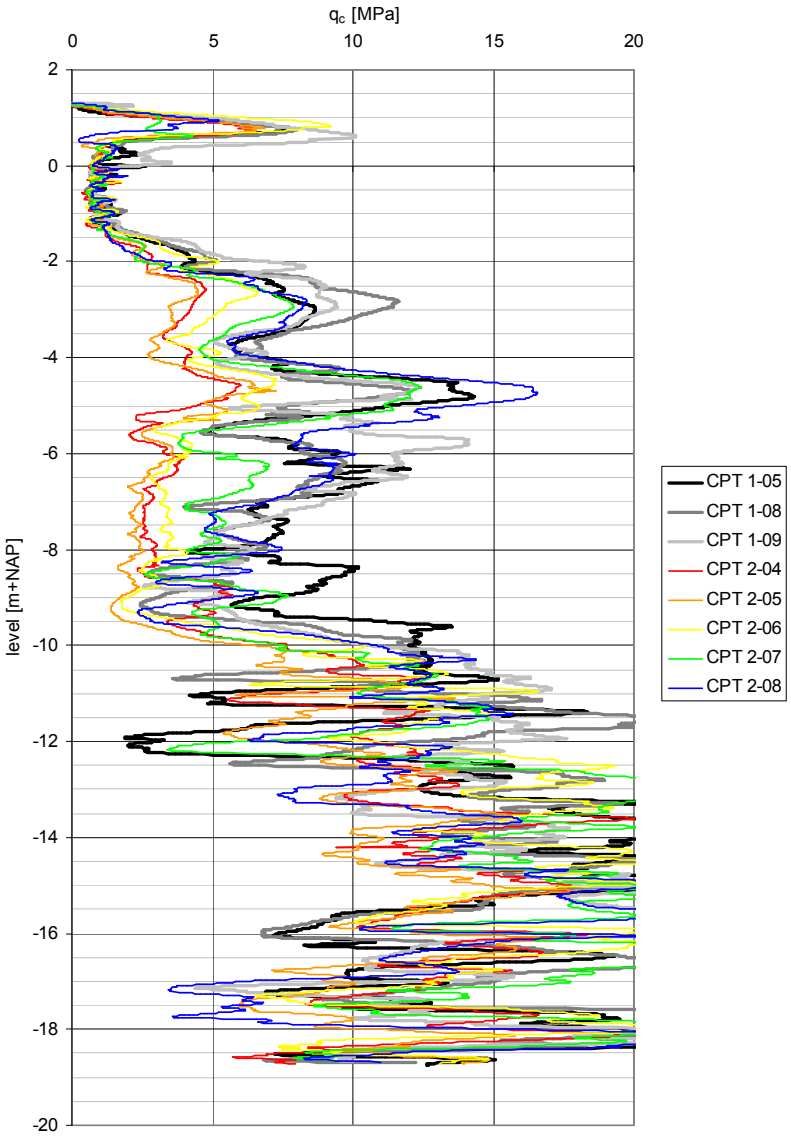

Cone resistance before and after installation, Z-section
serie 1: before installation, serie 2: after installation
CPT2-04: 0.5 m distance from wall
CPT2-05: 1.0 m distance from wall
CPT2-06: 1.5 m distance from wall
CPT2-07: 3.0 m distance from wall
CPT2-08: 5.0m distance from wall

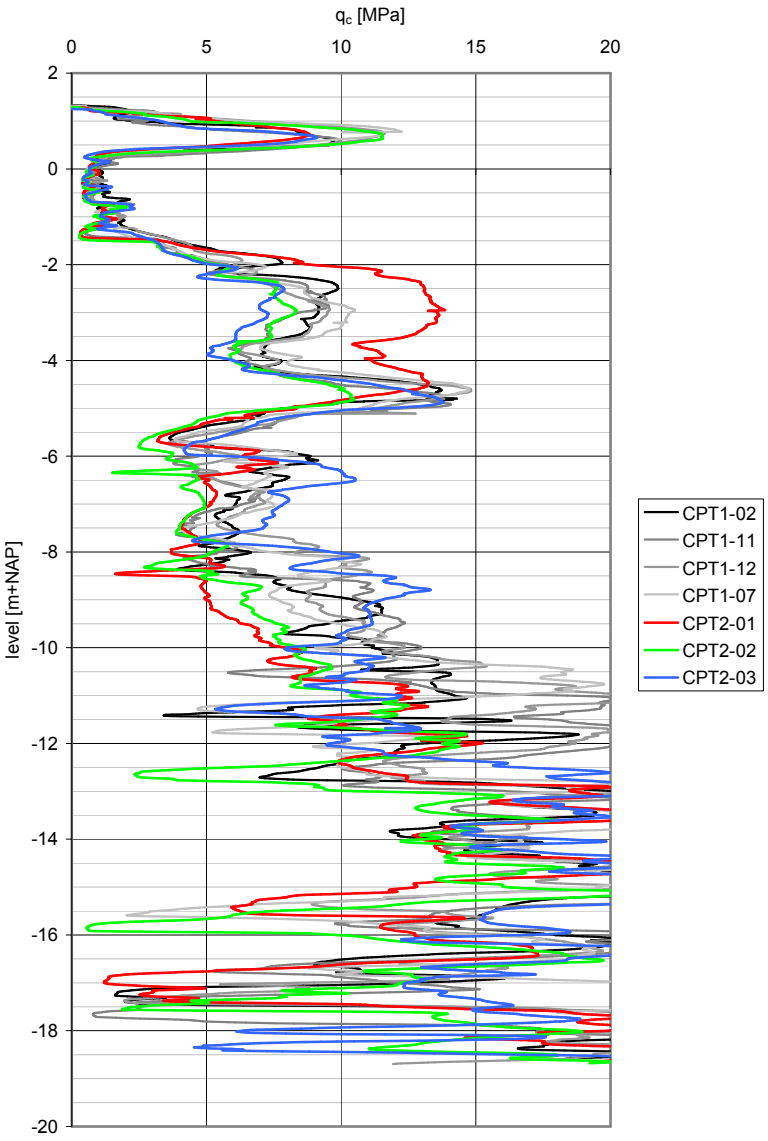

Cone resisance before and after installation, U-section;
serie 1 before installation, serie 2 after installation
CPT2-01: 0.5 m distance from wall
CPT2-02 1.0 m distance from wall
CPT2-03: 1.5 m distance from wall

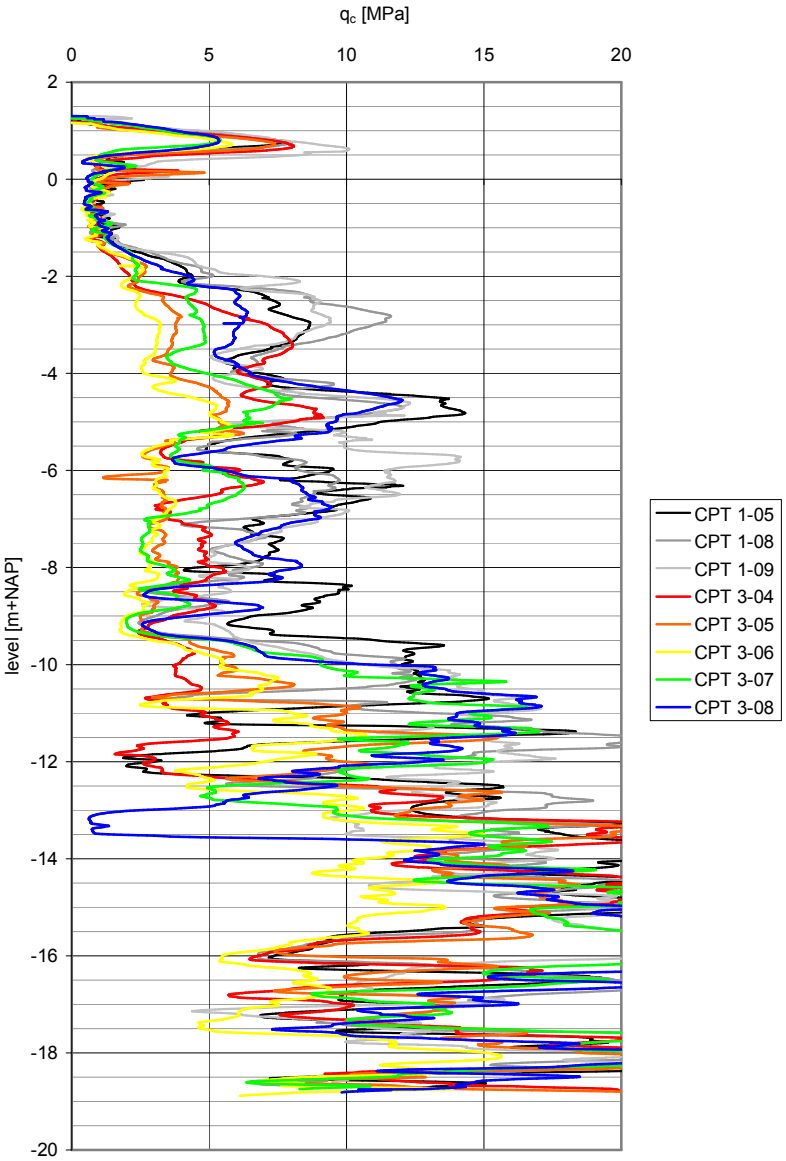

Cone resistance before installation and after removal, Z-section
serie 1: before installation, serie 3: after removal
CPT3-04: 0.5 m distance from wall
CPT3-05: 1.0 m distance from wall
CPT3-06: 1.5 m distance from wall
CPT3-07: 3.0 m distance from wall
CPT3-08: 5.0 m distance from wall

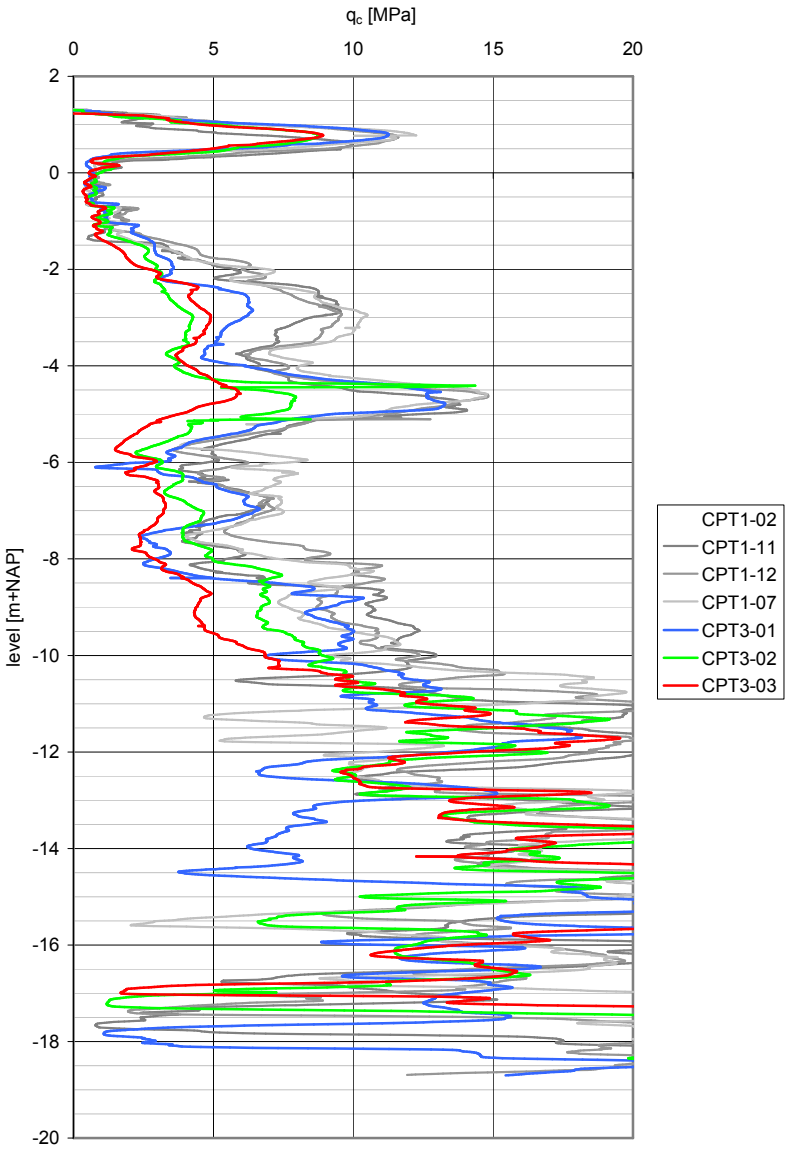

Cone resistance before installation and after removal, U-section
serie 1: before installation, serie 3: after removal
CPT3-01: 3.0 m distance from wall
CPT3-02: 1.5 m distance from wall
CPT3-03: 0.5 m distance from wall